Origins for dark matter particles : from the "WIMP miracle" to the "FIMP wonder"

Maíra Dutra

université PARIS-SACLAY

CIÊNCIA SEM FRONTEIRAS

UNIVERSITÉ PARIS SUD
Comprendre le monde, construire l'avenir

NNT : 2019SACLS059

Thèse de doctorat

Origins for Dark Matter Particles: from the WIMP miracle to a FIMP wonder

Thèse de doctorat de l'Université Paris-Saclay
préparée à l'Université Paris-Sud

Ecole doctorale n°576 Particules, Hadrons, Énergie, Noyau, Instrumentation, Imagerie, Cosmos et Simulation (PHENIICS)
Spécialité de doctorat: Astroparticules et Cosmologie

Thèse présentée et soutenue à Orsay, le 19 février 2019, par

MAÍRA DUTRA

Composition du Jury :

Asmâa Abada Professeur, Université Paris-Sud (UMR 8627)	Président
Laura Covi Professeur, Université de Göttingen	Rapporteur
Torsten Bringmann Professeur, Université de Oslo	Rapporteur
Gautam Bhattacharyya Professeur, Saha Institut de Physique Nucléaire	Examinateur
Pierre Fayet Professeur, École Normale Supérieure	Examinateur
Michel Tytgat Professeur, Université Libre de Bruxelles	Examinateur
Yann Mambrini Directeur de recherche, Université Paris-Sud (UMR 8627)	Directeur de thèse

Titre : Origines pour les particules de matière noire: du ”miracle WIMP” à une ”merveille FIMP”

Mots clés : Matière noire, l'univers primordial, phénoménologie

Résumé : Celà fait plus de 80 ans que nous avons des preuves qu'environ 26% de la densité d'énergie de l'univers actuel se présente sous la forme de matière noire, qui interagit avec la matière ordinaire strictement par gravitation. Avec les neutrinos massifs, l'existence de particules de matière noire (DM) indique qu'il faut étendre le modèle standard de la physique des particules (SM) pour en tenir compte. Dans cette thèse, nous explorons la relation étroite entre la nature des couplages reliant la DM aux particules du SM et la production de l'abondance de la DM dans l'univers primordial. Nous commençons par examiner la classe la plus prédictive de candidats DM, les particules massives à interaction faible (WIMP). Leurs masses et couplages sont comparables à ceux du SM, et donc les deux secteurs ont déjà été en équilibre thermique, et l'abondance de DM respecte automatiquement les limites cosmologiques – le ”miracle WIMP”. Les limites expérimentales actuelles repoussent l'espace paramétrique viable des modèles WIMP vers des limites complexes, rendant nécessaire l'ajout de particules supplémentaires dans le secteur sombre et la vérification plus précise de la condition de découplage. Après avoir considéré le statut phénoménologique d'une gamme significative de modèles pour les WIMP avec des masses dans l'intervalle $10 - 10^4\ GeV$, nous examinons la phénoménologie d'une DM sur l'échelle MeV dans un modèle de portail Z'. En plus de chercher à améliorer la recherche de WIMPs, il convient de considérer le cas dans lequel DM et SM interagissent si faiblement qu'ils n'ont jamais atteint l'équilibre. Les particules massives à interaction faible (FIMP) sont des candidats DM produits à partir du SM dans des processus hors d'équilibre, un mécanisme appelé ”*freeze-in*”. Nous montrons que si des champs lourds ($10^{10} - 10^{16}\ GeV$) interviennent dans les interactions MN-MS, le *freeze-in* est une possibilité naturelle qui fournit la bonne abondance de MN sans qu'il soit nécessaire d'imposer couplages extrêmement petits. Ces champs lourds sont en fait nécessaires dans des scénarios à hautes énergies théoriquement bien motivés tels que le GUT, le ≪see-saw≫, la leptogénèse et l'inflation – nous appelons cette coïncidence intéressante la ”merveille FIMP”. Nous explorons différentes réalisations de cette possibilité, avec des modèles impliquant des moduli, fermions, bosons de jauge et champs de spin-2 comme les médiateurs lourds. Nous montrons enfin dans quels cas la production de MN pendant le reheating après inflation a un impact sur l'espace paramétrique de tels modèles.

Title : Origins for dark matter particles: from the ”WIMP miracle” to a ”FIMP wonder”

Keywords : Dark matter, early universe, phenomenology

Abstract : For more than eighty years, we face evidence that about 26% of the energy budget of the universe today is in the form of dark matter, whose interaction with ordinary matter is felt only gravitationally. Along with massive neutrinos, the existence of dark matter particles (DM) indicate that we must extend the standard model of particle physics (SM) in order to account for them. In this thesis, we explore the close relationship between the nature of couplings connecting DM to the SM sector and the production of the DM relic density in the Early Universe. We start by considering the most predictive class of DM candidates, the weakly interacting massive particles (WIMPs). Their masses and couplings are comparable to the SM ones, which ensure that both sectors were once in thermal equilibrium and automatically render the DM relic density within the inferred range – the so-called “WIMP miracle”. The current experimental bounds push the viable parameter space of WIMP models to complex corners, making necessary to add extra particles in the dark sector and to check the decoupling condition more carefully. After reviewing the phenomenological status of a comprehensive spectrum of models for WIMPs with masses in the range $10 - 10^4\ GeV$, we consider the challenging phenomenology of an MeV DM in a Z' portal model. Besides seeking to improve the search for WIMPs, it is worth considering the case in which DM and SM interact so feebly that they had never reached equilibrium. Feebly interacting massive particles (FIMPs) are DM candidates produced from the SM thermal bath in out-of-equilibrium processes, a mechanism called freeze-in. We show that if heavy fields ($10^{10} - 10^{16}\ GeV$) mediate the DM-SM interactions, the freeze-in is a natural possibility that provide the right amount of DM in the universe without the need of extremely small gauge, yukawa or quartic couplings. Such heavy fields are actually needed in theoretically well motivated high-energy scenarios like for instance GUT, seesaw, leptogenesis and inflation – we call this interesting coincidence the “FIMP wonder”. We explore different realizations of such possibility, with models involving moduli, fermions, gauge bosons and spin-2 fields as heavy mediators. We finally show in which cases the DM production during reheating have impact on the parameter space of such models.

Université Paris-Saclay
Espace Technologique / Immeuble Discovery
Route de l'Orme aux Merisiers RD 128 / 91190 Saint-Aubin, France

For João Obá,
whom I joyfully discovered to be my great-great-grandfather last year.

In 1889, he led ex-slaves to celebrate the anniversary of the end of slavery in Brazil. Since then, the drums of Bembé do Mercado still play every May 13th in Santo Amaro, Bahia.

Acknowledgements

I thank immensely my mother, who always gave me the strength and the tools to follow and to fight for my way. I thank my father, who introduced me to Physics and motivated me to learn about Science and the world. I thank my beloved sister and brother Maiara and Guto, always so present and really fundamental in my life. Few relationships in life make us better people and put us beyond our own expectations. That is why I thank the love, the companionship and the care of Norberto Romanelli, with whom I want to be forever.

I am grateful for everything I have learned from and shared with my friend and collaborator Clarissa Siqueira. I also thank the moments full of music and confidence I was able to share with Nara Lordão here in Paris.

I thank Yann Mambrini for everything he taught me, for the opportunity to visit different places and to collaborate with different people, those were really great experiences. Moreover, I thank him for the motivation he gave me and for all the doors he has opened for me. It was a great honor and pleasure to have such a distinguished jury, and I am very happy to thank the time and the contributions of Asmâa Abada, Michel Tytgat, Gautam Bhattacharyya, Torsten Bringmann, Laura Covi and Pierre Fayet.

I have learned a lot in the last three years, and that was also thanks to the enlightening and pleasant discussions with Mathias Pierre, Nicolás Bernal, Farinaldo Queiroz, Pradipta Gosh, Giorgio Arcadi, Debtosh Chowdhury, Yasaman Farzan, Emilian Dudas and Takashi Toma. I also thank the contributions of Manfred Lindner, Stefano Profumo, Werner Rodejohann, Keith Olive and Marco Peloso for the works I discuss here. It was great discussing with Adam Falkowski, Andreas Goudelis, Marcos García, Geneviève Bélanger and Sudhir Vempati. I also thank the patience and generosity of Bryan Zaldívar, who introduced me to the CUBA package, very important for the work I have done. It was also very nice to know and to discuss with Meshkat Rajaee, Shiuli Chatterjee, Priyanka Lamba and Avik Banerjee. I am also very grateful for the excellent networks Elusives and Dark Side of the Universe.

The time I have spent in Orsay would not be so great without the nice discussions and lunch&coffee breaks with Olcyr Sumensary, Luiz Vale, Andrei Angelescu, Xavier Marcano, Matías Vásquez, Florian Nortier, Elie Mounzer, Sonali Verma, Elena Perdomo, Álvaro Cabezudo, Marco Fedele, Gabriel Jung, Antoine Lehébel, Martín Novoa-Brunet and Timothé Poulain. I also thank to Marie-Agnès Poulet, Henk Hilhorst, Jocelyne Raux, Sarah Meme, Sébastien Descotes-Genon and Philippe Molle for the friendly environment they have provided.

Finally, I acknowledge the support from the Brazilian PhD program "Ciência sem Fronteiras"/CNPq and the hospitality of the Laboratoire de Physique Théorique d'Orsay.

Publication list

- Giorgio Arcadi, MD, Pradipta Ghosh, Manfred Lindner, Yann Mambrini, Mathias Pierre, Stefano Profumo and Farinaldo S. Queiroz, ***The Waning of the WIMP? A Review of Models, Searches, and Constraints*** [1]

- MD, Manfred Lindner, Stefano Profumo, Farinaldo S. Queiroz, Werner Rodejohann, Clarissa Siqueira, ***MeV Dark Matter Complementarity and the Dark Photon Portal*** [2]

- e-ASTROGAM Collaboration, ***Science with e-ASTROGAM (A space mission for MeV-GeV gamma-ray astrophysics)*** [3]

- Nicolás Bernal, MD, Yann Mambrini, Keith A. Olive, Marco Peloso, Mathias Pierre, ***Spin-2 portal Dark Matter*** [4]

- Gautam Bhattacharyya, MD, Yann Mambrini, Mathias Pierre, ***Freezing-in dark matter through a heavy Z'*** [5]

- Debtosh Chowdhury, Emilian Dudas, MD, Yann Mambrini, ***Moduli portal to dark matter*** [6]

- MD, Yasaman Farzan, Yann Mambrini, ***Dynamical freeze-in of keV dark matter*** (work in progress) [7]

Contents

Chapter 1

Introduction

Contents

For more than eighty years, we face evidence that the baryonic matter* interacts gravitationally with an unknown type of matter that does not interact with light in a perceptible way, provided that our understanding of gravity is correct. It is interesting, and hopeful, to notice that fifty years before the appearance of the first pieces of evidence for dark matter, scientists were discussing whether the Milky Way comprised the entire universe [8].

As we are going to point out in Section 1.1, on one hand we need a matter component which was not affected by light and catalyzed the formation of the baryonic structures we see today. On the other hand, the behavior of stars in galaxies is better understood if we assume the presence of halos of gravitating matter which do not contribute to the measured luminosity. If these two components of non-baryonic matter are made of the same kind of particles, they should be stable and constitute a cosmic relic density accounting for about 26% of the energy budget of the Universe today, as inferred by the Planck satellite. We generically call them dark matter particles (DM). In Section 1.2, we explain the title of this thesis, once we advocate the interest in relating the dark matter genesis to processes taking place at very high energies in the early universe.

This thesis is structured as follows. Chapter 2 is devoted to technical details regarding the starting point of all the discussion covered in our works: the fluid equations and their collision terms. We also discuss in some detail the evolution of particle species taking into account the possibility of particle creation due to the decay of heavy fields, which is important to describe the evolution of dark matter in the early universe. In Chapter 3 we discuss mechanisms for the establishment of the relic density of DM. In Chapters 4, 5

*We remind the reader that, in cosmology, the term "baryonic matter" refers to all the known types of particles (electrons, protons, neutrons, etc).

and 6, we present our original works. Our general conclusions and perspectives are given in Chapter 7.

1.1 Why to believe there are and there were dark matter particles?

The first evidence for the presence of a large amount of non-luminous (dark) matter was inferred by Fritz Zwicky in the 1930's [9] by measuring velocity dispersion of galaxies in the Coma cluster, at a redshift of $z \sim 0.02$ from us ($z = 0$)*. Clusters of galaxies are bound systems, and we can use the Virial theorem to infer their masses. It was concluded that the mass necessary to explain the cohesion of the Coma cluster was much higher than its luminous mass [10], unless the laws of gravity at large-scales has to be modified [11]. At that moment, however, there were many observational limitations, and the credibility of both conclusions had to wait for decades. In what follows, we briefly discuss about the pieces of evidence for the presence of dark matter at increasing redshift (into the past).

About 40 years after the discoveries of Zwicky, Vera Rubin and others found that the rotation curves of stars in spiral galaxies are very different from what we expect for the baryonic matter [12, 13]. Such studies can be taken as the most convincing and direct evidence for the existence of halos of dark matter particles around galaxies [14, 15] and contributed greatly to its establishment as a real scientific problem. See [16] for a review on dark matter halos.

The rotation curves express the dependence of the speed of rotation of an object in orbit on its radial distance to the center of rotation. The orbit of an object (stars, dust, etc.) in a galaxy or in a cluster of galaxies is approximately spherical. From Newtonian dynamics, the equilibrium between the gravitational and centripetal forces on an object of mass m at the distance r from the center of rotation, with rotational velocity $v(r)$, give us the following relation

$$v(r) = \sqrt{\frac{GM(r)}{r}}\,, \tag{1.1}$$

where G is the Newton's gravitational constant and $M(r)$ is the total mass inside the radius r. Supposing spherical symmetry, for a given density profile $\rho(r)$, we find $M(r) = 4\pi \int \rho(r) r^2 dr$.

Outside the galaxy, where $M(r)$ becomes constant, $v(r) \propto r^{-1/2}$. It has been observed, though, that for many spiral galaxies the rotation speed is approximately constant even beyond the visible radius. This means that we observe the relation $M(r) \propto r$ instead of the expected one, $M(r) \approx M_{\text{total}} = \textit{constant}$. This could be caused by a density profile proportional to r^{-2}, but that matter would be outside the visible radius of the galaxies, as suggested by the measurements of luminosity.

*We postpone a more detailed introduction to the evolution of particles in an expanding universe to Sec. 2.2, where we have defined the redshift.

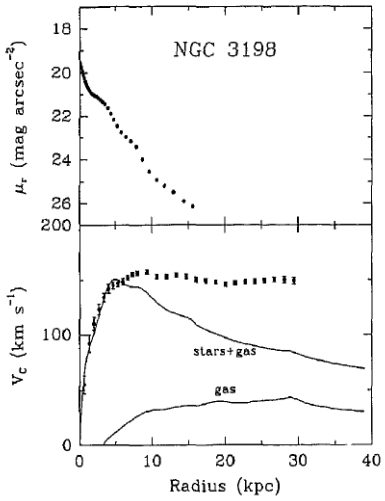

FIGURE 1.1 – *Comparison between the luminosity profile (upper panel) and rotation curve (lower panel) of galaxy NGC 3198 as a function of the radial distance. Figure from [20].*

In Fig. 1.1, we see the comparison between the luminosity and the rotation speed profiles as functions of the radial distance for a typical spiral galaxy [17]. We have two explanations for that which work: *a)* there is an approximately spherical distribution of matter with very low luminosity, *the halos of dark matter*, and/or *b)* Newton's Law does not apply at that scales. Proposals to modify Newtonian gravitation are collectively called as MOND (modified Newtonian dynamics). For recent review and constraints, see [18, 19].

The most immediate hypothesis is that black holes, low-luminosity stars, unseen planets and comets are dark matter. However, these massive compact halo objects (MACHOs) contribute with a very tiny fraction to the amount of dark matter needed [21]. This means that dark baryonic matter so far does not explain what we observe in rotation curves of galaxies. Studies of the Milky-Way are consistent with a halo of non-baryonic dark matter. As reviewed in [22], combining numerous and independent observations of stellar kinematics, the local density of DM at the location of the Sun is found to be in the range $\rho_\odot = 0.2 - 0.56\,\mathrm{GeV/cm^3}$, in agreement with results of N-body simulations of galaxy formation [*]. Of course, since we have not detected particles which would constitute this dark halo, dark non-baryonic particles need to interact with ordinary matter weakly enough.

Although we had evidence since the 1930's that the gravitational potential of galaxy clusters did not fully correspond to the visible matter of the system [24], we could not know whether this incompatibility was due to the presence of dark matter in all bands of the electromagnetic spectrum or was an indication that the gravitational laws which apply for the solar system do not apply at cluster of galaxies scales. This is because all the gravitating matter was inside the same volume. It is when two clusters collide that a

[*]This is indeed much below the upper limit on the dark matter density in the Solar System: $\rho_{\mathrm{dm}} < 78680, 7868$ and $6182\,\mathrm{GeV/cm^3}$ at the orbital distances of Earth, Mars and Saturn [23].

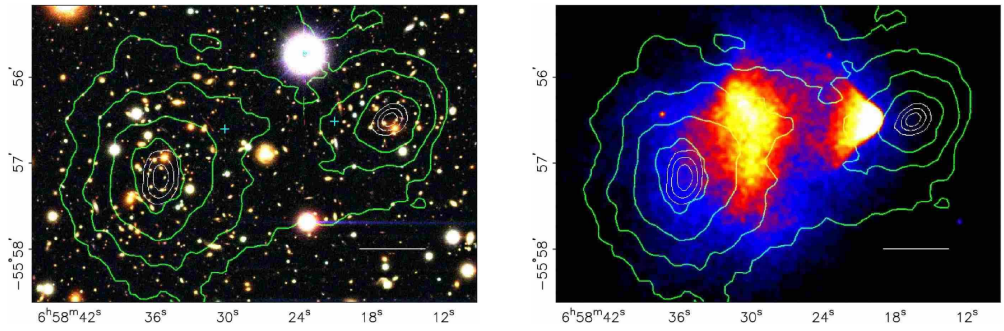

FIGURE 1.2 – *Optical (left) and X-ray (right) images of the merging Bullet cluster, obtained respectively by Magellan and Chandra observatories. The green contours show the weak lensing mapping of gravitational centers obtained by weak gravitational lenses. Figure from [25].*

dark matter content could be physically separated from the baryonic matter and become directly observable by its gravitational potential.

In 2006, it was observed that the mass centers of two colliding clusters of galaxies did not agree with those corresponding to the baryonic matter [25]. This cluster system (1E0657-558) is at $z = 0.296$ and is called the *Bullet cluster*, due to the shape of the smaller cluster passing through the larger one. This was done by comparing measurements of X-rays and weak gravitational lenses. The conclusion was that only about 10% of the observed baryons were in the gravitational centers (mapped by the gravitational lenses). The X-rays, which represent about 90% of the baryons, are displaced from the centers and show that the baryonic part of the clusters is affected by the collision (see Fig. 1.2). The invisible components of the clusters were found nearly collisionless. At the present time, explaining those observations with modified gravity theories is controversial [25–27], and subject to passionate debate.

Rotation curves of galaxies and observations of merging clusters therefore support the existence of particles which should be neutral, weakly interacting and non-baryonic. With gravity described by General Relativity, a collisionless fluid is included in the standard cosmological model, known as ΛCDM, and the success of this model constraints the strength of non-gravitational interactions between the visible and dark sectors.

Another study, with data from the Sloan Digital Sky Survey (SDSS) [28], favors the interpretation of dark matter particles at scales of galaxy clusters. They compare the predictions of ΛCDM and of MOND for the rms velocity of satellite galaxies in clusters, for two distinct luminosities. In Fig. 1.3, we see that according to their results, ΛCDM is clearly favored, with the galaxies hosting halos of dark matter particles with circular velocities of around 340 km/s (upper curve in the left panel) and 270 k/s (bottom curve in the left panel).

Such analyzes indicate as more plausible the existence of a large amount of dark matter which does not behave as baryonic matter and are more likely to be made of nonbaryonic particles, once modifications of gravity still have problems in explaining the observations. Merging clusters set bounds on the self-interaction of DM [29, 30].

The mapping of large-scale structures and the current understanding of their formation processes ($z \lesssim 10$) also point to the existence of dark matter [31–33].

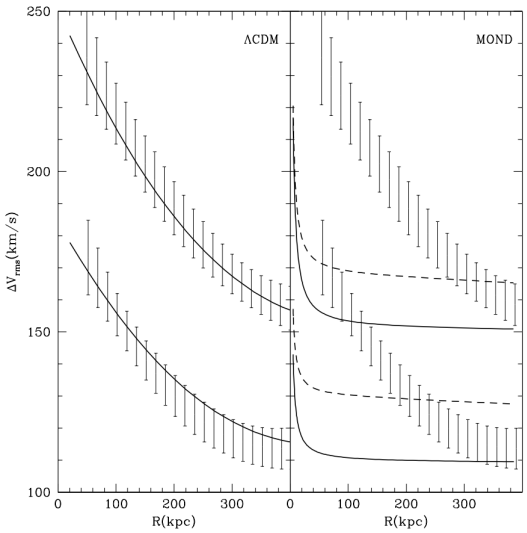

FIGURE 1.3 – *Predictions of ΛCDM (left) and MOND (right) for the rms velocities of satellite galaxies in clusters as a function of the distance to the center of the cluster. Figure from [28].*

In the standard understanding, supported by simulations and comparison with observations, the large-scale structures we observe today have evolved from small inomogeneities in the distribution of matter. We have basically two fundamental opposing forces in this process: the gravitational attraction of matter and the repulsion generated by the radiation pressure. Structures are able to form once the gravitational pull can overcome the pressure of the photons. *Cold* and *hot* fluids are limiting cases of species with small and large internal velocity dispersion, respectively. Smaller the velocity dispersion, smaller the structures that can be formed, and smaller the distances between two interactions, i.e., their "free-streaming". For this reason, cold species are slower than hot (or warm, as an intermediate case) ones. As small inomogeneities grows more and more by gravitational attraction, cold species clump more than hot species. If the matter content of the universe were restricted to baryonic matter, structures would start forming later than what is observed today. The addition of a cold dark matter content, which does not interact with radiation significantly but interacts gravitationally with ordinary matter, is able to explain why did ordinary matter start clumping before becoming non-relativistic.

Large-scale mapping of galaxies also points to the existence of dark matter and put serious problems for modified gravity alternatives. In Fig. 1.4, we show the result of an analysis performed in Ref. [34]. We see the variance in the distribution of galaxies as function of scale, in Fourier space. At large scales (small k), the variance is smaller than unity, implying an approximately homogeneous distribution. The structure formation requires inomogeneities of order of unity. The blue dashed line is the prediction of a model containing only baryonic matter, unable to form structures. The solid blue line is the prediction of a relativistic MOND theory, which can sufficiently amplify the oscillation of baryons but do not agree with the measurements (red squares with error bars). The solid black line is the theoretical prediction of ΛCDM, which in addition to allowing formation of structures agrees very well with observational data.

Despite providing evidence for DM, observational data at scales of galaxies and clusters of galaxies do not give us information about the total amount of DM in the universe, which

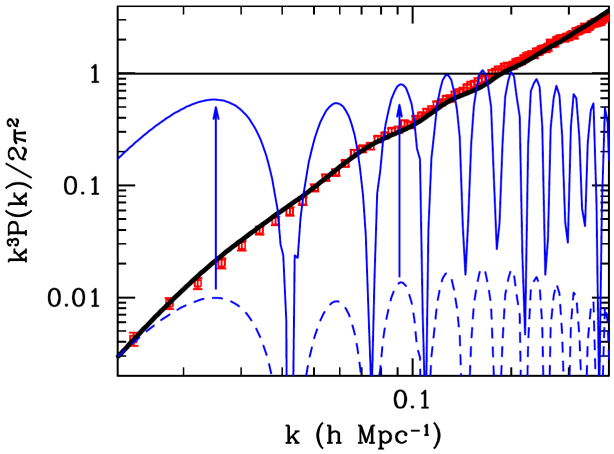

FIGURE 1.4 – *Data from SDSS (red squares with error bars) of the matter power-spectrum contrasted with predictions from a scenario with only baryonic matter (dashed blue curve), relativistic MOND (solid blue curve) and ΛCDM (solid black curve). Figure from [34].*

is achieved by the cosmological probes.

The last scattering surface of the cosmic microwave background (CMB), around $z \sim 1090$, is the farther we can *see* in the universe, the earliest direct probe of its thermal history. The CMB spectrum is the closest example of a black-body radiation source, and its tiny anisotropies make it possible to study the thermalization process of the photons at that epoch [35]. The injection of energy into the thermal bath of CMB photons are therefore strongly constrained, specially by the results of the Planck satellite [36]. *Inflationary theories* are nowadays the best explanation for the origin of those anisotropies, and subject to intense phenomenology [37]. See for instance [38] for an introduction. The Big Bang nucleosynthesis is a theory that predicts the formation of the first light elements and also the existence of the CMB radiation. For a recent review, see for instance [39]. It leaves no room for the dark matter content to be regarded as baryonic matter.

Finally, if dark matter is made of the same kind of particles, they must be stable enough as to have been present in the universe since its early stages. Also, as we discuss in the next Chapter, an unstable cold species would not be able to contribute to the cosmic energy, so that most of the dark matter content need to be stable in any particle physics model.

In Fig. 1.5 we illustrate the relation between the pieces of evidence discussed above – rotation curves [20], merging cluster [25], structure formation [40], CMB [36] and BBN [41] – with the properties that dark matter particles should have in any scenario accommodating them.

Agreement with structure formation, CMB and BBN constraints point out that the majority of the dark matter content was established as a relic, evolving independently of the thermal bath, before the last scattering surface. In Ref. [42], the authors have found that if all the DM was produced between the last scattering surface and the radiation-matter equality, the lower DM formation redshift is of $z_f \sim 1.08 \times 10^5$ at 99.73% C.L. from the SDSS data and $z_f > 9 \times 10^5$ at the same C.L. from the Lyman-α data. Together, the cosmological probes implies that the universe today has about 26% of its energy budget

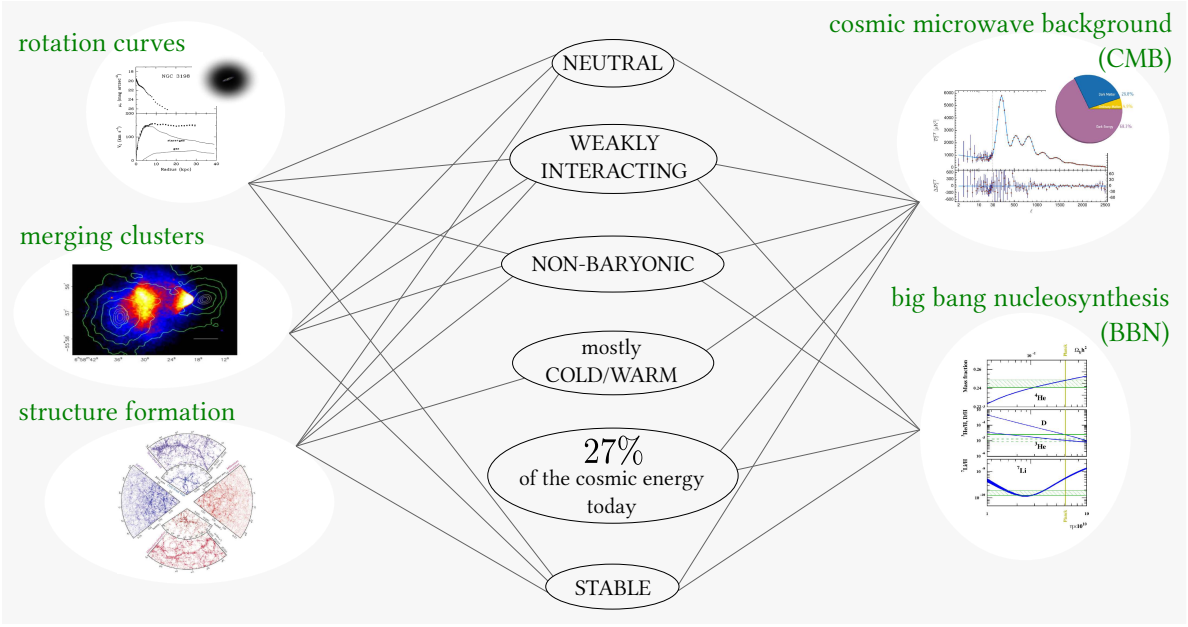

FIGURE 1.5 – *The dark matter puzzle.*

in the form of dark matter [43]. In this thesis, we consider that the dark matter density was established during the radiation era or even before, while the field responsible for the inflationary period, generically called inflaton, dominated the energy density of the universe. In Fig. 1.6, we put the events discussed above as function of redshift and temperature.

1.2 Why to relate the dark matter puzzle with very high-energy physics?

The 20$^{\text{th}}$ century witnessed the consolidation of quantitative descriptions of phenomena at subatomic and cosmological scales. On one hand, we had the emergence of quantum mechanics and special relativity that culminated in the quantum field theory when treating subatomic particles at high energies. This formalism allowed us to describe the fundamental interactions – weak, strong and electromagnetic. On the other hand, we had the emergence of the Einstein's gravitational theory that treats the gravitational interaction as the effect of energetic content curving the space-time, the general relativity (GR).

The standard model of particle physics (hereafter referred to as SM), besides mathematically consistent, had all its predictions experimentally confirmed to great accuracy over the last decades. The last predicted and unconfirmed particle of its spectrum, the Higgs boson, is very likely the 125 GeV scalar boson discovered at the LHC [44, 45], although there is still room for nonstandard properties [46]. Despite all that success, there are both experimental and theoretical reasons to consider beyond the SM (BSM) scenarios. The main, experimental, reason is that neutrinos are massless in the SM while we have evidence that they do have mass. We know that the universe contains more matter than

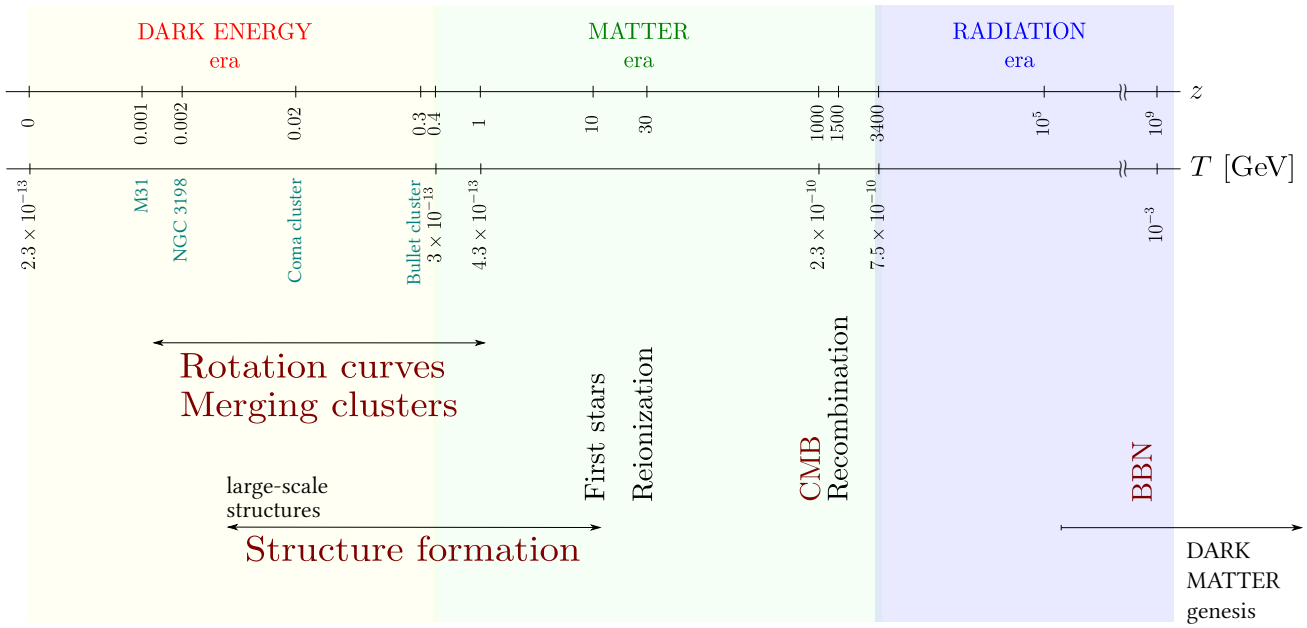

FIGURE 1.6 – *The cosmic timeline of the evidence for dark matter, in terms of redshift (z) and temperature (T).*

anti-matter, but we do not know yet why. In addition, there are problems of fine-tuned parameters such as the hierarchy problem, solved in theories such as supersymmetry (SUSY) and extra dimensions (ED). The number of fermionic families, as well as the hierarchy among particle masses, are also unanswered questions. See for instance Ref. [47] for an introduction to the SM and Refs. [48, 49] for discussions on BSM scenarios.

The once standard Big Bang model is the best we have nowadays to understand the evolution of the universe, having as observational pillars the cosmic expansion, the CMB and the BBN. The evidence for cold dark matter (CDM), dark energy (possibly a cosmological constant Λ) and the attempt to understand the origin of the gravitational perturbations generating the structures we observe today (inflationary models) put us beyond the Big Bang model, in a scenario known as ΛCDM – nowadays a successful cosmological standard model. Here we also have reasons to go beyond, for instance the famous cosmological constant problem [50] and the small-scale problems with CDM. See for instance Ref. [51] for a general discussion on extensions of ΛCDM.

Dark matter is a macroscopic problem, but as we have seen, it is likely made of particles. Since the SM has no viable DM candidate, it means that these particles are expected to be accommodated in some SM extension. In doing so, we also need to ensure that they are in agreement with what the ΛCDM already explains, being therefore part of it or a viable extension. Despite the often quoted deep discontent regarding the absence of signs for BSM physics, solutions apparently disconnected may be intertwined. The 21$^{\text{th}}$ century, if our species survives, is likely to witness significant advances in this interface of particle physics and cosmology, with the countless experiments seeking to detect new particles, with the advance of gravitational waves astronomy, even more precise studies of the CMB spectrum, etc.

Remarkably, the understanding of the early instants of the universe depends heavily on how high energy particles behave [52]. The phase transitions likely undergone by the

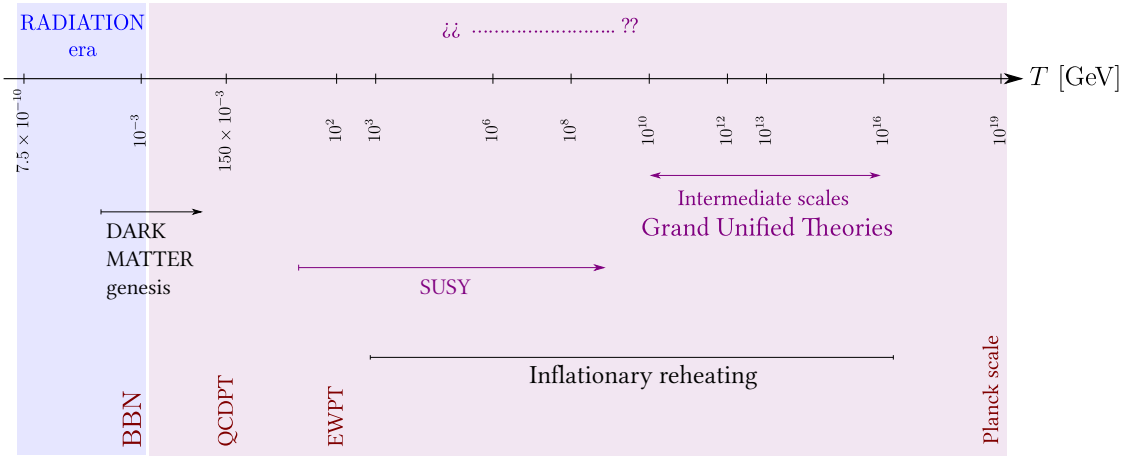

FIGURE 1.7 – *The landscape for dark matter particles production, as function of temperature (T).*

universe, for example, might be due to the breaking of a gauge symmetry. Indeed, the discovery of the Higgs boson made possible to study the process before which the weak and electromagnetic interactions were unified into an electroweak interaction, the spontaneous symmetry breaking (SSB). This also motivates the seek for unifying the electroweak and strong interactions, in grand unification theories (GUT), typically happening at scales of 10^{16} GeV, possibly through the breaking of symmetries at some intermediate scale $10^{10} - 10^{16}$ GeV.

In Fig. 1.7, we continue the cosmic timeline of Fig. 1.6 taking into account the discussion above. The BBN predicts very well how the first elements were formed, and this is well accommodated in the SM. We can therefore expect that earlier in the universe the quarks and gluons were free, before the QCD phase transition (QCDPT), around 150 MeV and that even earlier, around hundreds of GeV, the electromagnetic and weak interactions were unified, before the electroweak phase transition (EWPT). In Fig. 1.7, we indicate the mass scale of the hypothetical SUSY particles [53] and the intermediate scales of the breaking pattern of GUT scenarios. In the context of inflationary theories, we would expect that, after the period of exponential expansion of the universe, the universe changed from a cold phase in which its energy density was dominated by the inflaton field to a hot phase in which ultra-relativistic particles dominated its energy density. All the standard species would be therefore produced from the irreversible decay of the inflaton field, in a process called the inflationary reheating. In the next section, we discuss details of such a process. The scale at which the inflationary reheating took place is not known, and is highly model-dependent. In Fig. 1.7, we illustrate the energy interval in agreement with the constraints on the reheating scale found in Ref. [54].

In this context, connecting the dark matter production in the early universe with physical processes taking place at high energy scales is an appealing option, as we intend to show with different scenarios in this thesis. As we explain in detail in Chapter 3, in contrast to the so-called "WIMP miracle", we take the liberty – while asking for the excuse – of calling such a connection the "FIMP wonder". It is not a miraculous connection, whatever it might sound, but it is rather involved in appreciation toward something we cannot actually probe yet. Of course, with the purpose of going beyond the pure wondering towards the development of the FIMP phenomenology.

Chapter 2

Cosmological evolution of particles

Contents

In this chapter, we intend to provide the tools allowing us to understand (and/or modify) the thermal history of the universe at a first approximation *, in particular the evolution of dark matter particles and the establishment of its relic density.

2.1 Boltzmann and fluid equations

In order to describe the time evolution of particles of a species k, we need to track the path of its distribution function $f_k(t, \vec{x}_k, \vec{p}_k)$ in the phase-space, which depends on the interactions that such particles might feel. In a four-dimensional space-time, the path of particles is parametrized by some monotonically increasing variable λ. Through the four-momentum $P_k^\mu = (E_k, \vec{p}_k)$ of the species under study, we can trade the evolution over λ by the evolution over time by defining $P_k^\mu = dx^\mu/d\lambda$ [58, 59]. The Boltzmann equation is therefore

$$\frac{df_k}{d\lambda} = E_k \frac{df_k}{dt} = \widehat{C}[f_k]\,, \tag{2.1}$$

where $\widehat{C}$ is the collision operator, to be defined in what follows.

*See for instance [55–57].

The total time derivative of an homogeneous distribution function $f_k(t, \vec{p}_k)$ reads*

$$\frac{df_k}{dt} = \frac{\partial f_k}{\partial t} + \frac{\partial f_k}{\partial p_k}\frac{dp_k}{dt}\,. \tag{2.2}$$

In an expanding universe, time variation is related to the scale factor variation through the expansion rate of the universe, the Hubble rate $H = \frac{1}{a}\frac{da}{dt}$, with $a(t)$ the scale factor. In a flat, homogeneous and isotropic universe, the momenta of particles redshift as $p_k = \bar{p}/a$, with $\bar{p}$ the comoving momentum, and the Boltzmann equation is given by

$$\frac{\partial f_k}{\partial t} - Hp_k\frac{\partial f_k}{\partial p_k} = \frac{\widehat{C}[f_k]}{E_k}\,. \tag{2.3}$$

The total number of k particles in a unitary comoving volume $V = a^3$ is found after integrating over all the possible momenta†:

$$N_k = n_k a^3 = a^3\frac{\gamma_k}{(2\pi)^3}\int d\vec{p}_k f_k\,, \tag{2.4}$$

where n_k is the so-defined number density of the k particles and γ_k accounts for their spin degeneracy. The only way to change N_k over time is through transfer of energy and momentum via interactions with other species. All the microphysics governing these processes is encoded in the collision operator $\widehat{C}$ acting on the distribution function.

Let us consider the generic process $A \to B$, where the state A (B) is composed of particles of a species labeled as i (j). The collision operator for the evolution of a particle k (which may be part of state A or B) is defined as

$$\widehat{C}[f_k] \equiv \sum_{A\to B}\left[\left(\pm\frac{1}{2}\right)\mathcal{S}_A\mathcal{S}_B\int\prod_{\substack{i\in A\\ j\in B}}\left(d\Pi_{i\neq k}d\Pi_{j\neq k}|\overline{\mathcal{M}}|^2_{A\leftrightarrow B}\Phi_{i;j}\right)(2\pi)^4\delta^4\left(\textstyle\sum_i P_i - \sum_j P_j\right)\right]. \tag{2.5}$$

In the equation above, we sum over all the collision processes $A \to B$ involving the k particles. The overall plus (minus) sign holds for the collision operator acting on particles $k \in B$ ($k \in A$), since it will contribute to the production (annihilation) of particles k. We have included the factor $1/2$ for later convenience. The symmetrization factor $\mathcal{S}_{A(B)} = 1/n_{A(B)}!$ accounts for n_A (n_B) identical particles in the initial (final) state. $d\Pi_{i,j} = \gamma_{i,j}\frac{d\vec{p}_{i,j}}{(2\pi)^3 2E_{i,j}}$ are the phase space differential elements. We have assumed that the amplitude for a process $A \to B$ is equal to the amplitude for the process $B \to A$, as it will be the case throughout this thesis. The squared amplitude is averaged over initial and final spins, $|\overline{\mathcal{M}}|^2 \equiv \prod_{i,j}\frac{1}{\gamma_i\gamma_j}|\mathcal{M}|^2$, since in the cosmological context we do not know the spins of initial and final states. The 4-dimensional delta function ensures conservation of energy and momentum in any collision process.

*For the general case of a perturbed, non-homogeneous, version of the Boltzmann equation, see for instance Ref. [58].

†Remember that a quantum phase-space has a minimum momentum interval, $\Delta\vec{p} = h^3/V = (2\pi)^3\hbar/a^3$. Throughout this thesis, we work with natural units, so that $\hbar = c = 1$.

Finally, we have defined the phase-space factor $\Phi_{i;j}$ as

$$\Phi_{i;j} \equiv f_i(1+\zeta_j f_j) - f_j(1+\zeta_i f_i)\,. \tag{2.6}$$

In the classical limit $\zeta_{i,j}=0$, otherwise we have to distinguish between fermions ($\zeta_{i,j}=-1$) and bosons ($\zeta_{i,j}=+1$), in which case we have the quantum effects of Pauli blocking (due to the exclusion principle) and Bose enhancement (stimulated emission), respectively. Those effects should be taken into account if the medium populated by i,j species is dense enough. In this case, we have the so-called Boltzmann-Uehling-Uhlenbeck (BUU) equations, instead of the Boltzmann equation (in which $1\pm f=1$).

Equilibrium distributions are solutions of the Boltzmann or BUU equations leading to a vanishing collision term, and consequently, a constant total number of particles (for a detailed discussion, see for instance [60]). They take the form

$$f_i^{eq} = \frac{1}{e^{(E_i-\mu_i)/T}-\zeta_i} = \frac{\eta_i}{e^{E_i/T}-\zeta_i\eta_i}\,, \tag{2.7}$$

where we parametrize the dependence on the chemical potential μ_i through $\eta_i \equiv e^{\mu_i/T}$, with T the temperature achieved by the i particles. The Bose enhancement and the Pauli blocking for a species in equilibrium are given by

$$1+\zeta_i f_i^{eq} = \frac{e^{E_i/T}}{e^{E_i/T}-\zeta_i\eta_i}\,. \tag{2.8}$$

When the collision term of number conserving processes (e.g. $ij\to ij$) vanishes, we have the *kinetic equilibrium*. When the collision term of number violating processes (e.g. $ii\to jj$) vanishes, we have the *chemical equilibrium*, in which case, besides energy conservation which always holds ($\sum_i E_i = \sum_j E_j$), we have chemical potential conservation ($\sum_i \mu_i = \sum_j \mu_j$). The *thermal equilibrium* state is therefore characterized by the detailed balance equation (conservation of energy and chemical potential for equilibrium distributions):

$$\prod_{i,j} f_i^{eq}(1+\zeta_j f_j^{eq}) = \frac{\exp(\sum_i \mu_i/T)}{\prod_i(e^{E_i/T}-\zeta_i\eta_i)}\frac{\exp(\sum_j E_j/T)}{\prod_j(e^{E_j/T}-\zeta_j\eta_j)} = \prod_{i,j} f_j^{eq}(1+\zeta_i f_i^{eq})\,. \tag{2.9}$$

In Fig. 2.1 we plot the equilibrium distribution for a species i having Maxwell-Boltzmann (black), Bose-Einstein (blue) and Fermi-Dirac (red) statistics. We clearly see that particles in a thermal bath behave classically when their energies are much above the bath temperature.

The reader might find it useful to have the following convergent series:

$$f_i^{eq} = \sum_{\alpha=1}^{\infty} \zeta_i^{\alpha+1}\eta^\alpha e^{-\alpha E_i/T} \quad \text{and} \quad 1+\zeta_i f_i^{eq} = \sum_{\alpha=0}^{\infty}(\zeta_i\eta_i)^\alpha e^{-\alpha E_i/T}\,, \tag{2.10}$$

whose first term correspond to the Maxwell-Boltzmann statistics.

The six-dimensional phase-space integration in the Boltzmann equation is in general very difficult to treat. We can simplify our problem by taking the *moments of the distribution*

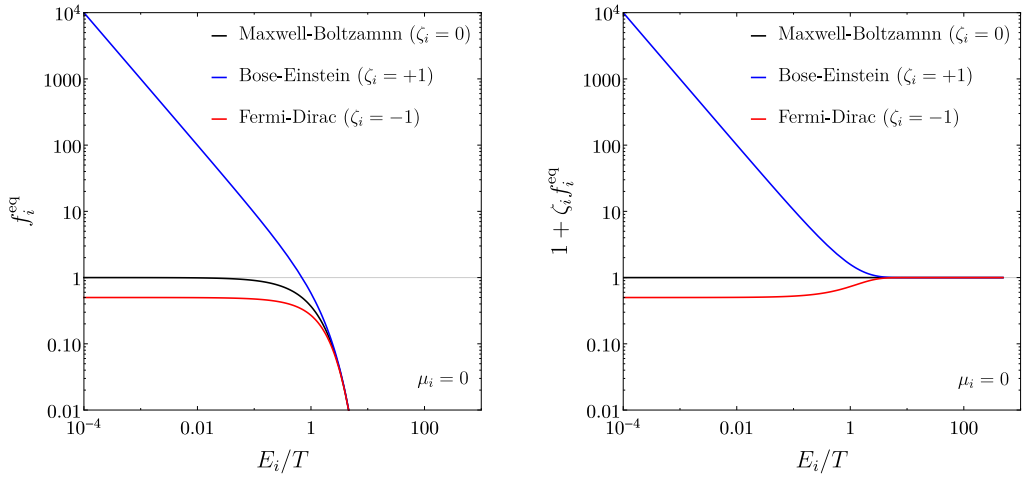

FIGURE 2.1 – *Equilibrium phase space distributions for a vanishing chemical potential. Notice that quantum effects might be important in the ultra-relativistic regime.*

functions, which does not need to be the equilibrium ones. Even though we lose information about the system in this procedure, it usually suffices to take only the first moments in order to describe the behavior of the species. The evolution equations for the moments of the distribution functions are the *fluid equations*.

From now on, we concentrate on macroscopic (measurable) quantities found after integrating over the momenta of the particles of a given species. The n-th moment of a distribution function for a species k is defined as

$$M_n(f_k) \equiv \frac{\gamma_k}{(2\pi)^3} \int d\vec{p}_k (\vec{p}_k)^n f_k(\vec{p}_k) \,. \tag{2.11}$$

The zero-th moment of f_k is the number density of species k, see Eq. (2.4):

$$n_k = \frac{\gamma_k}{(2\pi)^3} \int d\vec{p}_k f_k(\vec{p}_k) \,, \tag{2.12}$$

which is used to define the averaged value of a given quantity $\mathscr{O}$ over momenta:

$$\langle \mathscr{O}(\vec{p}_k) \rangle = \frac{1}{n_k} \frac{\gamma_k}{(2\pi)^3} \int d\vec{p}_k \mathscr{O}(\vec{p}_k) f_k(\vec{p}_k) \,. \tag{2.13}$$

Notice that the total number of particles is normalized to unity, with $\langle N_k \rangle = 1$.

The energy density of species k is the first moment of f_k:

$$\rho_k = n_k \langle E_k \rangle = \frac{\gamma_k}{(2\pi)^3} \int d\vec{p}_k E_k f_k(\vec{p}_k) \,, \tag{2.14}$$

while the pressure is related to the second moment by

$$\mathcal{P}_k = \frac{\gamma_k}{(2\pi)^3}\int d\vec{p}_k \frac{p_k^2}{3E_k} f_k(\vec{p}_k)\,. \tag{2.15}$$

It might be useful to define a "kinetic temperature" related to the zero-th and second moments of a generic distribution function as [61, 62],

$$T_k \equiv \frac{2}{3}\left\langle \frac{p_k^2}{2E_k}\right\rangle = \frac{1}{n_k}\frac{\gamma_k}{(2\pi)^3}\int d\vec{p}_k \frac{p_k^2}{3E_k} f_k(\vec{p}_k) = \frac{\mathcal{P}_k}{n_k}\,, \tag{2.16}$$

since it reduces to the thermal temperature when applied to an equilibrium distribution.

The CMB spectrum, close to a black-body spectrum, implies that the standard model species were in a common thermal bath in the Early Universe, beyond the surface of last scattering*. That is what allows us to use equilibrium thermodynamics in the study of the Early Universe. We can find analytical expressions for the number and energy densities and the pressure of a species i in thermal equilibrium after integrating Eqs. (2.12), (2.14) and (2.15) in the two limiting cases of the relativistic dispersion relation, $E_i^2 = m_i^2 + p_i^2$.

In the ultra-relativistic regime, $p_i \sim T \gg m_i, \mu_i$, the species behaves as radiation and we have

$$n_i^R = \frac{\gamma_i}{2\pi^2}\int_0^\infty \frac{E_i^2}{e^{E_i/T}-\zeta_i} dE_i = \begin{cases} \frac{\zeta(3)}{\pi^2}\gamma_i T^3 & \text{(bosons)} \\ \frac{3}{4}\frac{\zeta(3)}{\pi^2}\gamma_i T^3 & \text{(fermions)} \end{cases} \tag{2.17}$$

$$\rho_i^R = \frac{\gamma_i}{2\pi^2}\int_0^\infty \frac{E_i^3}{e^{E_i/T}-\zeta_i} dE_i = \begin{cases} \frac{\pi^2}{30}\gamma_i T^4 & \text{(bosons)} \\ \frac{7}{8}\frac{\pi^2}{30}\gamma_i T^4 & \text{(fermions)} \end{cases} \tag{2.18}$$

$$\mathcal{P}_i^R = \frac{\gamma_i}{6\pi^2}\int_0^\infty \frac{E_i^3}{e^{E_i/T}-\zeta_i} dE_i = \frac{1}{3}\rho_i^R \quad \text{(bosons and fermions)} \tag{2.19}$$

In the non-relativistic limit, $p_i \sim T \ll m_i, \mu_i$, the species behaves as matter and we have

$$n_i^M = \gamma_i \eta_i \left(\frac{m_i T}{2\pi}\right)^{3/2} e^{-m_i/T} \tag{2.20}$$

$$\rho_i^M = m_i n_i^M \tag{2.21}$$

$$\mathcal{P}_i^M = n_i^M T \ll \rho_i^M\,. \tag{2.22}$$

Since ρ_i^M and $\mathcal{P}_i^M$ are exponentially smaller than ρ_i^R and $\mathcal{P}_i^R$, the total energy density of the universe is dominated by the ultra-relativistic species. Throughout the expansion, as the universe cools down, when a species becomes non-relativistic it starts becoming too

*Hereafter, the temperature of the standard model thermal bath is referred to as simply T.

heavy as to be produced from the particles of the bath. After that moment, it cannot contribute anymore to the total energy density of the universe. This is the so-called *annihilation era* of that species. If the species is unstable, it decays into other species and do not contribute to the cosmic energy. If the species is stable, though, it might become a *cosmic relic*, possibly contributing to the total energy density. The total energy density is therefore given by

$$\rho = \rho_{relic} + \frac{\pi^2}{30} g_e T^4 \,, \tag{2.23}$$

where we have defined the energetic ultra-relativistic degrees of freedom

$$g_e \equiv \sum_{i=\text{bosons}} \gamma_i \left(\frac{T_i}{T}\right)^4 + \frac{7}{8} \sum_{i=\text{fermions}} \gamma_i \left(\frac{T_i}{T}\right)^4 \,. \tag{2.24}$$

Applying the Laws of Thermodynamics for a comoving volume, we find that any variation in the energy and pressure leads to a variation in entropy:

$$dS = d\left[\frac{(\rho + \mathcal{P})a^3}{T}\right] \equiv d[sa^3] \,. \tag{2.25}$$

The entropy density in a comoving volume s, defined above, is therefore given by

$$s = \frac{2\pi^2}{45} g_s T^3 \,, \tag{2.26}$$

where we have defined the entropic ultra-relativistic degrees of freedom

$$g_s \equiv \sum_{i=\text{bosons}} \gamma_i \left(\frac{T_i}{T}\right)^3 + \frac{7}{8} \sum_{i=\text{fermions}} \gamma_i \left(\frac{T_i}{T}\right)^3 \,. \tag{2.27}$$

In the absence of heat flows in a comoving volume, the total entropy is constant ($dS = 0$) and the temperature decreases with the inverse of the scale factor, $T \propto g_s^{-1/3} a^{-1}$. In general, in face of an entropy injection by a factor of $\Delta \equiv S_{\rm A}/S_{\rm B}$, the temperature, degrees of freedom, scale factor and entropy after (labeled by A) and before (labeled by B) any annihilation era are related by

$$\frac{T_{\rm A}}{T_{\rm B}} = \left(\Delta \frac{g_s^{\rm B}}{g_s^{\rm A}}\right)^{1/3} \frac{a_{\rm B}}{a_{\rm A}} \,. \tag{2.28}$$

We provide an estimate of the factor Δ in Sec. 2.3.1.

Going back to the general case in which *thermal equilibrium might not be reached*, we will hereafter work with the fluid equations for the number density (zeroth moment of the Boltzmann equation or continuity equation),

$$\dot{n}_k + 3Hn_k = R_k(t), \tag{2.29}$$

and for the energy density (first moment of the Boltzmann equation, conservation of energy),

$$\dot{\rho}_k + 3H(\rho_k + \mathcal{P}_k) = \mathscr{R}_k(t)\,. \tag{2.30}$$

We have defined the so-called *collision terms* for species k: the interaction rate $R_k(t)$, which is the number of interactions felt by species k per unit of time and volume,

$$R_k(t) \equiv \frac{\gamma_k}{(2\pi)^3}\int d\vec{p}_k \frac{\widehat{C}[f_k]}{E_k}\,, \tag{2.31}$$

and the interaction rate for a given energy, $\mathscr{R}_k$,

$$\mathscr{R}_k(t) \equiv \frac{\gamma_k}{(2\pi)^3}\int d\vec{p}_k \widehat{C}[f_k]\,. \tag{2.32}$$

We emphasize that those fluid equations hold even for out-of-equilibrium distribution functions, while the collision terms vanish when applied to equilibrium distributions.

2.1.1 Special cases of collision terms

The collision operators are the key quantities that allow us to track the evolution of particles in the phase-space,

$$\frac{\partial f_k}{\partial t} - Hp_k\frac{\partial f_k}{\partial p_k} = \frac{\widehat{C}[f_k]}{E_k}\,,$$

and to determine the interaction rates, or collision terms,

$$R_k = \frac{\gamma_k}{(2\pi)^3}\int d\vec{p}_k \frac{\widehat{C}[f_k]}{E_k}\,, \qquad \mathscr{R}_k = \frac{\gamma_k}{(2\pi)^3}\int d\vec{p}_k \widehat{C}[f_k]\,.$$

Here we will develop the collision terms for specific processes which will be useful for us, involving species labeled $1, 2, 3$ and 4: decays ($1 \to 34$), coalescences ($34 \to 1$) and scatterings ($12 \leftrightarrow 34$).

$\underline{1 \leftrightarrow 2 \text{ processes}}$

Let us start by considering the evolution of species 1 in a process $1 \leftrightarrow 34$. The collision term reads

$$\widehat{C}_{1\leftrightarrow 34}[f_1] = -\frac{S_{34}}{2}\int d\Pi_3 \int d\Pi_4 (2\pi)^4\delta^4(P_1 - P_3 - P_4)\frac{|\mathcal{M}|^2}{\gamma_1\gamma_2\gamma_3}\Phi_{1;34}\,, \tag{2.33}$$

with the phase-space factor given by

$$\Phi_{1;34} = f_1(1+\zeta_3 f_3)(1+\zeta_4 f_4) - f_3 f_4(1+\zeta_1 f_1)\,. \tag{2.34}$$

If the densities of species 1, 3 and 4 are not high enough, we can neglect the quantum-statistical factors $(1 + \zeta_{1,3,4} f_{1,3,4})$. In this case, we are in the classical regime of the phase-space:

$$\Phi_{1;34} \approx f_1 - f_3 f_4 \,. \tag{2.35}$$

The first term of Eq.(2.33) is straightforward since we do not have to integrate over f_1:

$$\widehat{C}_{1\to 34}[f_1] \supset -f_1 E_1 \Gamma_{1\to 34} \,, \qquad R_k(t) \supset -n_1 \Gamma_{1\to 34} \,, \qquad \text{and} \qquad \mathscr{R}_k(t) \supset -\rho_1 \Gamma_{1\to 34} \,,$$

where we have used the Fermi's Golden Rule for the transition from an initial state of m particles to a final state of n particles,

$$\Gamma_{m\to n} = \prod_{i=1}^{m} \frac{S_m S_n}{2E_i} \int \prod_{j=1}^{n} \frac{d\Pi_j}{\gamma_j} (2\pi)^4 \delta^4\Big(\textstyle\sum_i P_i - \sum_j P_j\Big) \frac{|\mathcal{M}|^2}{\gamma_i} \,. \tag{2.36}$$

If species 3 and 4 are in thermal equilibrium between each other, we can use the balance equation, Eq. (2.9), in the classical regime and the phase-space factor is simply

$$\Phi_{1;34} \approx f_1 - f_1^{eq} \,. \tag{2.37}$$

Notice that we are *not* assuming that species 1 is thermalized with species 3 and 4.

Therefore, in the classical regime, for species 1 decaying into and being produced by particles 3 and 4 which are thermalized between themselves, we have

$$\begin{aligned} \widehat{C}_{1\leftrightarrow 34}[f_1] &= -E_1 \Gamma_{1\to 34} (f_1 - f_1^{eq}) \\ R_1(t) &= -\Gamma_{1\to 34} (n_1(t) - n_1^{eq}(t)) \\ \mathscr{R}_1(t) &= -\Gamma_{1\to 34} (\rho_1(t) - \rho_1^{eq}(t)) \,. \end{aligned} \tag{2.38}$$

If the species 3 and 4 are *not* in thermal equilibrium, the interaction rate reads

$$\begin{aligned} R_1 &= -S_{34} \int \frac{d\Pi_1}{\gamma_1} \int \frac{d\Pi_3}{\gamma_3} \int \frac{d\Pi_4}{\gamma_4} (2\pi)^4 \delta^4(P_1 - P_3 - P_4) |\mathcal{M}|^2 (f_1 - f_3 f_4) \\ &\equiv -R_{1\to 34} + R_{34\to 1} \\ &\equiv -n_1 \Gamma_{1\to 34} + n_3 n_4 \langle \Gamma_{34\to 1} \rangle \,, \end{aligned} \tag{2.39}$$

where we have found convenient to define a *distribution averaged inverse decay rate* $\langle \Gamma_{34\to 1} \rangle$. Exploring the Lorentz-invariance of the phase-space integrand, we compute $R_{34\to 1}$ in the center-of-momentum frame, in this case the rest frame of species 1, and find

$$\langle \Gamma_{34\to 1} \rangle \equiv \frac{1}{n_3 n_4} \frac{\pi S_{34}}{m_1} \int \frac{d\Pi_3}{\gamma_3} \int \frac{d\Pi_4}{\gamma_4} f_3 f_4 \; \delta(m_1 - (E_3^* + E_4^*)) |\mathcal{M}|^2 \,. \tag{2.40}$$

Hereafter we label with an asterisk the quantities computed in a center-of-momentum frame. The integration over the phase-space of species 3 and 4 contains integration over the angle between their momenta, θ_{34}. We perform the change of variable from $\cos\theta_{34}$ to the Mandelstam variable $s = (P_1)^2 = (E_1^*)^2 = (P_3 + P_4)^2 = (E_3^* + E_4^*)^2$, which is

convenient for analytical and numerical purposes. The region of integration over the energies of species 4 depends on the masses of species 3 and 4 and is found after applying the constraint $|\cos\theta_{34}| \leq 1$:

- if $m_3 > 0$, $E_4^{\pm} = \frac{1}{2m_3^2}[E_3(s - m_3^2 - m_4^2) \pm p_3\sqrt{\lambda(s, m_3^2, m_4^2)}]$;
- if $m_3 = 0$, $E_4^- = \frac{\lambda(s,0,m_4^2)+4m_4^2p_3}{4p_3(s-m_4^2)}$, $E_4^+ = \infty$;
- if $m_3 = m_4 = 0$, $E_4^- = \frac{s}{4p_3}$, $E_4^+ = \infty$.

In this thesis we are interested in the production of dark matter from massless particles, something that is not commonly explored in the literature. We refer the reader to Refs. [63, 64] in this regard.

It is useful to have at hand the general result

$$\int \frac{d\Pi_i}{\gamma_i} \int \frac{d\Pi_j}{\gamma_j} = \frac{1}{4(2\pi)^4} \int ds \int_{m_i}^{\infty} dE_i \int_{E_j^-}^{E_j^+} dE_j \,. \tag{2.41}$$

If both species 3 and 4 are massive, it is convenient to work with the variables s, $E_+ = E_i + E_j$ and $E_- = E_i - E_j$ instead of with $\cos\theta_{34}$, E_3 and E_4:

$$\int \frac{d\Pi_i}{\gamma_i} \int \frac{d\Pi_j}{\gamma_j} = \frac{1}{8(2\pi)^4} \int ds \int_{\sqrt{s}}^{\infty} dE_+ \int_{\epsilon^-}^{\epsilon^+} dE_-, \tag{2.42}$$

where $\epsilon^{\pm} = |m_i^2 - m_j^2|\frac{E_+}{s} \pm 2p_{ij}\sqrt{E_+^2/s - 1}$, with $p_{ij} \equiv \sqrt{\lambda(s, m_i^2, m_j^2)}/(2\sqrt{s})$ and $\lambda(x, y, z) = (x - (\sqrt{y} + \sqrt{z})^2)(x - (\sqrt{y} - \sqrt{z})^2)$ the Källen function.

The distribution averaged inverse decay rate is therefore

$$\langle\Gamma_{34\to1}\rangle = \frac{1}{n_3 n_4} \frac{S_{34}}{4(2\pi)^3} |\mathcal{M}|^2 \int_{m_3}^{\infty} dE_3 f_3 \int_{E_4^-}^{E_4^+} dE_4 f_4 \,. \tag{2.43}$$

Although we are not going to consider quantum phase-space in this thesis, it is instructive to compute the collision term for the in-medium decay of a species 1 into thermalized species 3 and 4 (See also [65]). On one hand, it could give us intuition if we want to extrapolate classical results. On the other hand, it involves techniques which we also use in the case of the collision term of scatterings.

The quantum phase-space factor for thermalized 3 and 4 species reads

$$\begin{aligned} \Phi_{1;34} &= f_1(1 + \zeta_3 f_3^{eq})(1 + \zeta_4 f_4^{eq}) - f_3^{eq} f_4^{eq}(1 + \zeta_1 f_1) \\ &= (1 + \zeta_3 f_3^{eq})(1 + \zeta_4 f_4^{eq})[f_1 - (1 + \zeta_1 f_1)\eta_1 e^{-E_1/T}] \,, \end{aligned} \tag{2.44}$$

with the last equality coming from the detailed balance equation. In a general way, the balance equation allows us to factorize the phase-space factor into a part depending on initial distributions and another one depending on final distributions.

The difficulty arising from a quantum phase-space factor comes from the need to integrate over the distributions of species 3 and 4:

$$\widehat{C}_{1\leftrightarrow 34}[f_1] = -\frac{S_{34}}{2\gamma_1}[f_1 - (1+\zeta_1 f_1)\eta_1 e^{-E_1/T}] \times I_{34}\,, \tag{2.45}$$

with the integral over the quantum phase-space of species 3 and 4 given by

$$I_{34} = \frac{1}{4(2\pi)^2}\int \frac{d\vec{p}_3}{E_3}(1+\zeta_3 f_3^{eq}) \int \frac{d\vec{p}_4}{E_4}(1+\zeta_4 f_4^{eq})\delta^4(P_1 - P_3 - P_4)|\mathcal{M}|^2\,. \tag{2.46}$$

Since I_{34} is Lorentz-invariant, we can work in the center-of-momentum (rest frame of species 1), labeled with an asterisk:

$$\begin{aligned} I_{34} &= \frac{1}{4(2\pi)^2}\int \frac{d\vec{p}_3^{\,*}}{E_3^* E_4^*}(1+\zeta_3 f_3^{eq})(1+\zeta_4 f_4^{eq})\delta(m_1 - E_3^* - E_4^*)|\mathcal{M}|^2 \\ &= \frac{1}{8\pi}E_1\Gamma_{1\to 34}\int_{-1}^{+1} d\cos\theta_{13}^* \frac{p_*}{m_1}|\mathcal{M}|^2(1+\zeta_3 f_3^{eq})(1+\zeta_4 f_4^{eq})\,, \end{aligned} \tag{2.47}$$

where $p_* \equiv \sqrt{\lambda(m_1^2, m_3^2, m_4^2)}/(2m_1)$.

Now that we have $f_i^{eq} = f_i^{eq}(\cos\theta_{13}^*)$, we need to use a Lorentz boost from the reference frame of the distribution functions (E_3, E_4) to the rest frame of species 1 (E_3^*, E_4^*) with velocity $\vec{\beta} = \vec{p}_1/(m_1\gamma)$ [60]:

$$E_3(\cos\theta_{13}^*) = \frac{E_3^* E_1}{m_1} - \frac{p_* p_1}{m_1}\cos\theta_{13}^*\,; \qquad E_4(\cos\theta_{13}^*) = \frac{E_4^* E_1}{m_1} + \frac{p_* p_1}{m_1}\cos\theta_{13}^*\,. \tag{2.48}$$

For isotropic decays, we need to solve simply

$$I_{34} = \frac{1}{S_B}E_1\Gamma_{1\to 34}\int_{-1}^{+1} d\cos\theta_{13}^* \frac{e^{(E_3+E_4)/T}}{(e^{E_3/T}-\zeta_3\eta_3)(e^{E_4/T}-\zeta_3\eta_4)}\,. \tag{2.49}$$

The collision term is finally

$$\widehat{C}_{1\leftrightarrow 34}[f_1] = -E_1\Gamma_{1\to 34}\mathcal{Q}(p_1, p_*, \zeta_3, \zeta_4, \eta_3, \eta_4)\left[f_1 - (1+\zeta_1 f_1)\eta_1 e^{-E_1/T}\right]\,, \tag{2.50}$$

with a quantum statistical function defined as

$$\mathcal{Q} \equiv \frac{1}{(1-\zeta_3\zeta_4\eta_3\eta_4 e^{-E_1/T})}\left[1 + \frac{m_1 T}{2p_1 p_*}\ln\left(\frac{(1-\zeta_3\eta_3 e^{-E_3(-1)/T})}{(1-\zeta_3\eta_3 e^{-E_3(+1)/T})}\frac{(1-\zeta_4\eta_4 e^{-E_4(+1)/T})}{(1-\zeta_4\eta_4 e^{-E_4(-1)/T})}\right)\right]\,. \tag{2.51}$$

As expected, in the classical (Maxwell-Boltzmann) limit, $\mathcal{Q}(p_1, p_*, 0, 0, \eta_3, \eta_4) = 1$ and we recover the result of Eq.(2.38).

$2 \leftrightarrow 2$ processes

Let us now consider the evolution of species 3 in a process $12 \leftrightarrow 34$ where species 1 and 2 are thermalized between themselves ($f_1 f_2 = f_1^{eq} f_2^{eq}$). For the purposes of this thesis, we restrict ourselves to the classical phase-space. The collision operator for such a process reads

$$\begin{aligned}\widehat{C}_{12\leftrightarrow 34}[f_3] &= \frac{S_{12}S_{34}}{2\gamma_3}\int\frac{d\Pi_4}{\gamma_4}\int\frac{d\Pi_1}{\gamma_1}\int\frac{d\Pi_2}{\gamma_2}(2\pi)^4\delta^4(P_1+P_2-P_3-P_4)|\mathcal{M}|^2\Phi_{12;34}\\ &\equiv \frac{S_{12}S_{34}}{2\gamma_3}\int\frac{d\Pi_4}{\gamma_4}\times I_{12}^{\Phi}\,,\end{aligned} \tag{2.52}$$

with the phase-space factor given by

$$\begin{aligned}\Phi_{12;34} &= f_1 f_2(1+\zeta_3 f_3)(1+\zeta_4 f_4) - f_3 f_4(1+\zeta_1 f_1)(1+\zeta_2 f_2)\\ &= (1+\zeta_1 f_1^{eq})(1+\zeta_2 f_2^{eq})[\eta_3\eta_4 e^{-E_3/T}e^{-E_4/T}(1+\zeta_3 f_3)(1+\zeta_4 f_4) - f_3 f_4]\,.\end{aligned} \tag{2.53}$$

Neglecting the quantum-statistical factors and then using the balance equation, the phase-space factor reads

$$\Phi_{12;34} \approx f_1^{eq} f_2^{eq} - f_3 f_4 = f_3^{eq} f_4^{eq} - f_3 f_4\,. \tag{2.54}$$

Since the integral over the classical phase-space, I_{12}^{Φ}, is Lorentz-invariant, we can compute it in the center-of-momentum frame:

$$I_{12}^{\Phi} = \frac{1}{4(2\pi)^2}\int d\Omega_{13}^{*}\frac{p_{12}}{\sqrt{s}}|\mathcal{M}|^2(f_3^{eq}f_4^{eq} - f_3 f_4)\,, \tag{2.55}$$

where Ω_{13} is the solid angle between the initial and final momenta.

The classical collision operator for the scattering is therefore given by

$$\widehat{C}_{12\leftrightarrow 34}[f_3] = \frac{S_{12}S_{34}}{\gamma_3 p_3}\frac{1}{32(2\pi)^4}\int ds\frac{p_{12}}{\sqrt{s}}\int d\Omega_{13}^{*}|\mathcal{M}|^2\int_{E_4^-}^{E_4^+} dE_4(f_3^{eq}f_4^{eq} - f_3 f_4)\,. \tag{2.56}$$

As it is usual, interaction rates are written in terms of the *distribution averaged cross-sections*, $\langle\sigma v\rangle$. In our case, the interaction rate of species 3 reads

$$\begin{aligned}R_3 &= S_{12}S_{34}\int\frac{d\Pi_1}{\gamma_1}\int\frac{d\Pi_2}{\gamma_2}f_1 f_2 I_{34} - S_{12}S_{34}\int\frac{d\Pi_3}{\gamma_3}\int\frac{d\Pi_4}{\gamma_4}f_3 f_4 I_{12}\\ &\equiv R_{12\to 34} - R_{34\to 12}\\ &\equiv n_1 n_2\langle\sigma v\rangle_{12\to 34} - n_3 n_4\langle\sigma v\rangle_{34\to 12}\,.\end{aligned} \tag{2.57}$$

In order to understand it, notice that the integration over the phase-space of final state species in the center-of-momentum frame reads

$$\begin{aligned} S_{kl} I_{kl} &= (4 p_{ij} \sqrt{s}) \left(\frac{S_{kl}}{64 \pi^2 s} \frac{p_{kl}}{p_{ij}} \int d\Omega_{13}^{*} |\mathcal{M}|^2 \right) \\ &= \phi_{ij} \sigma_{ij \to kl} \, . \end{aligned} \tag{2.58}$$

The quantity ϕ_{ij} is the manifestly Lorentz-invariant incident flux defined in terms of the 4-currents $J_{i_\mu} = (2E_i, 2E_i \vec{\beta}_i)$ [63]:

$$\phi_{ij} \equiv (J_i \cdot J_j) v_{ij} = 4 (P_i \cdot P_j) v_{ij} = 4 p_{ij} \sqrt{s} \, , \tag{2.59}$$

with the Lorentz-invariant relative velocity given by

$$v_{ij} = \frac{\sqrt{(P_i \cdot P_j)^2 - m_i^2 m_j^2}}{(P_i \cdot P_j)} \, . \tag{2.60}$$

The distribution average is therefore defined from the interaction rate as

$$R_{ij \to kl} = n_i n_j \langle \sigma v \rangle_{ij \to kl} = \frac{S_{ij}}{(2\pi)^4} \int ds (P_i \cdot P_j) \sigma_{ij \to kl} v_{ij} \int_{m_k}^{\infty} dE_i f_i \int_{E_j^-}^{E_j^+} dE_j f_j \, . \tag{2.61}$$

If species 1 and 2 are in thermal equilibrium between themselves and if their interactions with species 3 and 4 are such that $\mathcal{M}_{12 \to 34} = \mathcal{M}_{34 \to 12}$, we can use the balance equation and write the interaction rate as

$$\begin{aligned} R_3 &= S_{12} S_{34} \int \frac{d\Pi_3}{\gamma_3} \int \frac{d\Pi_4}{\gamma_4} f_3^{eq} f_4^{eq} I_{12} - S_{12} S_{34} \int \frac{d\Pi_3}{\gamma_3} \int \frac{d\Pi_4}{\gamma_4} f_3 f_4 I_{12} \\ &\equiv n_3^{eq} n_4^{eq} \langle \sigma v \rangle_{34 \to 12} - n_3 n_4 \langle \sigma v \rangle_{34 \to 12} \, . \end{aligned} \tag{2.62}$$

Hence we can define the *thermally averaged annihilation cross section* $\langle \sigma v \rangle \equiv \langle \sigma v \rangle_{34 \to 12}$:

$$\langle \sigma v \rangle = \frac{1}{n_3^{eq} n_4^{eq}} \frac{S_{34}}{(2\pi)^4} \int ds (P_3 \cdot P_4) \sigma_{34 \to 12} v_{34} \int_{m_3}^{\infty} dE_3 f_3^{eq} \int_{E_4^-}^{E_4^+} dE_4 f_4^{eq} \, . \tag{2.63}$$

Hereafter, whenever we use $\langle \sigma v \rangle$ we mean average over equilibrium distributions of the species under study. If we specify the sense of the process, $\langle \sigma v \rangle_{ij \to kl}$, we will not be assuming that the average is thermal.

Finally, the collision terms read

$$R_3 = \langle \sigma v \rangle \left(n_3^{eq} n_4^{eq} - n_3 n_4 \right) \tag{2.64}$$

and

$$\mathscr{R}_3 = \langle \sigma v E_3 \rangle \left(n_3^{eq} n_4^{eq} - n_3 n_4 \right) \, . \tag{2.65}$$

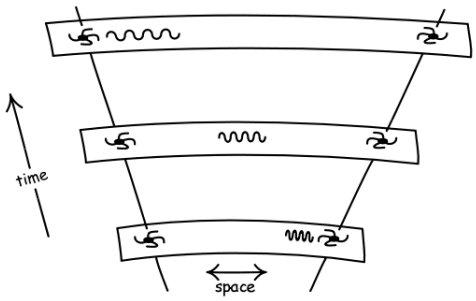

FIGURE 2.2 – *Redshift due to spacial expansion of the universe. Source:* http://www.pitt.edu/~jdnorton/teaching/HPS_0410/chapters/big_bang_FRW_spacetimes/index.html, *accessed on May 10, 2019.*

2.2 Evolution of matter and radiation in an expanding universe

The cosmic expansion, one of the pillars of the ΛCDM model, is inferred by the observed *redshift* in the spectra of distant luminous sources. By definition, the shift in wavelength is given by $z = \frac{\lambda_p - \lambda_e}{\lambda_e}$, where λ_p (λ_e) is the perceived (emitted) wavelength. By analyzing the spectra of the luminous sources, we recognize their chemical composition. If one observes that all the spectral lines are shifted to longer (shorter) wavelengths, we have a redshift (blueshift).

In 1929, Hubble observed a systematic redshift of distant galaxies, distinct to the peculiar redshift due to their movement, and inferred a linear relation between radial distance ($\vec{d}$) and velocity ($\vec{v}$), the Hubble's law [66]:

$$\vec{v} = H_0 \vec{d}\,, \tag{2.66}$$

where the proportionality constant H_0 is the so-called Hubble's constant*.

Nowadays, the standard interpretation of this observational fact, based on General Relativity, is that the space itself is expanding at large scales†, stretching the wavelengths of light. In Fig. 2.2 we see an illustration of the cosmic expansion.

The understanding that the whole universe expands linear and homogeneously (Hubble's law) makes it convenient for us to define a frame system x which is *comoving to the expansion*, with the time-dependence of the physical distance $d(t)$ parametrized by a scale factor $a(t)$: $d(t) = a(t)x$. The physical velocity is therefore

$$v(t) \equiv \dot{d}(t) = a(t)\dot{x} + \dot{a}(t)x = v_{\rm pec} + \frac{\dot{a}(t)}{a(t)} d(t)\,, \tag{2.67}$$

*As always, sub or superscripts "0" indicate the value of a cosmological quantity as measured today.

†The scale of expansion is the scale of clusters of galaxies, hundreds of Mpc, with $1\text{pc} \simeq 30.86 \times 10^{12}\,\text{km} \simeq 3.26\,\text{ly}$.

where the peculiar velocity $v_{\rm pec}$ is measured by a comoving observer. Hence, we see that the Hubble's constant is actually a time-dependent quantity, $H(t) \equiv \dot{a}/a$. Its value today is inferred by the Planck mission to be [36]

$$H_0 = 100\,h\,\mathrm{kms}^{-1}\mathrm{Mpc}^{-1} = 67.4 \pm 0.5 \mathrm{kms}^{-1}\mathrm{Mpc}^{-1}\,, \tag{2.68}$$

where h is a dimensionless parameter which quantifies the experimental uncertainty of this value.

2.2.1 Friedmann equations

In what follows, we briefly provide the key arguments leading to the equations governing the evolution of matter and radiation species in an expanding universe.

In the context of General Relativity (GR), the energetic content of the universe curves the space around it, and if it is homogeneous and isotropically distributed we can consider the space itself as homogeneous and isotropic. Mathematically, the Einstein tensor characterizing the space-time, $G_{\mu\nu}$, must be proportional to the stress-energy tensor, $T_{\mu\nu}$.

The most general metric of a homogeneous and isotropic space is the Robertson-Walker (RW) metric, and the invariant distance squared ds^2 is given by

$$ds^2 = g_{\mu\nu}dx^\mu dx^\nu = dt^2 - a^2(t)\left(\frac{dr^2}{1-kr^2} + r^2(d\theta^2 + \sin^2\theta d\phi^2)\right)\,, \tag{2.69}$$

where t, r, θ and ϕ are comoving coordinates and $a(t)$ is the scale factor of the spatial homogeneous expansion. The curvature constant k is commonly normalized to $0, +1$ and -1 for a space of zero, positive and negative curvature, respectively said to have a flat, closed or open geometry. The metric tensor of such curved space-time is given by

$$g_{\mu\nu} = \mathrm{diag}\left(1, -\frac{a^2(t)}{1-kr^2}, -a^2(t)r^2, -a^2(t)r^2\sin^2\theta\right)\,. \tag{2.70}$$

The conservation of energy, in the context of GR, is ensured by the vanishing of the covariant derivative of the stress-energy tensor. For that reason, the Einstein tensor must also have a vanishing covariant derivative. Moreover, in the limit of weak gravitational field, GR must describe Newtonian dynamics. With the tensor describing the space curvature, the Riemann-Crhistoffel tensor $R^\delta_{\mu\gamma\nu} = \frac{\partial\Gamma^\delta_{\mu\nu}}{\partial x^\gamma} - \frac{\partial\Gamma^\delta_{\mu\gamma}}{\partial x^\nu} + \Gamma^\delta_{\sigma\gamma}\Gamma^\sigma_{\mu\nu} - \Gamma^\delta_{\sigma\nu}\Gamma^\sigma_{\mu\gamma}$, we can find the Ricci's tensor and scalar:

$$R_{\mu\nu} \equiv R^\gamma_{\mu\gamma\nu} = \frac{\partial\Gamma^\gamma_{\mu\nu}}{\partial x^\gamma} - \frac{\partial\Gamma^\gamma_{\mu\gamma}}{\partial x^\nu} + \Gamma^\gamma_{\sigma\gamma}\Gamma^\sigma_{\mu\nu} - \Gamma^\gamma_{\sigma\nu}\Gamma^\sigma_{\mu\gamma} \tag{2.71}$$

and

$$R = g^{\mu\nu}R_{\mu\nu}\,, \tag{2.72}$$

where $\Gamma^{\gamma}_{\mu\nu}$ is the affine connection responsible for the parallel transport of vectors in a curved space. It is given by

$$\Gamma^{\gamma}_{\mu\nu} = \frac{g^{\gamma\lambda}}{2}\left(\frac{\partial g_{\mu\lambda}}{\partial x^{\nu}} + \frac{\partial g_{\nu\lambda}}{\partial x^{\mu}} - \frac{\partial g_{\mu\nu}}{\partial x^{\lambda}}\right) . \tag{2.73}$$

With these quantities, we have the field equations of GR, or Einstein equation, describing the relation between matter/radiation and space-time*:

$$G_{\mu\nu} \equiv R_{\mu\nu} - \frac{1}{2}g_{\mu\nu}R = 8\pi G T_{\mu\nu} . \tag{2.74}$$

The simplest example of a homogeneous and isotropically distributed energetic content is that of a perfect fluid, completely characterized by time-dependent energy density and pressure with an stress-energy tensor in the comoving frame given simply by $T_{\mu\nu} = \mathrm{diag}(\rho, -\mathcal{P}, -\mathcal{P}, -\mathcal{P})$.

We can finally replace the RW metric tensor and the stress-energy tensor of a perfect fluid in the GR field equation. Since they are both diagonal tensors, we have just the time and spacial components of the Einstein equation:

$$\ddot{a} = -\frac{4\pi G}{3}(\rho + 3\mathcal{P})a \tag{2.75}$$

and

$$a\ddot{a} + 2\dot{a}^2 + 2k = 4\pi G(\rho - \mathcal{P})a^2 , \tag{2.76}$$

respectively.

Combining the two equations above we can find the so-called Friedmann equation, which tells us how the scale factor (or the cosmic expansion rate $H(t) = \dot{a}/a$) evolves depending on the matter and radiation content of a comoving volume:

$$\left(\frac{8\pi G}{3H(t)^2}\rho(t) - 1\right)\left(\frac{\dot{a}(t)}{a(t)}\right)^2 = \frac{k}{a^2(t)} . \tag{2.77}$$

It is manifest that if the total energy density of the universe is equal to some critical density $\rho_{cr} \equiv 3H^2/(8\pi G) \equiv 3H^2 M_P^2$, with $M_P \simeq 2.43 \times 10^{18}$GeV being the reduced Planck mass, the geometry of the universe is flat ($k = 0$). The value of the critical energy density today is

$$\rho_{cr}(t_0) = \frac{3H_0^2}{8\pi G} \simeq 1.88h^2 \times 10^{-26}\,\mathrm{kg\ m^{-3}} \simeq 8.03 \times 10^{-47}h^2\,\mathrm{GeV}^4 . \tag{2.78}$$

It is therefore convenient to express the *abundance*, or the *relic density*, Ω_i of a given species i relative to ρ_{cr}: $\Omega_i \equiv \rho_i/\rho_{cr}$. The curvature of the universe can be inferred by analyzing the spectrum of the CMB, since the image we see of the surface of last scattering

*A cosmological constant Λ might be added either as a geometrical or an energetic term $g_{\mu\nu}\Lambda$.

is sensitive to the geometry of the space. The geometry of the universe is inferred by the Planck mission to be nearly flat, constraining the total abundance of the cosmic material to be $0.9974 \lesssim \Omega \lesssim 1.0012$ [36]. In what follows, we will be always assuming $k = 0$. This constraint is crucial to the conclusion that the universe today contains roughly 4.9% of baryonic matter ($\Omega_b^0 h^2 = 0.0224 \pm 0.0001$), 26% of cold dark matter ($\Omega_c^0 h^2 = 0.120 \pm 0.001$) and 68% of dark energy ($\Omega_\Lambda^0 = 0.679 \pm 0.013$) [36].

Finally, considering an equation of state of the form $\mathcal{P}_i = w\rho_i$ for a species i ($w = 1/3$ for radiation and $w = 0$ for matter, see Eqs. 2.19 and 2.22), the following relation holds in the absence of collisions and heat flows:

$$\rho_i = \rho_{i_0} \left(\frac{a}{a_0} \right)^{-3(1+w)} . \tag{2.79}$$

For a radiation (matter) dominated universe, the Friedmann equation give us $a \propto t^{1/2}$ ($t^{2/3}$), and the energy density decreases by a^{-4} (a^{-3}).

2.3 Evolution of inflaton-radiation system

With results of the previous sections, we can now take a step forward in the computation of dark matter evolution. Whether dark matter (labeled X) behaves as matter or as radiation, the evolution of its number density is governed by

$$\dot{n}_X + 3H(t) n_X = R_X(t) . \tag{2.80}$$

The evolution of the Hubble rate over time depend on the species present in the universe (Eq. (2.77)). For a flat universe, $H(t) = \left(\frac{8\pi G}{3} \rho(t) \right)^{1/2}$. As we have discussed, in order to be consistent with structure formation requirements, the dark matter content should have been established at most during the radiation era. In the context of inflationary theories, it is possible that the dark matter relic was already established before the radiation era, while the inflaton oscillations was dominating the energy density of the universe.

If a radiation (labeled by γ) and an unstable matter (labeled by ϕ) content contribute to the total energy density, the Hubble rate is found after solving the following coupled differential equations:

$$\begin{aligned} \dot{\rho}_\phi + 3H\rho_\phi &= \mathscr{R}_\phi(t) \\ \dot{\rho}_\gamma + 4H\rho_\gamma &= \mathscr{R}_\gamma(t) . \end{aligned} \tag{2.81}$$

As derived previously, Eq.(2.38), $\mathscr{R}_\phi = -\rho_\phi \Gamma_\phi$ when the backreactions from the decay products can be neglected. On the other hand, as a consequence of the First and Second Laws of Thermodynamics applied to an expanding universe, we know that $\mathscr{R}_\phi = -\dot{S}T/a^3$, with $S = sa^3$ and s respectively the total entropy and the entropy density in a comoving volume and T the temperature of the thermal bath into which the heat is flowing. Therefore, by conservation of energy, when a species decays it will add heat into the bath

of decay products and the entropy per comoving volume increases. During the inflaton decay*, the expansion of the universe is therefore adiabatic and irreversible [67, 68].

Regarding radiation as part of the decay products that eventually thermalize among themselves with a given rate Γ_{th} [69], we have $\mathscr{R}_\gamma \supset B_\gamma \rho_\phi \Gamma_\phi + \Gamma_{th}(\rho_\gamma - \rho_\gamma^{eq})$, where B_γ is the branching ratio of inflaton decay into radiation†. In what follows, our analysis will be restricted to instantaneous thermalization of the decay products (see for instance [70] for a relaxation of this hypothesis). We denote by $\mathscr{R}_{\gamma\to X}$ the collision term accounting for the production of dark matter from radiation.

The set of differential equations that we need to solve in order to track the evolution of dark matter is therefore

$$\begin{cases} \dot{n}_X + 3H(t)n_X = R_X(t) \\ \dot{\rho}_\phi + 3H(t)\rho_\phi = -\rho_\phi \Gamma_\phi \\ \dot{\rho}_\gamma + 4H(t)\rho_\gamma = B_\gamma \rho_\phi \Gamma_\phi - \mathscr{R}_{\gamma\to X}(t) \end{cases} , \tag{2.82}$$

with the evolution of the Hubble rate (see Eq.(2.77)) and of the total entropy in a comoving volume given by

$$H(t) \cong \frac{1}{\sqrt{3}M_P}\sqrt{\rho_\gamma(t) + \rho_\phi(t)} \quad \text{and} \quad \dot{S} = \frac{\Gamma_\phi}{T}\rho_\phi a^3 \,. \tag{2.83}$$

We will work under the approximation that the production of dark matter takes place while its contribution to the total energy density of the universe is negligible. This might not be the case for late DM production, as considered in [42].

In order to absorb the expansion of the universe, we rewrite the fluid equations in terms of the *total number of particles* of the matter and radiation content, (N) and $(\mathscr{N})$ respectively:

$$N_X \equiv n_X a^3, \qquad N_\phi \equiv n_\phi a^3 = \frac{\rho_\phi}{m_\phi}a^3 \qquad \text{and} \qquad \mathscr{N}_\gamma \equiv \rho_\gamma a^4 \,. \tag{2.84}$$

In the absence of collisions, these quantities can only remain constant, since the matter content would only dilute and the radiation content dilute and redshift with the expansion of the universe, as derived from the Friedmann equation.

The set of differential equations becomes

$$\begin{cases} \dot{N}_X = R_X(t)a^3 \\ \dot{N}_\phi = -\Gamma_\phi N_\phi \\ \dot{\mathscr{N}}_\gamma = B_\gamma N_\phi \Gamma_\phi m_\phi a - \mathscr{R}_{\gamma\to X}(t)a^4 \end{cases} , \tag{2.85}$$

*We hereafter also refer to ϕ as *inflaton*, but having in mind that it can be any unstable field.

†We will keep B_γ throughout our analysis in order to easily account for the possibility of inflaton decaying into other species, as dark matter for instance.

and now we have

$$H(t) \cong \frac{a^{-2}}{\sqrt{3}M_P}\sqrt{N_\phi m_\phi a + \mathscr{N}_\gamma} \quad \text{and} \quad \dot{S} = \frac{m_\phi}{T}\Gamma_\phi N_\phi = \frac{m_\phi}{T}|\dot{N}_\phi| \,. \tag{2.86}$$

Since we have explicit dependence on the scale factor, it is convenient to use it as the independent variable. From the definition of the Hubble rate, $da = aHdt$, and defining the dimensionless independent variable as $x = am_\phi$, we have

$$\begin{cases} N_X' = \frac{R_X(x)}{m_\phi^3 H(x)}x^2 \\ N_\phi' = -N_\phi \frac{\Gamma_\phi}{H(x)}x^{-1} \\ \mathscr{N}_\gamma' = B_\gamma N_\phi \frac{\Gamma_\phi}{H(x)} - \frac{\mathscr{R}_{\gamma\to X}(x)}{m_\phi^4 H(x)}x^3 \end{cases} , \tag{2.87}$$

where prime denotes derivation with respect to the variable x and

$$H(x) \cong \frac{m_\phi^2 x^{-2}}{\sqrt{3}M_P}\sqrt{xN_\phi + \mathscr{N}_\gamma} \quad \text{and} \quad S' = \frac{\Gamma_\phi}{H(x)}\frac{m_\phi}{T(x)}\frac{N_\phi}{x} \,. \tag{2.88}$$

As long as the radiation content thermalizes, we can define a temperature for the thermal bath from the definition of the energy density of radiation, $\rho_\gamma = \frac{\pi^2}{30}g_e T^4$:

$$T(x) = \left(\frac{\pi^2}{30}g_e(T)\right)^{-1/4}\frac{\mathscr{N}_\gamma^{1/4}(x)}{x}m_\phi \,. \tag{2.89}$$

Alternatively, and as it is more convenient for the study of the evolution of entropy, we can define temperature from the definition of the total entropy, $S = sa^3 = \frac{2\pi^2}{45}g_s T^3 a^3$:

$$T(x) = \left(\frac{2\pi^2}{45}g_s(T)\right)^{-1/3}\frac{S^{1/3}(x)}{x}m_\phi \,. \tag{2.90}$$

Making explicit the dependence on the evolving states, the coupled system of equations reads

$$\begin{cases} N_X' = \sqrt{3}\frac{M_P R_X(x)}{m_\phi^5}\frac{x^4}{\sqrt{xN_\phi+\mathscr{N}_\gamma}} \\ N_\phi' = -\sqrt{3}\frac{M_P\Gamma_\phi}{m_\phi^2}\frac{xN_\phi}{\sqrt{xN_\phi+\mathscr{N}_\gamma}} \\ \mathscr{N}_\gamma' = \sqrt{3}B_\gamma\frac{M_P\Gamma_\phi}{m_\phi^2}\frac{x^2N_\phi}{\sqrt{xN_\phi+\mathscr{N}_\gamma}} - \sqrt{3}\frac{M_P\mathscr{R}_{\gamma\to X}(x)}{m_\phi^6}\frac{x^5}{\sqrt{xN_\phi+\mathscr{N}_\gamma}} \,. \end{cases} \tag{2.91}$$

The entropy production is therefore governed by

$$S' = \left(\frac{2\pi^2}{45}g_s(x)\right)^{1/4}\frac{\sqrt{3}M_P\Gamma_\phi}{m_\phi^2}\frac{x^2N_\phi S^{-1/3}}{\sqrt{xN_\phi+\mathscr{N}_\gamma}} \,. \tag{2.92}$$

We will consider the evolution of entropy in Sec. 2.3.1. For the moment, however, it is important to have in mind that the non-triviality of the system of equations above mostly

relies on the fact that entropy is being produced. If the number of unstable particles (N_ϕ) were negligible, radiation would behave trivially and the dark matter evolution would be given by a simple integration over x.

Assuming that the production of dark matter from radiation is negligible with respect to the production of radiation from inflaton decays, which holds while

$$\mathscr{R}_{\gamma\to X}(x) \ll B_\gamma \Gamma_\phi m_\phi^4 N_\phi x^{-3}\,, \tag{2.93}$$

the evolution of radiation can be studied by considering only the first term in the last line of Eq.(2.91).

Our initial conditions are chosen as

$$x^I = 1; \qquad N_X^I = \mathscr{N}_\gamma^I = 0; \qquad N_\phi^I = \frac{3M_P^2 H_I^2}{m_\phi^4}\,. \tag{2.94}$$

The value of the Hubble rate at the end of the inflationary period, H_I, depends on the specific inflationary model. It has, however, an upper bound posed by the Planck mission [37]:

$$\frac{H_I}{M_{Pl}} < 2.7\times 10^{-5} \qquad \Rightarrow \qquad N_\phi^I < 1.9\times 10^{14}\left(\frac{10^{13}\,\mathrm{GeV}}{m_\phi}\right)^4\,. \tag{2.95}$$

Let us now focus on the evolution of the inflaton-radiation system, which is allowed since dark matter does not contribute to the Hubble rate during its production and does not change the number of radiation, under condition of Eq.(2.93). For an illustrative purpose, we fix $N_\phi^I = 1.03\times 10^{10}$, in the context of a Starobinsky-like potential [71, 72]. The mass and couplings of the inflaton are also, of course, model-dependent. Here we parametrize its decay width as $\Gamma_\phi = \alpha_\phi m_\phi$ and show our results for $\alpha_\phi = 10^{-8}$ and $m_\phi = 10^{13}\,\mathrm{GeV}$. We will assume that inflaton decays only into radiation ($B_\gamma = 1$).

In Fig. 2.3, we show the exact solution* of Eq.(2.91) for the total numbers of inflaton (solid purple curve) and radiation (blue curve). From $x = 1$ to $x = x_{\rm RH}$, to be defined bellow, the radiation content increases because of the inflaton decays, which is accompanied by the entropy production. This so-called *reheating process* finishes when the inflaton field decays completely and the entropy levels off, rendering the number of radiation constant – this is the onset of the radiation era. We also display the quantity xN_ϕ (dotted purple curve) in order to make explicit that it is always larger than $\mathscr{N}_\gamma$ while $N_\phi \approx N_\phi^I$, which is equivalent to the regime $\rho_\phi > \rho_\gamma$.

Therefore, with the Hubble rate dominated by inflaton ($H_{\rm ID}$), we can integrate the equation for the evolution of radiation in Eq.(2.91) up to $x_{\rm RH}$ and find its value by setting $\mathscr{N}_\gamma(x_{\rm RH}) = x_{\rm RH}N_\phi^I$:

$$\mathscr{N}_\gamma(x_{\rm RH}) \approx \frac{2}{5}\sqrt{3}B_\gamma\frac{M_P\Gamma_\phi}{m_\phi^2}\sqrt{N_\phi^I}(x_{\rm RH}^{5/2}-1) \sim x_{\rm RH}N_\phi^I\,. \tag{2.96}$$

*The results of this chapter were produced using Mathematica [73].

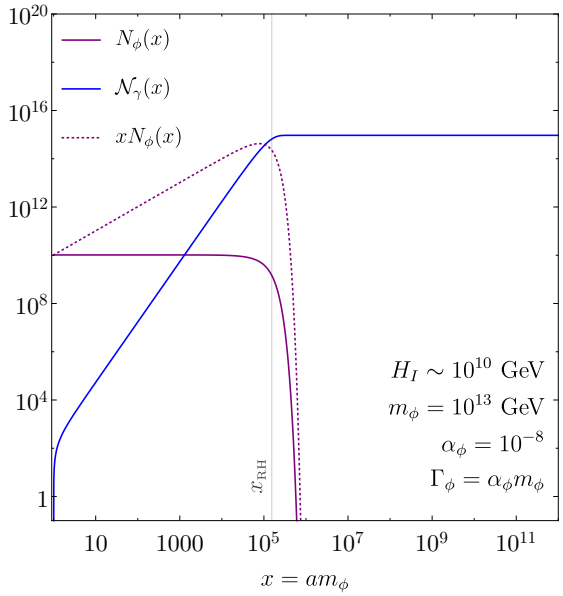

FIGURE 2.3 – *Solution of the set of differential equations, Eq. 2.91, for the total number of inflaton (solid purple) and radiation (blue). We also display the product xN_ϕ (dotted purple), which dominates over $\mathcal{N}_\gamma$ in the Hubble rate prior ϕ decay.*

As indicated by the vertical line in Fig. 2.3, this is a rough estimate of the moment when the radiation content is established, since the inflaton has started to decay efficiently. For the parameters we have chosen, we verify that $x_{\rm RH} \cong 1.54 \times 10^5$. By using equation Eq.(2.89), we find that the *reheating temperature*, $T(x_{\rm RH}) \equiv T_{\rm RH}$, is $T_{\rm RH} \cong 1.35 \times 10^{11}$ GeV. In Section 2.3.1, we provide a better estimate for the reheating temperature, which is defined as the temperature after which there is no more entropy production.

The evolution of temperature while inflaton dominates the cosmic expansion is found after replacing $\mathcal{N}_\gamma(x)$, as in Eq.(2.96) for any $x \leq x_{\rm RH}$, in Eq.(2.89) [74]:

$$\begin{aligned} T(x) &\approx 3^{3/8}\sqrt{\frac{2}{\pi}}\left(\frac{M_P B_\gamma \Gamma_\phi}{g_e}\right)^{1/4}\sqrt{m_\phi}(N_\phi^I)^{1/8}(x^{-3/2}-x^{-4})^{1/4} \\ &\equiv k(g_e)T_{\rm MAX}(x^{-3/2}-x^{-4})^{1/4}\,. \end{aligned} \tag{2.97}$$

This function has a maximum value, the maximal temperature achieved by the thermal bath, $T_{\rm MAX}$. We choose the function $k(g_e)$ so that $T = T_{\rm MAX}$ at $x = x_{\rm MAX}$. We find that $x_{\rm MAX} = (8/3)^{2/5} \cong 1.48$, which lead us to

$$k(g_e) = \left(\frac{8^8}{3^3 5^5}\right)^{1/20}\left(\frac{g_{\rm MAX}}{g_e}\right)^{1/4}\,. \tag{2.98}$$

From Eq.(2.97) we see that, when an *unstable matter* dominates the expansion of the universe, the temperature evolves as $T \propto x^{-3/8}$, which differs from the case in which either a stable matter or a radiation content dominates the *reversible* adiabatic expansion, with $T \propto x^{-1}$. For the *irreversible* adiabatic expansion due to the inflaton decay, temperature

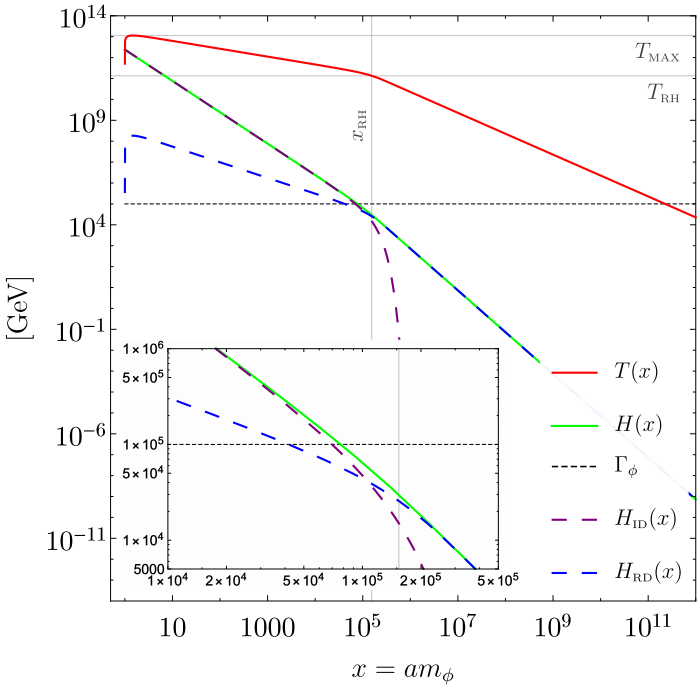

FIGURE 2.4 – *Evolution of temperature (red curve) and Hubble rate (green curve) and value of decay width (dashed black line). Approximate Hubble rates are shown for inflaton (purple dashed curve) and radiation (blue dashed curve) eras.*

and scale factor are related by

$$a^{-1} = m_\phi \left(\frac{T}{k(g_e) T_{\rm MAX}} \right)^{8/3} . \tag{2.99}$$

The maximal temperature reads

$$T_{\rm MAX} = \frac{3^{3/8}}{k(g_e)} \sqrt{\frac{2}{\pi}} \left(\frac{B_\gamma}{g_{\rm MAX}} \right)^{1/4} \sqrt{m_\phi} (M_P \Gamma_\phi)^{1/4} (N_\phi^I)^{1/8} . \tag{2.100}$$

The value of $T_{\rm MAX}$ found for the parameters of Fig. 2.3 is $T_{\rm MAX} \cong 1.14 \times 10^{13}$ GeV.

In Fig. 2.4, we show the evolution of temperature (red curve), the value of Γ_ϕ (dashed black line), the exact solution for the Hubble rate (green curve) and its approximations $H_{\rm ID}$ (dashed purple curve) and $H_{\rm RD}$ (dashed blue curve), found by respectively keeping only the inflaton and the radiation contributions in the total energy density. We indicate the above estimated values of $x_{\rm RH}$, $T_{\rm RH}$ and $T_{\rm MAX}$ (gray lines). In the inset, we see that for $x \gtrsim x_{\rm RH}$, the radiation content dominates the expansion.

The expressions for the Hubble rate under radiation and inflaton domination read, respectively:

$$H_{\rm RD} = \sqrt{\frac{\pi^2 g_e}{90}} \frac{T^2}{M_P} \tag{2.101}$$

and

$$H_{\rm ID} = \frac{\pi^2}{36}\frac{g_{\rm MAX}}{B_\gamma}\frac{T^4}{M_P^2\Gamma_\phi}\,. \tag{2.102}$$

2.3.1 Entropy production

The entropy production due to the decay of a heavy field, which characterizes the reheating process following inflation [67], is in fact a very important generic phenomenon that might have occurred at any time in the Early Universe. Actually, there is a vast literature pointing out the need for such episode with distinct arguments [75–85]. After such a process, the total energy density of the universe increases due to the contribution of the decay products. Any species which are not between the decay products will not receive such energy injection. As a consequence, the ratio between its energy density and the total energy density is reduced once the entropy production finishes.

As we will show in Section 2.4, it is convenient to track the evolution of a species through the dimensionless quantity $Y_i \equiv N_i/S$, the particle *yield*, which is comoving as long as there is no entropy production and can only possibly change when there is some departure from thermal equilibrium. Let us consider that before (after) the entropy production a species i have yield $Y_i^{\rm B}$ ($Y_i^{\rm A}$), total number $N_i^{\rm B}$ ($N_i^{\rm A}$) and the total entropy per comoving volume is $S_{\rm B}$ ($S_{\rm A}$). We define the *dilution factor* Δ as

$$\Delta \equiv \frac{S_{\rm A}}{S_{\rm B}} = \frac{s_{\rm A}a_{\rm A}^3}{s_{\rm B}a_{\rm B}^3} = \frac{g_s^{\rm A}(a_{\rm A}T_{\rm A})^3}{g_s^{\rm B}(a_{\rm B}T_{\rm B})^3}\,. \tag{2.103}$$

The reason why we call it dilution factor is manifest in the relation between the yields after and before the entropy production:

$$Y_i^{\rm A} = \frac{N_i}{S_{\rm A}} = \frac{N_i}{\Delta S_{\rm B}} = \frac{Y_i^{\rm B}}{\Delta}\,. \tag{2.104}$$

Let us therefore consider a generic unstable field called *diluton* (d) and compute Δ as function of the diluton mass (M_d) and decay width Γ_d (or lifetime $\tau_d = 1/\Gamma_d$). Our discussion follows closely Ref. [86].

As a very important general concept which is going to be discussed in more detail later, a species is said to be *decoupled* from another one if the interactions between them are slower than the cosmic expansion rate. In this case, both species evolve independently.

First of all, the diluton must decouple from the thermal bath because otherwise its abundance would reduce exponentially in its annihilation era, for $T \lesssim M_d$. If it decouples after becoming non-relativistic, the fraction of its energy that would give rise to a "new radiation" (the decay products) will be negligible compared to the energy of the "old radiation" and the entropy production would be also negligible. This is why the standard model annihilation eras do not produce entropy in a significant way.

On the other hand, if diluton decouples while ultra-relativistic, its presence would change the expansion rate, even if the universe were dominated by radiation, as long as they

become non-relativistic:

$$\frac{\rho_d}{\rho_\gamma} = \frac{45\zeta(3)}{\pi^4}\frac{\gamma_d}{g_e} M_d T^{-1} \propto a M_d \,. \tag{2.105}$$

The proportionality above holds for an isentropic expansion (inflationary or radiation eras, for instance). The energy density of the thermal bath is related to the total entropy per comoving volume by

$$\rho_\gamma = \frac{\pi^2}{30} g_e \, a^{-4} \, (\tilde{g}_s^{-1} S)^{4/3}, \tag{2.106}$$

where we define for simplicity $\tilde{g}_s \equiv \frac{2\pi^2}{45} g_s$. Therefore, the energy density always decreases because of the expansion (rarefaction and redshift, a^{-4}) but can increase when species become non-relativistic ($g_s^{-4/3}$) and if the entropy per comoving volume increases ($S^{4/3}$).

Since the diluton is unstable, it will interrupt the isentropic expansion at least when is starts decaying (around $t \sim \tau_d$), with $TdS = \Gamma_d \rho_d a^3 dt$. The evolution of ρ_d, as in Eq.(2.82), has the following solution:

$$\rho_d(t) = \rho_d^{\rm B} \left(\frac{a}{a_{\rm B}}\right)^{-3} e^{-\Gamma_d t} \,, \tag{2.107}$$

where the quantities labeled with "B" are given before the diluton decay ($t \ll \tau_d$). By using the definition of temperature as in Eq.(2.90), the change in entropy reads

$$\frac{dS}{dt} = S^{-1/3} \rho_d^{\rm B} a_{\rm B}^4 \tilde{g}_s^{\,1/3} \left(\frac{a}{a_{\rm B}}\right) \Gamma_d e^{-\Gamma_d t} \,. \tag{2.108}$$

The dilution factor is found after integrating Eq.(2.108) from a time much before diluton decay ($t \ll \tau_d$) up to a time much after that ($t \gg \tau_d$):

$$\Delta = \frac{S_{\rm A}}{S_{\rm B}} = \left(1 + \frac{4}{3}\frac{Y_d^{\rm B}}{(g_s^{\rm B})^{1/3}}\frac{M_d}{T_{\rm B}} \int_{t_{\rm B}}^{t_{\rm A}} d(\Gamma_d \, t) \; g_s^{1/3} \; \frac{a(t)}{a_{\rm B}} \; e^{-\Gamma_d t}\right)^{3/4} . \tag{2.109}$$

Now we can replace the solution for a final entropy at a given time in Eq.(2.106) in order to see the effect of entropy production in the energy density of the radiation content:

$$\begin{aligned} \rho_\gamma(t) &= \rho_\gamma^{\rm B} \left(\frac{a}{a_{\rm B}}\right)^{-4} \frac{g_e}{g_e^{\rm B}} \left(\frac{g_s}{g_s^{\rm B}}\right)^{-4/3} + \rho_d^{\rm B} \left(\frac{a}{a_{\rm B}}\right)^{-4} g_e g_s^{-4/3} \int d(\Gamma_d t) \; g_s^{1/3} \; \frac{a(t)}{a_{\rm B}} \; e^{-\Gamma_d t} \\ &= \rho_{old} + \rho_{new} \end{aligned} \tag{2.110}$$

We therefore see that the energy density in radiation is split in two terms: the first one is the "old radiation", which might not be present as in the case of reheating following inflation, and the second one is the "new radiation", the decay products.

Before solving the exact evolution of entropy, we can proceed with approximations which allow us to estimate the behavior of the entropy/energy density injected by decays as well as the dilution factor. In the early epoch ($t \ll \tau_d$, much before decay), we can suppose that the universe was dominated by either matter ($\rho_d^{\rm B}$) or radiation ($\rho_\gamma^{\rm B}$), it means

$a/a_{\rm B} = (t/t_{\rm B})^n$, and we can easily see that

$$S_{new}(t \ll \tau_d) \propto \begin{cases} a^{15/8} & (\rho_d^{\rm B} \text{ dominates}) \\ a^{9/4} & (\rho_\gamma^{\rm B} \text{ dominates}) \end{cases}, \quad \rho_{new}(t \ll \tau_d) \propto \begin{cases} a^{-3/2} & (\rho_d^{\rm B} \text{ dominates}) \\ a^{-1} & (\rho_\gamma^{\rm B} \text{ dominates}) \end{cases}.$$

At the late epoch ($t \gg \tau_d$, much after decay), the entropy per coming volume reaches its asymptotic value $S_{\rm A}$, which is determined by the species dominating the energy density during the decay process. Under diluton domination, $\frac{a(x)}{a_{\rm B}} \neq \left(\frac{t}{t_{\rm B}}\right)^n$ since n changes from 2/3 to 1/2 during the decay and we therefore need to solve the Friedmann equation more carefully. For simplicity, we define $\tilde{t} \equiv \Gamma_d t$. By defining the Hubble rate under diluton domination prior the decay as $H_{\rm B} = \sqrt{\rho_d^{\rm B}}/(\sqrt{3}M_P)$ and the abundance of a species i relative to the diluton energy density prior decay as $f_i = \rho_i/\rho_d^{\rm B}$, the Friedmann equation reads

$$\frac{a'}{a} = \frac{H_{\rm B}}{\Gamma_d}\sqrt{f_d + f_\gamma}\,, \tag{2.111}$$

where prime is derivation with respect to $\tilde{t}$.

In the late epoch, the energy density of radiation is dominated by the decay products and we have

$$f_d = \left(\frac{a}{a_{\rm B}}\right)^{-3} e^{-\tilde{t}} \quad \text{and} \quad f_\gamma \approx \left(\frac{a}{a_{\rm B}}\right)^{-4} g_s^{-1/3} \int_0^\infty d\tilde{t}\, g_s^{1/3} \frac{a(\tilde{t})}{a_{\rm B}} e^{-\tilde{t}} \tag{2.112}$$

The factor $H_{\rm B}/\Gamma_d$ can be eliminated if we define $y = (a/a_{\rm B})(H_{\rm B}/\Gamma_d)^{-2/3}$ and the Friedmann equation for a universe filled with diluton and its decay products becomes

$$\frac{y'}{y} = \left(y^{-3}e^{-\tilde{t}} + y^{-4} g_s^{-1/3} \int_0^\infty d\tilde{t}\, g_s^{1/3}\, y(\tilde{t})\, e^{-\tilde{t}}\right)^{1/2}. \tag{2.113}$$

We can estimate $y(\tilde{t})$ by noticing that the boundary conditions for the equation above is given by [86]

- $y_{\rm B} = \left(\frac{H_{\rm B}}{\Gamma_d}\right)^{-2/3} \propto a_{\rm B} \propto \tilde{t}_{\rm B}^{\,2/3} \quad \Rightarrow \quad \tilde{t}_{\rm B} \propto \left(\frac{H_{\rm B}}{\Gamma_d}\right)^{-1}$
- $\left.\frac{y'}{y}\right|_{\rm B} \propto \left.\frac{y'_{\rm B}}{y_{\rm B}}\right|_{\rm B} \propto \frac{2}{3}\tilde{t}_{\rm B}^{-1} \propto \frac{H_{\rm B}}{\Gamma_d} \quad \Rightarrow \quad \tilde{t}_{\rm B} \propto \frac{2}{3}\left(\frac{H_{\rm B}}{\Gamma_d}\right)^{-1}$

The solution compatible with these conditions is $y(\tilde{t}) = \left(\frac{3}{2}\tilde{t}\right)^{2/3}$, what makes the integration in Eq.(2.113) straightforward:

$$\int_0^\infty d\tilde{t}\; g_s^{1/3}\; y\; e^{-\tilde{t}} = \left(\frac{3}{2}\right)^{2/3} \bar{g}_s^{1/3}\, \Gamma(5/3)\,, \tag{2.114}$$

where $\bar{g}_s$ is an average value of the entropic degrees of freedom during the diluton decay.

We can finally provide a reliable estimate of the dilution factor:

$$\begin{aligned}\Delta &\simeq \left[1+\frac{4}{3}\left(\frac{3}{2}\right)^{2/3}\frac{\Gamma(5/3)}{3^{1/3}}\bar{g}_s^{1/3}\frac{(M_d Y_d^{\rm B})^{4/3}}{(M_P\Gamma_d)^{2/3}}\right]^{3/4} \\ &= 1.07\,\xi\,\bar{g}_s^{1/4}\frac{N_d^{\rm B}}{S_B}\frac{M_d}{\sqrt{M_P\Gamma_d}}\,,\end{aligned} \tag{2.115}$$

where all the uncertainties involved in our analytical approximations are fully encoded in the numerical factor ξ, to be found by comparison with the exact solution of Eq. (2.108).

It worth noting that the final entropy after dilution, $S_{\rm A} = \Delta S_{\rm B}$, *does not* depend on the initial entropy as it is manifest in the last line of the equation above. Instead, it depends purely on the physics of the heavy decaying field: its total number prior decay, its mass and its decay width.

It is therefore possible to define the temperature of the thermal bath just after the entropy release, the *reheating temperature*, even if we do not have information on the initial entropy and the dilution factor:

$$\begin{aligned}T_{\rm RH} &\equiv (\tilde{g}_s^{\rm RH})^{-1/3} S_{\rm A}^{1/3}\, a(c/\Gamma_d)^{-1} \\ &\simeq 1.48\,\xi^{1/3}\,c^{-2/3}\,(g_s^{\rm RH})^{-1/4}\sqrt{M_P\Gamma_d}\end{aligned} \tag{2.116}$$

The only ambiguity in the reheating temperature definition relies therefore on the time of decay completion, $t_d = c/\Gamma_d$ *. From Eq. (2.88), we see that the entropy production depends strongly on the ratio $\Gamma_\phi/H(x)$, which does not need to be exactly one. By equaling the time needed for the diluton to decay completely, t_d, to the Hubble time $t_H = 1/H$ which is a mixing between radiation ($H = H_{\rm RD}$) and matter ($d = 2/3$), we can define the reheating temperature as

$$\Gamma_d = \frac{c}{2/3}H_{\rm RD}(T_{\rm RH}) \qquad \Rightarrow \qquad T_{\rm RH} = \left(\frac{40}{c^2\pi^2 g_e^{\rm RH}}\right)^{1/4}\sqrt{M_P\Gamma_d}\,. \tag{2.117}$$

In the inset of Fig. 2.4, we have seen that using $\Gamma_d = H(x)$ to define the reheating correspond to the instantaneous reheating approximation (no mixed period of inflaton and radiation, $c/d = 1$). If the reheating is defined like that, we need to discount a factor of $\sim 1/8$ coming from the entropy production due to inflaton decay after $\Gamma_d = H(x)$, as shown in [74].

The exact evolution of the entropy depends strongly on its initial value. In Fig. 2.5, we solve Eq. (2.108) in two cases: when the initial entropy is equal to the total number of the decaying field (green curve), $S_{\rm B} = N_d^{\rm B} = 10^{10}$, and when it is much smaller (orange curve), $S_{\rm B} = 1$. We have set the same parameters as in Fig. 2.3 to complement our previous discussion on the reheating period. The total number of diluton is shown as the purple curve. For a sizable initial entropy, we start with an isentropic period, as a radiation era, disrupt temporally during diluton decay. Such a process might occur whenever a

*Notice that ξ also carry uncertainty regarding the decay completion, since we have defined $\tilde{t} = \Gamma_d\, t$.

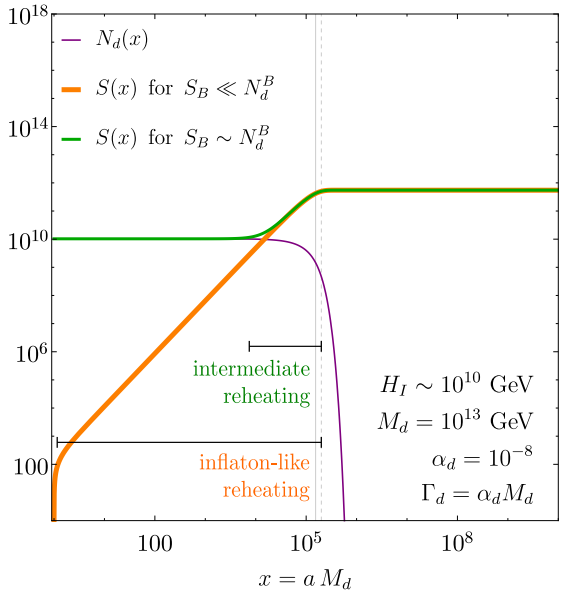

FIGURE 2.5 – *In purple: evolution of the total number of diluton as in Fig. 2.3. Vertical lines: $x = x_{RH}$ (solid) and $x = 1.3\,x_{RH}$ (dashed). In green and orange: solutions of Eq. 2.108 in the cases of $S_B = N_d^B$ and $S_B = 1$, respectively. Notice that both scenarios of initial low-entropy (inflaton-like) and sizable entropy (intermediate matter era, within radiation era) lead to the same final entropy, set by the diluton physics.*

heavy field starts dominating the energy density of the universe after having decoupled while ultra-relativistic. The smaller the initial entropy, the bigger the entropy production while diluton dominates, always respecting $S \propto x^{15/8}$ prior decay completion. One of the motivations for inflation is the low-entropy problem and the need to dilute dangerous relics in the early universe. Those two problems are solved by assuming a reheating epoch after the isentropic exponential increase of the scale factor, the inflationary period.

We have found that, in both scenarios of Fig. 2.5, the analytical expression for the dilution factor, Eq. (2.115), overestimates the exact entropy production by the same factor $\xi \simeq 1.3$. The vertical lines in Fig. 2.5 indicates $x = x_{\rm RH}$ (solid), estimated in the previous section, and $x = 1.3\,x_{\rm RH}$ (dashed), which is closer to the moment in which the entropy levels off and the radiation content dominates completely the Hubble expansion (see Fig. 2.4). Using Eq.(2.117), we recover the previously estimated $T(x_{\rm RH}) = 1.35 \times 10^{11}$ GeV for $c \simeq 2.60$ and find $T(1.3\,x_{\rm RH}) = 1.10 \times 10^{11}$ GeV for $c \simeq 3.91$.

In this thesis we are going to keep the reheating and maximal temperatures as free parameters. The important point we want to make after this discussion is that *hereafter the reheating temperature is such that there is no entropy production for $T < T_{RH}$*. Also, inspired in the results of this section, we fix $T_{\rm MAX} = 100\,T_{\rm RH}$ throughout our analysis.

2.4 Relic density of dark matter particles

We are now in a position to discuss the generic evolution of dark matter particles. In what follows, we show how to extract the relic density of dark matter from the discussion

above and derive approximate expressions for the relic density taking into account dark matter production during the radiation era and the reheating process, as well as the effect of dilution.

We have seen that the evolution of the total number of dark matter particles, in the presence of inflaton (ϕ) and radiation (γ), is governed by the following equation:

$$N'_X = \sqrt{3}\frac{M_P R_X(x)}{m_\phi^5}\frac{x^4}{\sqrt{xN_\phi + \mathscr{N}_\gamma}}\,,$$

where the time parameter is $x = m_\phi a$, with a the scale factor. The interaction rate $R_X(x)$ is a net rate of all interactions responsible for the creation and annihilation of dark matter particles. After the moment where those interactions cannot change N_X, we have the establishment of a *dark matter relic density* and the evolution of dark matter is said to be *decoupled* from the species they interact with.

The dark matter relic abundance today Ω_X^0 is given by

$$\Omega_X^0 \equiv \frac{\rho_X^0}{\rho_{cr}^0} = \frac{m_X n_X^0}{\rho_{cr}^0}\,, \tag{2.118}$$

since dark matter needs to behave as a non-relativistic fluid at least by the time of the last scattering.

Since $n_X^0 = N_X^0 a_0^{-3}$ and from the definition of temperature, Eq.(2.89), we can find an exact expression for the relic density. It is valid for any temperature $T < T_f$, after which the *final* number of dark matter does not change, and it reads

$$\Omega_X^0 h^2 = \frac{h^2}{\rho_{cr}^0}\left(\frac{\pi^2 g_e^0}{30\mathscr{N}_\gamma^0}\right)^{3/4} m_X N_X^f T_0^3 \tag{2.119}$$

Now, let us derive generic approximations for the final dark matter relic density by starting from the evolution of its number density over time,

$$\dot{n}_X + 3H(t)n_X = R_X(t)\,.$$

We have seen that for temperatures $T_{\rm RH} < T < T_{\rm MAX}$, the expansion of the universe is dominated by the energy in the inflaton field, while for $T < T_{\rm RH}$, it is dominated by the energy in the radiation content. It is therefore convenient to evolve the number density over temperature, instead of time or scale factor. Those relations, however, depend on the content which dominates the expansion.

From the definition of the total entropy in a comoving volume, $S = sa^3 = \frac{2\pi^2}{45} g_s T^3 a^3$, and of the Hubble rate, $aH = da/dt$, we have the general relation between time, temperature, degrees of freedom and entropy:

$$dt = -\frac{dT}{HT}\left(1 + \frac{1}{3}\frac{d\ln g_s}{d\ln T} - \frac{1}{3}\frac{d\ln S}{d\ln T}\right) \equiv -g_s^*\frac{dT}{HT} + \frac{dS}{3HS}\,, \tag{2.120}$$

where we account for the variation of the entropic degrees of freedom with the variable $g_s^* \equiv 1 + \frac{1}{3}\frac{d\ln g_s}{d\ln T}$.

During an *isentropic* period, as the radiation era, Eq.(2.120) becomes

$$\frac{dn_X}{dT} - 3g_s^*\frac{n_X}{T} = -g_s^*\frac{R_X}{HT} \qquad \Rightarrow \qquad g_s T^3 \frac{d}{dT}\left(\frac{n_X}{g_s T^3}\right) = -g_s^*\frac{R_X}{HT} \tag{2.121}$$

We can therefore see that it is convenient to express the dark matter relic density in terms of another dimensionless parameter, the *yield* (or the amount):

$$Y_X = \frac{N_X}{S} = \frac{n_X}{s}\,. \tag{2.122}$$

We can see that such quantity is comoving, i.e. does not depend on the scale factor, by noticing that $n_X \propto a^{-3}$ and $s \propto g_s T^3 \propto a^{-3}$ in the absence of entropy production.

The evolution of dark matter throughout an isentropic expansion reads

$$\frac{dY_X}{dT} = -g_s^*\frac{R_X}{HTs}\,. \tag{2.123}$$

For instance, suppose that dark matter may be produced via three distinct processes: $i \leftrightarrow XX$, $jj \leftrightarrow X$ and $kk \leftrightarrow XX$, with the species i, j and k having temperatures T_i, T_j and T_k, respectively, which may be different from the temperature of the thermal bath, T. Using the results of Sec. 2.1.1 for classical collision terms, the evolution of Y_X would be governed by the following equation:

$$\begin{aligned} -\frac{T}{g_s^*}\frac{dY_X}{dT} \supset & \sum_i Y_i(T_i)\frac{B_X\Gamma_{i\to XX}}{H(T)}\left(1 - \frac{Y_X}{Y_i}\frac{n_X\langle\Gamma_{XX\to i}\rangle}{B_X\Gamma_{i\to XX}}\right) \\ & + \sum_j Y_j(T_j)\frac{n_j\langle\Gamma_{jj\to X}\rangle}{H(T)}\left(1 - \frac{Y_X}{Y_j}\frac{B_k\Gamma_{X\to kk}}{n_j\langle\Gamma_{jj\to X}\rangle}\right) \\ & + \sum_k Y_k(T_k)\frac{n_k\langle\sigma v\rangle_{kk\to XX}}{H(T)}\left(1 - \frac{Y_X^2}{Y_k^2}\frac{\langle\sigma v\rangle_{XX\to kk}}{\langle\sigma v\rangle_{kk\to XX}}\right) \end{aligned} \tag{2.124}$$

From the equation above, it is clear that the establishment of the dark matter relic density ($dY_X/dT \to 0$) might happen either when the abundance of the species producing dark matter gets suppressed ($Y_{i,j,k} \to 0$) or when the interaction rate becomes much smaller then the expansion rate (universe expanding faster then the typical time of interactions).

For a generic interaction rate R_X, the dark matter yield today, Y_X^0, is given by

$$Y_X^0 - Y_X(T_{\rm RH}) = \int_{T_0}^{T_{\rm RH}} dT\, g_s^*\frac{R_X}{HTs} \tag{2.125}$$

In order to find the yield at the time of reheating, $Y(T_{\rm RH})$, we need to consider dark matter production during the reheating process. In this case, as we have seen, $dS \neq 0$.

From Eq.(2.99), we find

$$dt = -\frac{dT}{HT}\left(\frac{8}{3} - \frac{2}{3}\frac{d\ln g_e}{d\ln T}\right) \equiv -\frac{dT}{HT}\frac{8}{3}g_e^*\,, \tag{2.126}$$

where, analogously to g_s^*, we account for the variation of the energetic degrees of freedom with the variable $g_e^* \equiv 1 - \frac{1}{4}\frac{d\ln g_e}{d\ln T}$.

The Eq.(2.120) becomes

$$\frac{dn_X}{dT} - 8g_e^*\frac{n_X}{T} = -\frac{8}{3}g_e^*\frac{R_X}{HT} \qquad \Rightarrow \qquad g_e^2T^8\frac{d}{dT}\left(\frac{n_X}{g_e^2T^8}\right) = -g_e^*\frac{R_X}{HT} \tag{2.127}$$

Since under inflaton domination the total number of inflaton is constant, $N_\phi \approx N_\phi^I = n_\phi^I a^3$, the number density of inflaton (and not the density of entropy) is the quantity that redshifts as a^{-3}. From (2.99), we see that n_ϕ^I is proportional to $g_e^2T^8$. Hence, during inflaton domination, the comoving amount of dark matter is accounted for by the following dimensionless quantity:

$$Y_X^{\rm ID} \equiv \frac{N_X}{N_\phi^I} = \frac{n_X}{n_\phi^I}\,, \tag{2.128}$$

and the evolution of dark matter is governed by

$$\frac{dY_X^{\rm ID}}{dT} = -g_e^*\frac{8}{3}\frac{R_X}{HTn_\phi^I}\,, \qquad \text{for} \quad T_{\rm RH} \lesssim T < T_{\rm MAX}\,, \tag{2.129}$$

where the approximation remind us that the entropy levels off while $N_\phi \lesssim N_\phi^I$.

The explicit expression of n_ϕ^I reads

$$\begin{aligned} n_\phi^I &= \left(\frac{8^8}{3^3 5^5}\right)^{-1/5}\frac{g_e^2T^8}{g_{\rm MAX}^2T_{\rm MAX}^8}N_\phi^I m_\phi^3 \\ &= \frac{\pi^4}{432}\left(\frac{g_{\rm MAX}}{B_\gamma}\right)^2\frac{T^8}{m_\phi(M_P\Gamma_\phi)^2} \\ &= \frac{5\pi^2}{54c^2}\frac{g_{\rm MAX}^2}{g_{\rm RH}\,B_\gamma^2}\frac{T^8}{m_\phi T_{\rm RH}^4}\,. \end{aligned} \tag{2.130}$$

By definition, the yields $Y_X^{\rm ID}$ and Y_X are related through the number density of dark matter:

$$n_X = Y_X s = Y_X^{\rm ID} n_\phi^I\,. \tag{2.131}$$

The radiation-dominated yield at the reheating time is therefore given by the following expression:

$$Y_X(T_{\rm RH}) = \frac{25}{12\,c^2}g_{\rm RH}^{-3/2}\frac{T_{\rm RH}}{m_\phi}Y_X^{\rm ID}(T_{\rm RH})\,. \tag{2.132}$$

It is interesting to see that the entropy injection is automatically taken into account:

$$Y_X(T_{\rm RH}) = \frac{N_\phi^I}{S(T_{\rm RH})} Y_X^{\rm ID}(T_{\rm RH}) = \frac{N_\phi^I}{S^I \Delta} Y_X^{\rm ID}(T_{\rm RH}) \simeq 0.66\sqrt{c}/\xi (g_{\rm RH}/\bar{g}_s)^{1/4} \frac{T_{\rm RH}}{m_\phi} Y_X^{\rm ID}(T_{\rm RH})\,. \tag{2.133}$$

With these results, we can write a good approximation for the relic density of dark matter which takes into account the production during an inflaton-dominated period:

$$\begin{aligned}\Omega_X^0 h^2 &= \frac{m_X}{\rm GeV} \frac{Y_X^0}{3.62\times 10^{-9}} \\ &= \frac{m_X}{2.16\times 10^{-28}} \left(\int_{T_0}^{T_{\rm RH}} dT \frac{g_s^*}{g_s\sqrt{g_e}} \frac{R_X(T)}{T^6} + 1.6\, c\, B_\gamma\, g_{\rm RH}^{-3/2}\, T_{\rm RH}^7 \int_{T_{\rm RH}}^{T_{\rm MAX}} dT g_e^* \frac{R_X(T)}{T^{13}} \right)\,,\end{aligned} \tag{2.134}$$

where we have used $s_0 \simeq 2.23\times 10^{-38}$ GeV^3.

We identify the first and second terms in Eq.(2.134) with the radiation dominated (RD) and the inflaton dominated (ID) contributions, respectively,

$$\Omega_X^0 h^2 = \Omega_X^0 h^2_{\rm RD} + \Omega_X^0 h^2_{\rm ID} = \Omega_X^0 h^2_{\rm RD} \left(1 + \frac{\Omega_X^0 h^2_{\rm ID}}{\Omega_X^0 h^2_{\rm RD}} \right) \equiv \Omega_X^0 h^2_{\rm RD}\, \mathscr{B}(T_{\rm RH}, T_{\rm MAX})\,. \tag{2.135}$$

We then define the boost factor $\mathscr{B}$, a function of the reheating and maximal temperatures which quantifies the contribution of the production during reheating. In special cases, though, the boost factor might depend on model-dependent parameters present in the rate. It is also useful to define the fraction $f_{\rm RH}$ of dark matter produced during reheating, related to the boost factor as $f_{\rm RH} = (\mathscr{B}-1)/\mathscr{B}$. From Eq. (2.134) we can see that such a fraction might be relevant for sufficiently high temperature dependence in the rate.

For a qualitative understanding of the parameter space of a given model, we can in many occasions approximate $R_X(T) \propto T^n$. Integrating from an infra-red (IR) to a ultra-violet (UV) higher scale give us the following model-independent result:

$$\int_{T_{\rm IR}}^{T_{\rm UV}} dT\, T^{n-k} = \begin{cases} \dfrac{T_{\rm IR}^{-((k-1)-n)}}{(k-1)-n} \left(1 - \dfrac{T_{\rm IR}^{(k-1)-n}}{T_{\rm UV}^{(k-1)-n}} \right)\,, & n < k-1 \\ \ln\left(\dfrac{T_{\rm UV}}{T_{\rm IR}} \right)\,, & n = k-1 \\ \dfrac{T_{\rm UV}^{n-(k-1)}}{n-(k-1)} \left(1 - \dfrac{T_{\rm IR}^{n-(k-1)}}{T_{\rm UV}^{n-(k-1)}} \right)\,, & n > k-1 \end{cases} \tag{2.136}$$

We therefore see that the temperature dependence of the rate set a qualitative behavior of the dark matter production. If $n < k-1$ ($n > k-1$), the dark matter production would take place at the lowest (highest) scale available and is said to be IR-dominated (UV-dominated), while if $n = k-1$, we have an "inflection point" in the production regime with a logarithmic dependence of both scales which we refer to as IR-UV mix.

The radiation era contribution have an inflection point for $n = 5$ while for the inflaton era contribution it happens for $n = 12$.

We remind the reader that while estimating the contribution from the reheating process one assumes $N_\phi \approx N_\phi^I$ until the end of entropy injection, which brings uncertainty. Nevertheless, the analytical estimations we gave in this section are useful to guide our expectations regarding the viable parameter space of dark matter models.

Chapter 3

Origins for dark matter particles

Contents

As we have seen in the previous chapter, the comoving amount of dark matter particles (labeled X), the yield $Y_X = n_X/s$, changes in face of their interactions and throughout an isentropic cosmic expansion, its evolution might be put in the form

$$-\frac{T}{g_s^*}\frac{dY_X}{dT} = \frac{Y_i\mathcal{W}_{i\to X} - Y_X\mathcal{W}_{X\to i}}{H}\,, \tag{3.1}$$

where the *frequency of interactions* between dark matter and a species labeled i is denoted by $\mathcal{W}_{i\leftrightarrow X}$. It is related to the interaction rate simply by $\mathcal{W}_{i\to X} = R_{i\to X}/n_i$. The stronger the couplings between particles X and i, the higher the frequency of interactions.

We easily see from the equation above that there are only two ways of keeping the yield of dark matter constant through the expansion of the universe. On one hand, if the universe expands fast enough, the interactions between the two sectors do not happen in a significant way as to vary Y_X, in which case they are *decoupled* ($H \gg \mathcal{W}_{i\leftrightarrow X}$). On the other hand, if the interactions are frequent enough, but if both sectors are produced at the same rate, $R_{i\to X} = n_i\mathcal{W}_{i\to X} = n_X\mathcal{W}_{X\to i} = R_{X\to i}$, they are in an equilibrium situation and therefore the total number of both kinds of particles cannot change. Moreover, notice that for a given rate of change in the yield ($dY_X/d\ln T$), the effect of having $\mathcal{W}_{i\to X} > H$ is to make $Y_X \to Y_i$, which might lead to the *thermalization* of both sectors. Notice that the considerations above applies for the production during radiation era, while for the production during inflaton era we should compare $\mathcal{W}$ with a faster expansion rate H_{ID}.

The assumptions involved for the *initial condition* of the equation above, to be supported by the nature of the couplings, determine how the yield evolves. In what follows, we consider two widely considered assumptions in this regard.

3.1 Freeze-out of WIMPs

The weakly interacting massive particles (WIMPs) are dark matter candidates that interact with standard model (SM) particles with strengths which are weak but sizable enough as to have kept them in equilibrium in the early universe. By further assuming that the WIMP is heavier then the SM particles, this equilibrium would have been disrupt once the temperature of the thermal bath approaches the WIMP's mass. In this case the SM particles would no more have enough energy to produce WIMPs, which then annihilate until its decoupling ($H \gg \mathcal{W}_{i\leftrightarrow X}$). This is the most considered way of generating a dark matter relic abundance, the so-called *freeze-out* mechanism [87].

This is the mechanism behind the establishment of the abundances of the light elements, the BBN, and given the extraordinary agreement between BBN predictions and observations, it seems natural – or at least reasonable – to expect that the dark matter content was produced in the same way.

In what follows, we show how the DM relic density today depends on the mass and couplings of a WIMP. Since the moment of decoupling in this case depends on the relation between the temperature of the thermal bath (T) and DM mass (m_X), it is convenient to use the variable $x = m_X/T$ as the time parameter. If thermalized SM species interact with WIMPs via a $2 \to 2$ process, we have (Eq.(2.124)):

$$\frac{dY_X}{dx} = \sqrt{\frac{8\pi^2 g_*(x)}{45}} M_P m_X \frac{\langle\sigma v\rangle}{x^2}((Y_X^{eq})^2 - Y_X^2)\,, \tag{3.2}$$

where we use the usual definition $g_*^{1/2} \equiv g_s^* \frac{g_s}{\sqrt{g_e}}$. The equilibrium yield is (see Eq. (2.10))

$$\begin{aligned} Y_X^{eq} &= \frac{45\gamma_X}{4\pi^4 g_s}\frac{m_X^2}{T^2}\sum_{a=1}^{\infty}\zeta_X^{\alpha+1}\eta_X^{\alpha}\frac{K_2(\alpha\, m_X/T)}{\alpha} \\ &\approx \frac{45\gamma_X\eta_X}{4\pi^4}\frac{x^2}{g_s}K_2(x) \approx \frac{45\gamma_X\eta_X}{4\sqrt{2}\pi^{7/2}}\frac{x^{3/2}}{g_s}e^{-x}\,, \end{aligned} \tag{3.3}$$

with $K_\nu(x)$ being the modified Bessel function of order ν.

In Fig. 3.1, we show exact solutions* of Eq.(3.2), where the generic picture of the freeze-out mechanism can be appreciated. The equilibrium curve given by Eq.(3.3) is shown in gray. In this plot we have assumed a generic constant thermally averaged annihilation cross-section $\langle\sigma v\rangle = \lambda^4/m_X^2$ and the WIMP mass is set to $m_X = 100$GeV. The blue, green and red curves are the solutions for $\lambda = 0.005$, 0.07, and 1, respectively.

At the beginning ($x \ll 1$), the WIMPs are thermalized with the SM species. It is only when the WIMP becomes non-relativistic ($x \sim 10$) that its yield departs from its equilibrium value and the chemical decoupling takes place. When this happens, the frequency of interactions becomes comparable to the expansion rate, $\mathcal{W}(T_f) \sim H(T_f)$. The moment

*We have used Matlab 2016a [88].

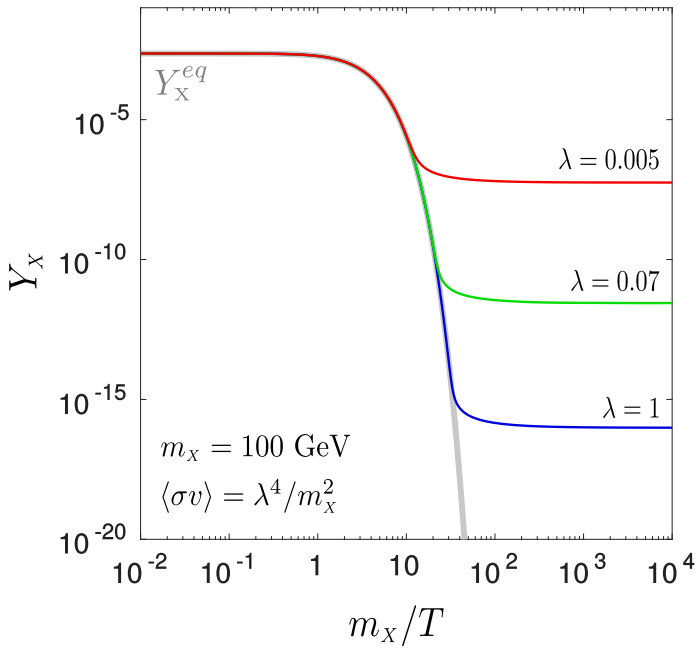

FIGURE 3.1 – *Exact solutions for the yield of a WIMP with mass* $m_X = 100 GeV$ *for three values of its coupling to SM:* $\lambda = 0.005$ *(blue curve),* $\lambda = 0.07$ *(green curve) and* $\lambda = 1$ *(red curve). Equilibrium curve is shown in gray. Notice that the stronger the interactions, the smaller the remaining WIMP relic.*

of decoupling is thus roughly

$$x_f = \ln\left(\sqrt{\frac{45}{4\pi^5}} M_P m_X \frac{\sqrt{x_f}}{\sqrt{g_e(x_f)}} \langle\sigma v\rangle_f\right) . \tag{3.4}$$

Taking for instance $m_X = 100$ GeV and $\langle\sigma v\rangle = \lambda^4/m_X^2$ with $\lambda = 0.07$, we find $x_f \simeq 23.8$, which correspond to what we see in Fig. 3.1.

The equation we have to solve in order to find an analytical expression for the WIMP relic density, the freeze-out approximation, reads

$$\frac{1}{Y_X^0} - \frac{1}{Y_X^f} = \sqrt{\frac{8\pi^2}{45}} M_P \int_{T_0}^{T_f} dT g_*^{1/2} \langle\sigma v\rangle . \tag{3.5}$$

Since the yield at decoupling ($Y_X(x_f) \equiv Y_X^f$) is still close to its equilibrium value, we can parametrize it with $Y_X^f \equiv Y_X^{eq,f}(1+\delta)$, where δ is a small number and $Y_X^{eq,f} \equiv Y_X^{eq}(x_f)$. Choosing $\delta = 1.5$ was shown to be a good approximation [89].

From Eq.(2.63), we know that the thermally averaged annihilation cross-section is given by

$$\langle\sigma v\rangle = \frac{\mathcal{S}_X m_X^{-4} T^{-1}}{8\gamma_X K_2(m_X/T)^2} \int_{4m_X^2}^{\infty} ds \sqrt{s}(s - 4m_X^2)\sigma K_1\left(\frac{\sqrt{s}}{T}\right) , \tag{3.6}$$

but in the non-relativistic limit, it usually does not depend on temperature.

By setting $m_X = 100$ GeV and $\langle\sigma v\rangle = 10^{-9}\,\mathrm{GeV}^{-2} = 10^{-26}\,\mathrm{cm}^{-3}/\mathrm{s}$, for which we have found $x_f = 23.8$, the WIMP relic density is automatically within a good scale:

$$\frac{\Omega_X^0 h^2}{0.12} \sim \left(\frac{x_f}{23.8}\right)\left(\frac{86.3}{g_*(x_f)}\right)^{1/2}\left(\frac{2\times 10^{-26}\,\mathrm{cm}^3\,\mathrm{s}^{-1}}{\langle\sigma v\rangle}\right). \tag{3.7}$$

The interesting thing about this value for the thermally averaged cross section is that it is easily satisfied by electroweak interactions.

For quartic or gauge interactions between WIMPs and SM fields with a strength λ, we have typically

$$\langle\sigma v\rangle \sim \frac{\lambda^4}{m_X^2} = 2\times 10^{-26}\,\mathrm{cm}^3\mathrm{s}^{-1}\times\begin{cases}\left(\frac{\lambda}{0.07}\right)^4\left(\frac{m_X}{100\ \mathrm{GeV}}\right)^{-2}\\ \left(\frac{\lambda}{0.2}\right)^4\left(\frac{m_X}{1000\ \mathrm{GeV}}\right)^{-2}\end{cases} \tag{3.8}$$

We therefore see that the yield depicted by the green curve in Fig.3.1 provides the right amount of dark matter.

If the interactions are mediated by a field of mass M, whose interactions with WIMPs and SM fields have strength λ_X and λ_f respectively, we find typically

$$\langle\sigma v\rangle \sim \lambda_X^2\lambda_f^2\frac{m_X^2}{M^4} = 2\times 10^{-26}\,\mathrm{cm}^3\mathrm{s}^{-1}\times\begin{cases}\left(\lambda_X\frac{\lambda_f}{0.1}\right)^2\left(\frac{m_X}{100\ \mathrm{GeV}}\right)^2\left(\frac{M}{456\ \mathrm{GeV}}\right)^{-4}\\ \left(\lambda_X\frac{\lambda_f}{0.1}\right)^2\left(\frac{m_X}{1000\ \mathrm{GeV}}\right)^2\left(\frac{M}{1000\ \mathrm{GeV}}\right)^{-4}\end{cases} \tag{3.9}$$

The couplings linking WIMPs and SM particles are bounded from above by theoretical particle physics requirements of perturbativity and from below by the need to provide thermalization in the early universe. Thus we usually work with $10^{-3} \lesssim \lambda \lesssim \sqrt{4\pi}$. The corresponding mass interval providing the good amount of dark matter today is typically of $100 \lesssim m_X/\mathrm{GeV} \lesssim 1000$, which is precisely the scale of masses of electroweak interactions.

Therefore, if the scales of masses and couplings of WIMPs are close to the SM ones, the right amount of dark matter relic density is easily achieved. Moreover, WIMP candidates are a common byproduct of models in which new physics at weak scales solves problems of the SM. This coincidence is the so-called *"WIMP miracle"*. The possibility of probing this scenario at colliders, underground detectors, telescopes and satellites had driven the efforts in the search for dark matter particles in the last decades.

3.2 Freeze-in of FIMPs

Despite all the effort put into the search for dark matter, specially WIMPs, in the last few decades, the null results from numerous experiments point out challenging possibilities for the dark matter properties. For example, their interactions with SM are much weaker

than expected, their masses are much lighter or much heavier than the probed mass range and the dark sector is not minimal since DM and SM particles may not interact directly.

If the SM-DM interactions are weak enough so that we have always $\mathcal{W}_{i\leftrightarrow X} < H$, both sectors would never thermalize and the freeze-out mechanism discussed above would not hold.

As we have shown, if the dark matter (X) interact with particles of the thermal bath (i), whenever $\mathcal{M}_{i\to X} = \mathcal{M}_{X\to i}$ we can use the balance equation to write $n_i \mathcal{W}_{i\to X} = n_X^{eq} \mathcal{W}_{X\to i}$. In this case, if dark matter is always far from equilibrium ($Y_X \ll Y_X^{eq}$), its evolution obey the following equation:

$$-\frac{T}{g_s^*}\frac{dY_X}{dT} = Y_X^{eq}\frac{\mathcal{W}_{X\to i}}{H}\left(1-\frac{Y_X}{Y_X^{eq}}\right) \approx Y_X^{eq}\frac{\mathcal{W}_{X\to i}}{H}\,. \tag{3.10}$$

The solution for this equation is highly dependent on the initial condition for Y_X, which is not Y_X^{eq} anymore, and the decoupling – or *freeze-in* – happens when $\mathcal{W}_{X\to i} \ll H$. Such dark matter candidates were considered at least since [90] and are nowadays referred to as feebly interacting massive particles (FIMPs) [91].

We will now study the evolution of FIMPs produced from ultra-relativistic species, which is the case of interest in the following chapters. Production from non-relativistic particles is also possible, though. For simplicity, we set the ultra-relativistic degrees of freedom to be $g_e = g_s = 100$.

In order to not make any further assumption regarding FIMP dark matter in our numerical computations, we work purely with interaction rates. The interaction rates of FIMPs are usually determined solely by their production terms, the *production rates* $R_{i\to X} = n_i^2 \langle\sigma v\rangle_{i\to X}$:

$$\begin{aligned} R_X \cong R_{i\to X} &= \frac{S_{12}}{(2\pi)^4}\int ds\, p_{12}\,\sqrt{s}\,\sigma_{12\to 34}\int_0^\infty dp_1 f_1 \int_{\frac{s}{4p_1}}^\infty dp_2 f_2 \\ &= \frac{S_{12}S_{34}}{32(2\pi)^6}\int_{4m_X^2}^\infty ds\,\sqrt{1-\frac{4m_X^2}{s}}\int d\Omega_{13}^*|\mathcal{M}|^2\int_0^\infty dp_1 f_1\int_{\frac{s}{4p_1}}^\infty dp_2 f_2\,, \end{aligned} \tag{3.11}$$

where we have used Eqs. (2.58), (2.59) and (2.61).

Notice that ultra-relativistic species are able to produce dark matter as long as their momenta are larger than the DM mass, as of course expected. The integration over the initial momenta is at least qualitatively given by $T\sqrt{s}K_1\left(\frac{\sqrt{s}}{T}\right)$, which makes the *threshold for dark matter production*, lead by the factor $\sqrt{1-\frac{4m_X^2}{s}}$, to happen almost exponentially when $T \lesssim 10\, m_X$. This is because the most energetic particles in the tail of the distributions are still able to produce dark matter for $T < m_X$. This is the so-called Boltzmann suppression, a general feature for production rates of species that become non-relativistic. Notice that this is also happening in the freeze-out mechanism.

In this thesis, we are interested in the dark matter production from "portals", which are mediators connecting the dark and visible sectors. For an s-channel exchange of a mediator with mass M and total width Γ, the integrated squared amplitude may be

n	$\xi^{FD}(k)$	$\xi^{MB}(k)$	$\xi^{BE}(k)$
4	2.71	4.00	10.82
6	26.01	32.00	46.24
8	6.89×10^2	7.68×10^2	9.00×10^2
10	3.48×10^4	3.69×10^4	3.96×10^4
12	2.86×10^6	2.95×10^6	3.05×10^6

TABLE 3.1 – *Factors coming from the statistics of incoming ultra-relativistic species in the production rate of FIMPs far from resonance. FD, MB and BE stand for Fermi-Dirac, Maxwell-Boltzmann and Bose-Einstein statistics. The power of the Mandelstam variable in the amplitudes (k) is related to the power of temperature in the rate (n) by* $n = 2k + 4$.

parametrized in the following way:

$$\int d\Omega_{13}^{*}|\mathcal{M}|^2 \equiv \frac{A(s)}{(s-M^2)^2+M^2\Gamma^2} \approx \begin{cases} \frac{\pi}{M\Gamma}A(s)\delta(s-M^2) & \text{near resonance} \\ \lambda_{tot}\frac{s^k}{\Lambda^{2k}} & \text{far from resonance} \end{cases} \tag{3.12}$$

where we have used the narrow width approximation (NWA) [92] which holds in the pole region ($s \sim M^2$), with $\Gamma \ll M$. λ_{tot} (Λ) encodes a dimensionless (dimension one in energy) function of the free parameters.

Under NWA, the production rate is given by (see Eqs. (2.134) and (2.135))

$$R_X(T)\Big|^{\text{NWA}} = \frac{\mathcal{S}_i\mathcal{S}_X}{64(2\pi)^5}\frac{T}{\Gamma}K_1\left(\frac{M}{T}\right)A(M^2)\,, \tag{3.13}$$

where we have used Maxwell-Boltzmann statistics. As long as $T_0 \ll M \ll T_{\text{RH}}$, and setting for instance $T_{\text{RH}} = 10^{10}\,\text{GeV}$, the final relic density is approximately

$$\begin{aligned} \frac{\Omega_X^0 h^2}{0.12}\Big|^{\text{NWA}} &\sim \mathscr{B}_{\text{NWA}}\frac{A(M^4)}{\text{GeV}^4}\frac{\text{GeV}}{\Gamma}\left(\frac{m_X}{100\text{GeV}}\right)\left(\frac{M}{4\times 10^5\text{GeV}}\right)^{-4} \\ &\sim \frac{\mathscr{B}_{\text{NWA}}}{20}\frac{(A(M^4)/\text{GeV}^4)(\text{GeV}/\Gamma)}{2\times 10^{20}}\left(\frac{m_X}{100\text{GeV}}\right)\left(\frac{M}{4\times 10^{11}\text{GeV}}\right)^{-4}. \end{aligned} \tag{3.14}$$

This relation might be useful once we have the specific model, so that we can constrain $A(M^2)$ and Γ in terms of masses and couplings. The boost factor becomes important whenever the mediator mass is close to the reheating scale.

Far from resonance, the production rate increases with temperature by some power $n = 2k + 4$, fixed by the microscopic processes under consideration, and the production rate reads

$$R_X(T)\Big|^{\text{FAR}} = \frac{\mathcal{S}_i\mathcal{S}_X}{32(2\pi)^6}\xi(k)\lambda_{tot}\frac{T^n}{\Lambda^{n-4}} \tag{3.15}$$

The parameter $\xi(k)$ encodes the statistics of the incoming ultra-relativistic particles and it is $2^{2k+2}k!(k+1)!$ for Maxwell-Boltzmann, $2^{2k+2}k!(k+1)!\zeta^2(k+2)$ for Bose-Einstein and $(2^{k+1}-1)^2k!(k+1)!\zeta^2(k+2)$ for Fermi-Dirac statistics, provided that $k > -1$. We

show in Table 3.1 how those numerical factors depend on the temperature dependence of the rate far from resonance. This is to have in mind the error coming from the use of Maxwell-Boltzmann statistics in such ultra-relativistic processes, which simplifies the analytical and numerical computations.

The relic density far from resonance reads (see Eq. (2.136))

$$\Omega_X^0 h^2\Big|^{\rm FAR} \approx 2.4\times 10^{18}\mathscr{B}\,\mathcal{S}_i\mathcal{S}_X\xi(k)\lambda_{tot}\times\begin{cases}\frac{1}{n-5}\left(\frac{m_X}{T_{\rm RH}}\frac{T_{\rm RH}^{n-4}}{\Lambda^{n-4}}-\frac{m_X}{T_f}\frac{T_f^{n-4}}{\Lambda^{n-4}}\right), & n\neq 5\\ \frac{m_X}{\Lambda}\ln\left(\frac{T_{\rm RH}}{T_f}\right), & n=5\end{cases}. \tag{3.16}$$

In what follows, we will show how the dependence on the energy of the scattering amplitude (or the microscopic description of the model) can completely change the picture, results and interpretation of the freeze-in mechanism. We recall the reader the distinction we have made regarding an infra-red (IR) and a ultra-violet (UV) production, after presenting the model-independent result of Eq. (2.136).

In the simplest case of $\int d\Omega_{13}^*|\mathcal{M}|^2=\lambda_{tot}$, so $k=0$ and $n=4$, the relic density is approximately

$$\frac{\Omega_X h^2}{0.12}\Big|_{n=4}\sim\mathscr{B}_4\frac{\lambda_{tot}}{1.25\times10^{-20}}\left(\frac{m_X}{T_f}-\frac{m_X}{T_{\rm RH}}\right)\sim\left(\frac{\sqrt{\lambda_{tot}}}{1.12\times10^{-10}}\right)^2, \tag{3.17}$$

where the last approximation comes from the fact that freeze-in in this case happens at $T_f\sim m_X$, since m_X is the only scale of the process, and assuming $m_X\ll T_{\rm RH}$.

This is the infra-red FIMP scenario (discussed for instance in [91]), in a sense that the production finishes at the smallest scale available, the dark matter mass. In this case, the agreement with the relic density constraints impose a need for very small couplings ($\sqrt{\lambda_{tot}}=\lambda\sim10^{-12}$). The boost factor in this case is safely negligible as long as $m_X\ll T_{\rm RH}$.

In the case of the exchange of a heavy field of mass M, $\int d\Omega_{13}^*|\mathcal{M}|^2=\lambda_{tot}\frac{s^2}{M^4}$, the relic density far from resonance reads

$$\frac{\Omega_X^0 h^2}{0.12}\Big|_{n=8}^{\rm FAR}\sim\frac{\mathscr{B}_8}{1.8}\frac{\lambda_{tot}}{0.1}\left(\frac{m_X}{100{\rm GeV}}\right)\left(\frac{T_{\rm RH}}{10^{10}{\rm GeV}}\right)^3\left(\frac{M}{9.8\times10^{12}{\rm GeV}}\right)^{-4}. \tag{3.18}$$

We therefore see that a natural scale for a mediator sequestering a GeV dark matter from the thermal bath is $M\simeq10^{13}$ GeV. This corresponds surprisingly to a natural mass for an intermediate Z' mediator compatible with many S0(10) scenarios, especially the ones including a right handed neutrino [93]. It is compelling to note that the value of λ_{tot} required in such constructions is easily accommodated in GUT models. Notice that the dark matter production in this case has a UV-dominated radiation contribution while having an IR-dominated inflaton contribution.

The boost factor is even more important in models with $\int d\Omega_{13}^*|\mathcal{M}|^2=\lambda_{tot}\frac{s^4}{\Lambda^8}$. At first sight, it looks strange to study interactions with such high power in mass suppression. However, once we write $|\mathcal{M}|^2=\left(\frac{\lambda}{\Lambda^2}\right)^2\frac{s^4}{M^4}$, we recognize models with a heavy mediator

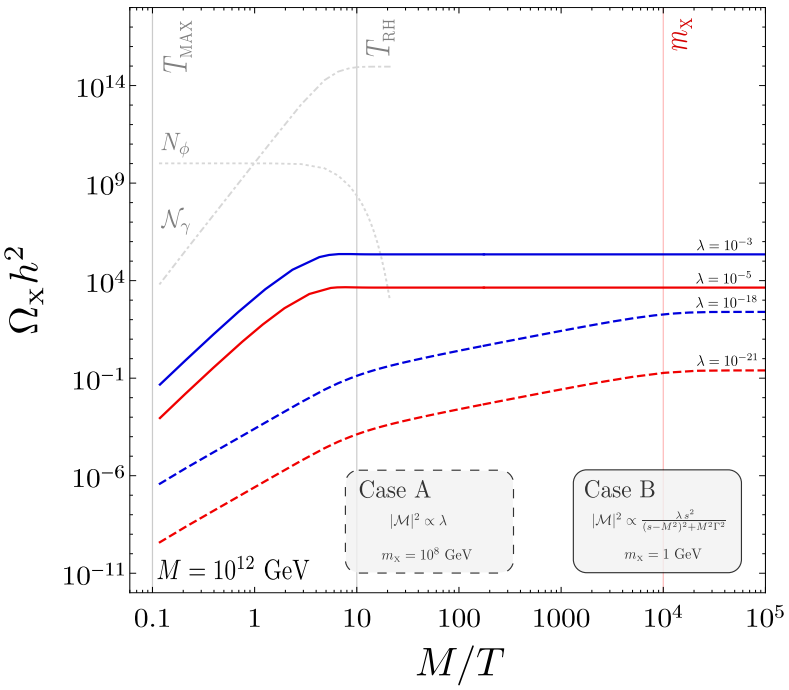

FIGURE 3.2 – *Exact solutions for the relic density of FIMPs, Eq.*(3.10)*, in two generic cases: for a constant squared amplitude (case A, dashed curves) and for the amplitude corresponding to the exchange of a mediator of mass* $M = 10^{12}$ *GeV (case B, solid curves). Smaller (larger) overall couplings are shown in red (blue).*

of mass $\simeq M$ coupling to the visible and dark matter through dimensional coupling of the form $\frac{\lambda}{\Lambda^2}$ (which is the case in SUSY models with gravitino dark matter, with Λ the Planck scale). In this case, one obtains

$$\frac{\Omega_X^0 h^2}{0.12}\Big|_{n=12}^{\rm FAR} \sim \frac{\mathscr{B}_{12}}{35.4}\left(\frac{\lambda}{0.1}\right)^2\left(\frac{m_X}{100{\rm GeV}}\right)\left(\frac{\Lambda}{10^{16}{\rm GeV}}\right)^{-4}\left(\frac{M}{1.3\times 10^8{\rm GeV}}\right)^{-4}\left(\frac{T_{\rm RH}}{10^{10}{\rm GeV}}\right)^7, \tag{3.19}$$

and the radiation contribution to the dark matter production is UV-dominated while the inflaton contribution happens at the inflection point to also become UV-dominated, with $\mathscr{B}_{12} \propto \ln(T_{\rm MAX}/T_{\rm RH})$. The dark matter production is therefore happening around the reheating scale.

Now, let us consider the evolution of FIMPs in two scenarios: when the amplitude is constant, as in the case of Eq. (3.17) ("case A", dashed), and for an s-channel exchange of a mediator of mass $M = 10^{12}$ GeV, as in Eq. (3.12) ("case B", solid). In Fig. 3.2, we show how the FIMP relic density varies with time, parametrized by M/T.

In order to consider the production during reheating, we have solved the set of differential equations (Eq. (2.91)), as discussed in the last Chapter *. For reference, we assume the split between the reheating and maximal temperature to be $T_{\rm MAX}/T_{\rm RH} = 100$ and show in

*We have produced this figure with the code developed during my Ph.D. which is written in C++.

light gray the solution for the numbers of inflaton and radiation. Therefore, the reheating scale is of $T_{\rm RH} = 10^{11}$ GeV and $T_{\rm MAX} = 10^{13}$ GeV. The initial condition for dark matter is set to be $N_X^I = 0$ in both cases. We indicate in vertical lines when the temperature equals $T_{\rm MAX}, T_{\rm RH}$ and the case A m_X.

In case A, we have set the FIMP mass to be $m_X = 10^8$ GeV, and since this is the only scale of the process, the relic density is established around that scale even though the freeze-in process starts slowly during the reheating period. As we have estimated, the contribution from production at temperatures $T > T_{\rm RH}$ is negligible whenever the FIMP mass is sufficiently smaller than the reheating scale. We show solutions of the case A for two values of the overall coupling, $\lambda = 10^{-21}$ (dashed red curve) and $\lambda = 10^{-18}$ (dashed blue curve).

In case B, $m_X = 1$ GeV and we can avoid the need for very small overall couplings by assuming a heavy mediator. We have chosen for this figure $\lambda = 10^{-5}$ (solid red curve) and $\lambda = 10^{-3}$ (solid blue curve). Since we have chosen a mediator with mass in the reheating process scale, most of the FIMPs were already produced before the reheating had finished. We can also verify that in this case most of the production takes place around $T_{\rm RH}$, the UV scale of the radiation contribution and IR scale of the inflaton contribution.

As it should be expected, we observe the opposite behavior relative to the freeze-out mechanism: the relic density is larger for larger couplings between dark matter and the sector from which it is produced.

3.3 Searches for dark matter particles

The main ways of searching for dark matter particles were considered in the review on simplified WIMP models whose results are going to be summarized in the next Chapter. We could detect DM particles through *i)* their scattering off nuclei and electrons in underground detectors (direct detection, or DD); *ii)* the products of DM annihilation into SM particles, to be distinguished from the background of known astrophysical sources (indirect detection, or ID); *iii)* their invisible production in colliders and accelerators, to be inferred by conservation of energy.

We end this introductory part of the thesis with the status of DD searches for dark matter. In Fig. 3.3 we see the constraints from a multitude of experiments, in the plane of dark matter mass versus cross sections for scattering off nucleons (upper panel) and electrons (bottom panel). Up to this moment, no unambiguous signal was reported and those are upper bounds on the cross sections. The shaded regions are the current upper bounds and in the yellow region in the left panel, for very tiny cross sections, dark matter would not be easily distinguished from neutrinos. The colored curves are expected bounds, with short, medium and long term future shown respectively in solid, dashed and dotted curves.

Details about these complex but useful plots can be found in Ref. [94], but here we want to emphasize that many WIMP scenarios are already excluded by the current bounds, as we are going to see in the next Chapter, and that an intense phenomenology of FIMPs might happen in a concrete future.

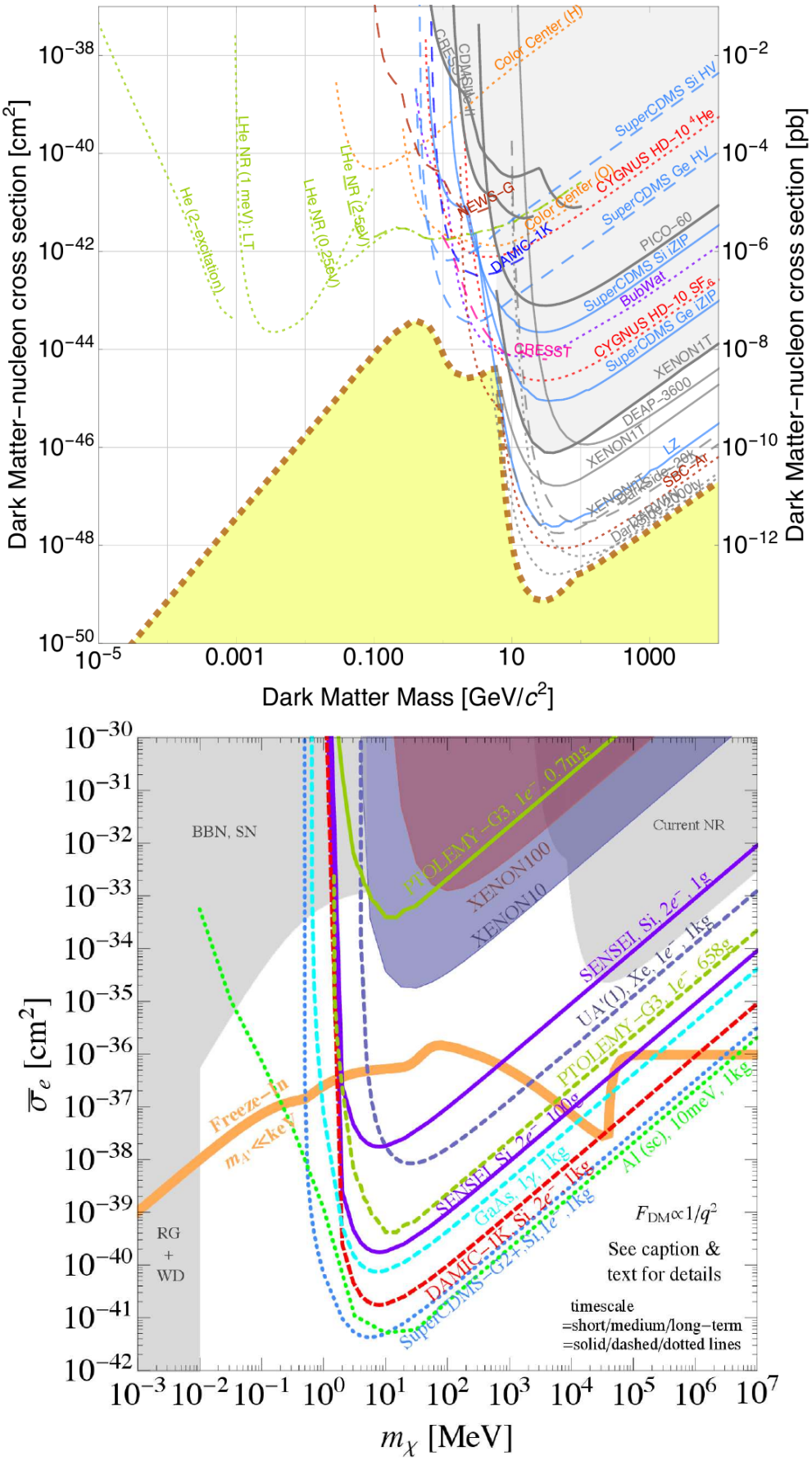

FIGURE 3.3 – *Status of dark matter detection searches, through scattering off nucleon (upper panel) and off electrons (bottom panel). Figure from [94].*

3.4 Discussion and conclusions

In this chapter, we could see that we have a considerable freedom to accommodate beyond standard model particles in such a way to produce the right amount of dark matter. Even though it worth exploring any scenario which could lead to a scientific prediction regarding dark matter particles, one of the reasons making a given possibility more appealing than others might be its ability to relate different open problems in an economic way. Moreover, detecting dark matter might shed some light on otherwise inaccessible phenomena.

With this in mind we turn to the following question: how to understand the tiny interactions needed for the freeze-in production? An appealing answer is that it is the effect of physical processes happening at very high energies in the Universe, since the exchange of heavy particles between two sectors suppresses the overall interaction between them. One important subtlety in this scenario is that, if the masses of those mediators are close to the reheating scale, the Universe expands faster than in the radiation era, due to the contribution of the inflaton for the total energy density. Dark matter would have been produced from the standard model ultra-relativistic particles as soon as they are produced by inflaton decay, *during* the reheating process, provided that the temperature dependence of the production rate is high enough. Nevertheless, well motivated DM models having this feature are under-explored in the literature.

In the freeze-in scenario, the scales providing the relic density of FIMPs within the inferred interval of $\Omega_x^0 h^2 \sim 0.12$ could link the dark matter puzzle to open questions of particle physics and cosmology, such as neutrino mass generation [95], vacuum stability of Higgs [95], hierarchy problem [96], left-right symmetric models [97], leptogenesis [98, 99], grand unified theories [91, 100, 101], quantum theories of gravity [102–104], inflation [105] and baryogenesis [106, 107]. In this thesis, we call such a connection the *FIMP wonder*. We advocate that it is a construction it worth being done from the theoretical side towards a new generation of phenomenological approaches. Indeed, in Refs. [108–111], we see that frozen-in dark matter is already expected to be within the sensitivity of direct and indirect detection, as well as of collider searches in a concrete future.

In the following chapters, we will present our original results.

We will start with an overview of many simplified WIMP models, with special attention to the usually most constraining direct detection bounds. We proceed by considering the usually less constrained low-mass (MeV-scale) regime of the parameter space of WIMPs in the context of an MeV-scale dark photon. In such a case, direct detection bounds join collider and CMB bounds to severely constrain the WIMP parameter space. We will show in which cases such bounds might be alleviated.

After considering the WIMP scenarios, we discuss an ongoing work of a keV-scale FIMP, which might be constrained as a warm dark matter candidate and with a UV completion of reheating scale mediators. We then proceed by exploring the FIMP wonder in three theoretically well-motivated realizations: heavy Z', spin-2 and moduli portals to dark matter.

Chapter 4

Status of simplified WIMP models and a sub-GeV dark photon portal

Contents

The reason why WIMPs are the most considered class of dark matter candidates relies on the fact that their masses and couplings are comparable to the masses and couplings of the standard model (SM) particles. It means that, although the overall interactions between the visible and dark sectors are expected to be weak, our current technology might be able to detect them. In this case, we are already able to constrain the free parameter space of the extensions of the SM accounting for DM particles.

In Section 4.1, we consider a wide variety of models for WIMPs and mediators in the $10 - 1000$ GeV mass range, since we will be focused on direct detection (DD) constraints. In Section 4.2, we explore the low-mass regime (MeV scale) of WIMPs and mediators in a very predictive dark photon model.

4.1 The waning of the WIMP?

Simplified models of dark matter which contain only a dark matter candidate and possibly a mediator field interacting with the dark and visible sectors – the *portal* – are a fair

starting point towards the understanding of what would be the underlying beyond the standard model (BSM) physics of dark matter.

In this work [1], we consider simplified models of WIMPs in a systematic way: scalar (χ), fermionic (ψ) and vector (V) dark matter candidates interact with SM fermions (f) through visible Higgs (H) and neutral vector boson (Z) as well as through dark scalars (S, Σ_f), fermions (Ψ_f) and neutral vector bosons (Z').

The notation regarding the couplings throughout this section is as follows:

- μ_i^j: dimensionful (energy) couplings for particle i to portal j ;
- λ_i^j, η_i^j: dimensionless couplings for scalar and vector i to portal j ;
- V_i^j and A_i^j: dimensionless vector and axial couplings for fermion i to portal j, respectively ;
- g and g_i: SM $SU(2)_L$ and BSM gauge couplings, respectively ;
- ξ: 1/2 for self-conjugated fields (real scalars and vectors, Majorana fermions) and 1 otherwise (complex scalars and vectors, Dirac fermions) .

Our Lagrangians are built following principles of gauge invariance and renormalizability, although in some cases we need to consider effective and/or higher dimensional operators to be embedded in UV completions. We are going to assume extensions of the standard model which do not bring CP-violation, so that all the new couplings are real.

In Ref. [1], we have considered the possibility of WIMPs with direct couplings to standard model fields. This can only be achieved for charged dark matter, and also possibly the mediator, under the standard model gauge group.

We have considered scalar and fermionic singlet WIMPs interacting directly with SM quarks and BSM scalars and fermions carrying SM quantum numbers. The cosmological stability of DM in this case could be ensured by assuming it to be lighter than the mediator and by particular choices of quantum numbers avoiding its decay. The freeze-out in this case would proceed via t-channel exchange of those charged mediators into quarks and co-annihilations would also play a role in the achievement of the relic density. We have found that Majorana WIMPs are the only current viable option, with respect to LUX and collider searches, and will be completely probed by the full run of XENON1T.

The other possibility for a direct coupling between the dark and visible sectors we have considered in Ref. [1] was a DM charged under SM $SU(2)_L$. DM would be the lightest neutral component of its multiplet, with its mass the only free parameter of the so called *minimal DM* model. Since in this case the interactions are usually very efficient, the relic density is usually suppressed unless DM is heavy enough. Interesting effects in such case would be Sommerfeld enhancement [112] and bound state formation [113]. Indirect detection would better probe such scenario [114].

If we construct our Lagrangians without direct couplings of the SM fields with the dark matter or the dark portal, we have the so-called *secluded portals*. Those portals are opened

as an effect of extra fields, or when some symmetry breaks down. This is the case of the mass mixing between the Higgs and a dark complex scalar and of the kinetic mixing between Abelian visible and dark gauge bosons.

In what follows, we summarize our findings regarding visible and dark portals to dark matter, by showing some representative cases of the constrained parameter space. The interested reader will find in Ref. [1] the results for all the models we have considered, along with analytical approximations for scattering and annihilation cross-sections.

4.1.1 SM portals

Let us consider the simplest and most predictive extension of the standard model with only one singlet field as dark matter candidate. The only free parameters in this case are the mass and couplings of dark matter.

For scalar and vector WIMPs which are singlet under the SM gauge group, a direct connection with the SM Higgs doublet would be mandatory. It would be described by the following terms in the Lagrangians:

$$\mathcal{L}_\chi \supset \xi \lambda_\chi^H \chi^* \chi H^\dagger H \quad \text{and} \quad \mathcal{L}_V \supset \xi \lambda_V^H V_\mu V^\mu H^\dagger H \,. \tag{4.1}$$

In the case of a fermionic WIMP, such Higgs portal is not renormalizable and the Lagrangian would contain at least a dimension-5 operator with a BSM unknown UV scale Λ:

$$\mathcal{L}_\psi \supset \xi \frac{\lambda_\psi^H}{\Lambda} \bar{\psi}\psi H^\dagger H \,. \tag{4.2}$$

After the electroweak symmetry breaking (EWSB), the Higgs doublet is expanded as $H = \begin{pmatrix} 0 & \frac{v_h+h}{\sqrt{2}} \end{pmatrix}^T$ in the unitary gauge, with v_h the Higgs vacuum expectation value (vev) and h the redefined Higgs scalar. In this context, the WIMPs receive at least a contribution to their masses with a mass term $m_i \supset v_h \sqrt{\lambda_i^H/2}$ for the scalar and vector cases and $m_i \supset v_h \lambda_i^H/2$ for the fermionic case, with the redefinition $\lambda_\psi^H \to \lambda_\psi^H v_h/\Lambda$ absorbing the UV scale.

The EWSB would also lead to the opening of a Z portal to dark matter, otherwise forbidden by gauge invariance. This could happen through a dimension-6 operator containing $H^\dagger i\overleftrightarrow{D^\mu} H$ * [115], since we have $H^\dagger i\overleftrightarrow{D^\mu} H \supset \frac{g v_h^2}{2 c_W} Z_\mu$, with c_W the cosine of the weak angle. For scalar, fermionic and self-conjugated vector WIMPs, we thus use this operator to

*With this operator we take into account the Hermitian derivative terms $(D_\mu H)^\dagger H \equiv H^\dagger \overleftarrow{D_\mu} H$, so that $H^\dagger i\overleftrightarrow{D^\mu} H = i H^\dagger (D_\mu - \overleftarrow{D_\mu})$ H.

build the Z portal:

$$\begin{aligned}
\mathcal{L}_\chi \supset \lambda_\chi^H \frac{H^\dagger i\overleftrightarrow{D_\mu} H}{2\Lambda^2}\chi^* i\overleftrightarrow{\partial^\mu}\chi \quad &\to \quad \lambda_\chi^Z \frac{g}{4c_W} Z_\mu \chi^* i\overleftrightarrow{\partial^\mu}\chi \\
\mathcal{L}_\psi \supset \frac{H^\dagger i\overleftrightarrow{D_\mu} H}{2\Lambda^2}\bar{\psi}\gamma^\mu(v_\psi^Z - a_\psi^Z\gamma_5)\psi \quad &\to \quad \frac{g}{4c_W} Z_\mu \bar{\psi}\gamma^\mu(V_\psi^Z - A_\psi^Z\gamma_5)\psi \\
\mathcal{L}_V \supset \eta_V^Z \frac{H^\dagger i\overleftrightarrow{D_\nu} H}{2\Lambda^2}\varepsilon^{\mu\nu\rho\sigma}V_\mu V_{\rho\sigma} \quad &\to \quad \eta_V^Z \frac{g}{4c_W} Z_\nu \varepsilon^{\mu\nu\rho\sigma}V_\mu V_{\rho\sigma}\,,
\end{aligned} \tag{4.3}$$

where we have redefined the couplings as $(\lambda, v, a, \eta)_\chi^Z v_h^2/\Lambda^2 \to (\lambda, V, A, \eta)_\chi^Z$. We will discuss the coupling between three vectors in the next chapter (Sec. 5.2).

If the WIMP is a complex vector, we can write a Lorentz invariant coupling to the Z boson as

$$\mathcal{L}_V \supset \eta_V^Z \frac{g}{4c_W}[[VVZ]]\,, \tag{4.4}$$

with the coupling chosen as to match the case of the real vector and

$$[[VVZ]] \equiv i\left(\frac{1}{2}V_{\mu\nu}V^{\dagger\,\mu}Z^\nu - V_{\mu\nu}^\dagger V^\mu Z^\nu + \frac{1}{2}Z_{\mu\nu}(V^\mu V^{\dagger\,\nu} - V^\nu V^{\dagger\,\mu})\right)\,.$$

Annihilation of the WIMP candidates into the visible fermions and gauge bosons take place then via s-channel exchanges of h and Z, while for heavy enough WIMPs the annihilation into h and Z might occur thought the t-channel exchange of dark matter fields. By taking into account all the kinematically accessible SM final states, we show in Fig. 4.1 the contours in agreement with the relic density constraint as inferred by the Planck satellite (red curves) in the two-dimensional (except for the UV scale absorbed in some couplings) parameter spaces of the Higgs and Z portal models. We contrast our parameter space with the current (XENON1T, blue regions) and future (XENON1T-2y and LZ, magenta and purple regions respectively) direct detection bounds (see Fig. 3.3), as well as the collider constraint coming from Higgs and Z decays into invisible states (brown regions).

As we have seen in the previous chapter, the less WIMPs annihilate, the more abundant they are. All the regions bellow the relic curves would therefore overclose the universe, in the sense that the curvature constant would be larger than zero.

A generic feature, which is present in every DM relic density contours (for WIMPs and FIMPs), can be noticed in Fig. 4.1: *whenever the amplitude for DM-SM interaction is enhanced (suppressed), the overall coupling needs to be lowered (raised) as to provide the same relic density value.* We can recognize the big enhancements due to pole regions, when the mediators are produced on-shell and subsequently decay into the SM states. This happens when the WIMP mass is half of the mediator mass, $m_{\rm DM} \sim 62.3$ for the Higgs portal and $m_{\rm DM} \sim 45.5$ for the Z portal. We also notice slight enhancements in the DM-SM interaction when some channel become available: around $m_{\rm DM} \sim 80, 91, 125$ and 173 GeV (W^+W^-, ZZ, hh and $\bar{t}t$) in the Higgs portal case and around $m_{\rm DM} \sim 80, 173$ and 216 GeV ($W^+W^-, \bar{t}t$ and hZ) in the Z portal case. Another generic feature is the need for larger couplings for lighter WIMPs, since less channels are kinematically available and the DM-SM interaction is suppressed.

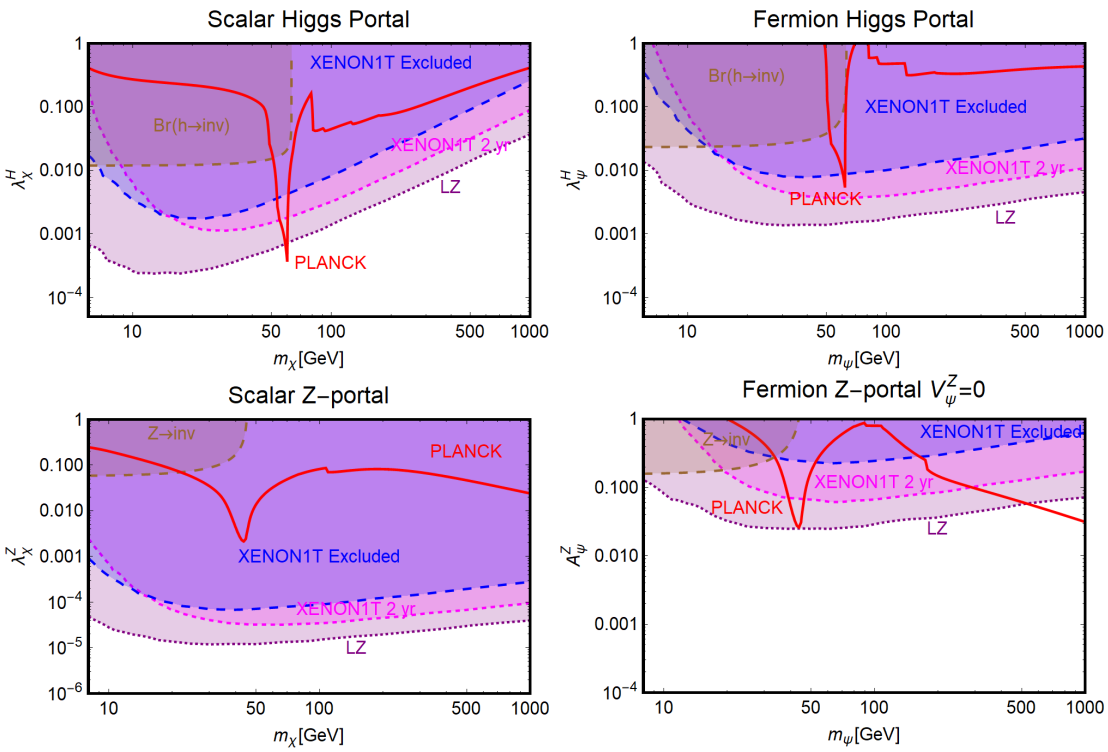

FIGURE 4.1 – *Constraints on the parameter space of the SM portal models, in the case of Higgs portal (upper panel) and Z portal (lower panel).*

In the case of Higgs portal, direct detection would happen via t-channel h exchange between the WIMPs and quarks, which is a SI process. We show in Fig. 4.1 the Higgs portal to a scalar (upper left panel) and fermionic (upper right panel) WIMP. The vector case is similar to the scalar one. We see that apart from the pole region, the Higgs portal is already excluded by the current DD constraint (XENON1T).

For the Z portal, the isospin violating interaction of Z with quarks enhance the scattering cross-section, leading to even stronger DD constraints. However, while the scalar, Dirac and vector (real and complex) WIMP cases are already excluded by XENON1T, the case of a Majorana WIMP is still viable in the pole and high mass regions. This is because the charge-conjugation properties of a Majorana fermion cancels out the contribution of a vector current to the scattering amplitudes [116], weakening the DD bounds.

We now turn our attention to portals with BSM spin-0 and spin-1 fields. Our parameter space is now augmented by at least two free parameters: the mediator mass and a coupling between the mediator and the SM fermions. We show our results in parameter space slices of the mass spectrum $(m_{\rm portal}, m_{\rm DM})$. As we are going to see, the interpretation of the relic density contours is not as obvious as in the case of the SM portals. Nevertheless, we do can recognize which processes are contributing for the establishment of the relic density depending on the relation between the dark matter and mediator masses. A detailed description of the relic density contours we show here can be found in Ref. [1].

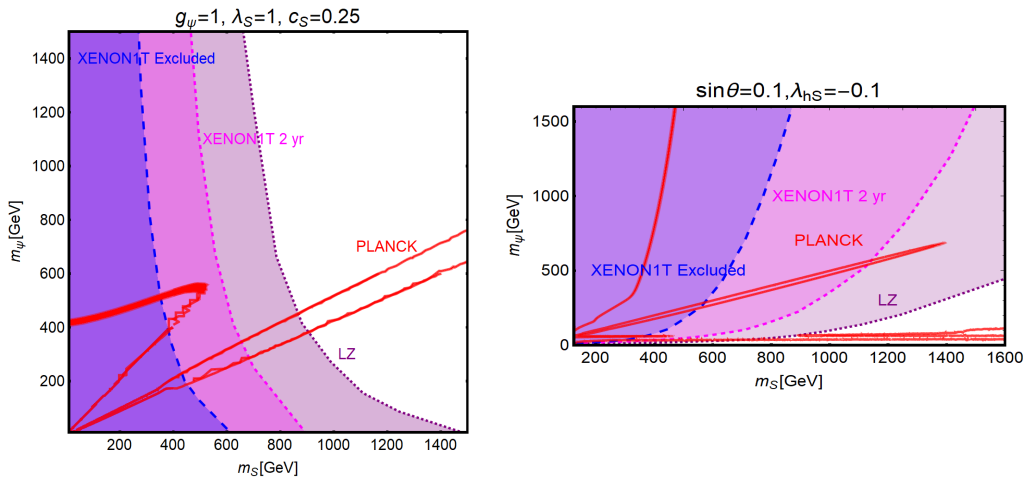

FIGURE 4.2 – *In the left (right) panel, we show the constraints on the parameter space of the BSM spin-0 portal in the absence (presence) of a mix with the Higgs boson, for the fermionic DM candidate.*

4.1.2 BSM Spin-0 portals

New scalars are needed in many SM extensions, usually to provide new mass scales for the BSM particles. Here we will assume that a generic BSM real scalar (S) might couple to the SM fermions through a Yukawa-like interaction:

$$\mathcal{L}_S \supset -\frac{c_S}{\sqrt{2}}\frac{m_f}{v_h}\bar{f}fS - \frac{1}{3!}\lambda_S m_S S^3\,, \tag{4.5}$$

where we also show the usually present trilinear self-coupling (often mandatory by symmetry), as it would lead to an annihilation channel for dark matter.

The s-channel annihilations of the scalar, fermionic and vector WIMPs arise from the following trilinear interactions with the new real scalar:

$$\mathcal{L}_\chi \supset -\xi\mu_\chi^S|\chi|^2 S\,,\quad \mathcal{L}_\psi \supset -\xi g_\psi\bar{\psi}\psi S \quad \text{and} \quad \mathcal{L}_V \supset \frac{\eta_V^S}{2}m_V V_\mu V^\mu S\,. \tag{4.6}$$

In the cases of scalar and vector WIMPs, contact BSM channels might also contribute to the relic density: $\mathcal{L}_\chi \supset -\xi(\lambda_\chi^S)^2|\chi|^2S^2$ and $\mathcal{L}_V \supset \frac{(\eta_V^S)^2}{8}V_\mu V^\mu S^2$ respectively. We assume $\mu_\chi^S = \lambda_\chi^S m_S$ and $m_V = \eta_V^S v_S/2$. The DD constrained parameter space of a fermionic DM interacting with SM fermions through the exchange of a real scalar BSM field is shown in Fig. 4.2 (left panel).

Even if new scalars do not couple directly to SM fermions but only to WIMPs, however, a portal between both sectors would be inevitably opened once both scalars develop vacuum expectation values (vevs). A mass mixing in this case would be allowed (therefore mandatory) by gauge symmetry and it could only be avoided by assuming very small mass mixing angles.

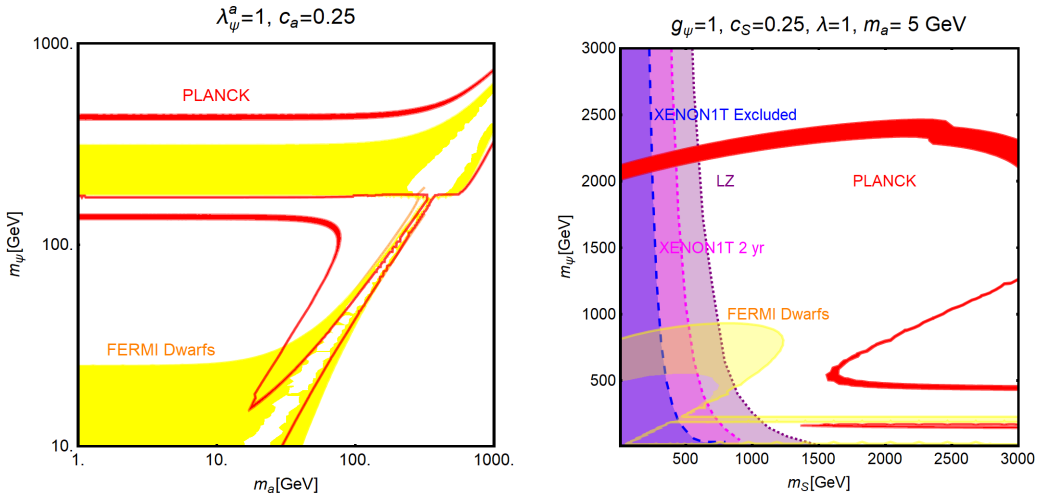

FIGURE 4.3 – *Constraints on the parameter space of the pseudoscalar (left) and scalar+pseudoscalar (right) portal models, for the fermionic DM.*

We therefore consider the global $U(1)$ symmetric Lagrangian containing the interaction of the Higgs and a scalar Φ, singlet under SM group:

$$\mathcal{L} \supset -\lambda_{hS} H^\dagger H \Phi^2 - \mu_\Phi^2 \Phi^2 - \lambda_\Phi \Phi^4 \,. \tag{4.7}$$

If the global $U(1)$ were also spontaneously broken, the new scalar could be expanded as $\Phi = (v_S + S)/\sqrt{2}$, with v_Φ its vev. After diagonilizing the mass matrix of H and Φ, we find the eigenvalues h, S, with a mixing angle θ and the mixing coupling λ_{hS} given by [117]

$$\sin 2\theta = \frac{2\lambda_{hS} v_h v_S}{m_h^2 - m_S^2} \quad \text{and} \quad \lambda_{hS} = s_\theta c_\theta \frac{m_h^2 - m_S^2}{v_h v_S} \,. \tag{4.8}$$

Notice that a heavy enough BSM scalar would close such portal. In Fig. 4.2 (right panel) we show the parameter space of a fermionic WIMP interacting with SM fermions through the exchange of h and S fields, in a case of small mixing $\sin\theta = 0.1$ and $\lambda_{hS} = -0.1$ (since we consider $m_S > m_h$).

In the case of a complex scalar mediator, the WIMP-SM interaction would also be mediated by a pseudoscalar field a. Since we restrict our analysis to CP-invariant interactions, only a fermionic DM would couple to the pseudoscalar. Such possibility is described by the Lagrangian

$$\mathcal{L} \supset -i\lambda^a_\psi \, \bar{\psi}\gamma_5\psi \, a - i\frac{c_a}{\sqrt{2}}\frac{m_f}{v_h}\bar{f}\gamma_5 f \, a \,. \tag{4.9}$$

In this case the scattering cross-section with nucleons is too tiny as to be probed by DD searches, but annihilation into SM fermions might be probed by ID searches (see also [118]). In Fig. 4.3, we show the parameter space of a fermionic WIMP interacting with SM fermions through a pseudoscalar (left panel) and though a scalar+pseudoscalar portal (right panel). We constrain the curves respecting the DM relic density (in red) with the current and expected DD bounds, same color code as in the previous figure. We also show the complementary indirect detection bounds (yellow regions), due to the non-observation

TABLE 4.1 – *Table of couplings between the SM fermions and a Z'.*

	$V_u^{Z'}$	$A_u^{Z'}$	$V_d^{Z'}$	$A_d^{Z'}$	$V_e^{Z'}$	$A_e^{Z'}$	$V_\nu^{Z'}$	$A_\nu^{Z'}$
SSM	$\frac{1}{4}-\frac{2}{3}s_W^2$	$\frac{1}{4}$	$-\frac{1}{4}+\frac{1}{3}s_W^2$	$\frac{1}{4}$	$-\frac{1}{4}+s_W^2$	$-\frac{1}{4}$	$\frac{1}{4}$	$\frac{1}{4}$
E_{6_χ}	0	$-\frac{1}{2\sqrt{10}}$	$-\frac{1}{\sqrt{10}}$	$\frac{1}{2\sqrt{10}}$	$\frac{1}{\sqrt{10}}$	$\frac{1}{2\sqrt{10}}$	$\frac{3}{\sqrt{10}}$	$-\frac{1}{2\sqrt{10}}$
E_{6_ψ}	0	$-\frac{1}{2\sqrt{6}}$	0	$\frac{1}{2\sqrt{6}}$	0	$\frac{1}{2\sqrt{6}}$	$\frac{1}{4\sqrt{6}}$	$-\frac{1}{2\sqrt{6}}$

of gamma-ray fluxes coming from dark matter-dominated Dwarf galaxies, as constrained by the Fermi-LAT satellite [119].

4.1.3 BSM Spin-1 portals

Extra $U(1)$ symmetries, dubbed $U(1)'$, are often present in extensions of the standard model group structure $SU(3)_c \times SU(2)_L \times U(1)_Y$, whether alone, from a phenomenological point of view, or as a consequence of a larger symmetry which was broken. See for instance [120] for a review. The new gauge boson is usually called Z' since their interactions could in principle be chiral.

If the SM fermions are charged under $U(1)'$, the spin-1 portal is opened by the following Lagrangian term

$$\mathcal{L}_{Z'} \supset g' \bar{f} \gamma^\mu (V_f^{Z'} - A_f^{Z'} \gamma_5) f Z'_\mu \,. \tag{4.10}$$

In this case we expect stronger constraints since we would have gauge-like interactions between the spin-1 mediator and SM quarks, which is strongly constrained by colliders.

We consider the spin-1 portal in three realizations. In the first one, we fix the couplings $g', V_f^{Z'}$ and $A_f^{Z'}$ according to the sequential standard model (SSM), where the couplings are the same as the SM ones, with $g' \approx 0.65$. On the other hand, Z' fields are low-scale remnants of breaking patterns in many grand unified theories (GUT) and string inspired models [121–125]:

$$E_6 \to SO(10) \times U(1)_\psi \to SU(5) \times U(1)_\chi \times U(1)_\psi \to G_{\rm SM} \times U(1)_{\theta_{E_6}} \,,$$

where the parameter θ_{E_6} is in the interval $[-90^\circ, 90^\circ]$, with $\theta_{E_6} = 0^\circ$ ($\theta_{E_6} = 90^\circ$) defining the ϕ (χ) model, E_{6_ψ} (E_{6_χ}) [121]. We therefore assign the couplings as in these two GUT-inspired realizations with $g' = \sqrt{5/3}\, g \tan\theta_W \approx 0.46$ [120]. The assignations of the vector and axial couplings we have used are reported in Table 4.1.

The couplings of the scalar, fermionic and vector WIMPs with Z'_μ are equivalent to the case of couplings with Z_μ (Eqs. (4.3) and (4.4)), with the replacement $g/(4c_W) \to g'$.

We have found that the SSM and E_{6_χ} would be completely excluded in case XENON1T do not confirm a WIMP signal in its full run, except for the case of a Majorana WIMP. The case of E_{6_ψ} evades the collider bounds for the three WIMP candidates considered, near the pole region $m_{\rm DM} \sim m_{Z'}/2$. For the fermionic and vector WIMP candidates, the t-channel annihilation cross-section into Z' bosons (in the $m_{\rm DM} > m_{Z'}$ regions of the parameter space) has the velocity dependency contribution proportional to $m_{\rm DM}^2/m_{Z'}^2$,

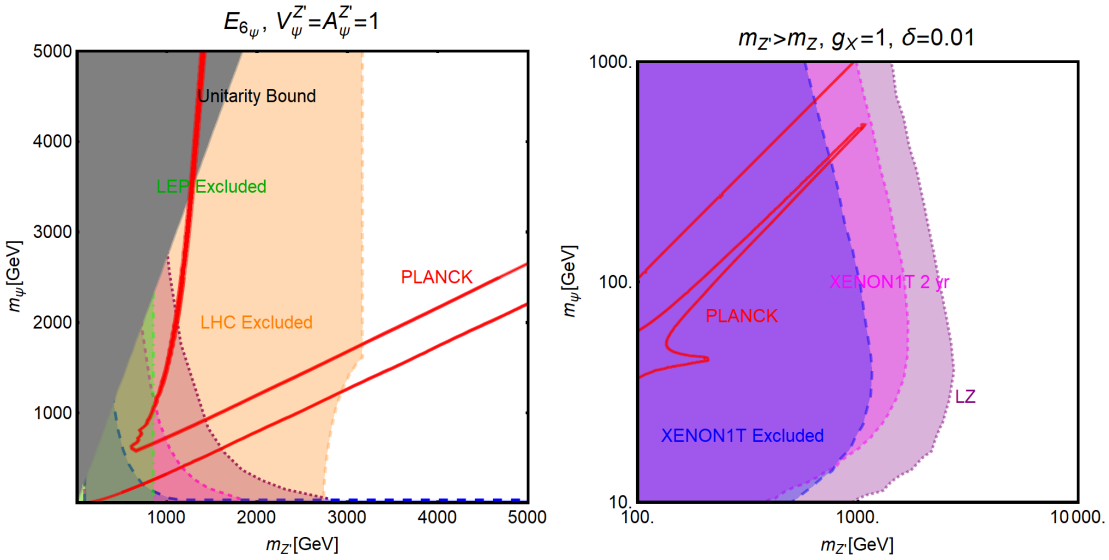

FIGURE 4.4 – *Constraints on the parameter space of the fermionic DM in the Z' portal model, without (left panel) and with (right panel) kinetic mixing between Z and Z'.*

leading to violation of perturbative unitarity which might be cured with the inclusion of new degrees of freedom in a UV completion of the model [126, 127].

In Fig. 4.4 (left panel), we show the parameter space for the fermionic WIMP in the case of the E_{6_ψ} framework. We have found that the constraints from LEP, Tevatron [128, 129] (green exclusion regions) and LHC [130] (orange exclusion regions) are competitive and even stronger than the DD bounds.

Finally, we might think that the bounds would be less restrictive when the standard fermions are not charged under $U(1)'$. However, in the presence of an extra Abelian gauge boson, a new renormalizable term could be present in the kinetic part of the extended Lagrangian and this would lead to a *kinetic mixing* between Z and Z'. After EWSB, a mass mixing would also be allowed and the kinetic mixing would have to be tiny due to precision electroweak constraints. The WIMP annihilation would be therefore suppressed, easily leading to an overproduction of WIMPs. This makes the model in tension with the current bounds, as we can see in the right panel of Fig. 4.4, in which the Z' kinetically mix with the Z boson with a mixing angle of $\delta = 0.01$.

4.2 MeV dark matter complementarity and the dark photon portal

Given the success of the standard model in describing matter fields (fermions) interacting through the exchange of gauge bosons, it is not implausible to suppose that dark matter is charged under a "dark" gauge symmetry. One possibility is to consider a new local $U(1)$ symmetry, $U(1)'$, whose force carrier was dubbed U *boson* [131]. If this gauge symmetry is broken, the U boson becomes massive and in general mixes with the SM hypercharge gauge boson. This is a very appealing possibility from a theoretical point of view, since

it is a renormalizable extension and might be related to supersymmetric completions of the standard model [132, 133], and also from a phenomenological point of view, since it would in general mix with photons which might affect electromagnetic interactions in many detectable ways [134–144].

We now discuss the phenomenology of one realization of such scenario, in which an MeV-scale Dirac fermion, our DM candidate, interact with SM fermions due to a BSM gauge boson which kinetically mixes with the SM photon, the *dark photon* [2].

In this work, we consider the interplay of many experiments looking for dark matter and dark photon in constraining the regions of our parameter space providing the correct relic density for the dark matter. We regard our DM candidate both as WIMP and FIMP.

Our dark matter candidate would be able to generate cosmic rays in the MeV range of the spectrum, which is currently not constrained but that would be probed in the next decade by the proposed e-ASTROGAM (enhanced ASTROGAM) mission, intended to study astrophysical phenomena in the photon energy range of 0.3 MeV - 3 GeV. This satellite would provide an opportunity to infer the presence of DM candidates with mass below ~ 10 MeV. Our work was considered by this mission as one of the many fundamental physics motivations for exploring the sky in this energy range [3].

4.2.1 The dark photon model

In the presence of two fields of the same kind, the gauge invariant Lagrangian has in general a non-canonical kinetic term. Therefore, the gauge sector of the standard model augmented by $U(1)'$ reads in general

$$\mathcal{L}_G = -\frac{1}{4}W^i_{\mu\nu}W^{i\,\mu\nu} - \frac{1}{4}\hat{B}_{\mu\nu}\hat{B}^{\mu\nu} - \frac{1}{4}\hat{U}_{\mu\nu}\hat{U}^{\mu\nu} - \frac{s_\chi}{2}\hat{B}_{\mu\nu}\hat{U}^{\mu\nu}\,, \tag{4.11}$$

where the hat symbols indicate that the kinetic energy matrix of the corresponding field is non-diagonal and s_χ is the sine of the *kinetic mixing* angle χ between such fields. Notice that the $SU(2)_L$ gauge fields are not kinetically affected by the presence of $U(1)'$.

We might regard such kinetic mixing as an effective term generated by the degrees of freedom of an underlying theory, such as fermions charged under both gauge groups or an extended scalar sector giving mass to them [133, 145], rather than a genuine physical phenomenon.

Therefore, from an effective point of view, in order to put this kinetic Lagrangian in the canonical form, we need to rotate and normalize the gauge fields. We can go from the mixed ($\{\hat{B}, \hat{U}\}$) to a canonical ($\{\bar{B}, \bar{U}\}$) basis by performing the non-orthonormal rotation

$$\begin{pmatrix} \hat{B}_\mu \\ \hat{U}_\mu \end{pmatrix} = \begin{pmatrix} 1 & -t_\chi \\ 0 & 1/c_\chi \end{pmatrix} \begin{pmatrix} \bar{B}_\mu \\ \bar{U}_\mu \end{pmatrix} \quad . \tag{4.12}$$

Finally, once the gauge fields acquire mass, there will be a mass mixing between $\bar{B}_\mu$ and $\bar{U}$, which might modify the weak mixing between $\bar{B}_\mu$ and W^3_μ.

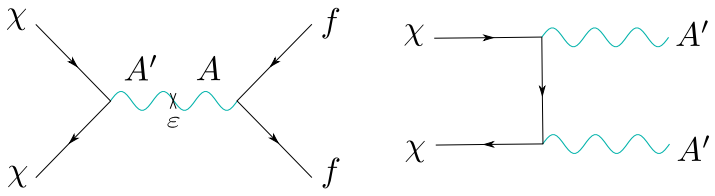

FIGURE 4.5 – *Feynman diagrams of the processes contributing to the production of our dark matter candidate.*

Given that in this context the SM neutral current would be written in terms of $\hat{B}_\mu$, the SM fermions would have an effective charge $t_\chi\, q_f\, e \equiv \varepsilon\, q_f\, e$ under $U(1)'$.

If the U boson is only vectorially coupled to visible (f_i) and dark matter (χ) fermions, it is regarded as a *dark photon* [146], hereafter denoted as A' *:

$$\mathcal{L} \supset \frac{1}{2} M_{A'}^2 A'^2 - \sum_i \overline{f}_i (e q_{f_i} \not{A} + \varepsilon e q_{f_i} \not{A}' + m_{f_i}) f_i - \overline{\chi}(g_D \not{A}' + m_\chi)\chi \,, \tag{4.13}$$

with m_{f_i}, m_χ and $M_{A'}$ respectively the SM fermion, DM and dark photon masses, g_D the coupling between the dark photon and the dark matter, and εe the dark photon coupling with the SM fermions of charge q_{f_i}.

The processes contributing for the establishment of DM relic density, whenever kinematically available, are depicted in Fig. 4.5. If $m_\chi > M_{A'}$, dark matter would mostly produce dark photons through t-channel (right panel), while for $m_\chi < M_{A'}$, the s-channel (left panel) annihilation into SM fermions dominate. In this work we consider only the second case, in which the kinetic mixing parameter plays the central role in the dark matter phenomenology, allowing us to explore the rich interplay of independent searches for dark photons.

The squared amplitude which is going to be important for us is therefore given by

$$|\mathcal{M}|^2_{\chi\chi\leftrightarrow ff} = \frac{16}{3}(\varepsilon e q_f g_D)^2 \left(1 + \frac{2m_f^2}{s}\right)\left(1 + \frac{2m_\chi^2}{s}\right) \frac{s^2}{(s - M_{A'}^2)^2 + M_{A'}^2 \Gamma_{A'}^2} \,, \tag{4.14}$$

where the total width of the dark photon is given by

$$\Gamma_{A'} = \frac{M_{A'}}{4\pi}\left[\sum_i (\varepsilon e q_{f_i})^2 \left(1 + \frac{2m_{f_i}^2}{M_{A'}^2}\right)\sqrt{1 - \frac{4m_{f_i}^2}{M_{A'}^2}} + g_D^2 \left(1 + \frac{2m_\chi^2}{M_{A'}^2}\right)\sqrt{1 - \frac{4m_\chi^2}{M_{A'}^2}}\right] . \tag{4.15}$$

Since we are going to consider dark matter masses in the range $10 - 100$ MeV, the SM fermions are just electrons.

*Notice that U bosons with both vector and axial couplings are also denoted as Z' in the literature, since they are usually heavy.

4.2.2 Dark matter production: freeze-out and freeze-in

The evolution of our dark matter candidate is governed by the following equation (see Eq. 2.124):

$$-\frac{T}{g_s^*}\frac{dY_\chi}{dT} = Y'_A \frac{B_\chi \Gamma_{A'\to\chi\chi}}{H}\left(1-\frac{Y_\chi}{Y'_A}\frac{n_\chi\langle\Gamma_{\chi\chi\to A'}\rangle}{\Gamma_{A'\to\chi\chi}}\right) + Y_f \frac{n_f\langle\sigma v\rangle}{H}\left(1-\frac{Y_\chi^2}{Y_f^2}\right), \tag{4.16}$$

where $\langle\Gamma_{\chi\chi\to A'}\rangle$ is the distribution averaged inverse decay rate, as given in Eq. (2.43) and $\langle\sigma v\rangle$ is the thermally averaged annihilation cross-section, since the SM fermions are in thermal equilibrium between themselves.

Hereafter we assume that the dark photons have already decoupled from the thermal bath, so that $Y'_A \ll Y_f$ and we can neglect the first term of the equation above. As we have discussed in the previous chapter, the strength of the couplings between the dark and visible sectors provides the initial conditions which determines the production mechanism: if $Y_\chi^I = Y_\chi^{eq}$, we are in the freeze-out regime, and if $Y_\chi^I \ll Y_f = Y_\chi^{eq}$, we are in the freeze-in regime. The interaction rates read respectively

$$\begin{aligned} R_{\rm FO}(T) &= (n_\chi^{\rm eq})^2\langle\sigma v\rangle_{\rm ann}\left(1-\frac{Y_\chi^2}{(Y_\chi^{\rm eq})^2}\right) \\ R_{\rm FI}(T) &= n_f^2\langle\sigma v\rangle_{\rm prod} \end{aligned} \tag{4.17}$$

As expected by the balance equation,

$$\begin{aligned} (n_\chi^{\rm eq})^2\langle\sigma v\rangle_{\rm ann} = n_f^2\langle\sigma v\rangle_{\rm prod} = \\ = \frac{T}{32(2\pi)^6}\int ds\sqrt{s}K_1\Big(\frac{\sqrt{s}}{T}\Big)\sqrt{1-\frac{4m_\chi^2}{s}}\sqrt{1-\frac{4m_f^2}{s}}\int d\Omega|\mathcal{M}|^2\,, \end{aligned} \tag{4.18}$$

where $\langle\sigma v\rangle_{\rm ann} = \langle\sigma v\rangle_{\chi\chi\to ff}$ and $\langle\sigma v\rangle_{\rm prod} = \langle\sigma v\rangle_{ff\to\chi\chi}$.

It is useful to have an analytical approximation for the thermally averaged annihilation cross section to also facilitate the understanding and interpretation of the bounds we will discuss further. In the limit $m_f^2 \ll m_\chi^2 \ll M_{A'}^2$, i.e. when the dark matter annihilation into pairs of fermion via the s-channel exchange of the dark photon is non-resonant, $\langle\sigma v\rangle_{\rm ann}$ scales as

$$\langle\sigma v\rangle_{\rm ann} \sim \frac{(g_D\varepsilon e)^2\, m_\chi^2}{M_{A'}^4}\,. \tag{4.19}$$

Therefore, if an experiment places a model-independent bound on $\langle\sigma v\rangle_{\rm ann}$, we can interpret such limit in the ε vs $M_{A'}$ plane for a fixed dark matter mass. Furthermore, this constraint should weaken with the dark photon mass. This feature will clearly be noticed in Figs. 4.8-4.10. Moreover, we are going to see that a very important region in the parameter space lies near resonance, when $M_{A'}^2 \sim s \sim 4m_\chi^2$ ($M_{A'} \sim 2m_\chi$).

In our numerical results regarding χ as WIMPs, we use the freeze-out approximation, Eq. (3.5), integrating over $\langle\sigma v\rangle_{\rm ann}$ as given in Eq. (4.18) with the squared amplitude of

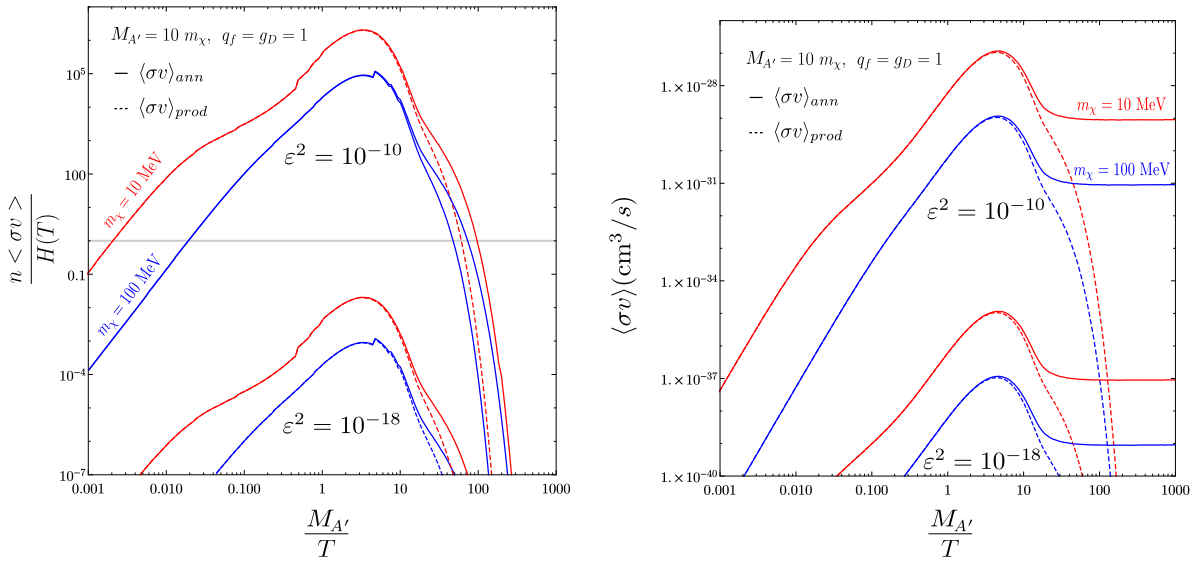

FIGURE 4.6 – *Left: Ratio of the frequency of interactions to the frequency of expansion for a set of parameters of interest. For $\varepsilon^2 \lesssim 10^{-15}$ DM is never thermalized with SM fermions and could be produced via freeze-in. Right: Evolution of the averaged annihilation and production cross-sections.*

Eq. (4.14). All the relic density computation in this work was performed with the numerical package CUBA [147].

In the freeze-in case, the relic density might in principle depend on the high energy scale from which we start the integration. However, since we consider here a reheating temperature that is $T_{\rm rh} \gg$ MeV, our results are not significantly affected by such an uncertainty *. Interestingly, as pointed out in [148], it is possible to constrain dark matter physics through its dependence on the reheating temperature by using CMB observables.

In Fig. 4.6 we compare the freeze-out and freeze-in production regimes. In the left panel we show the ratio of the frequency of interactions and the Hubble rate, $n\langle\sigma v\rangle(T)/H(T)$, as a function of $M_{A'}/T$, for different choices of the kinetic mixing coupling and dark matter mass. We highlight that in the freeze-out scenario, it is usual to work with the thermal annihilation cross section, which is $\langle\sigma v\rangle_{\rm ann} = R_{\rm FO}(T)/n_{\rm eq}^2$. Since both $R_{\rm FO}(T)$ and $n_{\rm eq}(T)$ decreases for $T \lesssim T_f$, the annihilation cross section becomes constant after the thermal decoupling. For the freeze-in scenario, we work instead with the production cross-section $\langle\sigma v\rangle_{\rm prod} = R_{\rm FI}(T)/n_f^2$. Since n_f is constant for $m_f < T < T_f$, $\langle\sigma v\rangle_{\rm prod}$ decreases after decoupling. We illustrate this in the right panel of figure 4.6.

Additionally, Fig. 4.6 shows that the maximal production rate occurs near resonance. To check consistency, we have estimated a rough upper bound on the kinetic mixing to be

*As we have discussed, this assumption has no experimental footing and the larger temperature of the radiation era could have been $\mathcal{O}$(MeV) as to agree with BBN [74]. Relaxing this assumption only means that we must consider the dark matter evolution as discussed in detail in the previous chapters.

within the freeze-in regime:

$$\varepsilon^2 < 7.4 \times 10^{-16} \left(\frac{g_e}{10}\right)^{1/2} \left(\frac{M'_A}{GeV}\right) \frac{r_f K_2(\sqrt{r_f}x)x^2}{(1+2r_f)\sqrt{1-4r_f}K_1(x)}, \tag{4.20}$$

where $x \equiv M'_A/T$ and $r_f \equiv m_f^2/M_{A'}^2$. For $M'_A \sim 100$ MeV, $g_e \sim 20$ and by considering electrons, $r_f \sim 10^{-5}$. Considering the maximum of the rate at $x \sim 3$, we find $\varepsilon^2 \lesssim 5 \times 10^{-15}$.

4.2.3 Experimental bounds on MeV dark matter

Our dark matter candidate would have an effective interaction with the photons, and is therefore called a "milicharged" dark matter. As we have discussed in the introduction, DM particles need to be neutral enough as to agree with observations ranging from galactic to cosmological scales. In particular, the spectrum of the cosmic microwave background (CMB) might constrain the possible injection of energy into the thermal bath from dark matter annihilation. Besides providing the interval for the dark matter relic abundance, the Planck collaboration precise measurements of the anisotropies in the CMB spectra [36, 128] renders competitive bounds on dark matter annihilation and decays between the recombination and reionization periods ($1100 < z < 10$). This is because annihilation and decay products might inject energy into the thermal bath, which might enlarge the surface of last scattering or increase the electron ionization fraction. See for instance [149] for a detailed discussion on the physical processes involved in decays and scatterings (s-wave and p-wave) of dark matter producing electrons, positrons and photons.

The energy per time per volume injected in the medium by DM is of course proportional to its annihilation cross-section and abundance, but only a fraction of it will be actually deposited in the medium. This is parametrized by the efficiency function $f(z)$:

$$\left.\frac{dE}{dt\,dV}\right|_{\rm dep}(z) = f(z)\frac{\langle\sigma v\rangle}{m_\chi}\rho_{cr}^2\Omega_\chi^2(1+z)^6 \equiv f(z)\left.\frac{dE}{dt\,dV}\right|_{\rm inj}(z)\,. \tag{4.21}$$

The efficiency function $f(z)$ was carefully computed in [150] and recently shown to be redshift-independent with a good precision, being rather an effective efficiency factor $f_{\rm eff}$ [151, 152].

This efficiency factor depends on the *energy spectra*, the number of final states f per dark matter annihilation as a function of energy, dN/dE^f, and can be computed numerically with Pythia or PPPC4DM [153, 154]. In our model, the final states are electron-positron pairs and photons resulting from final state radiation. We also need to account for the individual efficiency functions of the electron-positron pairs and photons, labeled $f_{\rm eff}^{e^+}$ and $f_{\rm eff}^{\gamma}$ respectively. They simply quantify how much these particles perturb the ionization history of the Universe as a function of energy and were obtained using the code from Ref. [151]. Having these quantities at hand, we can compute the overall efficiency factor, $f_{\rm eff}$, by integrating over energy [151]:

$$f_{\rm eff} = \frac{1}{2m_\chi}\int_0^{m_\chi} EdE\left(f_{\rm eff}^{\gamma}(E)\frac{dN}{dE^\gamma} + 2\, f_{\rm eff}^{e^+}(E)\frac{dN}{dE^{e^+}}\right),$$

where the factor 2 appear to account for electrons and positrons.

All the information about the model is therefore contained in an effective *annihilation parameter*, $P_{\rm ann} \equiv f_{\rm eff}\langle\sigma v\rangle/m_\chi$, which is currently constrained by Planck to be [36]

$$P_{\rm ann} < 3.2 \times 10^{-28}\,{\rm cm}^3\,{\rm s}^{-1}\,{\rm GeV}^{-1}\,. \tag{4.22}$$

At the time of our work, we used the available limit of $P_{\rm ann} < 4.1 \times 10^{-28}\,{\rm cm}^3\,{\rm s}^{-1}\,{\rm GeV}^{-1}$ [155].

In the left panel of Fig. 4.7, we show the thermal average of direct annihilation of dark matter into pairs of electron-positron as a function of dark matter mass. The red region indicates where the value of the cross-section would give an unacceptable injection of electron-positrons during recombination, as measured by the Planck satellite and inferred in Ref. [151]. More specifically, the bounds we are going to use is of $\langle\sigma v\rangle < 5.18 \times 10^{-30}\,{\rm cm}^3\,{\rm s}^{-1}$ for $m_\chi = 10$ MeV and $\langle\sigma v\rangle < 5.65 \times 10^{-29}\,{\rm cm}^3\,{\rm s}^{-1}$ for $m_\chi = 100$ MeV. The bounds on the process $\chi\chi \to 4e$ would be comparable [151], but this secluded regime would be suppressed by the factor $\epsilon^4 \times g_D^2$ and we will not consider here.

The annihilation of dark matter into electron, positron and photons could also lead to excesses, relative to the known astrophysical background, in cosmic ray fluxes measured by satellites and telescopes. The bounds posed from the study of the CMB spectrum can be therefore complemented with indirect detection searches for dark matter. Interesting studies in the energy range relevant for MeV-GeV gamma-ray indirect detection have been presented e.g. in Refs. [156–163]. However, the experimental bounds on this range is not yet developed. The e-ASTROGAM proposal is anticipated to fill this gap [164]. It would be a space observatory comprised of a silicon tracker, a calorimeter and an anti-coincidence system, sensitive to photons in the energy range from 0.3 MeV to 3 GeV. If accepted, it is expected to be launched in 2029. That said, Ref. [165] performed a dedicated sensitivity study of the e-ASTROGAM mission to MeV dark matter, which we use here to complement the CMB bound on annihilation of dark matter into pairs of electron-positron. In Fig. 4.7 (purple region in the left panel), we see that e-ASTROGAM can potentially discover dark matter for masses below 10 MeV, while offering a complementary and important probe for larger dark matter masses.

In the previous chapter, we have summarized the status of direct detection (DD) searches for dark matter. The DD of an MeV dark matter is challenging but possible [166, 167]. In particular, the strongest limits on MeV dark matter scattering off electrons stems from the XENON10 and -100 experiments [108, 168, 169]. These model-independent bounds can be interpreted in terms of the dark photon model we consider knowing that the dark matter-electron scattering cross section reads

$$\sigma_e = \frac{16\pi\mu_{\chi e}\alpha\varepsilon^2\alpha_D}{M_{A'}^2 + \alpha^2 m_e^2}\,, \tag{4.23}$$

where α is the fine-structure electromagnetic constant, $\alpha_D = g_D/4\pi$, and $\mu_{\chi e}$ is the dark matter-electron reduced mass. For a given dark matter mass $\mu_{\chi e}$ is determined and one can thus translate the experimental bound on σ_e into a bound on the ε vs $M_{A'}$ plane.

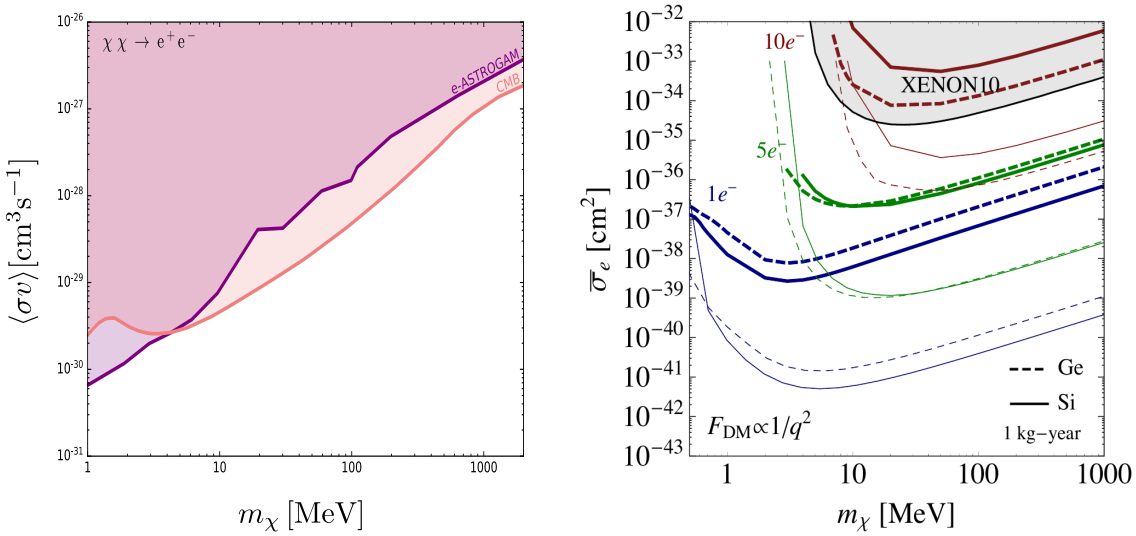

FIGURE 4.7 – *Left: Upper bounds on the thermally averaged annihilation cross section, from CMB [151] and prospects from e-ASTROGAM [165] on the channel $\chi\chi \to e^+e^-$. Right: Upper bounds on DM scattering off electrons as function of dark matter mass (Figure from [108]).*

4.2.4 Constrained parameter space

We can now show our results regarding the viability of our model.

Let us first regard our dark matter candidate as a WIMP. In this case, there is a rich current and expected phenomenology to be explored. In the following figures of this chapter, we constraint the curves providing the inferred relic density of WIMPs (in turquoise) with the previously specified DD (red hatched exclusion regions) and ID (purple hatched exclusion regions) bounds. We remind the reader that we are concerned here with the direct annihilation ($M'_A > m_\chi$) of dark matter into electrons, positrons and photons between recombination and reionization, highly dependent on the kinetic mixing parameter. This is why the bounds from the CMB here do not apply to the secluded regime. We complement those bounds with the results of a bunch of searches for dark photons. The gray regions represent current limits from BaBar [170], muon $g-2$ [171], E787/E949 [172–174] and NA64 [175] ranging from accelerators to colliders as reviewed in [94, 176]. The colored dashed lines account for projected sensitivities of a multitude of experiments such as NA64, LDMX, BELLE II etc [177–181].

In Fig. 4.8 we summarize the results for $m_\chi = 10$ MeV. In the left (right) panel we exhibit the limits for $g_D = 0.1$ ($g_D = 1$). From Fig. 4.7, we see that in this case e-ASTROGAM and CMB bound the DM annihilation into $e^\pm$ nearly in the same way. One can easily notice that the relic density curve is completely immersed in the exclusion region of the e-ASTROGAM/CMB probes for $g_D = 0.1$, whereas there is a small space for $g_D = 1$ that will be probed in the next generation of NA64 and LDMX.

Since the relic density in this case is produced by the freeze-out mechanism, all the regions below the turquoise lines provide an overabundant WIMP candidate. As we have discussed in some detail in Chapter 2, such overproduction might not be correct if, *after*

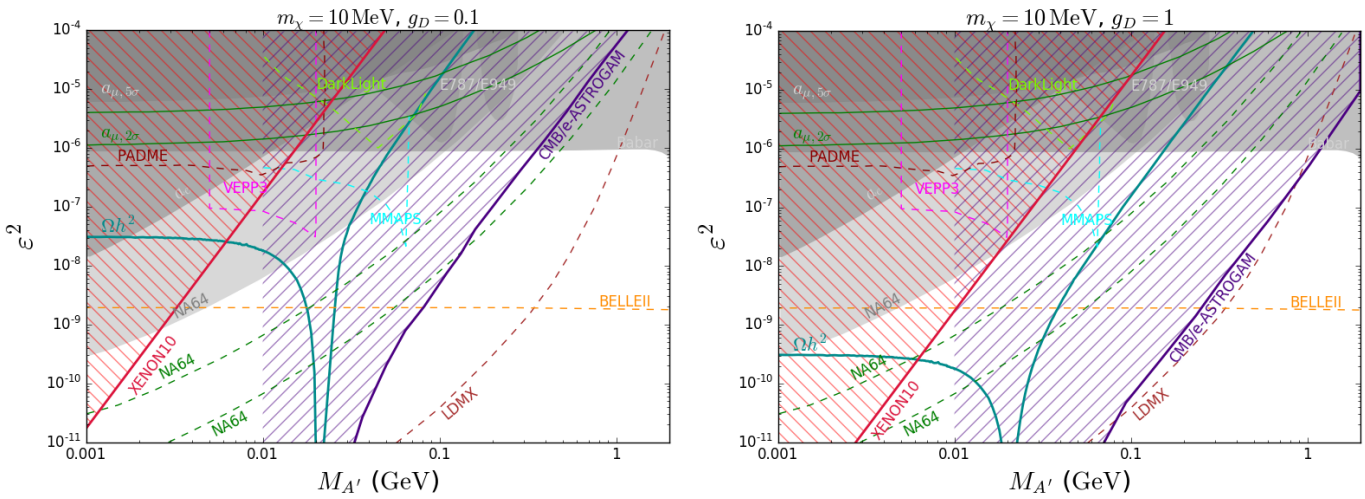

FIGURE 4.8 – *Bounds on the dark photon parameter space, for DM mass $m_\chi = 10$ MeV and dark coupling set as $g_D = 0.1$ (left panel) and $g_D = 1$ (right panel). We constrain the relic density curve (turquoise) with bounds from CMB, to be nearly probed by e-ASTROGAM (purple hatched region), DD (red hatched region), as well as current (gray regions) and expected (colored lines) dark photon searches.*

the DM freeze-out, some heavy field had dominated the Hubble rate in the early universe and subsequently decayed. In such a case, the relic density curves displayed in Fig. 4.8 would have to be corrected by the dilution factor Δ: $\Omega^0_\chi h^2 \to \Omega^0_\chi h^2/\Delta$. As we are going to show now, such a dilution might bring the relic density curves to viable regions of the parameter space. We regard the dilution factor Δ as a free parameter, having in mind that it is completely determined by the physics of the heavy decaying field and the total entropy before its decay. We should also have in mind a possible tension with BBN though [182]. That said, we cannot discuss the dilution factor for 10 MeV dark matter because the freeze-out would occur at BBN.

In the Fig. 4.9 we present the current bounds on the scenario for $m_\chi = 100$ MeV with $g_D = 0.1$ (left panel) and $g_D = 1$ (right panel). For $g_D = 0.1$, we see that $\Delta \gtrsim 10$ is needed to find a region of parameter space yielding the correct relic density while simultaneously obeying experimental limits. It is interesting to see that accelerators provide a complementary probe for MeV dark matter. Indeed, for $g_D = 1$, direct detection is very restrictive for $M_{A'} < 50$ MeV, accelerators for $\Delta \gtrsim 100$, and indirect detection for $M_{A'} > 100$ MeV. In this case, a 100 MeV dark matter could be perfectly consistent with all existing bounds with no need for non-standard cosmology.

In summary, in light of existing constraints only for a small region of parameter space we can accommodate an MeV dark matter candidate based on thermal production of dark matter and standard cosmology.

It is nonetheless important to have in mind prospects for MeV dark matter in the dark photon portal. To illustrate that, we display in Fig. 4.10 projected DD limits from SuperCDMS [183, 184] following the receipt given in [108]. We notice that a SuperCDMS-like detector is very important and might detect MeV dark matter, covering a large region of the parameter space of the model where a correct relic density is achieved either via

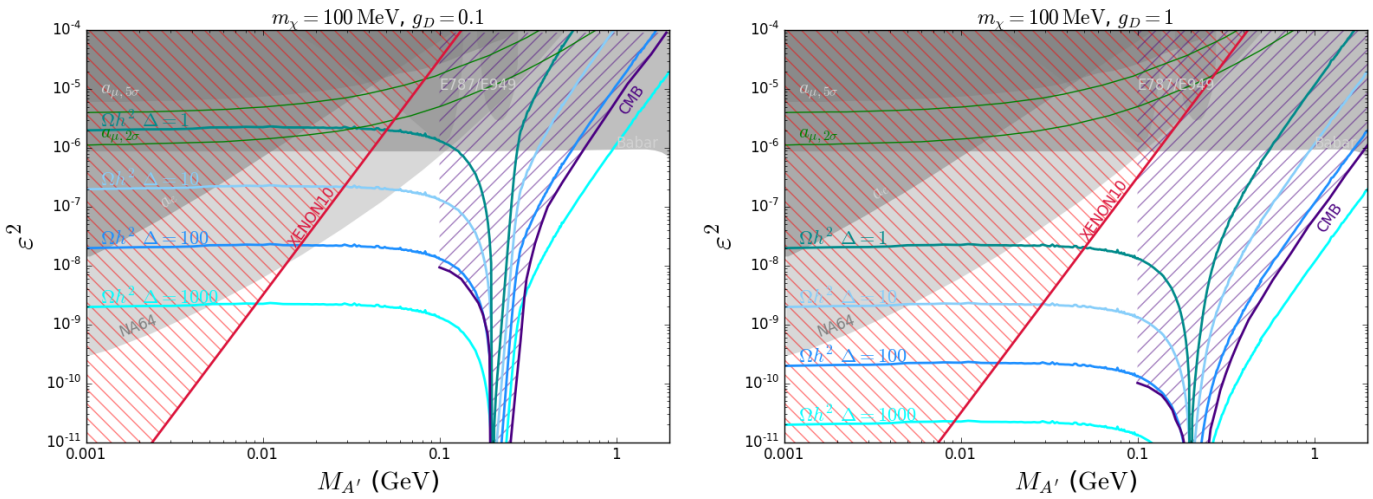

FIGURE 4.9 – *Current bounds on the dark photon parameter space, for DM mass $m_\chi = 100$ MeV and dark coupling set as $g_D = 0.1$ (left) and $g_D = 1$ (right). The relic density curves (bluish lines) account for different dilution factors ($\Delta = 1, 10, 100, 1000$). Same color code as Fig. 4.8.*

thermal production or intermediate reheating. It is exciting to see that such experiments can almost fully test the model, whether or not we assume the intermediate reheating process.

We now turn our attention to the case in which our dark matter candidate is a FIMP, produced from SM fermions through s-channel exchange of dark photons without having shared a thermal bath with them.

As we have seen, in order to fulfill the conditions of a freeze-in production, the kinetic mixing parameter has to be small enough, blinding the direct and indirect searches regarding this scenario. Nevertheless, we can pursue possible ways of detecting the effects of a FIMP, as we do in what follows.

Any weakly interacting light species that can be produced in a supernova event can potentially affect the energy loss and thus the luminosity of a supernova episode [185]. Since the neutrino observation from SN1987A [186, 187] strong limits have been imposed on new light particles such as axions and dark photons [188–191]. In our case, these new dark photons could be emitted in the channels like $p+p \to p+p+A'$ and $p+n \to p+n+A'$ via bremsstrahlung and also via pion emission for the second case. These emissions alter the energy loss of the supernova, which can be expressed in terms of the luminosity in the emitted light particle. The maximum energy loss ϵ_A permitted by the SN1987A observation is given by [192],

$$\epsilon_A = \frac{L_A}{M} \sim 10^{19}\,\frac{\text{erg}}{\text{g.s}}\,, \tag{4.24}$$

where M is the supernova mass and and L_A its luminosity. This constraint imposes a lower limit on the ε parameter. However, for large ε the dark photon could decay before having left the supernova core or get trapped and thermalize, which effectively produces an upper limit on ε for which constraints are effective [188]. In short, we find that supernova physics does not constrain the relic density curve of our model as one can

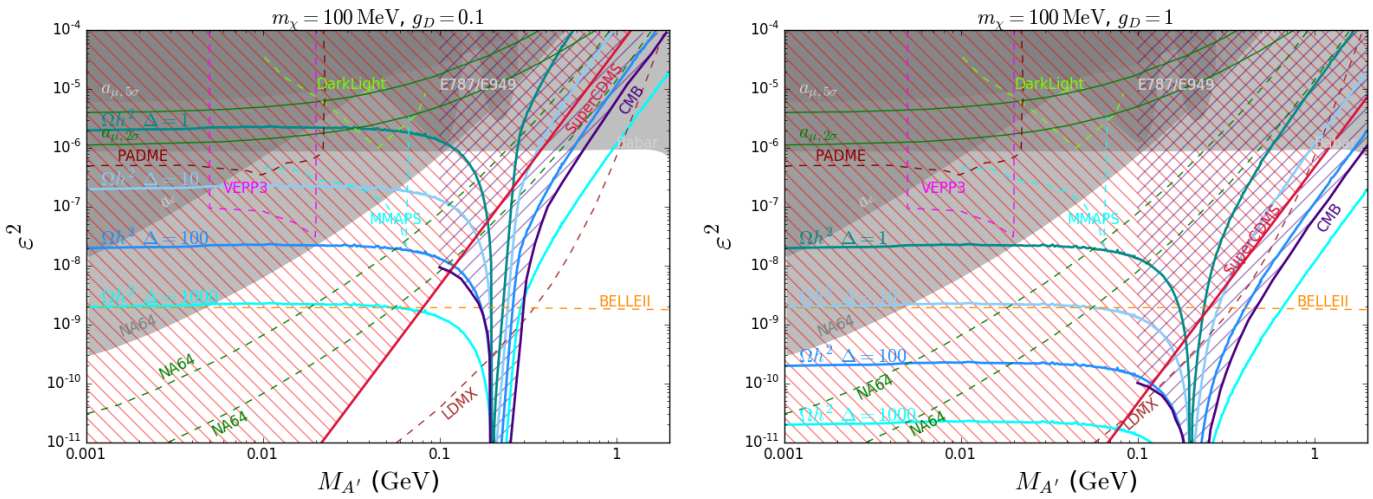

FIGURE 4.10 – *Current and prospect bounds on the dark photon parameter space, for DM mass $m_\chi = 100$ MeV and dark coupling set as $g_D = 0.1$ (left panel) and $g_D = 1$ (right panel). Same color code as Fig. 4.9.*

observe in Fig. 4.11. SN bounds, however, are still subject to study as we can read in Ref. [193] (which could probe our freeze-in scenario).

Big Bang nucleosynthesis constraints arising due to the cascade reaction induced by a very long lived dark photon are not directly applicable to our model either, because our dark photon decays into dark matter [194].

Hence, one can successfully produce MeV DM via freeze-in in the dark photon portal escaping most phenomenological constraints, unlike the thermal equilibrium case discussed above. This fact is clearly visible in Fig. 4.11 where the contours for $\Omega^0_\chi h^2 = 0.12$ are free from constraints, for dark matter masses either 10 MeV or 100 MeV. As shown in Ref. [109], though, such FIMP scenario is already probed by XENON1T for a $1-50$ GeV dark matter mass and will be probed by LZ for dark matter mass in the range of $15-4000$ GeV.

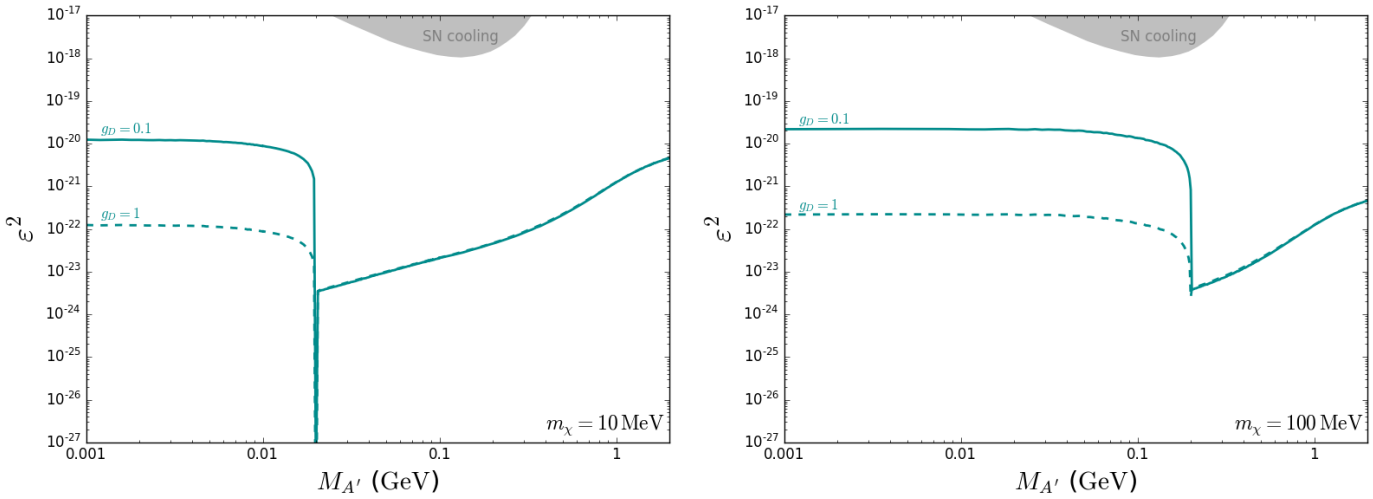

FIGURE 4.11 – *Parameter space of the dark photon in our freeze-in scenario of dark matter production, for DM masses of $m_\chi = 10$ MeV (left panel) and $m_\chi = 100$ MeV (right panel) and $g_D = 0.1$ (solid curves) and $g_D = 1$ (dashed curves). The turquoise curves provide the correct relic density. The gray regions stand for the bounds from Supernovae cooling.*

4.3 Discussion and conclusions

In this chapter we could explore the rich complementarity of experiments looking for WIMPs and BSM states in general.

We have discussed the main results of an extensive review of simplified WIMP models, mainly constrained by direct detection searches (LUX, XENON1T and future LZ, XENON1T 2y) and complemented by colliders (LHC, LEP) and indirect detection searches (FERMI). We found that the majority of the considered WIMP set-ups is ruled out, although BSM spin-0 portals (scalar and pseudoscalar) for any DM candidate and spin-1 portals (SM and BSM) with a Majorana fermion DM are still viable.

One way to avoid those strong constraints, which are for the $10-1000$ GeV DM mass range, is to consider lighter dark matter candidates. Achieving the relic density for light dark matter, though, is challenging in the freeze-out mechanism, since the final states of DM annihilation gets restricted. Light mediators, however, might enhance such annihilations and lead the relic density to acceptable ranges.

We have considered a gauge extension of the standard model with light (MeV-scale) dark matter and mediator, a dark photon. We have found that precise measurements of the CMB temperature and polarization power spectra leave small window for the thermal production of our DM candidate, a Dirac fermion. However, we have also found that this scenario would be partially in agreement with the experimental bounds if some heavy field had decayed during the radiation era, after DM decoupling. As we have discussed previously, such phenomenon could be even inevitable if there exist BSM physics in the $1 - 10^{19}$ GeV energy scale in the universe.

It is interesting to notice a generic conclusion of this chapter. Viable regions of our WIMP parameter space would depend on the presence of additional beyond the standard model

fields. For the WIMPs in the $10 - 1000\,\mathrm{GeV}$ mass range, considering mediators in that scale alleviate the current bounds. In the dark photon model featuring an MeV-scale WIMP candidate, most of the viable region would actually depend on the presence of an additional MeV-scale field, not just on the dark photon. Such additional field did not need to play a role in the freeze-out process. Such conspiracy would not alarm the particle physics community, though, given the multitude of arguments to expect the presence of BSM fields in the early universe.

Very heavy non-standard fermions charged under the dark and standard $U(1)$ symmetries would generate tiny kinetic mixing between the dark and standard photons. In this case, dark matter would never achieve thermal equilibrium with the visible sector. We have found that the freeze-in production of the fermionic dark matter through such dark photon portal is possible and currently viable.

Actually, the dark photon portal itself is a particular case of a "U portal", which appear in GUT-inspired extensions of the standard model. In what follows, we take this lesson as a motivation to develop models where the dark matter is produced through heavy mediators, in the context of the freeze-in mechanism.

Chapter 5

Heavy fermions portals to dark matter

Contents

Here starts our study on what we have called the FIMP wonder – the connection between the tiny couplings necessary to seclude dark matter from the thermal bath of standard model particles with physics at the intermediate scale ($10^{10} - 10^{16}$ GeV).

We keep the same philosophy used to approach the WIMP paradigm, *i.e.* we develop minimal scenarios, but this time aiming to directly connect the origin of dark matter with high-energy processes occurring in the early universe. From now on, we will consider the dark matter production from standard model fields in the symmetric phase of the standard model (SM), above the electroweak symmetry breaking (EWSB).

Heavy nonstandard fermions are present in the spectrum of many beyond the standard model (BSM) scenarios accounting for instance for the generation of the tiny neutrino masses [195, 196]. In this chapter, we study effective secluded BSM spin-0 and spin-1 portals. In Section 5.1, we present the first case, in which dark matter is the pseudoscalar component of a complex field featuring a global $U(1)$ symmetry whose breaking generate the mass of the heavy BSM fermions. The second scenario is presented in Section 5.2, with a local $U(1)$ symmetry under which the BSM fermions and dark matter candidates are charged. In both cases, by assuming that the heavy BSM fermions are charged under SM groups, we can generate a tiny effective connection between the dark and visible sectors, whose possible gauge invariant realizations are further discussed.

5.1 Dynamical freeze-in of a keV dark matter

In the work (in progress) we are going to discuss now [7], we propose a dynamical explanation for the freeze-in production of a dark matter candidate with mass in the keV range. Guided by a minimal model perspective, we assume that a set of heavy nonstandard fermions carry standard hypercharge and acquire mass from a SM singlet scalar field, after the breaking of a global $U(1)$ symmetry. Since global symmetries are expected to be broken at the Planck scale, a dark matter which couples to the real component of the singlet scalar is expected to experiment a feeble interaction with the SM hypercharge gauge bosons. In this context, we study the freeze-in production of the (pion-like) pseudo Nambu-Goldstone of the theory and of a sterile neutrino, which is completely neutral and acquire mass through (neutrino-like) tiny yukawa couplings.

5.1.1 Effective minimal models

One of the simplest extensions of the standard model is the addition of a complex scalar field $\Phi = (s + ia)/\sqrt{2}$, singlet under the standard groups. Our Lagrangian may be split in the following parts:

$$\mathcal{L} \supset \mathcal{L}^0_{\rm SM} - V(H, \Phi) + \mathcal{L}_{\rm int} \,,$$

with $\mathcal{L}^0_{\rm SM}$ the SM Lagrangian in the symmetric phase up to the scalar potential, which is modified by the presence of the singlet scalar. $\mathcal{L}_{\rm int}$ is the interaction term between the complex singlet scalar field and the standard gauge bosons and is explicit below.

We assume a global $U(1)_X$ symmetry under which $\Phi \to e^{i\alpha}\Phi$. The most general renormalizable potential for a singlet complex scalar (Φ) and the SM Higgs doublet (H) respecting respectively the global $U(1)_X$ and the electroweak symmetry reads

$$V(H, \Phi) = \mu_H^2 |H|^2 + \mu_\Phi^2 |\Phi|^2 + \lambda_H |H|^4 + \lambda_\Phi |\Phi|^4 + \lambda_{H\Phi} |\Phi|^2 |H|^2 \,. \tag{5.1}$$

In order for the potential to be bounded from below, we need to satisfy $\lambda_\Phi > 0, \lambda_H > 0$ and $|\lambda_{H\Phi}| < 2\sqrt{\lambda_H \lambda_\Phi}$. On the other hand, the $U(1)_X$ symmetry breaking will generate a massless Goldstone boson a. However, just like in the strong CP problem, instanton effects induce a small $U(1)_X$ breaking mass term in the potential of the form

$$-\frac{\epsilon_\Phi^2}{2}(\Phi^2 + \Phi^{\dagger 2})$$

where $\epsilon_\Phi \ll \mu_\Phi$. This term will then generate an explicit mass term for a, making it to be regarded as a pseudo Nambu-Goldstone boson.

In the early universe when the temperature is above $O(|\mu_H|)$, through the $\lambda_{H\Phi}$ coupling the quadratic term in Φ receives a correction of $\lambda_{H\Phi} T^2 |\Phi|^2/12$ [197]. Notice that this thermal correction can be both positive and negative. In principle, if $\mu_\Phi^2 - \epsilon_\Phi^2 + \lambda_{H\Phi} T^2/12 > 0$, the $U(1)_X$ symmetry will be restored: $\langle \Phi \rangle = 0$. We are however interested in the regime

$|\lambda_{H\Phi} T_{\rm RH}^2| \ll |\mu_\Phi^2 - \epsilon_\Phi^2|$ so for us, $U(1)_X$ is broken with

$$\langle \Phi \rangle = \frac{v_\Phi}{\sqrt{2}} = \left(\frac{|\mu_\Phi^2 - \epsilon_\Phi^2|}{2\lambda_\Phi} \right)^{1/2} .$$

We can then decompose

$$\Phi \equiv \frac{v_\Phi + s + ia}{\sqrt{2}} \tag{5.2}$$

The masses of these particles can be written as

$$m_a = \sqrt{2}\epsilon_\Phi \quad \text{and} \quad m_s = \sqrt{2|\epsilon_\Phi^2 - \mu_\Phi^2|}.$$

Since there exist a remaining Z_2 symmetry for the pseudoscalar [198], it insures its stability and allows us to regard it as a dark matter candidate.

We will parametrize the coupling of s and a to the standard hypercharge gauge boson in an axion-like way, with the dimension-5 Peccei-Quinn operator. As we shall see in Section 5.1.3, such couplings are generated in a complete set-up after the spontaneous breaking of $U(1)_X$, where s and a obtain couplings of the following form through loops in which chiral fermions under $U(1)_X$ propagate [*]:

$$\mathcal{L}_{\rm int} = \mathcal{L}_1 + \mathcal{L}_2 = \frac{1}{\Lambda_1} s B_{\mu\nu} B^{\mu\nu} + \frac{1}{\Lambda_2} a B_{\mu\nu} \tilde{B}^{\mu\nu} , \tag{5.3}$$

where $B_{\mu\nu} = \partial_\mu B_\nu - \partial_\nu B_\mu$ is the field strength of the hypercharge field B_μ and $\tilde{B}^{\mu\nu} \equiv \frac{1}{2}\epsilon^{\mu\nu\rho\sigma} B_{\rho\sigma}$ is its dual field strength[†]. Λ_1 and Λ_2 represent generic BSM scales, which are in principle different but should be related to the mass of the BSM heavy fermions, as we will develop in Section 5.1.3.

After the breaking, the relevant terms in the potential read

$$\begin{aligned} V(H,s,a) \supset & \frac{m_s^2}{2} s^2 + \frac{m_a^2}{2} a^2 + \mu_H^2 |H|^2 \left(1 + \frac{\lambda_{H\Phi}}{4\lambda_\Phi} \frac{m_s^2}{\mu_H^2} \right) \\ & + m_s \sqrt{\frac{\lambda_\Phi}{2}} (s a^2 + s^3) + m_s \frac{\lambda_{H\Phi}}{\sqrt{2\lambda_\Phi}} s |H|^2 \\ & + \lambda_H |H|^4 + \frac{\lambda_{H\Phi}}{2} (s^2 + a^2) |H|^2 + \frac{\lambda_\Phi}{4} (s^2 + a^2)^2 . \end{aligned} \tag{5.4}$$

Notice that in the scalar sector the axion-like particles are stable, since they only appear in pairs.

In order to have a successful electroweak symmetry breaking, we should have $\mu_H^2(1 + (\lambda_{H\Phi}/4\lambda_\Phi)(m_s^2/\mu_H^2)) < 0$. The SM Higgs mass, $m_h = 125$ GeV should then be given by

[*] For simplicity, we here consider the coupling of the dark field to the Abelian $U(1)_Y$ gauge fields of the Standard Model. Generalization to the non-Abelian case is straightforward and will not affect qualitatively our results.

[†] Notice that the axion-like particle interacts only through derivative couplings, since after integration by parts we have $a B_{\mu\nu} \tilde{B}^{\mu\nu} = -2\epsilon^{\mu\nu\rho\sigma} \partial_\mu a B_\nu \partial_\rho B_\sigma$.

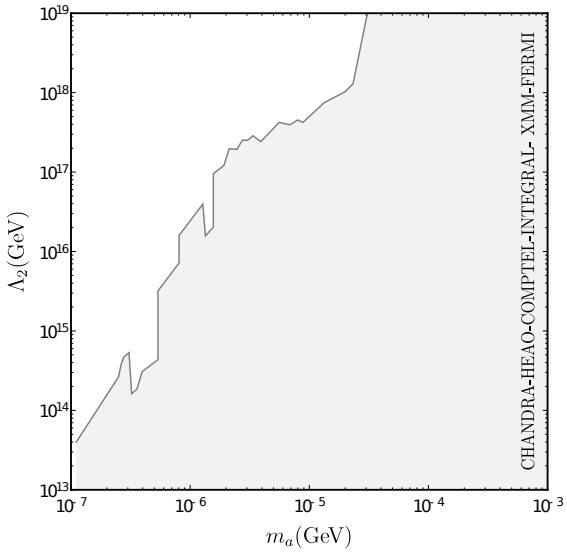

FIGURE 5.1 – *Constraint on the Peccei-Quinn operator energy scale as a function of the dark matter mass. The gray region is excluded by stability [200].*

$(2|\mu_H^2 + (\lambda_{H\Phi}/4\lambda_\Phi)m_s^2|)^{1/2}$. From Eq.(4.8), in the limit $m_s \gg m_a, m_h$, we have $\lambda_{H\Phi} \approx -s_\alpha c_\alpha \frac{m_s}{v_h}\sqrt{2\lambda_\Phi}$ and therefore, in order to agree with the current collider constraints [199] of $s_\alpha \leq 0.2$, we need to satisfy

$$\lambda_{H\Phi} \leq -2.6 \times 10^{-3}\sqrt{\lambda_\Phi} m_s/GeV\,. \tag{5.5}$$

The total widths of the real scalar and the pseudoscalar read respectively

$$\Gamma_s = \frac{m_s}{16\pi}\left[48\frac{m_s^2}{\Lambda_1^2} + \frac{\lambda_{H\Phi}^2}{\lambda_\Phi}\left(1 - \frac{4\mu_H^2}{m_s^2}\right)^{1/2} + \lambda_\Phi\left(1 - \frac{4m_a^2}{m_s^2}\right)^{1/2}\right] \tag{5.6}$$

and

$$\Gamma_a = \frac{m_a^3}{4\pi\Lambda_2^2}\,. \tag{5.7}$$

Since we will regard a as a metastable DM candidate, it is crucial to constrain its lifetime, which is given by

$$\tau_a = 8.3 \times 10^{28}\left(\frac{\text{keV}}{m_a}\right)^3\left(\frac{\Lambda_2}{10^{17}\text{ GeV}}\right)^2 \text{ sec}\,. \tag{5.8}$$

The agreement with observational constraints from gamma-ray line searches [101] provide us the following upper bound on dark matter mass:

$$\frac{m_a}{\text{keV}} \lesssim \left(\frac{8.3 \times 10^{28}\text{ sec}}{\tau_a^{obs}}\right)^{1/3}\left(\frac{\Lambda_2}{10^{17}\text{ GeV}}\right)^{2/3} \tag{5.9}$$

Notice that this is a generic constraint for any species decaying into gamma-rays, and does not require such species to be a dark matter candidate. In Fig. 5.1, we show this observational constraint over the (m_a, Λ_2) region of our parameter space.

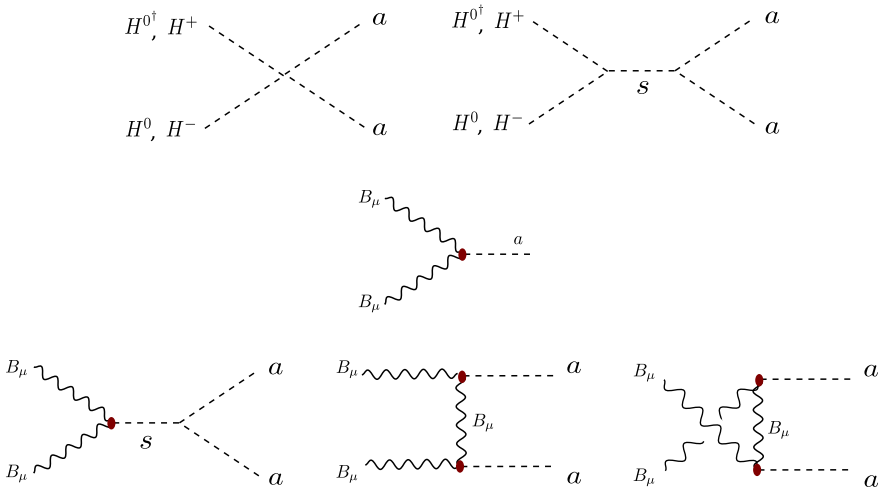

FIGURE 5.2 – *Feynman diagrams for the production of the pseudoscalar FIMP candidate.*

That said, in Fig.5.2 we show the production channels of the pseudoscalar dark matter candidate.

Let us stress an interesting point regarding the production of the pseudoscalar dark matter by Higgs-fusion. Above EWSB, $HH \to aa$ can proceed via contact and s-channel diagrams, with amplitudes

$$\mathcal{M}_c = -i\lambda_{H\Phi} \qquad \text{and} \qquad \mathcal{M}_s = -i\lambda_{H\Phi}\frac{m_s^2}{s - m_s^2 + im_s\Gamma_s}\,. \tag{5.10}$$

In the limit $m_s \gg \sqrt{s}, \Gamma_s$, the interference between these two diagrams makes this channel negligible, regardless of the strength of $\lambda_{H\Phi}$. This cancellation can be better understood if we decompose Φ in the form $\Phi = e^{ia/v_\Phi}(v_\Phi + s)/\sqrt{2}$ [*]. With this decomposition, it is trivial that a does not directly couple to H (*i.e.,* a disappears from the $\lambda_{H\Phi}$ term) and should be produced only via the decoupled particle, with interaction terms of the Lagrangian given by $-(\epsilon_\Phi^2/v_\Phi)sa^2$ and $s\,\partial_\mu a\,\partial^\mu a/(2v_\Phi)$ (coming from the kinetic term). It is therefore natural to expect the amplitude of $HH \to aa$ to be suppressed by s/m_s^2 and/or m_a^2/m_s^2. The sum of these two diagrams yield

$$|\mathcal{M}|^2_{\mathrm{HH}\to aa} = \lambda_{H\Phi}^2\frac{s^2 + m_s^2\Gamma_s^2}{(s - m_s^2)^2 + m_s^2\Gamma_s^2}\,. \tag{5.11}$$

The production from gauge bosons can happen through coalescence ($BB \to a$), with integrated amplitude squared given by

$$|\mathcal{M}|^2_{\mathrm{BB}\to a} = 8\frac{m_a^4}{\Lambda_2^2}, \tag{5.12}$$

[*]We recall the theorem on representation independence, see for instance [201–203].

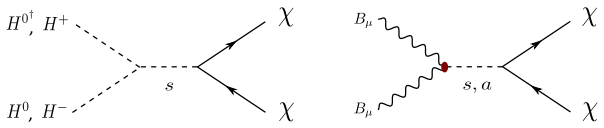

FIGURE 5.3 – *Feynman diagrams for the production of the sterile neutrino FIMP candidate.*

and through scattering,

$$\begin{aligned}
&\int d\Omega_{13}^{*}|\mathcal{M}|^2_{\mathrm{BB}\to aa} = \\
&= 64\pi\frac{s^2}{(s-m_s^2)^2+m_s^2\Gamma_s^2}\left(\lambda_\Phi\frac{m_s^2}{\Lambda_1^2}-4\sqrt{2\lambda_\Phi}\frac{m_s}{\Lambda_1}\frac{(s-m_s^2)}{\Lambda_2^2}\right) \\
&\quad+\frac{128\pi}{(1-\frac{2m_a^2}{s})}\frac{s^2}{\Lambda_2^4}\left[5-12\frac{m_a^6}{s^3}+14\frac{m_a^4}{s^2}-14\frac{m_a^2}{s}+\frac{8m_a^4}{s^2}\frac{(1-\frac{4m_a^2}{s}+\frac{3m_a^4}{s^2})}{\sqrt{1-\frac{4m_a^2}{s}}}\coth^{-1}\left(\frac{\frac{2m_a^2}{s}-1}{\sqrt{1-\frac{4m_a^2}{s}}}\right)\right] \\
&\approx 640\pi\frac{s^2}{\Lambda_2^4}+64\pi\frac{s^2}{(s-m_s^2)^2+m_s^2\Gamma_s^2}\left(\lambda_\Phi\frac{m_s^2}{\Lambda_1^2}-4\sqrt{2\lambda_\Phi}\frac{m_s}{\Lambda_1}\frac{(s-m_s^2)}{\Lambda_2^2}\right),
\end{aligned} \tag{5.13}$$

with the approximation holding in the limit $s \gg m_a^2$.

If the axion-like particle is a true (massless) Goldstone boson, it would be a dark radiation instead of dark matter candidate. On the other hand, if they are very heavy, they would not be produced from the thermal bath. However, if the mass of the lightest nonstandard fermion of this scenario lies below the maximal temperature achieved by the thermal bath, it is worth considering it as our dark matter FIMP candidate, hereafter referred to as χ.

Proceeding with our simplified approach, we assume that the fermionic FIMP interacts only with the singlet complex scalar, from which they would also acquire mass. They are therefore chiral under the global $U(1)_X$ and neutral under the standard group, being regarded as sterile neutrinos. Our Lagrangian (5.1) receives the following Yukawa term:

$$\mathcal{L}_\chi \supset -y_\chi \Phi \bar{\chi}_L \chi_R + \text{h.c.}\,. \tag{5.14}$$

After the breaking of the global $U(1)_X$, the dark matter candidate acquires mass and CP-even and odd interactions:

$$\mathcal{L}_\chi = \bar{\chi}(i\partial\!\!\!/ - m_\chi)\chi + \sqrt{2\lambda_\Phi}\frac{m_\chi}{m_s}(s\bar{\chi}\chi + ia\bar{\chi}\gamma_5\chi)\,. \tag{5.15}$$

The total width of the scalar is now

$$\Gamma_s = \frac{m_s}{16\pi}\left[48\frac{m_s^2}{\Lambda_1^2}+\frac{\lambda_{H\Phi}^2}{\lambda_\Phi}\left(1-\frac{4\mu_H^2}{m_s^2}\right)^{1/2}+\lambda_\Phi\left(1-\frac{4m_a^2}{m_s^2}\right)^{1/2}+4\lambda_\Phi\frac{m_\chi^2}{m_s^2}\left(1-\frac{4m_\chi^2}{m_s^2}\right)^{3/2}\right]. \tag{5.16}$$

The freeze-in of our fermionic dark matter candidate occur through the processes depicted in Fig. 5.3, with amplitudes given by

$$|\mathcal{M}|^2_{\text{HH}\to\chi\chi} = 2\lambda^2_{H\Phi}\frac{m_\chi^2(s-4m_\chi^2)}{(s-m_s^2)^2+m_s^2\Gamma_s^2} \tag{5.17}$$

and

$$|\mathcal{M}|^2_{\text{BB}\to\chi\chi} = 32\lambda_\Phi\frac{m_\chi^2}{m_s^2}\left(\frac{1}{\Lambda_1^2}\frac{(1-4m_\chi^2/s)}{(s-m_s^2)^2+m_s^2\Gamma_s^2}+\frac{1}{\Lambda_2^2}\frac{1}{(s-m_a^2)^2+m_a^2\Gamma_a^2}\right)s^3\,. \tag{5.18}$$

5.1.2 Production rates

The freeze-in production of our FIMP candidates is realized by the processes shown in Figs. 5.2 and 5.3, and therefore the total production rates have three contributions in the case of the pseudoscalar FIMP,

$$R_a(T) = R_{\text{HH}\to aa} + R_{\text{BB}\to aa} + R_{\text{BB}\to a}\,, \tag{5.19}$$

and two contributions in the case of sterile neutrino FIMP,

$$R_\chi(T) = R_{\text{HH}\to\chi\chi} + R_{\text{BB}\to\chi\chi}\,. \tag{5.20}$$

At this point, we are assuming that the production from the processes $s, ss \to aa, \chi\chi$ and $aa \to \chi\chi$ are suppressed by the negligible abundances of s and a relative to the abundances of HH, BB.

Let us first consider the only production channel which does not depend on mediators, the coalescence of gauge bosons into one pseudoscalar. Since we assume that the hypercharge bosons are already thermalized with the thermal bath while start producing dark matter, we use Eq. 2.38 to find

$$R_{\text{BB}\leftrightarrow a} = n_a^{\text{eq}}\,\Gamma_a\left(1-\frac{n_a(t)}{n_a^{\text{eq}}}\right)\approx n_a^{\text{eq}}\,\Gamma_a \simeq \begin{cases} \dfrac{\zeta(3)}{4\pi^3}\dfrac{m_a^3}{\Lambda_2^2}T^3 & (m_a \ll T) \\ \dfrac{1}{8\sqrt{2}\pi^{3/2}}\dfrac{m_a^{9/2}T^{3/2}}{\Lambda_2^2}e^{-m_a/T} & (m_a \gg T) \end{cases} \tag{5.21}$$

This contribution is therefore IR-dominated. Since it is always suppressed by $(m_a/\Lambda_2)^2$, we would need the channels mediated by the real scalar in order to achieve a good relic density for a keV-scale FIMP.

Approximate expressions for the production rate terms coming from all the $2 \to 2$ processes can be found in the limit where we can neglect the dark matter mass relative to the energies at which it is produced, but they necessarily depend on whether the mediator is far or close to its pole.

Just by looking to the Eqs. (3.13) and (3.15), we can find the temperature and parameters dependencies of the contributions to the total production rates.

For the pseudoscalar dark matter, we have

$$R_{\mathrm{HH}\to aa} \approx \begin{cases} c_0 \lambda_{H\Phi}^2 T^4 & (m_s \ll T) \\ c_{\mathrm{NWA}} \lambda_{H\Phi}^2 m_s^4 \frac{T}{\Gamma_s} K_1\left(\frac{m_s}{T}\right) & (m_s \sim T) \\ 0 & (m_s \gg T) \end{cases} \tag{5.22}$$

and

$$R_{\mathrm{BB}\to aa} \approx c_{tu} \frac{T^8}{\Lambda_2^4} + \begin{cases} c_0 \lambda_\Phi \frac{m_s^2}{\Lambda_1^2} T^4 - c_1 \sqrt{\lambda_\Phi} \frac{m_s}{\Lambda_1} \frac{T^6}{\Lambda_2^2} & (m_s \ll T) \\ c_{\mathrm{NWA}} \frac{T}{\Gamma_s} \lambda_\Phi \frac{m_s^2}{\Lambda_1^2} K_1\left(\frac{m_s}{T}\right) & (m_s \sim T) \\ c_2 \left(\frac{\lambda_\Phi}{m_s^2 \Lambda_1^2} + \frac{4\sqrt{2\lambda_\Phi}}{m_s \Lambda_1 \Lambda_2^2} \right) T^8 & (m_s \gg T) \end{cases} \tag{5.23}$$

Following our analysis in Chapter 3, we have defined numerical coefficients c_k, with k corresponding to the power of s in the squared amplitudes, and c_{NWA}, which encodes the numerical factors for the rate under narrow width approximation. We also encode numerical factors from the contribution of the t- and u-channels in the constant c_{tu}, which of course does not depend on the real scalar.

We therefore see that the production of pseudoscalars during reheating is always IR-dominated ($n < 12$) while their production during radiation era might be UV-dominated ($n > 5$) because of the gauge bosons contribution. Notice that for a heavy scalar, the production happens almost exclusively through gauge boson fusion, due to the interference of the channels of Higgs fusion.

By doing the same analysis for the fermionic dark matter, we find

$$R_{\mathrm{HH}\to \chi\chi} \approx \lambda_{H\Phi}^2 m_\chi^2 \times \begin{cases} c_{-1} T^2 K_0\left(\frac{2m_\chi}{T}\right) & (m_s \ll T) \\ c_{\mathrm{NWA}} (m_s^2 - 4m_\chi^2) \frac{T}{\Gamma_s} K_1\left(\frac{m_s}{T}\right) & (m_s \sim T) \\ c_1 \frac{T^6}{m_s^4} & (m_s \gg T) \end{cases} \tag{5.24}$$

and

$$R_{\mathrm{BB}\to \chi\chi} \approx \lambda_\Phi^2 \frac{m_\chi^2}{m_s^2 \Lambda_{1,2}^2} \times \begin{cases} c_1 T^6 & (m_s \ll T) \\ c_{\mathrm{NWA}} m_s^6 \frac{T}{\Gamma_s} K_1\left(\frac{m_s}{T}\right) & (m_s \sim T) \\ c_3 \frac{T^{10}}{m_s^4} & (m_s \gg T) \end{cases} \tag{5.25}$$

In the absence of a contact channel for the Higgs fusion in this case, the production of fermionic dark matter during radiation era is completely UV-dominated if happening through the exchange of heavy real scalars. Notice that in the case of gauge boson fusion, even the production through light real scalars would happen around the reheating scale.

These results imply that our dark matter candidates would be produced near the reheating temperature, the largest scale available in the radiation era, in a large part of our parameter space.

Φ	$(\mathbf{1},\mathbf{1};\ 0;-2)$
F_L	$(\mathbf{1},\mathbf{1};+1;-1)$
F_R	$(\mathbf{1},\mathbf{1};+1;+1)$
χ_L	$(\mathbf{1},\mathbf{1};\ 0;-1)$
χ_R	$(\mathbf{1},\mathbf{1};\ 0;+1)$

TABLE 5.1 – Charge assignation under $SU(3)_c, SU(2)_L; Y; X$

With these results, we would be able to constrain the parameter spaces of our keV dark matter candidates with relic density constraints, and also with structure formation bounds, since they could play the role of a warm dark matter content. The distribution functions of a and χ can be found directly from the collision operators, after solving the integro-partial differential equation (Eq. (2.3)). The current analysis we are performing is intended to determine whether our keV warm dark matter candidates satisfy the Lyman-α bounds, see for instance Ref. [204]. In this kind of study, the results of Chapter 2 become valuable.

5.1.3 UV completion of the Peccei-Quinn interaction

We have just seen that a simple global $U(1)$ extension of the standard model, $U(1)_X$, with a breaking scale above the reheating temperature can account for the right amount of dark matter via the freeze-in mechanism. However, the interaction terms between the scalars and the standard hypercharge bosons in Eq. 5.3 are effective and gauge-variant.

A simple way of generating the effective interactions of Eq. 5.3 at a microscopic level is by assuming the existence of heavy nonstandard fermions carrying standard hypercharge (Y_F). By assuming that such nonstandard fermionic current is vectorlike under $U(1)_Y$, we ensure that they do not introduce anomaly to the SM.

From a simplified model point of view, such fermions might acquire mass through yukawa-like couplings to the complex scalar:

$$\mathcal{L}_F = \bar{F}\not{D}F - y_F \Phi \bar{F}_L F_R + \text{h.c.}\,, \tag{5.26}$$

with the covariant derivative given by $D_\mu = \partial_\mu + ig' Y_F \bar{F}\gamma^\mu F B_\mu$.

Our model is invariant under both Abelian symmetries if one imposes for instance the charge assignment of Table 5.1.

After the breaking of $U(1)_X$, the heavy fermions acquire masses and CP-even and odd interactions. By making the assumption that the heavy fermions have equal masses and yukawa couplings, we have

$$\mathcal{L}_F \supset -m_F \bar{F}F + \frac{y_F}{\sqrt{2}}(s\bar{F}F + ia\bar{F}\gamma_5 F)\,, \tag{5.27}$$

with $m_F = \frac{y_F}{\sqrt{2}} v_\Phi$.

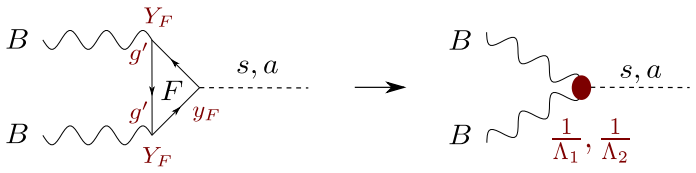

FIGURE 5.4 – *Feynman diagram allowed by Eq. (5.26) generating the Peccei-Quinn interaction of Eq. (5.3).*

As a consequence, the quartic coupling of the complex scalar is given in terms of the high energy physics:

$$\lambda_\Phi = \frac{y_F}{2}\frac{m_s}{m_F} \tag{5.28}$$

and in the case of interests for us, $\lambda_\Phi \ll 1$ which implies $m_F \gg m_s$.

The amplitudes for the interaction of the scalar and the pseudoscalar with two gauge bosons (depicted in Fig. 5.4) are completely analogous to the amplitude of SM Higgs interacting with two photons [205]:

$$\mathcal{M}_{s\to \mathrm{BB}} = \frac{\alpha'}{2\pi}\frac{y_F Y_F^2}{\sqrt{2}m_F}(\eta^{\mu\nu}(p_1\cdot p_2) - p_1^\nu p_2^\mu)\epsilon_\mu(p_1)\epsilon_\nu(p_2) f_{1/2}(\tau) \tag{5.29}$$

$$\mathcal{M}_{a\to \mathrm{BB}} = \frac{\alpha'}{4\pi}\frac{y_F Q_F^2}{\sqrt{2}m_F}\epsilon^{\mu\nu\alpha\beta}(p_1^\beta p_2^\alpha - p_1^\alpha p_2^\beta)\epsilon_\mu(p_1)\epsilon_\nu(p_2)\tilde{f}_{1/2}(\tilde{\tau}) \tag{5.30}$$

with $\alpha' = (g')^2/4\pi$.

Here, we have

$$\tau \equiv \frac{m_s^2}{4m_F^2} \qquad\qquad \tilde{\tau} \equiv \frac{m_a^2}{4m_F^2} \tag{5.31}$$

and the loop function are defined in such a way that they go to one in the limit $\tau, \tilde{\tau} \to 0$ and to zero in the limit $\tau, \tilde{\tau} \to \infty$ [206, 207]:

$$f_{1/2}(\tau) = 2\frac{\tau + (\tau-1)f(\tau)}{\tau^2} \qquad\qquad \tilde{f}_{1/2}(\tilde{\tau}) = 2\frac{f(\tilde{\tau})}{\tilde{\tau}} \tag{5.32}$$

with

$$f(\tau) = \begin{cases} \arcsin^2(\sqrt{\tau}) & (\tau < 1) \\ -\frac{1}{4}\left(\ln\left(\frac{1+\sqrt{1-1/\tau}}{1-\sqrt{1-1/\tau}}\right)\right)^2 & (\tau > 1) \end{cases} \tag{5.33}$$

The fact that the $sB_{\mu\nu}B^{\mu\nu}$ and $aB_{\mu\nu}\tilde{B}^{\mu\nu}$ are generated by loops of fermions whose mass are dynamical renders the scales Λ_1 and Λ_2 completely determined by the fundamental parameters of the theory:

$$\Lambda_1 = \frac{8\pi}{\alpha'}\frac{\sqrt{2}m_F}{y_F Y_F^2}\frac{1}{f_{1/2}(\tau)} \quad \text{and} \quad \Lambda_2 = \frac{8\pi}{\alpha'}\frac{\sqrt{2}m_F}{y_F Y_F^2}\frac{1}{\tilde{f}_{1/2}(\tilde{\tau})} \tag{5.34}$$

As we would have expected, in the limit $\tau \to 0$, $\Lambda_1, \Lambda_2 \simeq v_\Phi$.

5.2 Freezing-in dark matter through a heavy Z'

As we have seen in the previous chapter, extending the standard model group with an extra local $U(1)$ symmetry, $U(1)'$, is a very well-motivated and therefore widely considered option. The U boson, carrying this new interaction, might be coupled only to vector currents (visible and/or dark) and therefore be regarded as a dark photon. On the other hand, it might couple to (visible and/or dark) $V-A$ currents and be regarded as a nonstandard Z boson, the Z'.

If the SM fermions are charged under $U(1)'$, the interaction strengths are in general strong enough as to ensure thermalization between the visible and an eventual dark matter sector coupled to Z'. In this case, as we discussed in the previous chapter, the mass of Z' is usually in the range $10-10^3$ GeV as to comprise the WIMPs with the correct relic density, and the experimental constraints from collider searches on Z' are usually strong.

In the work we are going to discuss now [5], we assume that the standard model is neutral with respect to this new gauge interaction. On the other hand, heavy BSM fermions might be charged under both visible and dark $U(1)$ symmetries, as well as under the SM $SU(3)_c$. If the masses of those nonstandard fermions lie above the maximal temperature achieved by the thermal bath, there will be effective interactions between the Z' and the SM hypercharge bosons and gluons.

Effective interactions between three generic gauge bosons are dubbed *generalized Chern-Simons* (GCS) terms [208]. Dimension-4 and dimension-6 GCS operators connecting Z'_μ to an Abelian A_μ and a non-Abelian A^a_μ may be written respectively as

$$\lambda Z'_\alpha A_\mu \tilde{A}^{\alpha\mu} \qquad \text{and} \qquad \frac{1}{\Lambda^2}\partial^\alpha Z'_\alpha Tr[A^a_{\mu\nu}\tilde{A}^{a\,\mu\nu}]\,,$$

where $A_{\mu\nu}$ is the field strength of the gauge field A and $\tilde{A}_{\mu\nu} = \frac{1}{2}\epsilon^{\mu\nu\rho\sigma}A_{\mu\nu}$ its dual, λ is a dimensionless coupling and Λ is the new physics scale of the theory, the cut-off above which an effective approach is not valid. Both terms are *local gauge-variant* but, as we are going to discuss in Section 5.2.3, this is precisely what makes it possible for those theories to be consistent.

GCS effective interactions were first considered in the context of supergravity, string and high extra-dimension theories [209–211]. However, they can also be accommodated in field theories and were already assumed to play central role in the non-thermal [212] and thermal [213–215] production of dark matter particles.

We show in what follows that dark matter candidates which couple only to the Z' might be produced from standard model gauge bosons before the EWSB via the freeze-in mechanism. We first consider the dimension-6 operator above, relevant for the dark matter production in our model, and present an UV completion in Section 5.2.3.

We recall that in our context of a non-thermal dark matter, the upper limit of ~ 340 TeV [126] on its mass does not apply.

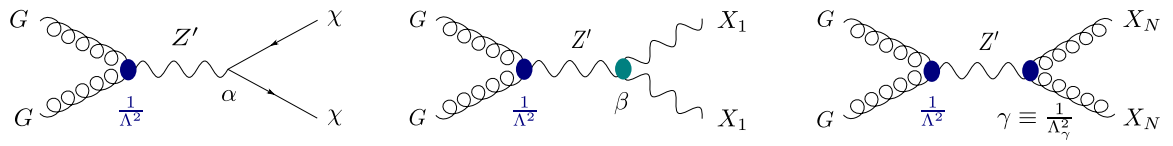

FIGURE 5.5 – *Feynman diagrams representing the production of our dark matter candidates (χ, X_1 and X_N) by annihilation of gluons (G) through the $U(1)'$ gauge boson (Z') in the early universe.*

5.2.1 The effective approach

Here we assume that the heavy fermions responsible for the GCS-like interaction are charged under $SU(3)_c$. In this case [216], our effective interaction Lagrangian is given by

$$\mathcal{L}_{\text{eff}} = \frac{1}{\Lambda^2}\partial^\alpha Z'_\alpha \epsilon^{\mu\nu\rho\sigma}\text{Tr}[G^a_{\mu\nu}G^a_{\rho\sigma}] + \mathcal{L}^i_{\text{DM}}\,, \tag{5.35}$$

where $\mathcal{L}^i_{\text{DM}}$ represents the interactions between Z' and the DM candidates, a fermion (χ), an Abelian (X_1) and a non-Abelian (X_N) vector fields, and read:

$$\mathcal{L}^{\chi}_{\text{DM}} = \alpha\ \bar{\chi}\gamma^\mu\gamma_5\chi Z'_\mu\,, \tag{5.36}$$

$$\mathcal{L}^{X_1}_{\text{DM}} = \beta\ \epsilon_{\mu\nu\rho\sigma}Z'^\mu X_1^\nu X_1^{\rho\sigma}\,, \tag{5.37}$$

and

$$\mathcal{L}^{X_N}_{\text{DM}} = \gamma\ \partial^\alpha Z'_\alpha \epsilon_{\mu\nu\rho\sigma}\text{Tr}[X_N^{\mu\nu}X_N^{\rho\sigma}]\,. \tag{5.38}$$

The stability of our vector dark matter candidates is automatic, in a sense that they only couple directly to fermions which are much heavier by construction. We need to ensure, though, that no kinetic mixing happens between X_1 and B and also between X_N and W^i or G^a.

Dark matter is therefore produced from gluon annihilation through s-channel exchange of Z', as depicted in Fig. 5.5. The respective squared amplitudes read

$$\int d\Omega^*_{13}|\mathcal{M}|^2_\chi = 2^{10}\pi\ \frac{\alpha^2}{\Lambda^4}\frac{m_\chi^2}{M^4_{Z'}}\frac{s^3(s-M^2_{Z'})^2}{(s-M^2_{Z'})^2+M^2_{Z'}\Gamma^2_{Z'}} \approx 2^{10}\pi\ \frac{\alpha^2}{\Lambda^4}\frac{m_\chi^2}{M^4_{Z'}}s^3\,, \tag{5.39}$$

$$\int d\Omega^*_{13}|\mathcal{M}|^2_{X_1} = 2^{10}\pi\ \frac{\beta^2}{\Lambda^4}\frac{s^3}{M^4_{Z'}}\frac{(s-4m^2_{X_1})(s-M^2_{Z'})^2}{(s-M^2_{Z'})^2+M^2_{Z'}\Gamma^2_{Z'}} \approx 2^{10}\pi\ \frac{\beta^2}{\Lambda^4}\frac{1}{M^4_{Z'}}s^4 \tag{5.40}$$

and

$$\int d\Omega^*_{13}|\mathcal{M}|^2_{X_N} = 2^{12}\pi\ \frac{\gamma^2}{\Lambda^4}\frac{s^5}{M^4_{Z'}}\frac{(s-4m^2_{X_N})(s-M^2_{Z'})^2}{(s-M^2_{Z'})^2+M^2_{Z'}\Gamma^2_{Z'}} \approx 2^{12}\pi\ \frac{\gamma^2}{\Lambda^4}\frac{1}{M^4_{Z'}}s^6\,. \tag{5.41}$$

Above, m_χ, m_{X_1}, m_{X_N}, and $M_{Z'}$ are respectively the masses of our dark matter candidates and of Z' and $\Gamma_{Z'}$ is the total decay width of Z'. The approximations hold whenever $\Gamma_{Z'} \ll M_{Z'}$, which is not the case only near resonance and, in the vector DM cases, when

DM mass lies much below the energy range at which it is produced. The approximations will be used only for an analytical description of the relic density, but are not considered in our numerical results. We point out that a vector coupling between Z' and χ does not contribute to the squared amplitude in the process depicted in Fig. 5.5. Because of that, in Eq. (5.36) we couple Z' to a purely axial current of dark matter without loss of generality for our purposes.

By looking to the expressions for the squared amplitudes, one might think that they all vanish exactly at the pole, when $s = M_{Z'}^2 = 4m_{\rm DM}^2$. However, in the same way that cross-sections do not diverge around resonances, the amplitudes here do not vanish exactly because the Z' has a finite decay width. It is nevertheless interesting to notice that in our scenario, around the pole region we observe a dip instead of a bump. The well-established Landau-Yang theorem prohibits spin-1 fields to decay into massless Abelian gauge bosons [217, 218] (see also [219]), based on Lorentz, gauge and statistical (Bose) symmetries. For non-Abelian fields, though, it was quite recently shown that the Landau-Yang theorem does not apply [220–222] In any case, due to the dimension-6 operator we are using, the decay of Z' (with 4-momentum p_1) into non-Abelian fields (massless or *massive*, with 4-momentum p_3 and p_4) vanishes exactly:

$$\begin{aligned}\mathcal{M} &= \epsilon_\mu(p_1)\epsilon^*_\sigma(p_3)\epsilon^*_\rho(p_4)[4i\gamma p_1^\mu \epsilon^{\sigma\rho\,\delta\eta}(p_{3\,\delta}p_{4\,\eta} - p_{3\,\eta}p_{4\,\delta})] \\ &= 4i\gamma\epsilon^{\sigma\rho\,\delta\eta}(p_1\cdot\epsilon_1)((p_3\cdot\epsilon_3^*)(p_4\cdot\epsilon_4^*) - (p_3\cdot\epsilon_3^*)(p_4\cdot\epsilon_4^*))\,.\end{aligned} \tag{5.42}$$

Since in the underlying theory there might be dark fermions lighter than Z' but uncharged with respect to the SM group and then not playing a role in the dark matter production, we take them into account in the computation of the total decay width of Z'. Therefore, allowing Z' to decay into N_ψ dark vector-like fermions ψ of charge Q_ψ and mass m_ψ, the total decay width is given by

$$\Gamma_{Z'} = \frac{M_{Z'}}{12\pi} N_\psi Q_\psi^2 \sqrt{1 - \frac{4m_\psi^2}{M_{Z'}^2}}\left(1 + \frac{2m_\psi^2}{M_{Z'}^2}\right) + \Gamma_{Z'\to\rm DM}\,, \tag{5.43}$$

where

$$\Gamma_{Z'\to\rm DM} = \frac{M_{Z'}}{12\pi} \times \begin{cases} \alpha^2\left(1 - \frac{4m_\chi^2}{M_{Z'}^2}\right)^{3/2} & \text{(fermionic DM)} \\ \frac{\beta^2}{2}\frac{M_{Z'}^2}{m_{\chi_1}^2}\left(1 - \frac{4m_{\chi_1}^2}{M_{Z'}^2}\right)^{5/2} & \text{(Abelian DM)} \\ 0 & \text{(non-Abelian DM)} \end{cases} \tag{5.44}$$

We finally have all the ingredients to compute the production rates, which are the key model-dependent quantities for the dark matter evolution. Before solving it numerically, it is useful to have analytical approximations. Far from the resonances and neglecting dark matter mass in the vector DM cases, we find

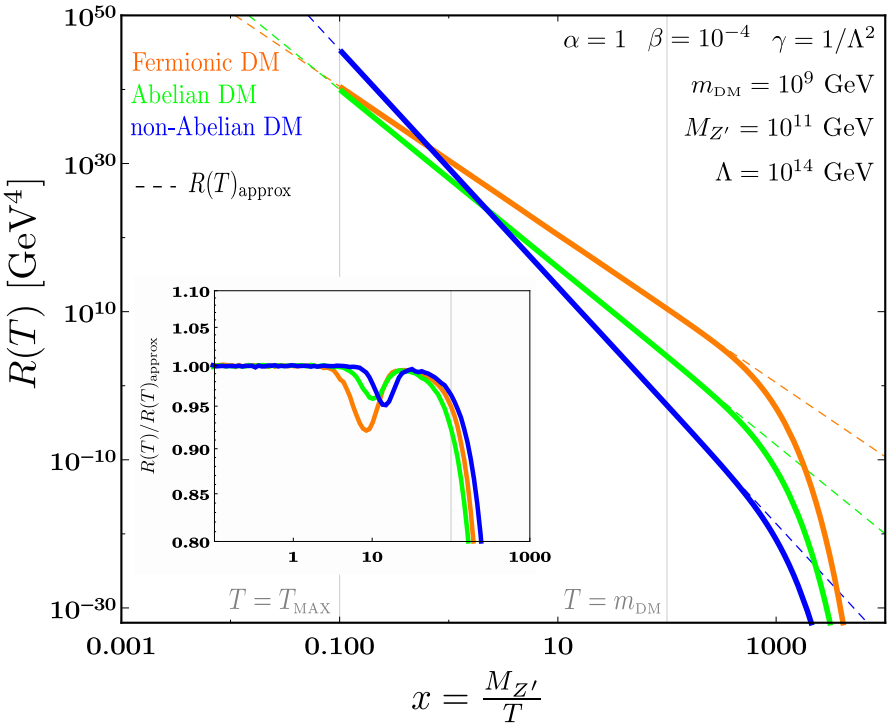

FIGURE 5.6 – *Exact solutions (solid curves) for the production rates of a fermionic (orange curves), Abelian (green curves) and non-Abelian (blue curves) dark matter, and respective approximations (dashed lines). Inset: Ratio between exact and approximate results.*

$$R(T)_{\rm approx} = \begin{cases} 2\times 10^2 \, \dfrac{\alpha^2}{\Lambda^4}\dfrac{m_\chi^2}{M_{Z'}^4} T^{10} & \text{(fermionic DM)} \\ 10^4 \, \dfrac{\beta^2}{\Lambda^4 M_{Z'}^4} T^{12} & \text{(Abelian DM)} \\ 2\times 10^9 \dfrac{\gamma^2}{\Lambda^4 M_{Z'}^4} T^{16} & \text{(non-Abelian DM)} \end{cases} \tag{5.45}$$

We notice from those approximate results that the operators connecting the visible and dark sectors lead to production rates with a high temperature dependence. As we have discussed, in an inflationary cosmology, it means that as long as the inflaton produce standard model particles, they are able to produce a significant amount of dark matter.

We have integrated numerically the production rates, as given in Eq. (3.11), considering the Bose-Einstein distributions of gluons and the exact squared amplitudes shown in Eqs. (5.39)-(5.41) *. In Fig. 5.6 we show the exact solutions for the production rates of the fermionic (orange curves), Abelian (green curves) and non-Abelian (blue curves) dark matter from gluon annihilation, along with the approximate solutions, in dashed lines. We fix the new physics cutoff Λ to be close to an intermediate scale, $\Lambda = 10^{14}$ GeV, and

*We have used the CUBA numerical package [147].

set the reheating scale to be $T_{\rm RH} = 10^{10}\,\text{GeV}$. Inspired by the results of Chapter 2, we keep the split between the reheating and the maximal temperature to be $T_{\rm MAX} = 100\,T_{\rm RH}$. Once we are interested in a heavy Z', we let its mass to be between the reheating and maximal temperatures, $M_{Z'} = 10^{11}\,\text{GeV}$. Before scanning over a wide range of dark matter mass, we fix it to $m_{\rm DM} = 10^{9}\,\text{GeV}$ for the three candidates. From now on, we fix the dark matter couplings to Z' as follows: in the fermionic case, since α is regarded as a gauge-like coupling, we set $\alpha = 1$; for the Abelian case, as we discuss in more detail in Section 5.2.3, β is related to gauge couplings of fermions running in the loops which generate this effective interaction and we set $\beta = 10^{-4}$; for the non-Abelian case, we assume that this interaction is generated in the same way as the interaction of Z' with gluons is generated and we therefore set $\gamma = 1/\Lambda^2$. Finally, regarding the Z' coupling to the vector-like current of fermions ψ, we fix $N_\psi = Q_\psi = 1$ and $m_\psi = 0.4\,M_{Z'}$.

In the inset of the figure, we show the ratio between the exact and approximated rates, where we are able to see the tiny dips we have anticipated by looking the squared amplitudes. Although negligible for the dark matter production in practice, those departures carry the special feature of our set-up, in which there is no resonances near the pole, as seen in the dark photon model we discussed in the previous chapter. The important failure of the approximation is in fact not model-dependent, but rather a general failure of approximated solutions neglecting the dark matter mass, since the Boltzmann suppression happening around $T \gtrsim 10\,m_{\rm DM}$ cannot be accounted for (we remind the reader the discussion following Eq. (3.11)).

Another feature of our model is that the s-channel exchange of Z' happens as if they were massless, without resonance. This is coming from the GCS operator and is due to the fact that Z' acquires mass à la Stueckelberg and is mainly a longitudinal spin-1 field [223, 224] and its propagator behaves as if it was a massless scalar (see for instance page 383 of Ref.[225]).

5.2.2 Agreement with relic density

We now proceed to the computation of the relic density of our dark matter candidates in order to find viable regions of our parameter space.

With the approximate rates of Eq. (5.45), given by power-laws of the temperature, we can use Eqs. (2.134)-(2.136), to write approximate expressions for the relic density:

$$\frac{\Omega^0_{\rm DM}h^2}{0.12} \sim \begin{cases} \left(\dfrac{\mathscr{B}_{10}}{3.68}\right)\left(\dfrac{\alpha}{1}\right)^2\left(\dfrac{m_\chi}{2.6\times10^7\,\text{GeV}}\right)^3\left(\dfrac{10^{11}\,\text{GeV}}{M_{Z'}}\right)^4\left(\dfrac{10^{14}\,\text{GeV}}{\Lambda}\right)^4\left(\dfrac{T_{\rm RH}}{10^{10}\,\text{GeV}}\right)^5 \\ \left(\dfrac{\mathscr{B}_{12}}{35.5}\right)\left(\dfrac{\beta}{10^{-4}}\right)^2\left(\dfrac{m_{X_1}}{5\times10^7\,\text{GeV}}\right)\left(\dfrac{10^{11}\,\text{GeV}}{M_{Z'}}\right)^4\left(\dfrac{10^{14}\,\text{GeV}}{\Lambda}\right)^4\left(\dfrac{T_{\rm RH}}{10^{10}\,\text{GeV}}\right)^7 \\ \left(\dfrac{\mathscr{B}_{16}}{3\times10^8}\right)\left(\dfrac{m_{X_2}}{5\times10^3\,\text{GeV}}\right)\left(\dfrac{10^{11}\,\text{GeV}}{M_{Z'}}\right)^4\left(\dfrac{10^{14}\,\text{GeV}}{\Lambda}\right)^8\left(\dfrac{T_{\rm RH}}{10^{10}\,\text{GeV}}\right)^{11} \end{cases} \tag{5.46}$$

We have set $\gamma = 1/\Lambda^2$ and considered $SU(2)$ as gauge group for the non-Abelian dark matter candidate. Notice the huge boost factor in the case of a non-Abelian dark matter,

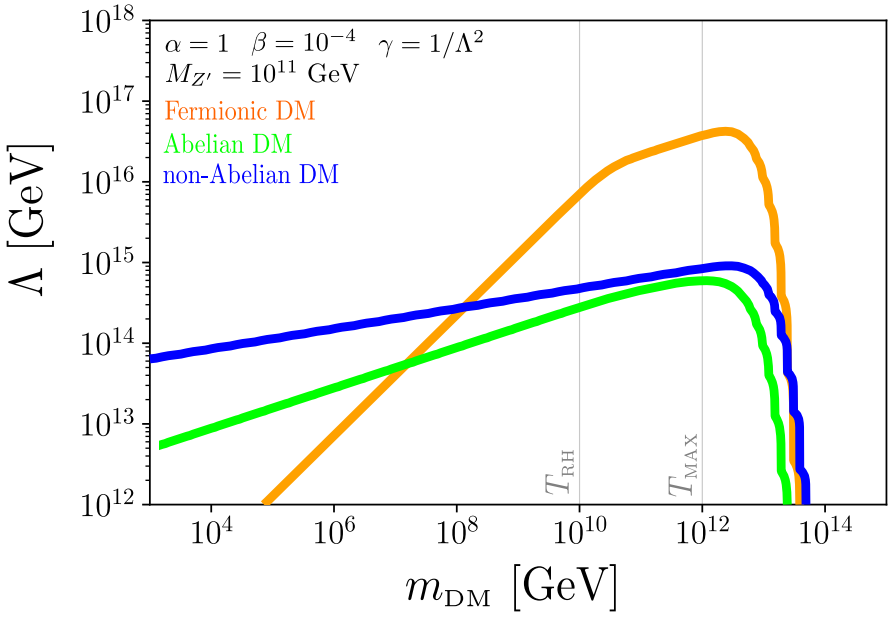

FIGURE 5.7 – *Relic density contours for the fermionic (orange curve), Abelian (green curve) and non-Abelian (blue curve) dark matter candidates. While the three cases are UV-dominated regarding production during radiation era, they are respectively IR-dominated, IR-UV mixed and UV-dominated regarding production during reheating.*

which means that the totality of dark matter was already produced before reheating had finished.

The exact solution for the relic density is found by simultaneously evolving the set of differential equations, Eq. (2.91), governing the inflaton, radiation and dark matter content. In Fig. 5.7, the contours providing $\Omega^0_{\rm DM}h^2 = 0.12$ in the plane of $(m_{\rm DM}, \Lambda)$ are shown in orange, green and blue, respectively for the fermionic, Abelian and non-Abelian dark matter candidates. The absence of pole regions made it possible to compute recursively the relic density using the Python package [226].

First of all, by using the approximations of Eq. (5.46), we can infer the orders of magnitude of the dark matter masses for a given value of Λ, as one can easily verify for the value we have chosen $\Lambda = 10^{14}$ GeV. It is also straightforward to understand all the different slopes that we see in the contours, as we show in what follows.

According to the discussion after Eq. (2.136), the *production during radiation era* of the three dark matter candidates considered here happens at the largest scale available, and is said to be UV-dominated ($n > 5$ in the three cases). Therefore, for $m_{\rm DM} < T_{\rm RH}$ the new physics scale providing the correct relic density depends on the other parameters as

$$\Lambda\Big|^{\chi}_{\rm RD} \sim 6.5\times 10^6 \alpha^{1/2} m_\chi^{3/4} T_{\rm RH}^{5/4} M_{Z'}^{-1}\,, \quad \Lambda\Big|^{X_1}_{\rm RD} \sim 1.5\times 10^7 \beta^{1/2} m_{X_1}^{1/4} T_{\rm RH}^{7/4} M_{Z'}^{-1} \quad \text{and} \quad \Lambda\Big|^{X_2}_{\rm RD} \sim 1.7\times 10^4 m_{X_2}^{1/8} T_{\rm RH}^{11/8} M_{Z'}^{-1/2}\,. \tag{5.47}$$

Indeed, we can verify in Fig. 5.7 that $\Lambda \propto m_{\rm DM}^{3/4}$, $m_{\rm DM}^{1/4}$ and $m_{\rm DM}^{1/8}$ for fermionic, Abelian and non-Abelian cases when $m_{\rm DM} < T_{\rm RH}$.

On the other hand, the contributions for the *production during reheating* of our three dark matter candidates are qualitatively different. For the fermionic dark matter, production during reheating happens at the lowest scale available ($n < 12$), and if $T_{\rm RH} < m_\chi < T_{\rm MAX}$ we find two distinct slopes for the dependence of Λ on m_χ, easily verified in Fig. 5.46:

$$\Lambda\Big|_{\rm ID}^{\chi} \sim 9.3 \times 10^6 c^{1/4} \alpha^{1/2} M_{Z'}^{-1} \times \begin{cases} m_\chi^{3/4} T_{\rm RH}^{5/4}\,, & \text{for} \quad m_\chi \sim T_{\rm RH} \\ m_\chi^{1/4} T_{\rm RH}^{7/4}\,, & \text{for} \quad T_{\rm RH}^2 \ll m_\chi^2 \ll T_{\rm MAX}^2\,. \end{cases} \tag{5.48}$$

For the Abelian dark matter, the production during reheating has a logarithmic dependence on both IR and UV scales. In case $T_{\rm RH} < m_\chi < T_{\rm MAX}$, we also have two different slopes but they are very smoothly connected:

$$\begin{aligned} \Lambda\Big|_{\rm ID}^{X_1} &\sim 2.8 \times 10^7 c^{1/4} \beta^{1/2} M_{Z'}^{-1} m_{X_1}^{1/4} T_{\rm RH}^{7/4} \left(\ln\left(\frac{m_{X_1}}{T_{\rm RH}}\right) + \ln\left(\frac{T_{\rm MAX}}{m_{X_1}}\right)\right)^{1/4} \\ &\approx 2.8 \times 10^7 c^{1/4} \beta^{1/2} M_{Z'}^{-1} m_{X_1}^{1/4} T_{\rm RH}^{7/4} \ln\left(\frac{T_{\rm MAX}}{T_{\rm RH}}\right)^{1/4}\,. \end{aligned} \tag{5.49}$$

Finally, the production of a non-Abelian dark matter from gluons is so highly dependent on temperature that it is UV-dominated even while inflaton dominate the expansion of the universe. In this case, for $T_{\rm RH} < m_\chi < T_{\rm MAX}$, we have

$$\begin{aligned} \Lambda\Big|_{\rm ID}^{X_2} &\sim 2.1 \times 10^4 c^{1/8} M_{Z'}^{-1/2} m_{X_2}^{1/8} T_{\rm RH}^{11/4} \left(\frac{m_{X_2}^4}{T_{\rm RH}^4} + \frac{T_{\rm MAX}^4}{T_{\rm RH}^4}\right)^{1/2} \\ &\approx 2.1 \times 10^4 c^{1/8} M_{Z'}^{-1/2} m_{X_2}^{1/8} T_{\rm RH}^{11/4} \left(\frac{T_{\rm MAX}^4}{T_{\rm RH}^4}\right)^{1/2}\,. \end{aligned} \tag{5.50}$$

For $m_{\rm DM} \gtrsim 10 T_{\rm MAX}$, only very energetic gluons in the tail of their distributions are able to produce dark matter and a huge suppression on the cut off scale is needed as to compensate it. Notice however that for $\Lambda < m_{\rm DM}$ our effective description is not valid anymore.

Finally, Fig.5.7 make explicit the "natural" scales of our allowed parameter space. For a very large range of the DM mass, from $\mathcal{O}$(TeV) to $T_{\rm MAX}$, values of the BSM scale Λ range from $T_{\rm MAX}$ to GUT/string scale and can still populate the Universe with the correct relic abundance of dark matter. This means that the heavy spectrum of masses above the reheating temperature $T_{\rm RH}$ generates naturally small couplings of an invisible Z' to the SM bath to satisfy the cosmological constraints through the freeze-in process. This constitutes the most important conclusion of our work.

We now proceed to the discussion on possible UV completions of our scenarios.

5.2.3 UV completion of generalized Chern-Simons interaction

We now turn our attention to the underlying physics responsible for the generalized Chern-Simons couplings leading to the production of our dark matter candidates. Such interactions might come from string theory frameworks, but here we consider them as a low-energy consequence of a quantum field theory involving currents of heavy nonstandard fermions.

First of all, if the currents of heavy nonstandard fermions are vectorlike with respect to the standard and nonstandard gauge groups, all the possible operators that might lead to a low-scale interaction between three gauge bosons vanishes exactly [216]. Therefore, the effective GCS couplings would in principle introduce anomalies in the theory, since they necessarily involve chiral fermionic currents. Hereafter, we assume that the BSM fermionic degrees of freedom couple only vectorially to the SM gauge groups such that no anomalous processes appear in the standard sector.

Our starting point is to assume the existence of a complex scalar field, Φ', singlet under the standard group, which spontaneously breaks $U(1)'$ at the highest scale of our theory. If the real component of Φ', h', is much heavier than the breaking scale V, it is convenient to use the exponential parametrization of the complex scalar,

$$\Phi' = \frac{1}{\sqrt{2}}(V + h')\, e^{i\, a'/V}\,, \tag{5.51}$$

with a' the Stueckelberg axion associated to $U(1)'$. All the processes we are going to consider happen at temperatures much below the $U(1)'$ phase transition scale, such that the radial component of the scalar field is always decoupled from the theory. Our Z' will be therefore primarily longitudinal, absorbing its Stueckelberg axion.

The next step is to ensure that the masses of all the BSM fermionic degrees of freedom are invariant both under the standard and non-standard gauge groups.

Our microscopic gauge-invariant Lagrangian, including the Stueckelberg axion a', the massive Z' and the set of heavy fermions Ψ^i (vectorlike under the SM group and chiral under $U(1)'$) reads therefore

$$\begin{aligned}\mathcal{L} =& \mathcal{L}_{\rm SM} + \frac{1}{2}(\partial_\mu a' - M_{Z'} Z'_\mu)^2 - M_i\ \overline{\Psi}^i_L e^{ia'/V(q_L - q_R)}\Psi^i_R \\ &+ i\overline{\Psi}^i_L \gamma^\mu(\partial_\mu - i\frac{\tilde{g}}{2} q^i_L Z'_\mu)\Psi^i_L + i\overline{\Psi}^i_R \gamma^\mu(\partial_\mu - i\frac{\tilde{g}}{2} q^i_R Z'_\mu)\Psi^i_R\end{aligned} \tag{5.52}$$

which is manifestly invariant under the (nonlinear) $U(1)'$ transformation of parameter α,

$$\begin{aligned}&\Psi^i_R \to \Psi^i_R e^{i\frac{\tilde{g}}{2} q_R \alpha}\ ; \qquad \Psi^i_L \to \Psi^i_L e^{i\frac{\tilde{g}}{2} q_L \alpha} \\ &Z'_\mu \to Z'_\mu + \partial_\mu \alpha\ ; \qquad a' \to a' + \frac{\tilde{g} V}{2}\ \alpha \equiv a' + M_{Z'}\ \alpha\,.\end{aligned}$$

From the Lagrangian in Eq. (5.52), we compute the triangle loops shown in Fig. 5.8 and integrate out the heavy fermions. We then obtain the effective Lagrangians as in Eqs. (5.35), (5.37) and (5.38).

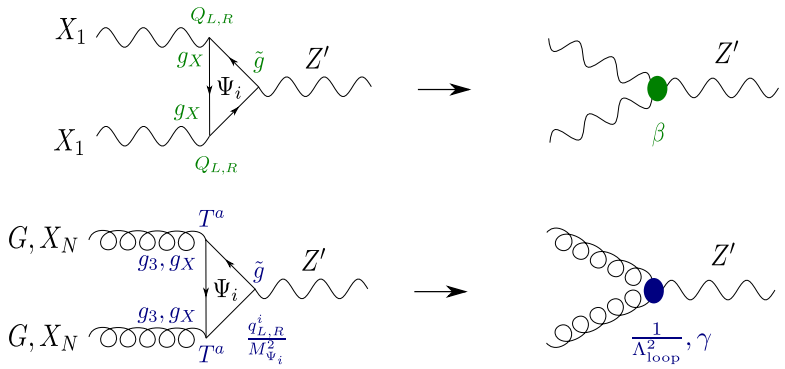

FIGURE 5.8 – *Triangle loops of the proposed UV completions for the generalized Chern-Simons interactions.*

Let us first consider the dimension-4 effective interaction between three Abelian gauge fields,

$$\mathcal{L} \supset \beta\, \epsilon_{\mu\nu\rho\sigma} Z'^{\mu} X_1^{\nu} X_1^{\rho\sigma}\,.$$

The first thing we notice is the apparent non-decoupling of this effective interaction, since β is a dimensionless coupling independent of the heavy fermion masses. It is also true that this term is gauge-variant, as well as the dimension-6 effective interaction term of Z' with two non-Abelian gauge bosons X_i^a,

$$\mathcal{L} \supset \frac{1}{\Lambda_i^2} \partial^{\alpha} Z'_{\alpha} \epsilon^{\mu\nu\rho\sigma} \mathrm{Tr}[X^{\,a}_{i\,\mu\nu} X^{\,a}_{i\,\rho\sigma}]\,.$$

Fortunately, those two problems might be accommodated in a consistent (anomaly-free) underlying theory. Here is where the Stueckelberg axion of Z' plays a central role. As in the case of the global Peccei-Quinn interaction considered previously, there will be effective Lagrangians as low-scale consequences of the heavy fermions receiving mass from the scalar Φ' and charged under the SM group. In the present case, though, the gauge-variance of this effective Lagrangian compensate the gauge variance of the three-gauge bosons effective interaction. As a consequence, the full theory is anomaly-free. This is the idea behind the Green-Schwarz mechanism [227]. See also Ref. [214] for a detailed discussion.

The heaviness of the colored nonstandard fermions have two important consequences here. First of all, even though cosmologically stable, the Boltzmann suppression in their production rates would have decoupled them from the thermal bath even in the beginning of reheating, which hide them from the thermal bath species. Therefore, they would not be able to directly produce dark matter and this bring us to the need for the effective GCS interactions. Another consequence is that, even though in principle these states contribute to the running of g_3, their contribution is too suppressed as to modify it during the remaining phase up to the GUT scale.

We now focus on the fermionic dark matter case. We can express the effective coupling of the dimension-6 Lagrangian in terms of the parameters of the microscopical theory. In

agreement with Ref. [216], we obtain

$$\mathcal{L}_{\rm loop} = \frac{1}{\Lambda^2_{\rm loop}} \partial^\alpha Z'_\alpha \epsilon^{\mu\nu\rho\sigma} {\rm Tr}[G^a_{\mu\nu} G^a_{\rho\sigma}] \,, \tag{5.53}$$

with

$$\frac{1}{\Lambda^2_{\rm loop}} = \frac{g_3^2 \ \tilde{g}}{96\pi^2} \sum_i \frac{q^i_L - q^i_R}{M^2_{\Psi_i}} {\rm Tr}[T^a T^a] \,. \tag{5.54}$$

Defining for simplicity $\sum_i \frac{q^i_L - q^i_R}{M^2_{\Psi_i}} {\rm Tr}[T^a T^a] \equiv \frac{N_\Psi Q_\Psi}{M^2_\Psi}$ (which corresponds to a set of N_Ψ fermions of effective "charges" Q_Ψ and masses M_Ψ) we obtain $\Lambda_{\rm loop} \simeq \frac{50}{\sqrt{N_\Psi Q_\Psi}} \frac{M_\Psi}{\sqrt{\tilde{g}}}$, where we used the SM expected value of g_3 at 10^{12} GeV.

We can now re-express the production rate of the fermionic dark matter candidate in terms of the fundamental parameters of the microscopic theory:

$$R_\chi(T) \sim 5 \times 10^{-4} \left(\frac{\alpha \ N_\Psi Q_\Psi}{y^2_\Psi \tilde{g}} \right)^2 \frac{m^2_\chi}{V^8} T^{10} \,, \tag{5.55}$$

where $M_\Psi = y_\Psi V$ and $M_{Z'} = \frac{\tilde{g}}{2} V$. The approximate solution for the relic density of our fermionic dark matter candidate becomes

$$\frac{\Omega_\chi h^2}{0.12} \sim \left(\frac{\mathscr{B}_{10}}{2} \right) \left(\frac{\alpha N_\Psi Q_\Psi}{\tilde{g} y^2_\Psi} \right)^2 \left(\frac{m_\chi}{10^{10}} \right)^3 \left(\frac{T_{\rm RH}}{10^{12}} \right)^5 \left(\frac{10^{14}}{V} \right)^8 \,. \tag{5.56}$$

We could keep V as a free fundamental parameter of the model, which is determined by the potential of Φ'. However, to be more complete, we investigated UV scenarios in which V is determined as an intermediate scale by the unification condition of the gauge coupling constants, in $SO(10)$ GUT constructions (as an example). Indeed, in such set-ups, the $SO(10)$ group is not directly broken into the SM in one step but goes through an intermediate gauge group $G_{\rm int}$ like $SO(10) \to G_{\rm int} \to SU(3)_c \times SU(2)_L \times U(1)_Y$. The scale $M_{\rm int}$ at which the intermediate gauge group is broken is fixed by the unification condition $g_1 = g_2 = g_3$ at a higher unified scale. It was shown in Refs. [100] (at one loop) and [95, 101] (at two loops) that $V = M_{\rm int}$ can range from 10^9 to 10^{15} GeV depending on $G_{\rm int}$ and the representation in which the Higgs field responsible for $G_{\rm int}$ breaking lies.

We show in Fig. 5.9 the parameter space providing the correct relic density for our fermionic dark matter candidate in several intermediate scenarios. Here, we take $V = M_\Psi = M_{\rm int}$, which is a reasonable approximation. The numerical results, obtained by solving the complete set of Boltzmann equations for the exact production rate, are in a reasonable agreement with our analytical approximation of Eq. (5.56).

We observe that in these unified scenarios DM density corresponding to the Planck measurements [36] can be directly produced from annihilation of SM particles even if the mediator Z' is extremely heavy and no SM particles charged under the extra $U(1)'$.

We can see in Fig. 5.9 that the natural hierarchy between the parameters of the theory is $M_{\rm int} \sim T_{\rm MAX} \sim 10^2 \ T_{\rm RH} \sim 10^2 \ m_{\rm DM}$, corresponding to the correct DM relic abundance. Therefore, the intermediate scale in such unified constructions could be closely related

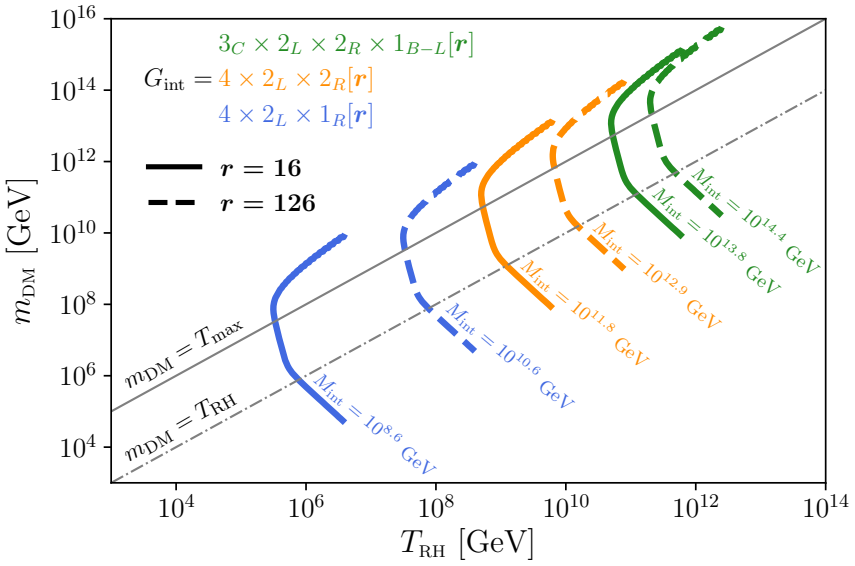

FIGURE 5.9 – *Relic density curves for the fermionic DM case in several $SO(10)$ breaking schemes and for different representations $[r]$ for the Higgs field responsible for intermediate scale breaking. We take $N_\Psi = Q_\Psi = y_\Psi = 1$ for illustrative purposes.*

to the inflaton mass as one expects it to be of the order of the maximum temperature reached by the SM thermal bath. The large hierarchy between these scales and the SM electroweak VEV naturally provides the suppressed DM-SM effective coupling required to produce the correct DM density non thermally via the freeze-in mechanism.

5.3 Discussion and conclusions

In this chapter, we studied generic effects of heavy non-standard fermions carrying standard model charges.

We have first assumed a non-standard complex scalar, singlet under the standard group, giving mass to those heavy fermions. We have considered an axion-like dark matter candidate, coming from the complex scalar itself. In this case, such axion-like particles would be able to decay into photons and the bounds on the new physics scale restrict their masses to be in the keV range. This is because the global symmetry directly connect their mass to their coupling. We have further considered that those scalars are too heavy as to be produced from the thermal bath, as it would be natural if they are to give mass to the heavy decoupled fermions. In this case, the lightest of the non-standard fermions would fit as a dark matter candidate. We are currently studying other possible constraints on such scenarios, especially regarding the warmness of the keV scale dark matter.

By extending the standard model gauge group with an extra local $U(1)$ symmetry, $U(1)'$, we have seen that even if all the standard model particles are uncharged under $U(1)'$, the new gauge boson Z' is able to mediate the production of dark matter particles. This is achieved by assuming the presence of heavy nonstandard fermions which are already needed for the theory to be consistent, once the cancellation of the gauge anomalies arising from this extension generate the generalized Chern-Simons couplings producing dark matter.

We have consistently found that for an intermediate scale Z', with mass in the range $10^{10} - 10^{14}\,\text{GeV}$, the parameter space providing the correct amount of dark matter in the universe is such that the new physics scale of the theory (Λ), and so the fermions we are integrating out, lies at least above the intermediate scale. The dark matter mass, though, can easily range from the TeV scale (if it is a fermion) or even from the keV scale (if it is a vector) to one order of magnitude above the maximal temperature achieved by the thermal bath.

In this work, we have also shown an interesting theoretical framework in which the temperature dependence of the dark matter production rate is high enough so that the production is UV-dominated even during the reheating process. This situation is not common in the literature, where the temperature dependence of interaction rates are usually as high as T^{12} for well-motivated models [74]. Indeed, this is the case when gluons produce vector dark matter, with $R_{X_1} \propto T^{12}$ ($R_{X_N} \propto T^{16}$) for an Abelian (a non-Abelian) dark matter candidate.

Chapter 6

Spin-2 and moduli portals to FIMPs

Contents

Open problems of the standard model of particle physics can be addressed by non-minimal, structural, extensions such as supersymmetry and string theory, as we have pointed out in Chapter 1. In such extensions, gravity can be consistently incorporated in a unified description of nature, along with the other fundamental interactions, in which general relativity and standard model are effective theories with nonstandard heavy particles in the spectrum. In this context, *feeble interactions* of the standard model fields to such nonstandard sector, comprised for instance of spin-2 and moduli fields, would be rather mandatory for the effective description to be consistent. As a consequence, these kinds of frameworks naturally accommodate the freeze-in of dark matter.

Here we study the freeze-in of scalar, fermionic and vector dark matter candidates from all standard model fields though the exchange of massless and massive spin-2 (Section 6.1) and moduli (Section 6.2) fields.

6.1 Spin-2 portal

Since all the evidence pointing to the existence of dark matter come from its gravitational interaction with the standard sector, it is very appealing to investigate how the freeze-in mechanism would proceed in an effective scenario which could be embedded in a theory of quantum gravity.

In general relativity, gravity is the effect of energy curving the space-time – a geometrical property instead of a fundamental interaction. Keeping this approach, a possible quantization of gravity is loop quantum gravity [228]. Another possibility, which is of interest for us, is that gravity is a fundamental interaction between particles, mediated by *gravitons*. A consistent theory of quantum gravity comprising the standard model and general relativity in the low-energy limit is string theory [229]. The (up to now) experimental fact that the rest and the gravitational masses are equal [230–233] base the *equivalence principle* which is the starting point of general relativity. Quantum gravity theories, though, might cause a tiny but detectable deviation of this equality, motivating the search for its violation [234–237].

In the same way that electromagnetism is mediated by photons, massless spin-1 fields A_μ, and have vector currents as its sources, $\bar{\psi}\gamma^\mu\psi$, gravity is thought to be mediated by massless * *spin-2 fields* $h_{\mu\nu}$, since its source is the stress-energy tensor $T^{\mu\nu}$ – everything that have energy, and this is certainly redundant, gravitates. A discussion on the detectability of such fields is performed for instance in [239]. It is interesting to notice that the possibility of the LHC to have detected a 125 GeV [44, 45] spin-2 particle, rather than the standard Higgs, was discussed in [240].

The gravity sector might also be comprised of massive spin-2 fields [241], a challenging possibility [242, 243] which have also found motivation in supergravity frameworks [244]. Mass terms in this case might be built by contracting the metric with a second metric, in the so-called bimetric theories. Consistent ghost-free theory of massive gravity is a promising area with recent important developments [245–251].

The freeze-out of scalar, fermionic and vector WIMPs with masses in the $100 - 1000\,\mathrm{GeV}$ range, through massive spin-2 fields and radions (scalars also coming from compactification of extra-dimensions) were considered in Ref. [252]. In this framework, the phenomenology of a massive spin-2 mediator at colliders [253], direct [254] and indirect [255] detection searches were considered.

The idea of spin-2 fields as dark matter candidates [256], was pursued in Refs. [102, 257, 258]. They have found that frozen-in spin-2 dark matter satisfies relic density and stability constraints if its mass lies in the range $1 - 66\,\mathrm{TeV}$, and if one considers self-interactions, it is lowered to the MeV range [259]. The freeze-in of scalar dark matter interacting with SM through the exchange of gravitons during reheating was considered in Ref. [103, 104, 260], they have found that the dark matter mass lies in the $10^9 - 10^{17}\,\mathrm{GeV}$ range.

*The recent observations of gravitational waves provide an upper bound on the mass of graviton of $m_h < 7.7 \times 10^{-23}\ \mathrm{eV}/c^2$ [238].

In this work [4], we generalize the previous analysis by considering spin-$0, \frac{1}{2}, 1$ dark and visible particles interacting through the exchange of gravitons and massive spin-2 fields, and we explore the impact of a resonant production of spin-2 mediators during reheating.

6.1.1 A minimal model of graviton and massive spin-2 portal

Our effective model of dark and visible particles interacting with gravitons ($h_{\mu\nu}$) and massive spin-2 fields ($\tilde{h}_{\mu\nu}$) is in the context of simplified DM models [252, 253]. We consider the following dimension-5 operators connecting the dark and visible sectors to gravity:

$$\mathcal{L} \supset \frac{1}{2M_{\rm P}} h_{\mu\nu} \left(\sum_i T_i^{\mu\nu} + T_j^{\mu\nu} \right) + \frac{1}{\Lambda} \tilde{h}_{\mu\nu} \left(g_{\rm SM} \sum_i T_i^{\mu\nu} + g_{\rm DM} T_j^{\mu\nu} \right) . \tag{6.1}$$

Notice we respect the equivalence principle, with an universal coupling to gravitons which depends only on the reduced Planck mass $M_{\rm P} \simeq 2.4 \times 10^{18}$ GeV [261]. In the case of the massive spin-2, while we do not need to assume universal couplings, for our purposes, we only differentiate its couplings to the visible ($g_{\rm SM}$) and dark ($g_{\rm DM}$) sectors. $\Lambda \lesssim M_P$ is an intermediate scale and governs the strength of the massive spin-2 interactions. Of course only two of the three parameters $(\Lambda, g_{\rm SM}, g_{\rm DM})$ are independent.

Finally, $T_i^{\mu\nu}$ ($T_j^{\mu\nu}$) is the stress-energy tensor of a standard model (dark matter) particle of spin-i (spin-j) and reads

$$\begin{aligned} T^0_{\mu\nu} &= \frac{1}{2} \left(\partial_\mu \phi \, \partial_\nu \phi + \partial_\nu \phi \, \partial_\mu \phi - g_{\mu\nu} \partial^\alpha \phi \, \partial_\alpha \phi \right) , \\ T^{1/2}_{\mu\nu} &= \frac{i}{4} \bar{\psi} \left(\gamma_\mu \partial_\nu + \gamma_\nu \partial_\mu \right) \psi - \frac{i}{4} \left(\partial_\mu \bar{\psi} \gamma_\nu + \partial_\nu \bar{\psi} \gamma_\mu \right) \psi , \\ T^1_{\mu\nu} &= \frac{1}{2} \left(F^\alpha_\mu F_{\nu\alpha} + F^\alpha_\nu F_{\mu\alpha} - \frac{1}{2} g_{\mu\nu} F^{\alpha\beta} F_{\alpha\beta} \right) . \end{aligned} \tag{6.2}$$

Our dark matter candidates in this work can be a real scalar (φ), a Dirac fermion (ψ) and a real vector (V). The freeze-in would proceed through s-channel annihilation of standard particles through graviton and massive spin-2 fields, assumed to have negligible abundances relative to that of the standard species.

The Feynman rules for the relevant interactions (for both visible and dark sectors) are given by

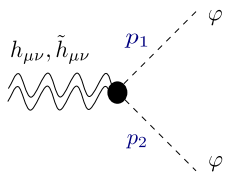

$$\propto -i \Big(\eta^{\mu\nu} (m_\phi^2 + (p_1 \cdot p_2)) - p_1^\mu p_2^\nu - p_1^\nu p_2^\mu \Big) ,$$

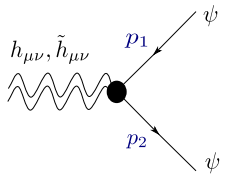

$$\propto -i\Big[\eta^{\mu\nu}(m_\psi + \frac{1}{2}(\not{p}_1 - \not{p}_2)) + \frac{1}{4}\gamma^\mu(p_1 - p_2)^\nu + \frac{1}{4}\gamma^\nu(p_1 - p_2)^\mu\Big]\,,$$

and

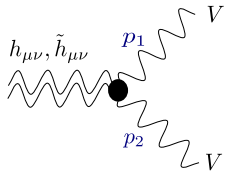

$$\propto -i\Big[(m_V^2 + (p_1 \cdot p_2))C^{\mu\nu}_{\rho\sigma} + D^{\mu\nu}_{\rho\sigma}\Big]\,,$$

where $\eta_{\mu\nu} = \text{diag}(1-1-1-1)$ is the Minkowski metric and the proportionality constants are just the corresponding couplings found in Eq. 6.1. We have defined

$$C^{\mu\nu}_{\rho\sigma} \equiv \eta^\mu_\rho \eta^\nu_\sigma + \eta^\mu_\sigma \eta^\nu_\rho - \eta^{\mu\nu}\eta_{\rho\sigma}\,,$$

$$D^{\mu\nu}_{\rho\sigma} \equiv \eta^{\mu\nu} p_{1\,\sigma} p_{2\,\rho}(\eta^\mu_\sigma p_1^\nu p_{2\,\rho} + \eta^\mu_\rho p_{1\,\sigma} p_2^\nu - \eta_{\rho\sigma} p_1^\mu p_2^\nu + (\mu \leftrightarrow \nu))\,.$$

Once spin-2 particles are not common in the dark matter literature, we here provide general results necessary for the computations done in this work. The propagator of a graviton with four-momentum k can be expressed in the Lorentz gauge as [262]

$$\Pi^h_{\mu\nu,\alpha\beta}(k) = \frac{\frac{1}{2}\eta_{\alpha\nu}\eta_{\beta\mu} + \frac{1}{2}\eta_{\alpha\mu}\eta_{\beta\nu} - \frac{1}{2}\eta_{\alpha\beta}\eta_{\mu\nu}}{k^2}\,. \tag{6.3}$$

The propagator of a massive spin-2 with four-momentum k can be written as [252, 262]

$$\Pi^{\tilde{h}}_{\mu\nu,\alpha\beta}(k) = \frac{iP_{\mu\nu,\alpha\beta}}{k^2 - m^2_{\tilde{h}} + im_{\tilde{h}}\Gamma_{\tilde{h}}}\,. \tag{6.4}$$

The sum over spin polarization states is given by

$$\sum_{s=1}^{5} \varepsilon_{\mu\nu}(k,s)\varepsilon_{\alpha\beta}(k,s) = P_{\mu\nu,\alpha\beta}\ , \tag{6.5}$$

where

$$P_{\mu\nu,\alpha\beta} = \frac{1}{2}(G_{\mu\alpha}G_{\nu\beta} + G_{\nu\alpha}G_{\mu\beta}) - \frac{1}{3}G_{\mu\nu}G_{\alpha\beta}, \tag{6.6}$$

with $G_{\mu\nu} \equiv \eta_{\mu\nu} - \frac{k_\mu k_\nu}{m^2_{\tilde{h}}}$.

An interesting detail to notice is that, even though we are only considering s-channel exchanges of spin-2 fields, the stress-energy tensor operator makes the squared amplitudes to depend on the Mandelstam variable t and not only on s as in the previous s-channel cases. We refer to the Appendix B of the journal version of this work [4] for their approximate expressions, under the limit $s, t \gg m^2_{\rm DM}, \mu^2_H$. After integrating over t (or $\cos\theta^*_{13}$), the

contribution of an initial state $i = H, f, G$ to the squared amplitude for the production of a dark matter candidate $j = \phi, \psi, V$ reads

$$\int d\Omega_{13}^{*}|\mathcal{M}_{ij}|^2 = \frac{\pi s^2}{60 M_{\rm P}^4} f_{ij}^{h}(s, m_X) + \frac{\pi g_{\rm SM}^2 g_{\rm DM}^2}{15\Lambda^4} \frac{s^4}{(s - m_{\tilde{h}}^2)^2 + m_{\tilde{h}}^2 \Gamma_{\tilde{h}}^2} f_{ij}^{\tilde{h}}(s, m_X)\,. \tag{6.7}$$

We have defined the functions $f_{ij}^{h}(s, m_X)$ and $f_{ij}^{\tilde{h}}(s, m_X)$ of the the Mandelstam variable s and dark matter mass m_X, which will be only order one numbers in the limit $s \gg m_X^2$. Here, for completeness, we provide the exact expressions of our amplitudes. In the expressions bellow, the first, second and third lines correspond respectively to $i = H, f$ and G.

We find for the scalar dark matter

$$f_{i\phi}^{h} = \begin{cases} \frac{1}{2} + \frac{\mu_H^2 + m_X^2}{s} + \frac{3\mu_H^4 + 3m_X^4 + 12\mu_H^2 m_X^2}{s^2} \\ \quad - \frac{4\mu_H^4 m_X^2 + 4\mu_H^2 m_X^4}{s^3} + \frac{28\mu_H^4 m_X^4}{s^4} \\ \frac{1}{4}\left(1 - \frac{4m_X^2}{s}\right)^2 \\ \left(1 - \frac{4m_X^2}{s}\right)^2 \end{cases} \qquad f_{i\phi}^{\tilde{h}} = \begin{cases} \frac{1}{3}\left(1 - \frac{4m_X^2}{s}\right)^2 \left(1 - \frac{4\mu_H^2}{s}\right)^2 \\ \left(1 - \frac{4m_X^2}{s}\right)^2 \\ 4\left(1 - \frac{4m_X^2}{s}\right)^2 \end{cases},$$

for the fermionic dark matter

$$f_{i\psi}^{h} = \left(1 - \frac{4m_X^2}{s}\right) \begin{cases} \frac{1}{4}\left(1 - \frac{4\mu_H^2}{s}\right)^2 \\ \quad + \frac{m_X^2}{2s}\left(3 - \frac{4\mu_H^2}{s} + \frac{28\mu_H^4}{s^2}\right) \\ \frac{3}{4}\left(1 + \frac{8m_X^2}{3s}\right)^2 \\ 3\left(1 + \frac{8m_X^2}{3s}\right)^2 \end{cases} \qquad f_{i\psi}^{\tilde{h}} = \left(1 - \frac{4m_X^2}{s}\right)\left(1 + \frac{8m_X^2}{s}\right) \begin{cases} \frac{1}{3}\left(1 - \frac{4\mu_H^2}{s}\right)^2 \\ 1 \\ 4 \end{cases},$$

and for the vector dark matter

$$f_{iV}^{h} = \begin{cases} \frac{3}{2}\left(1 + \frac{2m_X^2}{s} + \frac{6m_X^4}{s^2}\right) \\ \quad - \frac{\mu_H^2}{s}\left(1 + \frac{6m_X^2}{s}\right)\left(7 + \frac{2m_X^2}{s}\right) \\ \quad + \frac{\mu_H^4}{s^2}\left(19 + \frac{68m_X^2}{s} + \frac{84m_X^4}{s^2}\right) \\ \frac{1}{4}\left(13 + \frac{56m_X^2}{s}\frac{48m_X^4}{s^2}\right) \\ \left(13 + \frac{56m_X^2}{s}\frac{48m_X^4}{s^2}\right) \end{cases} \qquad f_{iV}^{\tilde{h}} = \left(13 + \frac{56m_X^2}{s}\frac{48m_X^4}{s^2}\right) \begin{cases} \frac{1}{3}\left(1 - \frac{4\mu_H^2}{s}\right)^2 \\ 1 \\ 4 \end{cases}.$$

We can therefore see from those expressions that if $s \gg m_X^2, \mu_H^2$ is a fair approximation while dark matter is being produced, the contributions of the graviton and a light $\tilde{h}$ set most of the production to happen near the reheating scale, since it would be UV-dominated regarding radiation era ($k = 2, n = 8$, following our previous analysis). A

heavy $\tilde{h}$, though, would dominate the production and establish most of the relic density before reheating had finished ($k = 4, n = 12$).

A very important piece of the amplitudes is the total decay width of the massive spin-2 field. Their decay modes into (visible or dark) scalars, fermions and vectors read

$$\Gamma_{\tilde{h}\to\varphi\varphi} = N_\varphi \frac{g_\varphi^2}{960\pi}\frac{m_{\tilde{h}}^3}{\Lambda^2}(1-4r_\varphi)^{5/2}\,, \tag{6.8}$$

$$\Gamma_{\tilde{h}\to\psi\psi} = N_\psi \frac{g_\psi^2}{160\pi}\frac{m_{\tilde{h}}^3}{\Lambda^2}\left(1+\frac{8}{3}r_\psi\right)(1-4r_\psi)^{3/2}\,, \tag{6.9}$$

and

$$\Gamma_{\tilde{h}\to VV} = N_V \frac{g_V^2}{960\pi}\frac{m_{\tilde{h}}^3}{\Lambda^2}(13+56r_V+48r_V^2)(1-4r_V)^{1/2}\,, \tag{6.10}$$

where $r_i \equiv m_i^2/m_{\tilde{h}}^2$, and therefore its total decay width reads

$$\begin{aligned}\Gamma_{\tilde{h}} =& 4\Gamma_{\tilde{h}\to\varphi\varphi} + 45\Gamma_{\tilde{h}\to\psi\psi} + 12\Gamma_{\tilde{h}\to VV} + \Gamma_{\tilde{h}\to\mathrm{DM}} \\ =& \frac{43 g_{\mathrm{SM}}^2 m_{\tilde{h}}^3}{96\pi\Lambda^2} + \Gamma_{\tilde{h}\to\mathrm{DM}}\,,\end{aligned} \tag{6.11}$$

with the appropriate $\Gamma_{\tilde{h}\to\mathrm{DM}}$ given in Eqs.(6.8)-(6.10).

We are now in a position to understand the behavior of the production rates in this model. Regardless of the spin of the dark matter candidate, this model present the following approximated production rates:

$$R_X(T)\Big|^{h} \approx \alpha\frac{T^8}{M_{\mathrm{P}}^4}\,, \qquad R_X(T)\Big|^{\tilde{h}} \approx \frac{g_{\mathrm{DM}}^2 g_{\mathrm{SM}}^2}{\Lambda^4}\times\begin{cases}\beta_1 T^8 & (m_{\tilde{h}}\ll T)\\ \beta_2 m_{\tilde{h}}^8 \frac{T}{\Gamma_{\tilde{h}}} K_1\left(\frac{m_{\tilde{h}}}{T}\right) & (m_{\tilde{h}}\sim T)\\ \beta_3 \frac{T^{12}}{m_{\tilde{h}}^4} & (m_{\tilde{h}}\gg T)\end{cases} \tag{6.12}$$

The values of α, β_1, β_2 and β_3 are collected in Table 6.1 at the end of this subsection.

In Fig. 6.1 we show the exact solution of the production rate for a scalar dark matter candidate (solid black curve), while in the cases of fermionic and vector dark matter the result would only be re-scaled. As we have done in Chapter 5, we show the rate as a function of the dimensionless parameter $x = m_{\tilde{h}}/T$ in order to understand the different regimes of the mediator. We have set the couplings to unity, $m_X = 1$ GeV, $m_{\tilde{h}} = 10^{12}$ GeV and $\Lambda = 10^{16}$ GeV.

We can clearly distinguish the three main regimes we have seen earlier in the case of the keV-scale dark matter: the light, the pole and the heavy ones. In addition, in this model we have a forth regime, due to the exchange of a graviton, which is independent of $m_{\tilde{h}}$ but that can only dominate the production of dark matter if the massive spin-2 field is too heavy as to produce dark matter. This forth regime is therefore referred to as a *decoupling* or *superheavy* regime, which is suppressed even relative to the Planck suppressed interaction. Once we have always $\Lambda < M_{\mathrm{P}}$, it is easy to understand why only in this decoupling regime the contribution of the graviton to the dark matter production

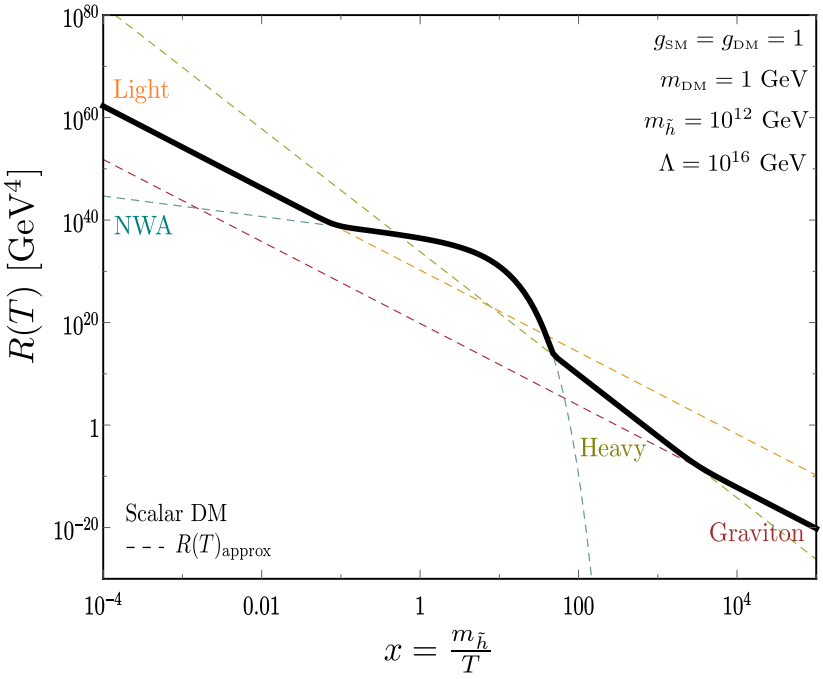

FIGURE 6.1 – *Exact evolution of the production rate (solid black curve) and its approximate results (dashed colored curves) as function of $m_{\tilde{h}}/T$, for a scalar dark matter of mass $m_X = 1$ GeV.*

can possibly be relevant. To guide the eye, we display in Fig. 6.1 coloured dashed lines corresponding to the approximate results of Eq. 6.12.

TABLE 6.1 – *Coupling coefficients*

Spin	α	β_1	β_2	β_3
0	1.9×10^{-4}	2.8×10^{-3}	1.2×10^{-5}	10.9
1/2	1.1×10^{-3}	1.7×10^{-2}	7.0×10^{-5}	65.2
1	2.3×10^{-3}	3.7×10^{-2}	1.5×10^{-4}	141

6.1.2 Agreement with relic density

We can now study the parameter space allowed by the relic density constraints.

Again, before solving the set of differential equations in order to find the relic density, we can use Eqs. (2.134)-(2.135) to estimate its behavior.

We first examine the contribution of the exchange of a graviton. As expected, we see that it is necessary to assume high values of dark matter mass and reheating temperature to overcome the Planck suppressed interaction:

$$\frac{\Omega_X^0 h^2}{0.12} \sim \left(\frac{\mathscr{B}_8}{1.8}\right)\left(\frac{\alpha}{\alpha^0}\right)\left(\frac{T_{\rm RH}}{10^{13}\,{\rm GeV}}\right)^3\left(\frac{m_X}{7.6\times 10^{12}\,{\rm GeV}}\right), \tag{6.13}$$

where we normalize the numerical factor α with its value in the scalar dark matter case.

The way a massive spin-2 mediator contributes to the dark matter production, as we have seen, depends on the relation between its mass and the temperature scale of the production. For the kind of interactions we have, we have also seen that most of the production is expected to happen around the reheating scale, since the production is UV-dominated relative to the radiation era and IR relative to the inflaton era (except for the heavy regime, where it is IR-UV mixed).

While the spin-2 mediator mass is much lighter then the reheating temperature, we have

$$\frac{\Omega_X^0 h^2}{0.12} \sim \left(\frac{\mathscr{B}_8}{1.8}\right)\left(\frac{\beta_1}{\beta_1^0}\right)\left(\frac{T_{\rm RH}}{10^{10}\,{\rm GeV}}\right)^3\left(\frac{\Lambda}{10^{16}\,{\rm GeV}}\right)^{-4}\left(\frac{m_X}{1.6\times 10^{11}\,{\rm GeV}}\right). \tag{6.14}$$

If the mediator mass is around the reheating scale, the contribution from the pole region dominates the production. In this case, there is no analytical expression for the integration over temperature in Eq. (2.134), but we can compute it numerically to estimate the parameter space providing the interred relic density value:

$$\frac{\Omega_X^0 h^2}{0.12} \sim \frac{\beta_2}{\beta_2^0}\left(\frac{10^{16}\,{\rm GeV}}{\Lambda}\right)^2 \times \begin{cases} \dfrac{\mathscr{B}_{\rm NWA}}{4.17}\,\dfrac{I_{\rm NWA}(10^{11}{\rm GeV})}{2.4\times 10^{-2}}\,\dfrac{m_X/{\rm GeV}}{0.31}\,\dfrac{m_{\tilde h}/{\rm GeV}}{10^{10}} \\ \dfrac{\mathscr{B}_{\rm NWA}}{2.3\times 10^{3}}\,\dfrac{I_{\rm NWA}(5\times 10^{13}{\rm GeV})}{1.5\times 10^{-7}}\,\dfrac{m_X/{\rm GeV}}{0.075}\,\dfrac{m_{\tilde h}/{\rm GeV}}{1.2\times 10^{15}}. \end{cases} \tag{6.15}$$

Notice that we have taken into account the width as given in Eq. (6.11), which gives the smaller dependence on the new physics scale. We denote by $I_{\rm NWA}$ the integration performed in this estimation, which is a function of the reheating temperature and of course of the spin-2 mediator mass. By defining $x = m_{\tilde h}/T$, $x_{\rm RH} = m_{\tilde h}/T_{\rm RH}$ and $x_0 = m_{\tilde h}/T_0$, it reads

$$I_{\rm NWA}(T_{\rm RH}) = \int_{x_{\rm RH}}^{x_0} dx\, x^3 K_1(x)\,.$$

As it is clear from Eq. (6.15), the boost factor depend strongly on the reheating temperature and mediator mass, through $I_{\rm NWA}$ and also through the corresponding integration over temperature from $T_{\rm RH}$ until $T_{\rm MAX}$.

Finally, under the heavy mediator regime, we have

$$\frac{\Omega_X^0 h^2}{0.12} \sim \left(\frac{\mathscr{B}_{12}}{35.4}\right)\left(\frac{\beta_3}{\beta_3^0}\right)\left(\frac{T_{\rm RH}}{10^{10}\,{\rm GeV}}\right)^7\left(\frac{\Lambda}{10^{16}\,{\rm GeV}}\right)^{-4}\left(\frac{m_X}{4.7\times 10^{10}\,{\rm GeV}}\right)\left(\frac{m_{\tilde h}}{10^{11}\,{\rm GeV}}\right)^{-4}. \tag{6.16}$$

In Fig. 6.2 we scan over a wide range of spin-2 mediator mass and reheating temperature and show the contours providing $\Omega_X^0 h^2 = 0.12$ for two values of dark matter mass: $m_X = 1$ GeV (dashed curve) and $m_X = 10^{10}$ GeV (solid curve). We show the results for a scalar dark matter, with $g_{\rm SM} = g_{\rm DM} = 1$ and a new physics scale of $\Lambda = 10^{16}$ GeV. In what follows, we describe our results from smaller to larger values of spin-2 mediator mass.

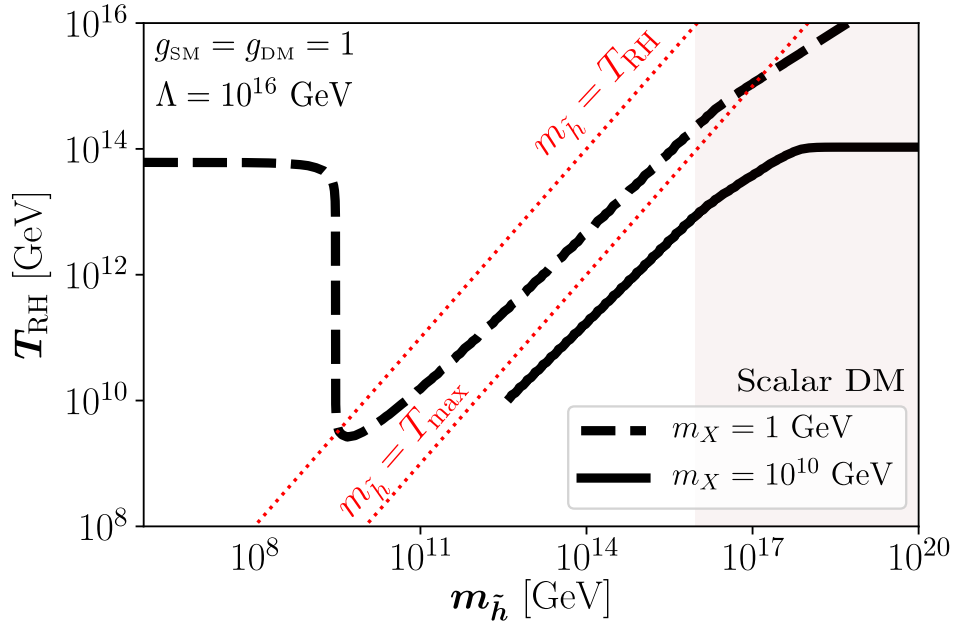

FIGURE 6.2 – *Values of T_{RH} and $m_{\tilde{h}}$ giving rise to the observed scalar DM relic abundance for $m_X = 1$ GeV and 10^{10} GeV, $g_{DM} = g_{SM} = 1$ and $\Lambda = 10^{16}$ GeV. The dotted diagonal lines with $m_{\tilde{h}} = T_{RH}$ and $m_{\tilde{h}} = T_{max} = 100\, T_{RH}$ are shown for reference.*

First of all, when $m_{\tilde{h}} < 2m_X$, the production is only possible through off-shell exchange of spin-2 mediators.

When $m_{\tilde{h}} \ll T_{\rm RH}$, the production happens under the light mediator regime, which is independent of the mediator mass and, for a given dark matter mass, the relic density value is entirely set by the reheating temperature. By using Eq. (6.14) for $m_X = 1$ GeV, we find a good relic density for $T_{\rm RH} \simeq 5.4 \times 10^{13}$ GeV, while from the exact solution shown in Fig. 6.2 we find $T_{\rm RH} \simeq 6.5 \times 10^{13}$ GeV.

While $m_{\tilde{h}}$ is still much smaller than $T_{\rm RH}$, we can integrate $I_{\rm NWA}$ from 0 to infinity, which give us just a factor $3\pi/2$ and in this case we have $\mathscr{B}_{\rm NWA} = 1$. We can therefore find the moment where the pole region starts dominating the production by equaling Eqs. (6.14) and (6.15) accordingly, which happens for $m_{\tilde{h}} \simeq 6.7 \times 10^9$ GeV, in an acceptable agreement with the vertical dashed line at $m_{\tilde{h}} \simeq 3 \times 10^9$ GeV. This happens because the on-shell production of the massive spin-2 mediator enhances the cross-section, so that smaller values of reheating temperature is needed to not overclose the universe. For heavier mediators, $I_{\rm NWA}$ starts to depend on $T_{\rm RH}$ and $m_{\tilde{h}}$, so that the relic contours monotonically increase. This also happens when $m_{\tilde{h}} > T_{\rm MAX}$, as we can see for the case of $m_X = 10^{10}$ GeV.

As expected from Fig. (6.1), when the spin-2 mediator mass start to be much larger than the reheating temperature, the contribution of the heavy regime starts to dominate the production. Estimating when it happens in this case is not possible since both pole and heavy regimes depend on $T_{\rm RH}$ and $m_{\tilde{h}}$, but we can still verify whether our approximations are reliable. If we take the value of $m_{\tilde{h}}$ when it is equal to the maximal temperature, $m_{\tilde{h}} \simeq 1.2 \times 10^{17}$ GeV, Eq. (6.16) leads us to a good relic density if $T_{\rm RH} \simeq 10^{15}$ GeV.

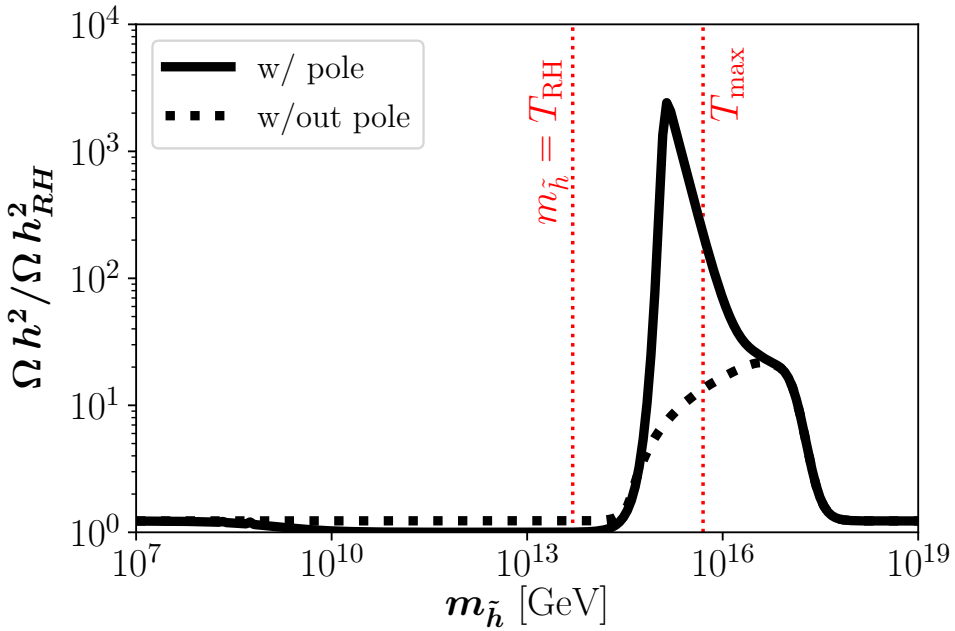

FIGURE 6.3 – *Boost factor behavior as function of $m_{\tilde{h}}$, for $T_{RH} = 5 \times 10^{13}$ GeV and $T_{MAX} = 5 \times 10^{15}$ GeV.*

For even higher values of $m_{\tilde{h}}$, the contribution of the heavy regime starts to become more suppressed than the Planck suppressed production through graviton exchange and therefore the agreement with relic density is again set only by the reheating temperature value for a given dark matter mass. We see this happening in the case of $m_X = 10^{10}$ GeV. However, the region of our parameter space with $m_{\tilde{h}} > \Lambda$ is not reliable since our effective approach is not valid. This is indicated by the shaded red region.

We end this section with a clear picture of the relevance in properly considering the production during reheating. In Fig. 6.3, we show the ratio of the relic abundance computed with the exact numerical solution, Ωh^2, to the instantaneous reheating approximation, $\Omega h^2_{\rm RH}$, which assumes that the relic density of dark matter at reheating is zero and instantaneously increases to the value set by the model of dark matter production. The solid curve stand for the exact calculation of the rate while the dashed curve only neglects the width of the massive spin-2 mediator. Here we remind the reader the definition of the boost factor:

$$\mathscr{B}(T_{\rm RH}, T_{\rm MAX}) \equiv 1 + \frac{\Omega^0_X h^2_{\rm ID}}{\Omega^0_X h^2_{\rm RD}} \simeq 1 + 1.6\, c\, T^7_{\rm RH} \left(\int_{T_{\rm RH}}^{T_{\rm MAX}} dT \frac{R_X(T)}{T^{13}} \right) \left(\int_{T_0}^{T_{\rm RH}} dT \frac{R_X(T)}{T^6} \right)^{-1} ,$$

so that the ratio in Fig. 6.3 encodes the uncertainties of the approximations on the rate as well of the constant c.

There are several effects of non-instantaneous reheating, depending on the mass of the mediator $m_{\tilde{h}}$ relative to $T_{\rm RH}$ and $T_{\rm MAX}$:

- If $m_{\tilde{h}} \ll T_{\rm RH}$, the dark matter production happens mainly through the exchange of the massive spin-2 mediator in its light regime, with $\mathscr{B} \approx 1.8$. This is seen by the horizontal part of the solid line at the smallest values of $m_{\tilde{h}}$.

- When $m_{\tilde{h}}$ approaches the scale of dark matter production in our model, $T_{\rm RH}$, the contribution from the pole of the massive spin-2 mediator starts dominating the production, first with $\mathscr{B}_{\rm NWA} = 1$ and $I_{\rm NWA}$ nearly independent of the mediator mass and reheating temperature. If we ignore the pole in this region of the parameter space, the abundance follows as in the light mediator regime. It turns out that the ratio of the integrals over the Bessel function exhibit a wild maximal value for a given mediator mass but, as far as we could see, this is to be found numerically. For the reheating temperature chosen in this figure, $T_{\rm RH} = 5 \times 10^{13}$ GeV, we have verified in Eq. (6.15) that $\mathscr{B}_{\rm NWA} \simeq 2.3 \times 10^3$ when $m_{\tilde{h}} \simeq 1.5 \times 10^{15}$ GeV.
- The effect of the pole is felt until the moment where $m_{\tilde{h}}$ is much higher than the typical temperature of dark matter production, so that the rate enters in the heavy mediator regime. In this case, the boost factor drops from its peak due to the pole, to the shoulder at around $m_{\tilde{h}} = 10^{17}$ GeV, where the rate is proportional to T^{12}. Here, the boost factor is approximately 20, smaller but not very far from the approximated value. The dotted line ignores the effect of the pole and shows the smooth transition between rates which vary as T^8 to T^{12} to T^8.
- Finally, at the largest values of $m_{\tilde{h}}$ shown in the figure, the production rate is dominated by graviton exchange, and the rate again varies as T^8, with a boost factor close to 1.8.

6.2 Moduli portal

In the low-energy limit of higher-dimensional supergravity or string theory extensions of the standard model, weakly coupled scalar fields (moduli) are usually present. They might come from the compactification of the higher-dimensional metric, dilaton or various anti-symmetric tensors. In particular, internal volumes and shapes and their axionic partners are abundant in such constructions. Most of them are flat directions at tree-level and get potentials and therefore masses by various perturbative and non-perturbative effects. Their resulting masses and vacuum expectation values are model-dependent and will be taken as free parameters in what follows. Their vacuum expectation determine values of four-dimensional parameters: gauge and Yukawa couplings, wave functions of various fields and Planck mass. If one assumes that the low-energy theory, obtained after their decoupling, is the standard model or a phenomenologically motivated extension of it, then their couplings can be obtained by starting from the low-energy theory and expanding the low-energy parameters in a power series. If moduli fields are heavier than the reheating temperature, then they can be safely replaced by their vacuum expectation values. If they are lighter however, they can lead to various physical effects. This strategy was used in early papers [234, 263–271] in order to study various low-energy effects of the moduli fields.

As weakly-coupled fields, easily long-lived, out-of-equilibrium moduli decays could produce large amount of entropy if they come to dominate the universe after having decoupled while ultra-relativistic. This so-called *cosmological moduli problem* [272–274] is in fact a well-motivated disaster, and a consequence of the generic phenomenon that we discussed in detail in Section 2.3.1. As we have discussed in Ref. [6], this problem would be avoided if the moduli mass is lighter than 10^{-26} eV or heavier than 10 TeV.

Given their feeble interactions, moduli fields are naturally embedded in the context of freeze-in production. Indeed, they were considered good FIMP candidates [91, 275] and could also non-thermally produce dark matter [276–280]. The higher-dimensional and derivative operators that usually couple moduli to the other fields implies that they may become very important at high energies, being therefore potentially relevant for the freeze-in mechanism during reheating.

In the work we discuss now [6], we intend to contribute to the list of interesting consequences of moduli fields by studying their possible role as mediators between the visible and dark sectors.

6.2.1 A minimal model for the moduli portal

Let us consider a complex modulus field $\mathcal{T}$, decomposed as $\mathcal{T} \equiv t + ia$. One can define its couplings to a standard model field k by expanding its wave-function $\mathcal{Z}_k$:

$$\mathcal{Z}_k(\mathcal{T}, \bar{\mathcal{T}}) \approx 1 + \frac{c_k}{\Lambda}\mathcal{T} + \frac{d_k}{\Lambda}\bar{\mathcal{T}} \equiv 1 + \frac{\alpha_k}{\Lambda}t + i\frac{\beta_k}{\Lambda}a\,. \tag{6.17}$$

In this work, we restrict ourselves to CP-conserving Lagrangians, so that c_k and d_k are real coefficients of order one. We defined the couplings to the real and imaginary components of $\mathcal{T}$ as $\alpha_k = c_k + d_k$ and $\beta_k = c_k - d_k$ respectively.

Consistency of the effective field theory requires that the new physics scale Λ is the largest mass scale of the theory, in particular larger than dark matter or mediator masses, and the maximal temperature of the thermal bath. It can be identified as a string, unification or SUSY/SUGRA breaking scale, for instance. For simplicity, we will consider only one modulus field throughout our work. Generalization to several fields is straightforward and would share the same kind of considerations.

We can then express generic couplings of the modulus field to the visible sector as

$$\begin{aligned}\mathcal{L}_{\mathcal{T}}^{\text{SM}} \supset\ & \mathcal{Z}_H|D_\mu H|^2 - \mu^2(\mathcal{T}, \bar{\mathcal{T}})|H|^2 - \lambda(\mathcal{T}, \bar{\mathcal{T}})|H|^4 \\ & + \frac{1}{2}\left(\mathcal{Z}_L \bar{f}_L i\not{D} f_L + \mathcal{Z}_R \bar{f}_R i\not{D} f_R + \text{h.c.}\right) \\ & - \frac{1}{4}\mathcal{Z}_G\, G_{\mu\nu}G^{\mu\nu} - \mathcal{Z}'_G\, G_{\mu\nu}\tilde{G}^{\mu\nu}\,,\end{aligned} \tag{6.18}$$

where $\mathcal{Z}_H (= 1 + \frac{\alpha_H}{\Lambda}t)$, $\mathcal{Z}_{L,R} (= 1 + \frac{\alpha_{L,R}}{\Lambda}t + i\frac{\beta_{L,R}}{\Lambda}a)$, $\mathcal{Z}_G (= 1 + \frac{\alpha_G}{\Lambda}t)$ and $\mathcal{Z}'_G (= \frac{\beta_G}{\Lambda}a)$ are the wave-functions of the standard scalar (H), fermionic (f) and gauge (G_μ) fields respectively. In the above equation, $G_{\mu\nu}$ is the field strength tensor of the gauge field (G_μ) and $\tilde{G}^{\mu\nu} (= \frac{1}{2}\epsilon^{\mu\nu\rho\sigma}G_{\rho\sigma})$ is its dual field strength tensor.

From the first line of Eq.(6.18) we see that the scalar potential depends on the mass parameter μ which is also a function of the moduli fields. We can parametrize the contribution of the modulus to the μ-parameter in a similar fashion as in Eq.(6.17):

$$\mu^2 = \mu_0^2\left(1 + \frac{\alpha_H}{\Lambda}\,t\right)\,, \tag{6.19}$$

with μ_0 being the SM μ-parameter that reproduces the observed Higgs mass at the electroweak scale. As Λ is the highest scale in the theory, contribution to the Higgs mass due to moduli is small. On the other hand there is a second possibility that the μ-parameter gets generated at a scale ($\sqrt{\langle F\rangle}$) close to the Planck scale. In this case the effective μ-parameter can be written as

$$\mu^2 = \mu_0^2 + \frac{\langle F\rangle}{M_{\rm P}}\, t\,, \tag{6.20}$$

where $\sqrt{\langle F\rangle}$ is the vev of the "spurion" field. In this case, a considerable amount of fine-tuning is needed as to reproduce the observed Higgs mass since the coupling of t to the Higgs is quite large. In order to ensure that the width of t is smaller than its mass, m_t, we demand $\langle F\rangle \lesssim m_t M_P$.

The effective interactions between the components of the modulus and SM fields, at the first order in $1/\Lambda$, read

$$\begin{aligned}\mathcal{L}_{\mathcal{T}}^{\rm SM} \supset & \frac{\alpha_H}{\Lambda}\, t\, |D_\mu H|^2 - \frac{\alpha_H}{\Lambda}\, \mu_0^2\, t\, |H|^2 \\ & + \left(\frac{1}{2\Lambda}\, t\, \bar f i\gamma^\mu(\alpha_{\rm V}^f - \alpha_{\rm A}^f\gamma_5) D_\mu f + \text{h.c.}\right) + \frac{1}{2\Lambda}\partial_\mu a\, \bar f\gamma^\mu(\beta_{\rm V}^f - \beta_{\rm A}^f\gamma_5) f \\ & - \frac{1}{4}\frac{\alpha_G}{\Lambda}\, t\, G_{\mu\nu}G^{\mu\nu} + 2\frac{\beta_G}{\Lambda}\, \partial_\mu a\, \epsilon^{\mu\nu\rho\sigma} G_\nu \partial_\rho G_\sigma\,,\end{aligned} \tag{6.21}$$

where we have identified the chiral couplings as $\alpha_{\rm V}^f = (\alpha_L + \alpha_R)/2$ and $\alpha_{\rm A}^f = (\alpha_L - \alpha_R)/2$, with analogous definitions for the couplings of the imaginary part of the moduli.

At this point we can make some remarks. Since the kinetic term of Higgs needs to be real, the Higgs sector only couples to the real part of the modulus field t. Interestingly, this features were already noticed in the effective model of a keV-scale dark matter, with a global $U(1)$ symmetry in the potential (Section 5.1). In the present case, though, one observes a shift symmetry in the Lagrangian regarding the imaginary part of the moduli ($a \to a +$ const), making the nature of its couplings to differ from the real moduli case.

By analogy, one can write the same type of couplings to the dark matter particles, considered as scalars (φ), fermions (ψ) and vectors (V). Their interactions with moduli read

$$\mathcal{L}_{\mathcal{T}}^{\varphi} = \frac{\alpha_\varphi}{\Lambda}\, t\, |\partial_\mu \varphi|^2\,, \tag{6.22}$$

$$\mathcal{L}_{\mathcal{T}}^{\psi} = \left(\frac{1}{2\Lambda}\, t\, \bar\psi i\gamma^\mu(\alpha_{\rm V}^\psi - \alpha_{\rm A}^\psi\gamma_5)\, \partial_\mu\psi + \text{h.c.}\right) + \frac{1}{2\Lambda}\, \partial_\mu a\, \bar\psi\gamma^\mu(\beta_{\rm V}^\psi - \beta_{\rm A}^\psi\gamma_5)\psi\,, \tag{6.23}$$

and

$$\mathcal{L}_{\mathcal{T}}^{V} = -\frac{1}{4}\frac{\alpha_V}{\Lambda}\, t\, V_{\mu\nu}V^{\mu\nu} + 2\frac{\beta_V}{\Lambda}\, \partial_\mu a\, \epsilon^{\mu\nu\rho\sigma} V_\nu \partial_\rho V_\sigma\,. \tag{6.24}$$

As in the case of the Higgs sector, the scalar dark matter does not couple to the imaginary part of the moduli. An immediate consequence, which will be discussed in what follows, is that only the real part of moduli contributes to the freeze-in of a scalar dark matter – regardless of the standard model initial states.

SM \ DM	spin-0	spin-$\frac{1}{2}$	spin-1
spin-0	$f_H^2(s)$	$2f_H^2(s)$	$1/2\ f_H^2(s)$
spin-1/2	0	0	0
spin-1	$1/2\ \alpha_G^2$	α_G^2	$1/4\ \alpha_G^2$

SM \ DM	spin-0	spin-$\frac{1}{2}$	spin-1
spin-0	0	0	0
spin-1/2	0	0	0
spin-1	0	$16\beta_G^2$	$64\beta_G^2$

TABLE 6.2 – *Coefficients of the squared amplitudes: $\lambda^t_{s_i,s_f}$ (left panel) and $\lambda^a_{s_i,s_f}$ (right panel) (Eqs. 6.26, 6.27 and 6.28).*

The interactions of fermions (Ψ, standard or dark) with moduli are essentially different from the scalar and vector cases, due to their chirality. The first aspect of this remark is evident from the amplitudes for their interactions with moduli:

$$\begin{aligned}\mathcal{M}_{t\bar{\Psi}\Psi} &= -\frac{i}{2\Lambda}\bar{u}(p_1)(\not{p}_1 - \not{p}_2)(\alpha_{\rm V}^{\Psi} - \alpha_{\rm A}^{\Psi}\gamma_5)v(p_2) = -i\frac{\alpha_{\rm V}^{\Psi} m_\Psi}{\Lambda}\bar{u}(p_1)v(p_2)\,,\\ \mathcal{M}_{a\bar{\Psi}\Psi} &= \frac{1}{2\Lambda}\bar{u}(p_1)(\not{p}_1 + \not{p}_2)(\beta_{\rm V}^{\Psi} - \beta_{\rm A}^{\Psi}\gamma_5)v(p_2) = -\frac{\beta_{\rm A}^{\Psi} m_\Psi}{\Lambda}\bar{u}(p_1)\gamma_5 v(p_2)\,,\end{aligned} \tag{6.25}$$

where p_1 and p_2 are the four-momenta of the fermions and m_Ψ is the mass of the fermion. We notice that if the fermions are on-shell, we have an explicit dependence on their mass due to the Dirac equation. As a consequence, *above the electroweak scale, standard fermions cannot produce any of the dark matter particles.* The other aspect we point out is that the fermionic coupling to the real part of the moduli is CP-even, so that the corresponding rates will depend only on the vector coupling ($\alpha_{\rm V}^{\Psi}$); and that the fermionic coupling to the imaginary part of the moduli is CP-odd and therefore the corresponding rates will depend only on the axionic coupling ($\beta_{\rm A}^{\Psi}$).

The squared amplitudes of s-channel SM annihilations into DM candidates of spin s_f ($|\mathcal{M}|^2_{s_f}$) can be put in a compact form:

$$|\mathcal{M}|^2_0 = \frac{\alpha_\varphi^2}{\Lambda^4}\frac{s^4\left(1-\frac{2m^2_{\rm DM}}{s}\right)^2}{(s-m_t^2)^2+m_t^2\Gamma_t^2}\sum_{s_i}\lambda^t_{s_i,0}(s) \tag{6.26}$$

$$|\mathcal{M}|^2_{1/2} = \frac{(\alpha_V^\psi)^2}{\Lambda^4}\frac{m^2_{\rm DM}s^3\left(1-\frac{4m^2_{\rm DM}}{s}\right)}{(s-m_t^2)^2+m_t^2\Gamma_t^2}\sum_{s_i}\lambda^t_{s_i,1/2}(s) + \frac{(\beta_A^\psi)^2}{\Lambda^4}\frac{m^2_{\rm DM}s^3}{(s-m_a^2)^2+m_a^2\Gamma_a^2}\sum_{s_i}\lambda^a_{s_i,1/2}(s) \tag{6.27}$$

$$|\mathcal{M}|^2_1 = \frac{\alpha_V^2}{\Lambda^4}\frac{s^4\left(1-\frac{4m^2_{\rm DM}}{s}+\frac{6m^4_{\rm DM}}{s^2}\right)}{(s-m_t^2)^2+m_t^2\Gamma_t^2}\sum_{s_i}\lambda^t_{s_i,1}(s) + \frac{\beta_V^2}{\Lambda^4}\frac{s^4\left(1-\frac{4m^2_{\rm DM}}{s}\right)}{(s-m_a^2)^2+m_a^2\Gamma_a^2}\sum_{s_i}\lambda^a_{s_i,1}(s). \tag{6.28}$$

We parametrize the contribution of the SM initial state with spin s_i for the production of DM of spin s_f through the exchange of a field j by $\lambda^j_{s_i,s_f}$, which may be a function of

the Mandelstam variable s, the masses and couplings involved in the processes. They are given in Table 6.2.

The computation of the decay widths of the moduli fields is straightforward. The real component of the modulus may decay into standard scalars and vectors, since the decay into fermions is not allowed above the electroweak symmetry breaking. We have therefore

$$\Gamma_t = 4\,\Gamma_{t\to HH} + 12\,\Gamma_{t\to GG} + \Gamma_{t\to \mathrm{DMDM}} = \frac{m_t^3}{\pi\Lambda^2}\Big(\frac{f_H(m_t^2)^2}{8}\sqrt{1-\frac{4\mu_0^2}{m_t^2}} + \frac{3}{16}\alpha_{\mathrm{G}}^2\Big) + \Gamma_{t\to \mathrm{DMDM}}, \tag{6.29}$$

The distinct ways of writing the mass parameter of the Higgs lead us to define the function

$$f_H(x) \equiv \begin{cases} \alpha_H & \text{(case of Eq. (6.19))} \\ \alpha_H\Big(1-\frac{2\mu_0^2}{x}\Big) + \frac{2\Lambda}{x}\frac{\langle F\rangle}{M_P} & \text{(case of Eq. (6.20))} \end{cases} \tag{6.30}$$

In the case of the imaginary component, decay into scalars is prohibited, and we have simply

$$\Gamma_a = 12\,\Gamma_{a\to GG} + \Gamma_{a\to \mathrm{DMDM}} = \frac{m_a^3}{\pi\Lambda^2}3\beta_{\mathrm{G}}^2 + \Gamma_{a\to \mathrm{DMDM}}. \tag{6.31}$$

The partial decay widths of the real and imaginary parts of the modulus into dark matter read respectively

$$\Gamma_{t\to \mathrm{DMDM}} = \frac{m_t^3}{\pi\Lambda^2}\sqrt{1-\frac{4m_{\mathrm{DM}}^2}{m_t^2}} \times \begin{cases} \frac{\alpha_\varphi^2}{32}\Big(1-\frac{2m_{\mathrm{DM}}^2}{m_t^2}\Big)^2, & \text{for } \varphi \\ \frac{(\alpha_V^\psi)^2}{8}\frac{m_{\mathrm{DM}}^2}{m_t^2}\Big(1-\frac{4m_{\mathrm{DM}}^2}{m_t^2}\Big), & \text{for } \psi \\ \frac{\alpha_V^2}{64}\Big(1-\frac{4m_{\mathrm{DM}}^2}{m_t^2}+\frac{6m_{\mathrm{DM}}^4}{m_t^4}\Big), & \text{for } V \end{cases} \tag{6.32}$$

and

$$\Gamma_{a\to \mathrm{DMDM}} = \frac{m_a^3}{\pi\Lambda^2}\sqrt{1-\frac{4m_{\mathrm{DM}}^2}{m_a^2}} \times \begin{cases} 0, & \text{for } \varphi \\ \frac{1}{8}(\beta_A^\psi)^2\frac{m_{\mathrm{DM}}^2}{m_a^2}, & \text{for } \psi \\ \frac{\beta_V^2}{4}\Big(1-\frac{4m_{\mathrm{DM}}^2}{m_a^2}\Big), & \text{for } V \end{cases} \tag{6.33}$$

From the squared amplitudes, we can conclude that also in this moduli portal the production of any of our dark matter candidates are UV-dominated with respect to the radiation era. The production during reheating is IR-UV mixed in the scalar and vector dark matter cases, while IR-dominated for the fermionic dark matter, because of the helicity split.

Far from the pole of the propagators, we might assume $\Gamma_{t,a} \ll m_{t,a}$. In the limit $m_{\mathrm{DM}} \ll T$, we can obtain analytical solutions for the production rate $R_{s_f}^j$ of a dark matter of spin s_f

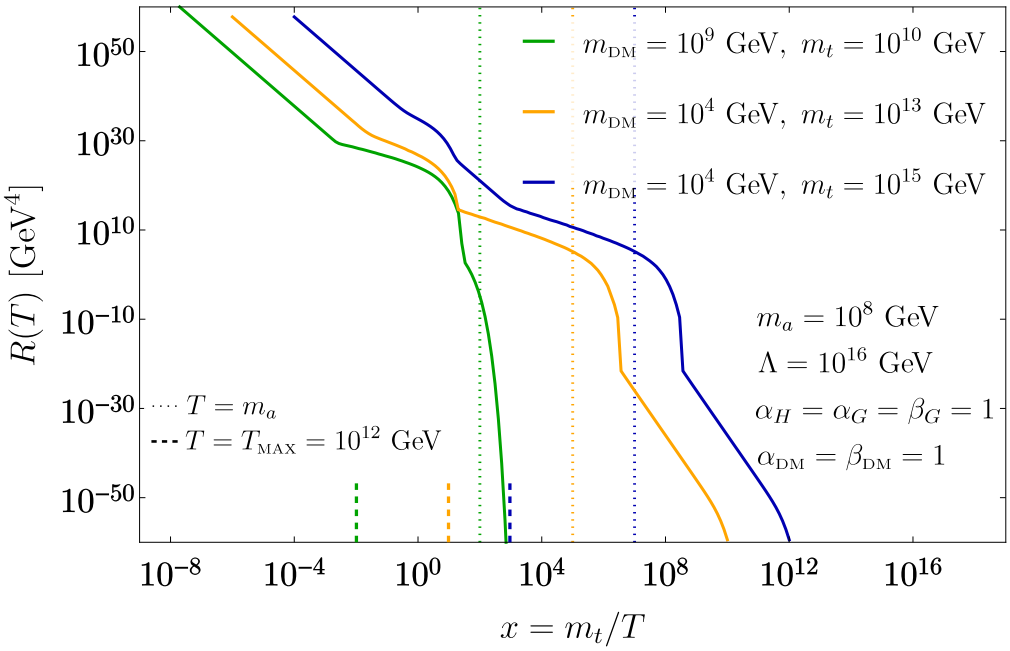

FIGURE 6.4 – *Evolution of the production rate of fermionic dark matter as function of temperature, for different masses of dark matter and real component of the modulus field.*

due to the exchange of a mediator j:

$$R^j_{0,1}(T) = \delta^j_{0,1} \times \begin{cases} \dfrac{T^8}{\Lambda^4} & (m_j \ll T) \\ \dfrac{m_j^8}{\Lambda^4}\dfrac{T}{\Gamma_j} K_1\left(\dfrac{m_j}{T}\right) & (m_j \sim T) \\ \dfrac{T^{12}}{m_j^4 \Lambda^4} & (m_j \gg T) \end{cases} \quad , \quad R^j_{\frac{1}{2}}(T) = \delta^j_{\frac{1}{2}} \times \begin{cases} \dfrac{m_{\rm DM}^2 T^6}{\Lambda^4} & (m_j \ll T) \\ \dfrac{m_{\rm DM}^2 m_j^6}{\Lambda^4}\dfrac{T}{\Gamma_j} K_1\left(\dfrac{m_j}{T}\right) & (m_j \sim T) \\ \dfrac{m_{\rm DM}^2 T^{10}}{m_j^4 \Lambda^4} & (m_j \gg T) \end{cases} \tag{6.34}$$

where the proportionality constants $\delta^j_{s_f}$ are given in Table 6.3, at the end of this section.

In Fig. 6.4, we show the exact solutions of the total production rate * of the fermionic dark matter for a representative set of free parameters, as a function of the variable $x = m_t/T$. We set the new physics scale Λ to be 10^{16} GeV (GUT scale), $T_{\rm MAX} = 10^{12}$ GeV and the mass of the axionic modulus to be 10^8 GeV. For simplicity, all the couplings are set to unity. From left to right, the mass of the real component of the modulus is set to 10^{10}, 10^{13} and 10^{15} GeV (green, orange and blue curves, respectively). The mass of the fermionic dark matter is set to be between the mediator masses in the first case (10^9 GeV) and to be relatively light in the second and third cases (10^4 GeV).

*We have used the CUBA package [147], with Bose-Einstein distribution function for the Higgs and gauge bosons in the initial states.

As it is by now clear, there are two generic features of the production rates. The first one is the strong temperature dependence: the higher the temperature (small x region), the more dark matter would be produced. The second one is the threshold for dark matter production which is due to the Boltzmann suppressed photon distribution having $T > M_{DM}$ (large x). This happens just after $x = 10$, 10^9 and 10^{11} for the three cases respectively.

Between those two extremes, we can notice the effects of the pole regions once T reaches m_t ($x \sim 1$) and m_a ($x = 10^2$, 10^5 and 10^7 for $m_t = 10^{10}$, 10^{13} and 10^{15} GeV respectively). Notice that the production rates for the scalar dark matter would not have the effect of the poles of a since it couples only to t. The production rate of a vector dark matter would have the same qualitative features of the fermionic case but with a steeper bend far from resonances, since the temperature dependencies in the light and heavy regimes are T^8 and T^{12} in the scalar and vector dark matter cases and T^6 and T^{10} in the fermionic case.

The presence of the pole regions depend on the low and high temperature thresholds. It will not appear if the Boltzmann suppression takes place before it (as in the green curve, for $x \sim 100$). Since the radiation content has a maximal temperature, fixed to 10^{12} GeV in Fig. 6.4, the production rate will have maximal values at $x = 10^{-2}, 10$ and 10^3. As a consequence, the pole due to the real component exchange would not contribute for the cases in orange and blue.

That said, we can now proceed to the study of our viable parameter space.

t \ DM	spin-0	spin-$\frac{1}{2}$	spin-1
Light	$\frac{\pi^3}{108000}\alpha_\varphi^2\alpha_{\rm SM}^2$	$\frac{\zeta(3)^2}{8\pi^5}\left(\alpha_V^\psi\right)^2\alpha_{\rm SM}^2$	$\frac{\pi^3}{21600}\alpha_V^2\alpha_{\rm SM}^2$
NWA	$\frac{1}{1024\pi^4}\alpha_\varphi^2\alpha_{\rm SM}^2$	$\frac{1}{256\pi^4}\left(\alpha_V^\psi\right)^2\alpha_{\rm SM}^2$	$\frac{1}{2048\pi^4}\alpha_V^2\alpha_{\rm SM}^2$
Heavy	$\frac{64\pi^7}{19845}\alpha_\varphi^2\alpha_{\rm SM}^2$	$\frac{72\zeta(5)^2}{\pi^5}\left(\alpha_V^\psi\right)^2\alpha_{\rm SM}^2$	$\frac{32\pi^7}{19845}\alpha_V^2\alpha_{\rm SM}^2$

a \ DM	spin-0	spin-$\frac{1}{2}$	spin-1
Light	0	$\frac{6\zeta(3)^2}{\pi^5}\left(\beta_A^\psi\right)^2\beta_G^2$	$\frac{8\pi^3}{225}\beta_V^2\beta_G^2$
NWA	0	$\frac{3}{16\pi^4}\left(\beta_A^\psi\right)^2\beta_G^2$	$\frac{3}{8\pi^4}\beta_V^2\beta_G^2$
Heavy	0	$\frac{3456\zeta(5)^2}{\pi^5}\left(\beta_A^\psi\right)^2\beta_G^2$	$\frac{8192\pi^7}{6615}\beta_V^2\beta_G^2$

TABLE 6.3 – *Coefficients appearing the approximate rates, Eq. 6.34: $\delta_{s_f}^t$ (left) and $\delta_{s_f}^a$ (right). We have defined $\alpha_{SM}^2 \equiv 2\alpha_H^2 + 3\alpha_G^2$, since we assume $\mu_0^2 \ll s$. Except for the NWA cases, we have used Bose-Einstein statistics for the initial state distribution functions.*

6.2.2 Agreement with relic density

As in the previous works, before showing the numerical results on the contours providing the correct relic density for our dark matter candidates, we show analytical approximations

in order to have an idea about our free parameter space. Taking the limit of heavy moduli, we find *

$$\frac{\Omega^0_{\rm DM}h^2}{0.12} \sim \begin{cases} \frac{\mathscr{B}_{12}}{35.5}\alpha_\varphi^2\frac{\alpha_{\rm SM}^2}{5}\left(\frac{m_{\rm DM}}{1.2\times10^{14}}\right)\left(\frac{T_{\rm RH}}{10^{10}}\right)^7\left(\frac{10^{15}}{\Lambda}\right)^4\left(\frac{10^{13}}{m_t}\right)^4, & \text{for } \varphi \\ \frac{\mathscr{B}_{10}}{3.68}\left(\frac{m_{\rm DM}}{3.2\times10^{10}}\right)^3\left(\frac{T_{\rm RH}}{10^{10}}\right)^5\left(\frac{10^{15}}{\Lambda}\right)^4\left[\frac{\left(\alpha_{\rm V}^{\psi}\right)^2}{2}\frac{\alpha_{\rm SM}^2}{5}\left(\frac{10^{13}}{m_t}\right)^4+\frac{\left(\beta_{\rm A}^{\psi}\right)^2}{2}\beta_G^2\left(\frac{10^{12}}{m_a}\right)^4\right], & \text{for } \psi \\ \frac{\mathscr{B}^{12}}{35.5}\left(\frac{m_{\rm DM}}{1.5\times10^{12}}\right)\left(\frac{T_{\rm RH}}{10^{10}}\right)^7\left(\frac{10^{15}}{\Lambda}\right)^4\left[\frac{\alpha_V^2}{2}\frac{\alpha_{\rm SM}^2}{25}\left(\frac{10^{13}}{m_t}\right)^4+\frac{\beta_V^2}{2}\beta_G^2\left(\frac{10^{12}}{m_a}\right)^4\right], & \text{for } V \end{cases} \tag{6.35}$$

It is important to underline that the expressions above are computed for heavy moduli fields, especially in the limit $m_t \gg T_{\rm MAX}$. Comparing Eq.(6.35) with our numerical results, we noticed that pole effects due to the exchange of t can be important even when $m_{\rm DM}$ lies above $T_{\rm MAX}$ as the enhancement due to a small width can compensate the Boltzmann suppression $e^{-m_{\rm DM}/T_{\rm MAX}}$. Moreover, the regimes of the real and the imaginary components of the moduli are independent. For instance, the pole regime of the real component and the heavy regime of the imaginary component might be equaling contributing to a given value of the relic density. Our results are summarized in Figs. 6.5 and 6.6, where we have plotted the contours in the parameter space $(m_{\rm DM}, \Lambda)$ corresponding to $\Omega^0_{\rm DM}h^2 = 0.12$ for the scalar, vector and fermionic dark matter candidates (blue, green and red curves, respectively). While we are always solving the set of differential equations of Eq. (2.91), for the evolution of the system dark matter/inflaton/radiation, we show in the upper panels the results for *approximate production rates* of dark matter†, as given in Eq. 6.34, and we show in the lower panels the *numerical results* (solid curves).

The approximate results help to understand the physical features of the relic density contours, especially where the numerical solution is not reliable. We have computed the triple integral of the production rates using a Monte Carlo method (Vegas), as given by the Cuba package [147]. Depending on the parameter choice, the Monte Carlo integration output (thus the relic density) close to the pole regions is highly oscillatory, rendering unreliable results. Because of this, the numerical solutions shown in the lower panels of Figs. 6.5 and 6.6 (solid curves) are interpolated following the behavior of the approximate results (dotted curves).

For simplicity, all the couplings in the Lagrangian are set to unity. We have set the reheating scale to be 10^{10} GeV and, as we have done previously, we chose the split between the reheating and maximal temperatures to be $T_{\rm MAX} = 100\,T_{\rm RH}$. In Fig. 6.5 we have set $m_a = 10^8$ GeV and $m_t = 10^{11}$ GeV, whereas we explore a scenario with heavier mediators in Fig. 6.6, with $m_a = 10^{10}$ GeV and $m_t = 10^{13}$ GeV. With this set of parameters, it is imperative to consider the presence of the inflaton energy density in the Hubble rate.

The first thing the reader might notice in each figure is the stronger (cubic) dependence of the fermionic contour on the dark matter mass, as compared to the scalar and vector cases which have a linear dark matter mass dependence coming from the relic density

*All the dimensionful parameters are given in GeV.

†At a given temperature, the production rate due to the exchange of a mediator j is approximated by $R^j(T) = e^{-m_{\rm DM}/T}(\min(\mathrm{R}^{\rm j}_{\rm light}, \mathrm{R}^{\rm j}_{\rm heavy}) + \mathrm{R}^{\rm j}_{\rm NWA})$, in this way we can account for the different regimes as well as for the Boltzmann suppression.

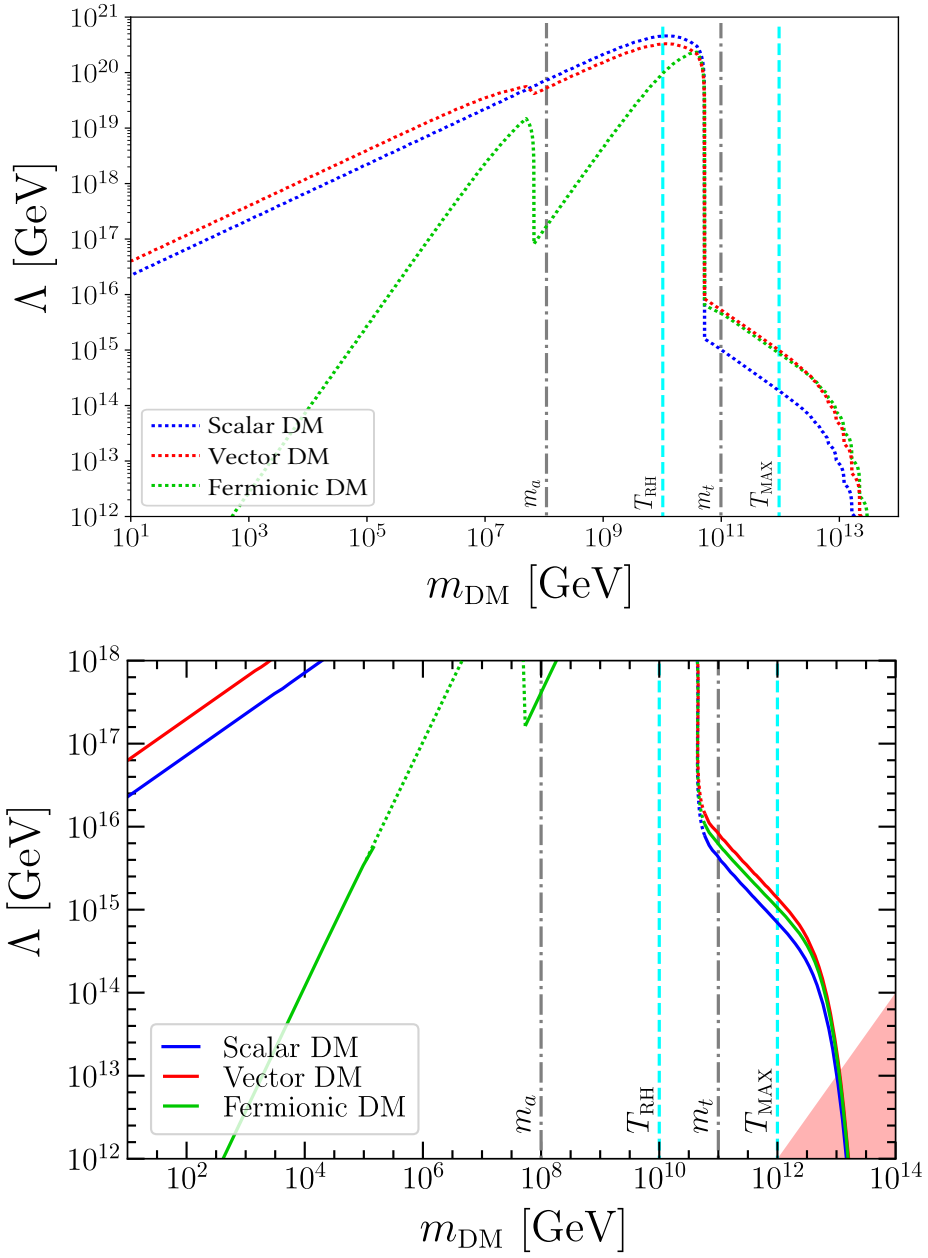

FIGURE 6.5 – *Contours respecting* $\Omega^0_{DM}h^2 = 0.12$ *in the* (m_{DM}, Λ) *plane for real and imaginary parts of modulus with masses* $m_t = 10^{11}$ *GeV and* $m_a = 10^8$ *GeV, respectively. For an illustrative purpose, we set* $T_{RH} = 10^{10}$ *GeV,* $T_{MAX} = 100\,T_{RH}$ *and all couplings are set to unity. The region in red is not reliable since* $\Lambda < m_{DM}$*. Upper: results for approximate rates. Lower: results for exact rates (solid curves) qualitatively interpolated following the approximate results (dotted curves).*

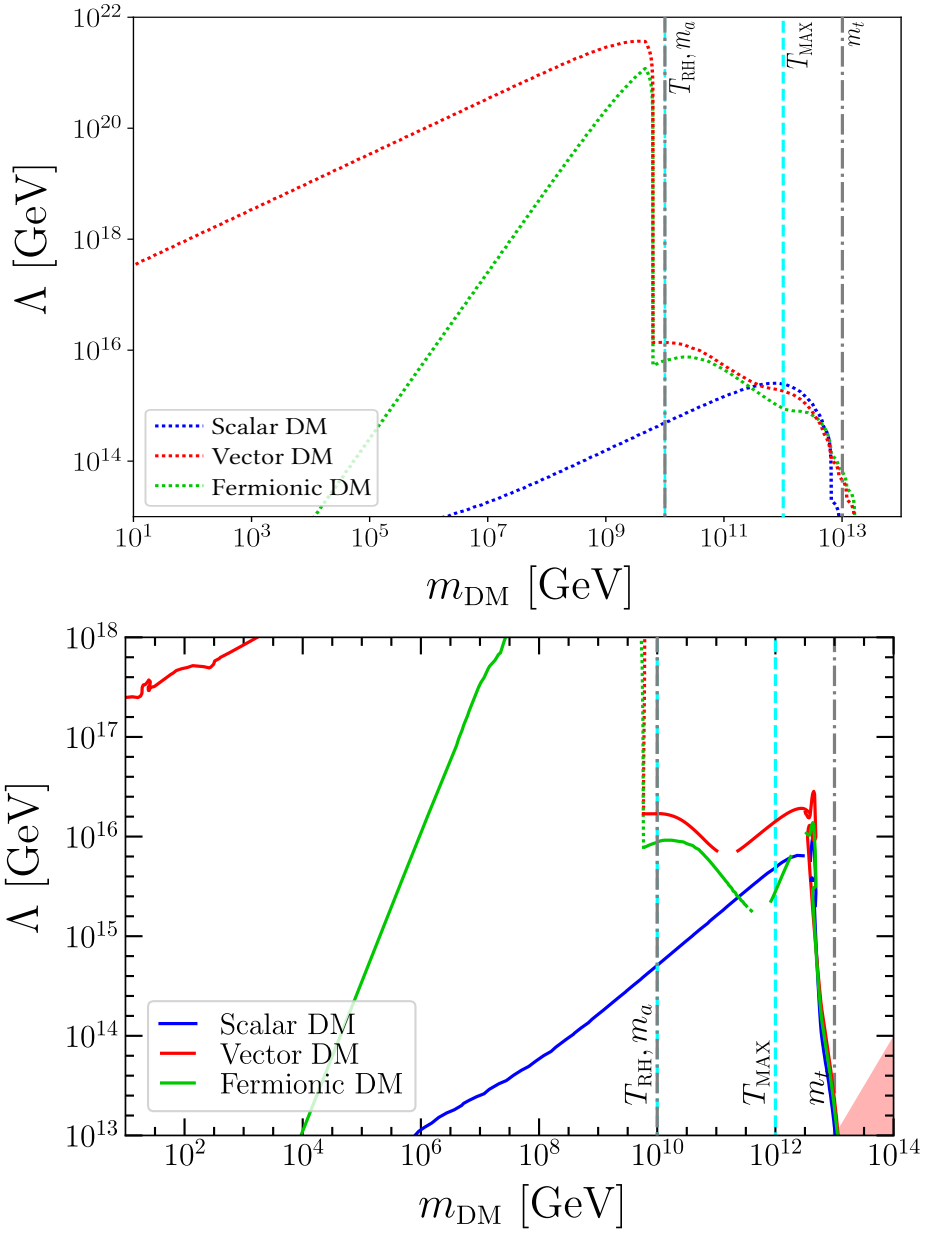

FIGURE 6.6 – *Contours respecting* $\Omega h^2 = 0.12$ *in the* (m_{DM}, Λ) *plane for all parameters set as in Fig. 6.5 but for heavier moduli:* $m_a = 10^{10}$ *GeV and* $m_t = 10^{13}$ *GeV. Upper: results for approximate rates. Lower: results for exact rates (solid curves) qualitatively interpolated following the approximate results (dotted curves).*

definition. This is easy to understand since the amplitude for the annihilation of the standard model states into fermionic dark matter depend explicitly on the dark matter mass (see Eq.(6.25)). It is therefore easier to see in the fermionic contours the following generic feature: the lighter the dark matter, the smaller the new physics scale for the same relic density value. On the other hand, the contours of the scalar and vector dark matter have similar behaviors, as suggested by the approximate expressions for the rate in Eq.(6.34). Comparing the scalar and vector cases in each figure, we see that for any dark matter mass, the same relic density value is achieved for larger values of Λ in the vector case, since a vector dark matter receives contribution from the imaginary part of modulus and the rate is therefore higher. This feature is more accentuated in Fig. 6.6, as we will be able to understand in what follows.

In the parameter region where $m_{t,a} > 2m_{\rm DM}$, the mediators can decay on-shell into dark matter whenever the pole can be reached ($m_{t,a} \lesssim T_{\rm MAX}$). The dark matter production in this region of the parameter space is therefore enhanced and we can understand that by increasing $m_{\rm DM}$ the Λ needs to be increased as well to provide the same relic density. So, the contour of $\Omega^0_{\rm DM}h^2 = 0.12$ monotonically increases as $m_{\rm DM}$ is increased until the threshold for on-shell production is reached, for $m_{\rm DM} \simeq m_{t,a}/2$. In the parameter region with $m_{\rm DM} > m_{t,a}/2$, the freeze-in proceeds through off-shell mediators. Thus in this regime, the rates are much lower compared to the pole-enhanced region and Λ needs to be also decreased to much lower values. This is why we can observe very sharp transitions between the on-shell and off-shell production regimes. This decreasing in Λ continues as we increase the dark matter mass, and becomes drastically accentuated because of the Boltzmann suppression in the rates, as we saw in Fig. 6.4. The heavier the dark matter, the less it is produced, and then a smaller Λ is needed to compensate the suppression. The process follows until the point where the freeze-in is kinematically forbidden. In fact, if dark matter is that heavy, our effective theory approach is no longer in a firm footing since we would enter into a unreliable region of our parameter space, with $\Lambda < m_{\rm DM}$ (red shaded region in lower panels).

Because of their accentuated dark matter mass dependence, the fermionic dark matter contours allow for much lower effective scale values for the entire region where dark matter is produced through the on-shell decay of the mediators. As the dark matter mass increases to $m_{\rm DM} \gtrsim m_{t,a}/2$ the off-shell production becomes the dominant one and the fermionic contour slowly approaches the scalar and vector ones. As the dark matter mass reaches $m_{\rm DM} \simeq m_a/2$, the dark matter production through imaginary part of the moduli becomes off-shell while production through the real part of the moduli remains on-shell. At this point, the dark matter production rate reduces and as a result there is a dip in the curve to compensate this change. Above this regime, the slope of the curve changes as the dominant contribution to the rate is only through the on-shell exchange of the real part of the moduli.

Finally, we can understand the main difference between Figs. 6.5 and 6.6. Heavier mediators lead to suppressed rates, which brings the effective scale to lower, and in our case more reasonable, values. In the fermionic and vector dark matter contours, we observe in Fig. 6.6 viable regions which could not be present in Fig. 6.5, corresponding to the combination of off-shell production from imaginary modulus and on-shell production of real modulus that happens for dark matter masses between $T_{\rm RH}$ and $T_{\rm MAX}$. Concerning the scalar contour, we see in Fig. 6.6 that the enhancement of the on-shell production

from the real modulus (the only mediator possible in this case) is not more efficient than the suppression due to the exchange of a very heavy modulus.

6.3 Discussion and conclusions

In this chapter, we have seen primary examples of "FIMP wonder" realizations. The two scenarios considered here can be viewed as part of the low-energy spectrum of string theory frameworks, in which gravitons, massive spin-2, and moduli fields might leave in hiding. In fact, if that is the case such fields would be playing together the role of mediators between the dark and visible sectors. In both scenarios, dark matter would always be produced near reheating.

It is interesting to see that, even though the stress-energy tensors of scalar, fermions and vectors are different, the gravity interactions between them are not significantly distinct. Interactions through moduli, though, are sensitive to the chirality of the fields, weakening the temperature-dependence of the production rate of fermionic dark matter.

The production through the exchange of a light spin-2 and moduli fields is always IR-dominated with respect to the reheating period (T^6 for fermionic DM produced through moduli, T^8 in all other cases). This is also the case for the heavy moduli exchange in the production of fermions (T^{10}). Otherwise, heavy spin-2 and moduli exchanges produce dark matter in intermediate stages of reheating (T^{12}). It is remarkable that even very heavy mediators can still populate the universe with the right amount of dark matter.

If the mediator masses are close to the reheating scale, their resonant production inside the reheating period might be huge, significantly lowering the values of reheating temperature (Fig. 6.2) and increasing the values of new physics scale (Figs. 6.5-6.6) in the contours providing the correct relic density of dark matter. As we have shown, the boost factor usually depends only on the ratio $T_{\rm MAX}/T_{\rm RH}$, which is completely set by the inflationary theory. However, when the production rate cannot be approximated by a power-law, the boost factor becomes strongly dependent on the physics of the sector producing dark matter.

As a generic conclusion, we can say that in models exhibiting a high temperature dependence in the production rate, the presence of a mediator with mass between the reheating and the maximal temperatures can drastically change the predictions of the parameter space relative to instantaneous reheating approximation. Indeed, we have shown that neglecting this effect might represent an underestimation of many orders of magnitude, depending on the mediator mass, the reheating and the maximal temperatures.

Chapter 7

Concluding remarks

In this thesis we have studied different possibilities for the underlying physics of dark matter (DM) particles. While it is possible that our understanding of gravity is not complete, and not valid at large scales, we have now evidence that a non-baryonic matter content affects the motion of the standard species in very crucial ways – catalyzing the formation of large-scale structures and binding galaxies together. We here make the ockhamiam assumption that all those effects are caused by the same kind of particles, which therefore need to be stable. Actually, perhaps we can say that there is no unique way of using the Ockam's razor in dark matter particle physics. Multi-component dark matter sectors, for instance, might be found as simplistic as the scenarios advocated here. The criterion we use is the possibility of embedding our models in frameworks which would be able to explain other open problems of particle physics which might find solution in the early stages of the universe.

Along with the fact that neutrinos have mass, the existence of DM particles implies that we should extend the standard model of particle physics to account for their (hypothetical) interactions with standard model (SM) particles. The strength of those interactions may or may not be strong enough as to keep DM and SM particles in thermal equilibrium in the early universe. Weakly interacting massive particles (WIMPs) are the most studied and testable class of DM candidates that were once coupled to the SM thermal bath, since their masses and couplings are comparable to the SM ones. Feebly interacting massive particles (FIMPs) are DM candidates produced from the SM thermal bath in out-of-equilibrium processes (freeze-in mechanism).

The waning of the WIMP?

In Section 4.1, we have discussed the status of simplified WIMP scenarios, mainly constrained by direct detection (DD) bounds, complemented with collider and indirect detection (ID) bounds. In Section 4.2, a gauge extension of the SM comprising a dark photon and a fermionic dark matter candidate was considered.

We could see from our analysis that simple models for WIMPs in the range of $\mathcal{O}(10 - 1000)$ GeV will be mostly probed in the next decades, but are currently very constrained. In the case of an MeV WIMP in the dark photon portal, we have also found a very restrictive scenario whose tensions with CMB, DD and ID bounds would be alleviated if

one assumes an intermediate reheating epoch after dark matter decoupling. Therefore, we may conclude that

- WIMPs would not come alone, since non-standard mediators are in general needed.

The problematic issue in this case is the need for thermal equilibrium between the visible and dark sectors, comprising dark matter and mediators, since the strengths of the couplings cannot be indefinitely lowered as for the models to agree with the complementary bounds. In the absence of detection in the next decades, though, we are still left with the possibility of much lighter or much heavier WIMPs and mediators – and of course a much challenging phenomenology. Nevertheless, the efforts on direct detection searches for sub-GeV dark matter particles are already rendering important constraints, as we could see in our MeV scenario.

The FIMP wonder

In our dark photon model, we could find two ways of alleviating the bounds: diluting the relic density of dark matter with an intermediate reheating process or giving up of thermal equilibrium between dark matter and electrons. Such model, though, is already hiding extra degrees of freedom: the kinetic mixing is expected to be caused by the presence of heavy fields interacting with both gauge bosons.

The approach we followed from this point was to wonder if indeed the connection between dark and standard matter is due to the presence of heavy fields. In this case, naturally tiny couplings would be generated and allow for the out-of-equilibrium production of dark matter.

We first considered the effect of very heavy fermions charged under the standard model group. In Section 5.1, we discussed an ongoing study in which the heavy fermions connect the standard gauge bosons to the scalar giving mass to the fermions after the breaking of a global $U(1)$ symmetry. The axion-like particle arising from this scalar field was considered a dark matter candidate, with the stability requirement constraining its mass to be below the keV range. We have also considered fermionic dark matter in such scenario. We have found that heavy scalars would bring the production of our dark matter candidates to the early stages of the radiation era. In Section 5.2, we have considered instead a gauge $U(1)$ symmetry, and assumed that the scalar giving mass to the fermions are also too heavy as to be considered a degree of freedom. In this way, we were left with an effective interaction between two standard gluons and the new Abelian field, pushing the production of dark matter for even earlier stages.

We have considered scenarios inspired in structural extensions of the standard model, in which the description of the early stages of the universe would be consistently unified. We therefore studied the freeze-in through the exchange of spin-2 and moduli fields, in Sections 6.1 and 6.2 respectively. We have consistently found that the relic density in this case is satisfied in natural regions of the parameter space.

Finally, we have shown that if the temperature dependence of the production rates of FIMPs is strong enough, which can be achieved in models with derivative couplings, FIMPs would have already been produced in the beginning of the radiation era. Perhaps the main conclusion of our work is that

- neglecting a resonant production of mediators during reheating might lead to an underestimation of the DM relic density of many orders of magnitude.

In this thesis we have provided a complete route to estimate the regions in the parameter space of a dark matter model providing the correct relic density. It starts from the squared amplitudes of the processes contributing to the production of dark matter and take into account the production *during* a reheating phase. Under appropriate approximations, the rate might be mostly given as a power-law of the temperature. If this temperature dependence is high enough ($n > 5$), the dark matter production takes place near the reheating scale. Increasing this temperature dependence means producing dark matter at earlier stages, and if $n > 12$, the production takes place at the earliest moments of the post-inflationary reheating process. We emphasize that the equation 2.134 is a good master equation for this kind of inquiry, and it provides results which are close to the full solution of the set of integro-differential equations in Eq. (2.91) in a satisfactory way, provided that we integrate exactly the production rates. The use of approximate results for the production rates in many cases lead to significant discrepancies, but solving a multidimensional integration as in Eq. (2.134) is much easier and faster than evolving the integro-differential equations.

Beyond the wondering

The puzzle of dark matter suffers from many theoretical and astrophysical uncertainties. With this in mind, next steps in this line of research may be guided by:

- putting computational efforts to test the validity of usual approximations and better explore the parameter space of the DM models;
- relating the dark matter theory with open problems of particle physics and cosmology, mainly the generation of neutrino mass and baryon asymmetry;
- trying to understand how the astrophysical environments affect DM in a model-independent point of view.

Relating dark matter physics with the earliest stages of the universe demand more careful work towards the understanding of thermalization processes between dark matter, inflaton and the other degrees of freedom. The formalism of fluid equation used in this thesis would not be appropriate and is only a first approach to this problem.

Effects coming from finite temperature corrections and quantum-statistical Bose enhancement factors might be important in high energy and density environments, respectively. The possible impact of such effects in the evolution of DM in the early universe, filled with a quark-gluon plasma, and possibly on dense astrophysical environments are worth exploring.

With the analyzes of the CMB becoming even more accurate, the possibility of constraining specific inflationary models motivate the study of producing dark matter with a direct influence of inflaton candidates.

In a time where we start to be able to detect gravitational waves and possibly the light of the first stars, it is appropriate to study DM astrophysical signatures and cosmological consequences in a way as generic and complementary as possible.

Bibliography

[1] G. Arcadi, M. Dutra, P. Ghosh, M. Lindner, Y. Mambrini, M. Pierre, S. Profumo, and F. S. Queiroz. "The Waning of the WIMP? A Review of Models, Searches, and Constraints". In: *The European Physical Journal C* 78.3 (2018). DOI: 10.1140/epjc/s10052-018-5662-y. arXiv: 1703.07364.

[2] M. Dutra, M. Lindner, S. Profumo, F. S. Queiroz, W. Rodejohann, and C. Siqueira. "MeV dark matter complementarity and the dark photon portal". In: *Journal of Cosmology and Astroparticle Physics* 2018.3 (2018), pp. 037–037. DOI: 10.1088/1475-7516/2018/03/037. arXiv: 1801.05447.

[3] A. De Angelis et al. "Science with e-ASTROGAM (A space mission for MeV-GeV gamma-ray astrophysics)". In: *Journal of High Energy Astrophysics* 19 (2018), pp. 1–106. DOI: 10.1016/j.jheap.2018.07.001. arXiv: 1711.01265.

[4] N. Bernal, M. Dutra, Y. Mambrini, K. Olive, M. Peloso, and M. Pierre. "Spin-2 portal dark matter". In: *Physical Review D* 97.11 (2018). DOI: 10.1103/PhysRevD.97.115020. arXiv: 1803.01866.

[5] G. Bhattacharyya, M. Dutra, Y. Mambrini, and M. Pierre. "Freezing-in dark matter through a heavy invisible Z'". In: *Phys.Rev.* D98.3 (2018), p. 035038. DOI: 10.1103/PhysRevD.98.035038. arXiv: 1806.00016.

[6] D. Chowdhury, E. Dudas, M. Dutra, and Y. Mambrini. "Moduli Portal Dark Matter". In: (2018). arXiv: 1811.01947.

[7] M. Dutra, Y. Farzan, and Y. Mambrini. "Dynamical freeze-in of keV dark matter". In: *(work in progress)* (2019). arXiv: 1903.XXXXX.

[8] H. Shapley and H. D. Curtis. "The Scale of the Universe". In: *Bulletin of the National Research Council, Vol. 2, Part 3, No. 11, p. 171-217* 2 (1921), pp. 171–217.

[9] F. Zwicky. "Republication of: The redshift of extragalactic nebulae". In: *Gen Relativ Gravit* 41.1 (2009), pp. 207–224. DOI: 10.1007/s10714-008-0707-4.

[10] J. H. Oort. "The force exerted by the stellar system in the direction perpendicular to the galactic plane and some related problems". In: *Bulletin of the Astronomical Institutes of the Netherlands* 6 (1932), p. 249.

[11] M. Milgrom. "A modification of the Newtonian dynamics as a possible alternative to the hidden mass hypothesis". In: *The Astrophysical Journal* 270 (1983), pp. 365–370. DOI: 10.1086/161130.

[12] V. C. Rubin and W. K. Ford Jr. "Rotation of the Andromeda Nebula from a Spectroscopic Survey of Emission Regions". In: *The Astrophysical Journal* 159 (1970), p. 379. DOI: 10.1086/150317.

[13] Y. Sofue and V. Rubin. "Rotation Curves of Spiral Galaxies". In: *Annual Review of Astronomy and Astrophysics* 39.1 (2001), pp. 137–174. DOI: 10.1146/annurev.astro.39.1.137. arXiv: astro-ph/0010594.

[14] S. M. Faber and J. S. Gallagher. "Masses and mass-to-light ratios of galaxies". In: *Annual Review of Astronomy and Astrophysics* 17 (1979), pp. 135–187. DOI: 10.1146/annurev.aa.17.090179.001031.

[15] G. Bertone, D. Hooper, and J. Silk. "Particle Dark Matter: Evidence, Candidates and Constraints". In: *Physics Reports* 405.5 (2005), pp. 279–390. DOI: 10.1016/j.physrep.2004.08.031. arXiv: hep-ph/0404175.

[16] P. Salucci and M. Persic. "Dark Halos around Galaxies". In: Dark and Visible Matter in Galaxies and Cosmological Implications. Vol. 117. 1997, p. 1. arXiv: astro-ph/9703027.

[17] S. M. Kent. "Dark matter in spiral galaxies. II - Galaxies with H I rotation curves". In: *The Astronomical Journal* 93 (1987), p. 816. DOI: 10.1086/114366.

[18] D. V. Bugg. "Mond – a review". In: *Canadian Journal of Physics* 93.2 (2015), pp. 119–125. DOI: 10.1139/cjp-2014-0057. arXiv: 1405.1695.

[19] A. Hees, B. Famaey, G. W. Angus, and G. Gentile. "Combined Solar System and rotation curve constraints on MOND". In: *Monthly Notices of the Royal Astronomical Society* 455.1 (2016), pp. 449–461. DOI: 10.1093/mnras/stv2330. arXiv: 1510.01369.

[20] K. G. Begeman. "HI rotation curves of spiral galaxies. I - NGC 3198". In: *Astronomy and Astrophysics* 223 (1989), pp. 47–60.

[21] M. A. Monroy-Rodríguez and C. Allen. "The end of the MACHO era- revisited: new limits on MACHO masses from halo wide binaries". In: *The Astrophysical Journal* 790.2 (2014), p. 159. DOI: 10.1088/0004-637X/790/2/159. arXiv: 1406.5169.

[22] J. I. Read. "The Local Dark Matter Density". In: *Journal of Physics G: Nuclear and Particle Physics* 41.6 (2014), p. 063101. DOI: 10.1088/0954-3899/41/6/063101. arXiv: 1404.1938.

[23] N. P. Pitjev and E. V. Pitjeva. "Constraints on dark matter in the solar system". In: *Astron. Lett.* 39.3 (2013), pp. 141–149. DOI: 10.1134/S1063773713020060. arXiv: 1306.5534.

[24] F. Zwicky. "On the Masses of Nebulae and of Clusters of Nebulae". In: *The Astrophysical Journal* 86 (1937), p. 217. DOI: 10.1086/143864.

[25] D. Clowe, M. Bradac, A. H. Gonzalez, M. Markevitch, S. W. Randall, C. Jones, and D. Zaritsky. "A direct empirical proof of the existence of dark matter". In: *The Astrophysical Journal* 648.2 (2006), pp. L109–L113. DOI: 10.1086/508162. arXiv: astro-ph/0608407.

[26] J. R. Brownstein and J. W. Moffat. "The Bullet Cluster 1E0657-558 evidence shows Modified Gravity in the absence of Dark Matter". In: *Monthly Notices of the Royal Astronomical Society* 382.1 (2007), pp. 29–47. DOI: 10.1111/j.1365-2966.2007.12275.x. arXiv: astro-ph/0702146.

[27] C. Lage and G. Farrar. "Constrained Simulation of the Bullet Cluster". In: *The Astrophysical Journal* 787.2 (2014), p. 144. DOI: 10.1088/0004-637X/787/2/144. arXiv: 1312.0959.

[28] A. Klypin and F. Prada. "Testing gravity with motion of satellites around galaxies: Newtonian gravity against Modified Newtonian Dynamics". In: *The Astrophysical Journal* 690.2 (2009), pp. 1488–1496. DOI: 10.1088/0004-637X/690/2/1488. arXiv: 0706.3554.

[29] S. W. Randall, M. Markevitch, D. Clowe, A. H. Gonzalez, and M. Bradač. "Constraints on the Self-Interaction Cross Section of Dark Matter from Numerical Simulations of the Merging Galaxy Cluster 1E 0657–56". In: *ApJ* 679.2 (2008), p. 1173. DOI: 10.1086/587859. arXiv: 0704.0261.

[30] N. Golovich et al. "Merging Cluster Collaboration: Optical and Spectroscopic Survey of a Radio-Selected Sample of Twenty Nine Merging Galaxy Clusters". In: (2017). arXiv: 1711.01347.

[31] J. Silk. "Cosmology and structure formation". In: *Nuclear Physics B - Proceedings Supplements*. Proceedings of the International Workshop on Particles in Astrophysics and Cosmology: From Theory to Observation 81 (2000), pp. 3–10. DOI: 10.1016/S0920-5632(99)00851-8.

[32] C. Knobel. "An Introduction into the Theory of Cosmological Structure Formation". In: (2012). arXiv: 1208.5931.

[33] A. L. Coil. "The Large-Scale Structure of the Universe". In: *Planets, Stars and Stellar Systems: Volume 6: Extragalactic Astronomy and Cosmology*. Ed. by T. D. Oswalt and W. C. Keel. Dordrecht: Springer Netherlands, 2013, pp. 387–421. DOI: 10.1007/978-94-007-5609-0_8.

[34] S. Dodelson. "The Real Problem with MOND". In: *International Journal of Modern Physics D* 20.14 (2011), pp. 2749–2753. DOI: 10.1142/S0218271811020561. arXiv: 1112.1320.

[35] W. Hu and J. Silk. "Thermalization and spectral distortions of the cosmic background radiation". In: *Phys. Rev. D* 48.2 (1993), pp. 485–502. DOI: 10.1103/PhysRevD.48.485.

[36] Planck Collaboration. "Planck 2018 results. VI. Cosmological parameters". In: (2018). arXiv: 1807.06209.

[37] Planck Collaboration. "Planck 2018 results. X. Constraints on inflation". In: (2018). arXiv: 1807.06211.

[38] D. Baumann. "TASI Lectures on Inflation". In: (2009). arXiv: 0907.5424.

[39] R. H. Cyburt, B. D. Fields, K. A. Olive, and T.-H. Yeh. "Big bang nucleosynthesis: Present status". In: *Rev. Mod. Phys.* 88.1 (2016), p. 015004. DOI: 10.1103/RevModPhys.88.015004.

[40] V. Springel, C. S. Frenk, and S. D. M. White. "The large-scale structure of the Universe". In: *Nature* 440 (2006), pp. 1137–1144. DOI: 10.1038/nature04805.

[41] A. Coc and E. Vangioni. "Primordial nucleosynthesis". In: *International Journal of Modern Physics E* 26.8 (2017), p. 1741002. DOI: 10.1142/S0218301317410026. arXiv: 1707.01004.

[42] A. Sarkar, S. Das, and S. K. Sethi. "How Late can the Dark Matter form in our universe?" In: *Journal of Cosmology and Astroparticle Physics* 2015.3 (2015), pp. 004–004. DOI: 10.1088/1475-7516/2015/03/004. arXiv: 1410.7129.

[43] M. Fukugita and P. J. E. Peebles. "The Cosmic Energy Inventory". In: *The Astrophysical Journal* 616.2 (2004), pp. 643–668. DOI: 10.1086/425155. arXiv: astro-ph/0406095.

[44] ATLAS Collaboration. "Observation of a new particle in the search for the Standard Model Higgs boson with the ATLAS detector at the LHC". In: (2012). DOI: 10.1016/j.physletb.2012.08.020.

[45] CMS Collaboration. "Observation of a new boson at a mass of 125 GeV with the CMS experiment at the LHC". In: (2012). DOI: 10.1016/j.physletb.2012.08.021.

[46] T. Lenz. "Searches for h(125) properties beyond the Standard Model at the CMS experiment". In: (2018). arXiv: 1808.09193.

[47] S. F. Novaes. "Standard Model: An Introduction". In: (2000). arXiv: hep-ph/0001283.

[48] E. Dudas. "Top-down Beyond the Standard Model Review". In: (2013). arXiv: 1306.2920.

[49] C. Csaki and P. Tanedo. "Beyond the Standard Model". In: (2016). DOI: 10.5170/CERN-2015-004.169. arXiv: 1602.04228.

[50] J. Martin. "Everything You Always Wanted To Know About The Cosmological Constant Problem (But Were Afraid To Ask)". In: *Comptes Rendus Physique* 13.6 (2012), pp. 566–665. DOI: 10.1016/j.crhy.2012.04.008. arXiv: 1205.3365.

[51] P. Bull et al. "Beyond ΛCDM: Problems, solutions, and the road ahead". In: *Physics of the Dark Universe* 12 (2016). arXiv: 1512.05356, pp. 56–99. DOI: 10.1016/j.dark.2016.02.001.

[52] E. Kolb and M. Turner. *The Early Universe*. Avalon Publishing, 1994. 594 pp.

[53] M. Tanabashi. "Supersymmetric Particle Searches". In: *Phys. Rev. D* (2018), p. 110.

[54] V. Domcke and J. Heisig. "Constraints on the reheating temperature from sizable tensor modes". In: *Physical Review D* 92.10 (2015). DOI: 10.1103/PhysRevD.92.103515.

[55] T. Binder, L. Covi, A. Kamada, H. Murayama, T. Takahashi, and N. Yoshida. "Matter power spectrum in hidden neutrino interacting dark matter models: a closer look at the collision term". In: *J. Cosmol. Astropart. Phys.* 2016.11 (2016), p. 043. DOI: 10.1088/1475-7516/2016/11/043. arXiv: 1602.07624.

[56] M. Drewes. "On finite density effects on cosmic reheating and moduli decay and implications for Dark Matter production". In: *Journal of Cosmology and Astroparticle Physics* 2014.11 (2014), pp. 020–020. DOI: 10.1088/1475-7516/2014/11/020. arXiv: 1406.6243.

[57] A. Hohenegger, A. Kartavtsev, and M. Lindner. "Deriving Boltzmann Equations from Kadanoff-Baym Equations in Curved Space-Time". In: *Physical Review D* 78.8 (2008). DOI: 10.1103/PhysRevD.78.085027. arXiv: 0807.4551.

[58] S. Dodelson. *Modern Cosmology*. Academic Press, 2003. 440 pp.

[59] O. F. Piattella. "Lecture Notes in Cosmology". In: *arXiv:1803.00070 [astro-ph, physics:gr-qc, physics:hep-th]* (2018). DOI: 10.1007/978-3-319-95570-4. arXiv: 1803.00070.

[60] H. van Hees. "Introduction to Relativistic Transport". In: *CNT Lectures on Hot / Dense Matter 2015, Variable Energy Cyclogron Center in Kolkata, India* (2018), p. 48.

[61] T. Bringmann and S. Hofmann. "Thermal decoupling of WIMPs from first principles". In: *Journal of Cosmology and Astroparticle Physics* 2007.4 (2007), pp. 016–016. DOI: 10.1088/1475-7516/2007/04/016. arXiv: hep-ph/0612238.

[62] T. Binder, T. Bringmann, M. Gustafsson, and A. Hryczuk. "Early kinetic decoupling of dark matter: When the standard way of calculating the thermal relic density fails". In: *Physical Review D* 96.11 (2017). DOI: 10.1103/PhysRevD.96.115010.

[63] T. A. Weaver. "Reaction rates in a relativistic plasma". In: *Physical Review A* 13.4 (1976), pp. 1563–1569. DOI: 10.1103/PhysRevA.13.1563.

[64] M. Cannoni. "Relativistic and nonrelativistic annihilation of dark matter: a sanity check using an effective field theory approach". In: *The European Physical Journal C* 76.3 (2016). DOI: 10.1140/epjc/s10052-016-3991-2. arXiv: 1506.07475.

[65] G. Bélanger, F. Boudjema, A. Goudelis, A. Pukhov, and B. Zaldívar. "micrOMEGAs 5.0 : Freeze-in". In: *Computer Physics Communications* 231 (2018), pp. 173–186. DOI: 10.1016/j.cpc.2018.04.027. arXiv: 1801.03509.

[66] E. Hubble. "A Relation between Distance and Radial Velocity among Extra-Galactic Nebulae". In: *Proceedings of the National Academy of Science* 15 (1929), pp. 168–173. DOI: 10.1073/pnas.15.3.168.

[67] M. S. Turner. "Coherent scalar-field oscillations in an expanding universe". In: *Physical Review D* 28.6 (1983), pp. 1243–1247. DOI: 10.1103/PhysRevD.28.1243.

[68] A. K. Sanyal and S. Debnath. "Thermodynamics of irreversible particle creation phenomena and its cosmological consequence". In: (2018), pp. 171–198. DOI: 10.1007/978-3-319-70957-4_8. arXiv: 1708.04857.

[69] A. Mazumdar and B. Zaldívar. "Quantifying the reheating temperature of the universe". In: (2013). DOI: 10.1016/j.nuclphysb.2014.07.001. arXiv: 1310.5143v2.

[70] M. A. G. Garcia and M. A. Amin. "Pre-thermalization Production of Dark Matter". In: *Physical Review D* 98.10 (2018). DOI: 10.1103/PhysRevD.98.103504. arXiv: 1806.01865.

[71] A. A. Starobinsky. "A new type of isotropic cosmological models without singularity". In: *Physics Letters B* 91.1 (1980), pp. 99–102. DOI: 10.1016/0370-2693(80)90670-X.

[72] J. Ellis, M. A. G. Garcia, D. V. Nanopoulos, K. A. Olive, and M. Peloso. "Post-Inflationary Gravitino Production Revisited". In: (2015). DOI: 10.1088/1475-7516/2016/03/008. arXiv: 1512.05701.

[73] Wolfram Research, Inc. *Mathematica, Version 11.3*. Champaign, IL, 2018.

[74] G. F. Giudice, E. W. Kolb, and A. Riotto. "Largest temperature of the radiation era and its cosmological implications". In: *Physical Review D* 64.2 (2001). DOI: 10.1103/PhysRevD.64.023508. arXiv: hep-ph/0005123.

[75] T. Asaka and M. Kawasaki. "Cosmological Moduli Problem and Thermal Inflation Models". In: *Physical Review D* 60.12 (1999). DOI: 10.1103/PhysRevD.60.123509. arXiv: hep-ph/9905467.

[76] P. Adhya, D. R. Chaudhuri, and S. Hannestad. "Late-time entropy production from scalar decay and the relic neutrino temperature". In: *Phys. Rev. D* 68.8 (2003), p. 083519. DOI: 10.1103/PhysRevD.68.083519. arXiv: hep-ph/0304291.

[77] T. Asaka, M. Shaposhnikov, and A. Kusenko. "Opening a new window for warm dark matter". In: *Physics Letters B* 638.5 (2006), pp. 401–406. DOI: 10.1016/j.physletb.2006.05.067. arXiv: hep-ph/0602150.

[78] J. Hasenkamp and J. Kersten. "Leptogenesis, Gravitino Dark Matter and Entropy Production". In: *Physical Review D* 82.11 (2010). DOI: 10.1103/PhysRevD.82.115029. arXiv: 1008.1740.

[79] P. Di Bari, S. F. King, and A. Merle. "Dark Radiation or Warm Dark Matter from long lived particle decays in the light of Planck". In: *Physics Letters B* 724.1 (2013), pp. 77–83. DOI: 10.1016/j.physletb.2013.06.003. arXiv: 1303.6267.

[80] C. Kelso, C. A. d. S. Pires, S. Profumo, F. S. Queiroz, and P. S. R. da Silva. "A 331 WIMPy Dark Radiation Model". In: *The European Physical Journal C* 74.3 (2014). DOI: 10.1140/epjc/s10052-014-2797-3. arXiv: 1308.6630.

[81] H. Baer, K.-Y. Choi, J. E. Kim, and L. Roszkowski. "Dark matter production in the early Universe: beyond the thermal WIMP paradigm". In: (2014). DOI: 10.1016/j.physrep.2014.10.002. arXiv: 1407.0017.

[82] G. Kane, K. Sinha, and S. Watson. "Cosmological Moduli and the Post-Inflationary Universe: A Critical Review". In: *International Journal of Modern Physics D* 24.8 (2015), p. 1530022. DOI: 10.1142/S0218271815300220. arXiv: 1502.07746.

[83] J. Bramante and J. Unwin. "Superheavy Thermal Dark Matter and Primordial Asymmetries". In: *Journal of High Energy Physics* 2017.2 (2017). DOI: 10.1007/JHEP02(2017)119. arXiv: 1701.05859.

[84] E. Dimastrogiovanni and L. M. Krauss. "$\Delta N_{\rm eff}$ and entropy production from early-decaying gravitinos". In: *Phys. Rev. D* 98.2 (2018), p. 023006. DOI: 10.1103/PhysRevD.98.023006. arXiv: 1706.01495.

[85] S. Hoof and J. Jaeckel. "QCD axions and axionlike particles in a two-inflation scenario". In: *Physical Review D* 96.11 (2017). DOI: 10.1103/PhysRevD.96.115016. arXiv: 1709.01090.

[86] R. J. Scherrer and M. S. Turner. "Decaying particles do not "heat up" the Universe". In: *Phys. Rev. D* 31.4 (1985), pp. 681–688. DOI: 10.1103/PhysRevD.31.681.

[87] M. Srednicki, R. Watkins, and K. A. Olive. "Calculations of relic densities in the early universe". In: *Nuclear Physics B* 310.3 (1988), pp. 693–713. DOI: 10.1016/0550-3213(88)90099-5.

[88] MATLAB and Statistics Toolbox. *Release 2016a*. Natick, Massachusetts, United States: The MathWorks Inc., 2010.

[89] P. Gondolo and G. Gelmini. "Cosmic abundances of stable particles: Improved analysis". In: *Nuclear Physics B* 360.1 (1991), pp. 145–179. DOI: 10.1016/0550-3213(91)90438-4.

[90] D. J. H. Chung, E. W. Kolb, and A. Riotto. "Production of massive particles during reheating". In: *Physical Review D* 60.6 (1999). DOI: 10.1103/PhysRevD.60.063504. arXiv: hep-ph/9809453.

[91] L. J. Hall, K. Jedamzik, J. March-Russell, and S. M. West. "Freeze-In Production of FIMP Dark Matter". In: *Journal of High Energy Physics* 2010.3 (2010). DOI: 10.1007/JHEP03(2010)080. arXiv: 0911.1120.

[92] T. M. P. Tait. "TASI Lectures on Resonances". In: (2009), p. 32.

[93] E. Dudas, Y. Mambrini, and K. Olive. "Monochromatic neutrinos generated by dark matter and the see-saw mechanism". In: *Physical Review D* 91.7 (2015). DOI: 10.1103/PhysRevD.91.075001. arXiv: 1412.3459.

[94] M. Battaglieri et al. "US Cosmic Visions: New Ideas in Dark Matter 2017: Community Report". In: *arXiv:1707.04591 [astro-ph, physics:hep-ex, physics:hep-ph]* (2017). arXiv: 1707.04591.

[95] Y. Mambrini, N. Nagata, K. A. Olive, and J. Zheng. "Vacuum Stability and Radiative Electroweak Symmetry Breaking in an SO(10) Dark Matter Model". In: *Physical Review D* 93.11 (2016). DOI: 10.1103/PhysRevD.93.111703. arXiv: 1602.05583.

[96] T. Cohen, R. T. D'Agnolo, and M. Low. "Freezing-in the Hierarchy Problem". In: (2018). arXiv: 1808.02031.

[97] A. Biswas, D. Borah, and A. Dasgupta. "A UV Complete Framework of Freeze-in Massive Particle Dark Matter". In: (2018). arXiv: 1805.06903.

[98] M. Lucente, A. Abada, G. Arcadi, V. Domcke, M. Drewes, and J. Klaric. "Freeze-in leptogenesis with 3 right-handed neutrinos". In: *PoS* ICHEP2018 (2018), p. 306.

[99] M. Lucente, A. Abada, G. Arcadi, and V. Domcke. "Leptogenesis, dark matter and neutrino masses". In: *arXiv:1803.10826 [astro-ph, physics:hep-ph]* (2018). arXiv: 1803.10826.

[100] Y. Mambrini, K. A. Olive, J. Quevillon, and B. Zaldivar. "Gauge Coupling Unification and Non-Equilibrium Thermal Dark Matter". In: *Physical Review Letters* 110.24 (2013). DOI: 10.1103/PhysRevLett.110.241306. arXiv: 1302.4438.

[101] Y. Mambrini, N. Nagata, K. A. Olive, J. Quevillon, and J. Zheng. "Dark Matter and Gauge Coupling Unification in Non-supersymmetric SO(10) Grand Unified Models". In: *Physical Review D* 91.9 (2015). DOI: 10.1103/PhysRevD.91.095010. arXiv: 1502.06929.

[102] E. Babichev, L. Marzola, M. Raidal, A. Schmidt-May, F. Urban, H. Veermäe, and M. von Strauss. "Heavy spin-2 Dark Matter". In: (2016). DOI: 10.1088/1475-7516/2016/09/016.

[103] M. Garny, M. Sandora, and M. S. Sloth. "Planckian Interacting Massive Particles as Dark Matter". In: *Phys. Rev. Lett.* 116.10 (2016), p. 101302. DOI: 10.1103/PhysRevLett.116.101302. arXiv: 1511.03278.

[104] M. Garny, A. Palessandro, M. Sandora, and M. S. Sloth. "Theory and phenomenology of Planckian interacting massive particles as dark matter". In: *J. Cosmol. Astropart. Phys.* 2018.2 (2018), p. 027. DOI: 10.1088/1475-7516/2018/02/027. arXiv: 1709.09688.

[105] S. Nurmi, T. Tenkanen, and K. Tuominen. "Inflationary Imprints on Dark Matter". In: *Journal of Cosmology and Astroparticle Physics* 2015.11 (2015), pp. 001–001. DOI: 10.1088/1475-7516/2015/11/001. arXiv: 1506.04048.

[106] G. Arcadi, L. Covi, and M. Nardecchia. "Out-of-equilibrium Baryogenesis and SuperWIMP Dark Matter". In: *Physical Review D* 89.9 (2014). DOI: 10.1103/PhysRevD.89.095020. arXiv: 1312.5703.

[107] L. J. Hall, J. March-Russell, and S. M. West. "A Unified Theory of Matter Genesis: Asymmetric Freeze-In". In: (2010). arXiv: 1010.0245.

[108] R. Essig, M. Fernández-Serra, J. Mardon, A. Soto, T. Volansky, and T.-T. Yu. "Direct detection of sub-GeV dark matter with semiconductor targets". In: *J. High Energ. Phys.* 2016.5 (2016), p. 46. DOI: 10.1007/JHEP05(2016)046.

[109] T. Hambye, M. H. G. Tytgat, J. Vandecasteele, and L. Vanderheyden. "Direct Detection is testing Freeze-in". In: *Physical Review D* 98.7 (2018). DOI: 10.1103/PhysRevD.98.075017. arXiv: 1807.05022.

[110] M. Heikinheimo, T. Tenkanen, and K. Tuominen. "Prospects for indirect detection of frozen-in dark matter". In: *Physical Review D* 97.6 (2018). DOI: 10.1103/PhysRevD.97.063002. arXiv: 1801.03089.

[111] R. T. Co, F. D'Eramo, L. J. Hall, and D. Pappadopulo. "Freeze-In Dark Matter with Displaced Signatures at Colliders". In: *JCAP* 1512.12 (2015), p. 024. DOI: 10.1088/1475-7516/2015/12/024. arXiv: 1506.07532.

[112] T. Hambye, F.-S. Ling, L. L. Honorez, and J. Rocher. "Scalar Multiplet Dark Matter". In: *Journal of High Energy Physics* 2010.5 (2010). DOI: 10.1007/JHEP05(2010)066. arXiv: 0903.4010.

[113] J. Choquette and J. M. Cline. "Minimal nonabelian model of atomic dark matter". In: *Physical Review D* 92.11 (2015). DOI: 10.1103/PhysRevD.92.115011. arXiv: 1509.05764.

[114] M. Cirelli, T. Hambye, P. Panci, F. Sala, and M. Taoso. "Gamma ray tests of Minimal Dark Matter". In: *Journal of Cosmology and Astroparticle Physics* 2015.10 (2015), pp. 026–026. DOI: 10.1088/1475-7516/2015/10/026. arXiv: 1507.05519.

[115] B. Grzadkowski, M. Iskrzynski, M. Misiak, and J. Rosiek. "Dimension-Six Terms in the Standard Model Lagrangian". In: *Journal of High Energy Physics* 2010.10 (2010). DOI: 10.1007/JHEP10(2010)085. arXiv: 1008.4884.

[116] A. Hoefer. "On the Possibilities of Distinguishing Majorana from Dirac Neutrinos". In: (1997). arXiv: hep-ph/9705362.

[117] M. Dutra, C. A. d. S. Pires, and P. S. R. da Silva. "Majorana Dark Matter in Minimal Higgs Portal Models after LUX". In: *Journal of High Energy Physics* 2015.9 (2015). DOI: 10.1007/JHEP09(2015)147. arXiv: 1504.07222.

[118] C. Boehm, M. J. Dolan, C. McCabe, M. Spannowsky, and C. J. Wallace. "Extended gamma-ray emission from Coy Dark Matter". In: *Journal of Cosmology and Astroparticle Physics* 2014.5 (2014), pp. 009–009. DOI: 10.1088/1475-7516/2014/05/009. arXiv: 1401.6458.

[119] The Fermi-LAT and DES Collaborations. "Searching for Dark Matter Annihilation in Recently Discovered Milky Way Satellites with Fermi-LAT". In: *The Astrophysical Journal* 834.2 (2017). arXiv: 1611.03184, p. 110. DOI: 10.3847/1538-4357/834/2/110.

[120] P. Langacker. "The physics of heavy Z' gauge bosons". en. In: *Reviews of Modern Physics* 81.3 (2009), pp. 1199–1228. DOI: 10.1103/RevModPhys.81.1199.

[121] M. Cvetic and S. Godfrey. "Discovery and Identification of Extra Gauge Bosons". In: *arXiv:hep-ph/9504216* 16 (1997), pp. 383–415. DOI: 10.1142/9789812830265_0007. arXiv: hep-ph/9504216.

[122] J. L. Hewett and T. G. Rizzo. "Low-energy phenomenology of superstring-inspired E6 models". In: *Physics Reports* 183.5 (1989), pp. 193–381. DOI: 10.1016/0370-1573(89)90071-9.

[123] M. Cvetic and P. Langacker. "New Gauge Bosons from String Models". In: *Modern Physics Letters A* 11.15 (1996), pp. 1247–1262. DOI: 10.1142/S0217732396001260. arXiv: hep-ph/9602424.

[124] M. Cvetic and P. Langacker. "Z' Physics and Supersymmetry". In: *Perspectives on Supersymmetry*. Vol. Volume 18. Advanced Series on Directions in High Energy Physics Volume 18. arXiv: hep-ph/9707451, DOI: 10.1142/9789812839657_0012. World Scientific, 1998, pp. 312–331.

[125] J. K. Mizukoshi, C. A. d. S. Pires, F. S. Queiroz, and P. S. R. da Silva. "WIMPs in a 3-3-1 model with heavy Sterile neutrinos". In: *Physical Review D* 83.6 (2011). DOI: 10.1103/PhysRevD.83.065024. arXiv: 1010.4097.

[126] K. Griest and M. Kamionkowski. "Unitarity limits on the mass and radius of dark-matter particles". In: *Phys. Rev. Lett.* 64.6 (1990), pp. 615–618. DOI: 10.1103/PhysRevLett.64.615.

[127] F. Kahlhoefer, K. Schmidt-Hoberg, T. Schwetz, and S. Vogl. "Implications of unitarity and gauge invariance for simplified dark matter models". In: *Journal of High Energy Physics* 2016.2 (2016). DOI: 10.1007/JHEP02(2016)016. arXiv: 1510.02110.

[128] The LEP Collaboration, ALEPH Collaboration, DELPHI Collaboration, L3 Collaboration, OPAL Collaboration, and the LEP Electroweak Working Group. "A Combination of Preliminary Electroweak Measurements and Constraints on the Standard Model". In: *arXiv:hep-ex/0612034* (2006). arXiv: hep-ex/0612034.

[129] CDF Collaboration and T. Aaltonen. "Search for New Physics in High Mass Electron-Positron Events in ppbar Collisions at sqrt(s) = 1.96 TeV". In: *Physical Review Letters* 99.17 (2007). arXiv: 0707.2524. DOI: 10.1103/PhysRevLett.99.171802.

[130] ATLAS Collaboration. "Search for high-mass new phenomena in the dilepton final state using proton-proton collisions at $\sqrt{s} = 13$ TeV with the ATLAS detector". In: *Physics Letters B* 761 (2016). arXiv: 1607.03669, pp. 372–392. DOI: 10.1016/j.physletb.2016.08.055.

[131] P. Fayet. "Extra $U(1)'$s and new forces". In: *Nuclear Physics B* 347.3 (1990), pp. 743–768. DOI: 10.1016/0550-3213(90)90381-M.

[132] P. Fayet. "Effects of the spin-1 partner of the goldstino (gravitino) on neutral current phenomenology". In: *Physics Letters B* 95.2 (1980), pp. 285–289. DOI: 10.1016/0370-2693(80)90488-8.

[133] P. Fayet. "The light U boson as the mediator of a new force, coupled to a combination of Q, B, L and dark matter". In: *The European Physical Journal C* 77.1 (2017). DOI: 10.1140/epjc/s10052-016-4568-9. arXiv: 1611.05357.

[134] P. Fayet. "A la recherche d'un nouveau boson de spin un". In: *Nuclear Physics B* 187.1 (1981), pp. 184–204. DOI: 10.1016/0550-3213(81)90122-X.

[135] P. Fayet. "Parity violation effects induced by a new gauge boson". In: *Physics Letters B* 96.1 (1980), pp. 83–88. DOI: 10.1016/0370-2693(80)90217-8.

[136] P. Fayet. "U-boson detectability, and Light Dark Matter". In: (2006). arXiv: hep-ph/0607094.

[137] H. An, M. Pospelov, J. Pradler, and A. Ritz. "Direct Detection Constraints on Dark Photon Dark Matter". In: *Physics Letters B* 747 (2015), pp. 331–338. DOI: 10.1016/j.physletb.2015.06.018. arXiv: 1412.8378.

[138] J.P. Lees on behalf of the BaBar Collaboration. "Search for a dark photon in e+e- collisions at BaBar". In: *Physical Review Letters* 113.20 (2014). DOI: 10.1103/PhysRevLett.113.201801. arXiv: 1406.2980.

[139] CERN NA48/2 Collaboration. "Search for the dark photon in π^0 decays". In: *arXiv:1504.00607 [hep-ex]* (2015). arXiv: 1504.00607.

[140] A. Aguilar-Arevalo et al. "First Direct-Detection Constraints on eV-Scale Hidden-Photon Dark Matter with DAMIC at SNOLAB". In: *Physical Review Letters* 118.14 (2017). DOI: 10.1103/PhysRevLett.118.141803. arXiv: 1611.03066.

[141] LHCb Collaboration. "Search for dark photons produced in 13 TeV *pp* collisions". In: *Physical Review Letters* 120.6 (2018). DOI: 10.1103/PhysRevLett.120.061801. arXiv: 1710.02867.

[142] M. Ablikim et al. "Dark Photon Search in the Mass Range Between 1.5 and 3.4 GeV/c^2". In: *Physics Letters B* 774 (2017), pp. 252–257. DOI: 10.1016/j.physletb.2017.09.067. arXiv: 1705.04265.

[143] J. P. Lees on behalf of the BaBar Collaboration. "Search for Invisible Decays of a Dark Photon Produced in e^+e^- Collisions at BaBar". In: *Physical Review Letters* 119.13 (2017). DOI: 10.1103/PhysRevLett.119.131804. arXiv: 1702.03327.

[144] K.-Y. Choi, K. Kadota, and I. Park. "Constraining dark photon model with dark matter from CMB spectral distortions". In: *Physics Letters B* 771 (2017), pp. 162–167. DOI: 10.1016/j.physletb.2017.04.062. arXiv: 1701.01221.

[145] B. Holdom. "Two $U(1)$'s and ϵ charge shifts". In: *Physics Letters B* 166.2 (1986), pp. 196–198. DOI: 10.1016/0370-2693(86)91377-8.

[146] M. Pospelov, A. Ritz, and M. B. Voloshin. "Secluded WIMP Dark Matter". In: *Physics Letters B* 662.1 (2008), pp. 53–61. DOI: 10.1016/j.physletb.2008.02.052. arXiv: 0711.4866.

[147] T. Hahn. "Cuba—a library for multidimensional numerical integration". In: *Computer Physics Communications* 168.2 (2005), pp. 78–95. DOI: 10.1016/j.cpc.2005.01.010. arXiv: hep-ph/0404043.

[148] D. Maity and P. Saha. "Connecting CMB anisotropy and cold dark matter phenomenology via reheating". In: (2018). arXiv: 1801.03059.

[149] H. Liu, T. R. Slatyer, and J. Zavala. "The Darkest Hour Before Dawn: Contributions to Cosmic Reionization from Dark Matter Annihilation and Decay". In: *Physical Review D* 94.6 (2016). DOI: 10.1103/PhysRevD.94.063507. arXiv: 1604.02457.

[150] T. R. Slatyer. "Energy Injection And Absorption In The Cosmic Dark Ages". In: *Physical Review D* 87.12 (2013). DOI: 10.1103/PhysRevD.87.123513. arXiv: 1211.0283.

[151] T. R. Slatyer. "Indirect Dark Matter Signatures in the Cosmic Dark Ages I. Generalizing the Bound on s-wave Dark Matter Annihilation from Planck". In: (2015). DOI: 10.1103/PhysRevD.93.023527. arXiv: 1506.03811.

[152] T. R. Slatyer. "Indirect Dark Matter Signatures in the Cosmic Dark Ages II. Ionization, Heating and Photon Production from Arbitrary Energy Injections". In: *Physical Review D* 93.2 (2016). DOI: 10.1103/PhysRevD.93.023521. arXiv: 1506.03812.

[153] M. Cirelli, G. Corcella, A. Hektor, G. Hütsi, M. Kadastik, P. Panci, M. Raidal, F. Sala, and A. Strumia. "PPPC 4 DM ID: A Poor Particle Physicist Cookbook for Dark Matter Indirect Detection". In: (2010). DOI: 10.1088/1475-7516/2011/03/051.

[154] T. Sjöstrand, S. Ask, J. R. Christiansen, R. Corke, N. Desai, P. Ilten, S. Mrenna, S. Prestel, C. O. Rasmussen, and P. Z. Skands. "An Introduction to PYTHIA 8.2". In: (2014). DOI: 10.1016/j.cpc.2015.01.024.

[155] Planck Collaboration. "Planck 2015 results. XIII. Cosmological parameters". In: *Astronomy & Astrophysics* 594 (2016), A13. DOI: 10.1051/0004-6361/201525830. arXiv: 1502.01589.

[156] C. Boehm, D. Hooper, J. Silk, and M. Casse. "MeV Dark Matter: Has It Been Detected?" In: *Physical Review Letters* 92.10 (2004). DOI: 10.1103/PhysRevLett.92.101301. arXiv: astro-ph/0309686.

[157] D. Hooper, F. Ferrer, C. Boehm, J. Silk, J. Paul, N. W. Evans, and M. Casse. "Possible Evidence for MeV Dark Matter In Dwarf Spheroidals". In: *Physical Review Letters* 93.16 (2004). DOI: 10.1103/PhysRevLett.93.161302. arXiv: astro-ph/0311150.

[158] J. F. Beacom, N. F. Bell, and G. Bertone. "Gamma-Ray Constraint on Galactic Positron Production by MeV Dark Matter". In: *Physical Review Letters* 94.17 (2005). DOI: 10.1103/PhysRevLett.94.171301. arXiv: astro-ph/0409403.

[159] K. Ahn and E. Komatsu. "Dark Matter Annihilation: the origin of cosmic gamma-ray background at 1-20 MeV". In: *Physical Review D* 72.6 (2005). DOI: 10.1103/PhysRevD.72.061301. arXiv: astro-ph/0506520.

[160] D. Hooper, M. Kaplinghat, L. E. Strigari, and K. M. Zurek. "MeV Dark Matter and Small Scale Structure". In: *Physical Review D* 76.10 (2007). DOI: 10.1103/PhysRevD.76.103515. arXiv: 0704.2558.

[161] T. Bringmann, A. Galea, A. Hryczuk, and C. Weniger. "Novel Spectral Features in MeV Gamma Rays from Dark Matter". In: *Physical Review D* 95.4 (2017). DOI: 10.1103/PhysRevD.95.043002. arXiv: 1610.04613.

[162] K. K. Boddy and J. Kumar. "Indirect Detection of Dark Matter Using MeV-Range Gamma-Ray Telescopes". In: *Physical Review D* 92.2 (2015). DOI: 10.1103/PhysRevD.92.023533. arXiv: 1504.04024.

[163] C. Garcia-Cely and A. Rivera. "General calculation of the cross section for dark matter annihilations into two photons". In: *Journal of Cosmology and Astroparticle Physics* 2017.3 (2017), pp. 054–054. DOI: 10.1088/1475-7516/2017/03/054. arXiv: 1611.08029.

[164] A. De Angelis et al. "The e-ASTROGAM mission (exploring the extreme Universe with gamma rays in the MeV-GeV range)". In: (2016). DOI: 10.1007/s10686-017-9533-6.

[165] R. Bartels, D. Gaggero, and C. Weniger. "Prospects for indirect dark matter searches with MeV photons". In: *Journal of Cosmology and Astroparticle Physics* 2017.5 (2017), pp. 001–001. DOI: 10.1088/1475-7516/2017/05/001. arXiv: 1703.02546.

[166] Q. Arnaud et al. "First results from the NEWS-G direct dark matter search experiment at the LSM". In: *Astroparticle Physics* 97 (2018), pp. 54–62. DOI: 10.1016/j.astropartphys.2017.10.009. arXiv: 1706.04934.

[167] The CRESST Collaboration. "Results on light dark matter particles with a low-threshold CRESST-II detector". In: *The European Physical Journal C* 76.1 (2016). DOI: 10.1140/epjc/s10052-016-3877-3. arXiv: 1509.01515.

[168] R. Essig, T. Volansky, and T.-T. Yu. "New Constraints and Prospects for sub-GeV Dark Matter Scattering off Electrons in Xenon". In: (2017). DOI: 10.1103/PhysRevD.96.043017.

[169] R. Essig, A. Manalaysay, J. Mardon, P. Sorensen, and T. Volansky. "First Direct Detection Limits on sub-GeV Dark Matter from XENON10". In: (2012). DOI: 10.1103/PhysRevLett.109.021301.

[170] J. P. Lees on behalf of the BaBar Collaboration. "Search for Invisible Decays of a Dark Photon Produced in e+e- Collisions at BaBar". In: *Physical Review Letters* 119.13 (2017). DOI: 10.1103/PhysRevLett.119.131804. arXiv: 1702.03327.

[171] H. Davoudiasl, H.-S. Lee, and W. J. Marciano. "Muon g-2, Rare Kaon Decays, and Parity Violation from Dark Bosons". In: *Physical Review D* 89.9 (2014). DOI: 10.1103/PhysRevD.89.095006. arXiv: 1402.3620.

[172] E787 Collaboration. "Further search for the decay $K^+ \to \pi^+\nu\bar{\nu}$ in the momentum region $P < 195\text{MeV}/c$". In: *Physical Review D* 70.3 (2004). DOI: 10.1103/PhysRevD.70.037102. arXiv: hep-ex/0403034.

[173] E949 Collaboration. "New measurement of the $K^+ \to \pi^+, nu, \bar{n}u$ branching ratio". In: *Physical Review Letters* 101.19 (2008). DOI: 10.1103/PhysRevLett.101.191802. arXiv: 0808.2459.

[174] R. Essig, J. Mardon, M. Papucci, T. Volansky, and Y.-M. Zhong. "Constraining Light Dark Matter with Low-Energy $e+e-$ Colliders". In: *Journal of High Energy Physics* 2013.11 (2013). DOI: 10.1007/JHEP11(2013)167. arXiv: 1309.5084.

[175] NA64 Collaboration. "Search for vector mediator of Dark Matter production in invisible decay mode". In: *Physical Review D* 97.7 (2018). DOI: 10.1103/PhysRevD.97.072002. arXiv: 1710.00971.

[176] J. Alexander et al. "Dark Sectors 2016 Workshop: Community Report". In: (2016).

[177] B. Wojtsekhowski, D. Nikolenko, and I. Rachek. "Searching for a new force at VEPP-3". In: (2012).

[178] M. Raggi and V. Kozhuharov. "Proposal to search for a dark photon in e^+ on target collisions at DAΦNE linac". In: (2014). DOI: 10.1155/2014/959802.

[179] M. Raggi, V. Kozhuharov, and P. Valente. "The PADME experiment at LNF". In: (2015).

[180] J. Balewski et al. "The DarkLight Experiment: A Precision Search for New Physics at Low Energies". In: (2014).

[181] B. Wojtsekhowski et al. "Searching for a dark photon: Project of the experiment at VEPP-3". In: (2017). DOI: 10.1088/1748-0221/13/02/P02021.

[182] M. Kawasaki, K. Kohri, and N. Sugiyama. "Cosmological Constraints on Late-time Entropy Production". In: *Physical Review Letters* 82.21 (1999), pp. 4168–4171. DOI: 10.1103/PhysRevLett.82.4168. arXiv: astro-ph/9811437.

[183] SuperCDMS Collaboration. "Projected sensitivity of the SuperCDMS SNOLAB experiment". In: *Physical Review D* 95.8 (2017). DOI: 10.1103/PhysRevD.95.082002. arXiv: 1610.00006.

[184] SuperCDMS Collaboration. "Results from the Super Cryogenic Dark Matter Search (SuperCDMS) experiment at Soudan". In: (2017). DOI: 10.1103/PhysRevLett.120.061802.

[185] M. S. Turner. "Axions from SN1987A". In: *Phys. Rev. Lett.* 60.18 (1988), pp. 1797–1800. DOI: 10.1103/PhysRevLett.60.1797.

[186] K. Hirata et al. "Observation of a neutrino burst from the supernova SN1987A". In: *Phys. Rev. Lett.* 58.14 (1987), pp. 1490–1493. DOI: 10.1103/PhysRevLett.58.1490.

[187] R. M. Bionta et al. "Observation of a neutrino burst in coincidence with supernova 1987A in the Large Magellanic Cloud". In: *Phys. Rev. Lett.* 58.14 (1987), pp. 1494–1496. DOI: 10.1103/PhysRevLett.58.1494.

[188] H. K. Dreiner, J.-F. Fortin, C. Hanhart, and L. Ubaldi. "Supernova Constraints on MeV Dark Sectors from e^+e^- Annihilations". In: *Physical Review D* 89.10 (2014). DOI: 10.1103/PhysRevD.89.105015. arXiv: 1310.3826.

[189] D. Kazanas, R. N. Mohapatra, S. Nussinov, V. L. Teplitz, and Y. Zhang. "Supernova Bounds on the Dark Photon Using its Electromagnetic Decay". In: *Nuclear Physics B* 890 (2015), pp. 17–29. DOI: 10.1016/j.nuclphysb.2014.11.009. arXiv: 1410.0221.

[190] C. Mahoney, A. K. Leibovich, and A. R. Zentner. "Updated Constraints on Self-Interacting Dark Matter from Supernova 1987A". In: *Physical Review D* 96.4 (2017). DOI: 10.1103/PhysRevD.96.043018. arXiv: 1706.08871.

[191] J. Smolinsky and P. Tanedo. "Dark Photons from Captured Inelastic Dark Matter Annihilation: Charged Particle Signatures". In: *Physical Review D* 95.7 (2017). DOI: 10.1103/PhysRevD.95.075015. arXiv: 1701.03168.

[192] G. G. Raffelt. *Stars as Laboratories for Fundamental Physics: The Astrophysics of Neutrinos, Axions, and Other Weakly Interacting Particles*. 2nd edition. Chicago: University of Chicago Press, 1996. 686 pp.

[193] J. H. Chang, R. Essig, and S. D. McDermott. "Revisiting Supernova 1987A Constraints on Dark Photons". In: *Journal of High Energy Physics* 2017.1 (2017). DOI: 10.1007/JHEP01(2017)107. arXiv: 1611.03864.

[194] A. Fradette, M. Pospelov, J. Pradler, and A. Ritz. "Cosmological Constraints on Very Dark Photons". In: *Physical Review D* 90.3 (2014). DOI: 10.1103/PhysRevD.90.035022. arXiv: 1407.0993.

[195] R. N. Mohapatra and A. Y. Smirnov. "Neutrino Mass and New Physics". In: *Journal of Physics: Conference Series* 53 (2006), pp. 44–82. DOI: 10.1088/1742-6596/53/1/003. arXiv: hep-ph/0603118.

[196] A. Abada, P. Hosteins, F.-X. Josse-Michaux, and S. Lavignac. "Successful leptogenesis in SO(10) unification with a left–right symmetric seesaw mechanism". In: *Nuclear Physics B* 809.1 (2009), pp. 183–217. DOI: 10.1016/j.nuclphysb.2008.09.043. arXiv: 0808.2058.

[197] A. Katz and M. Perelstein. "Higgs Couplings and Electroweak Phase Transition". In: *Journal of High Energy Physics* 2014.7 (2014). DOI: 10.1007/JHEP07(2014)108. arXiv: 1401.1827.

[198] L. M. Krauss and F. Wilczek. "Discrete gauge symmetry in continuum theories". In: *Phys. Rev. Lett.* 62.11 (1989), pp. 1221–1223. DOI: 10.1103/PhysRevLett.62.1221.

[199] G. Chalons, D. Lopez-Val, T. Robens, and T. Stefaniak. "The Higgs singlet extension at LHC Run 2". In: (2016). arXiv: 1611.03007.

[200] Y. Mambrini, S. Profumo, and F. S. Queiroz. "Dark Matter and Global Symmetries". In: *Physics Letters B* 760 (2016), pp. 807–815. DOI: 10.1016/j.physletb.2016.07.076. arXiv: 1508.06635.

[201] S. Coleman, J. Wess, and B. Zumino. "Structure of Phenomenological Lagrangians. I". In: *Phys. Rev.* 177.5 (1969), pp. 2239–2247. DOI: 10.1103/PhysRev.177.2239.

[202] C. G. Callan, S. Coleman, J. Wess, and B. Zumino. "Structure of Phenomenological Lagrangians. II". In: *Phys. Rev.* 177.5 (1969), pp. 2247–2250. DOI: 10.1103/PhysRev.177.2247.

[203] J. F. Donoghue, E. Golowich, and B. R. Holstein. "Dynamics of the standard model". In: *Camb.Monogr.Part.Phys.Nucl.Phys.Cosmol.* 2 (2014), pp. 1–540. DOI: 10.1017/CBO9780511524370.

[204] K. J. Bae, A. Kamada, S. P. Liew, and K. Yanagi. "Light Axinos from Freeze-in: production processes, phase space distributions, and Ly-α constraints". In: *Journal of Cosmology and Astroparticle Physics* 2018.1 (2018), pp. 054–054. DOI: 10.1088/1475-7516/2018/01/054. arXiv: 1707.06418.

[205] W. J. Marciano, C. Zhang, and S. Willenbrock. "Higgs Decay to Two Photons". In: *Physical Review D* 85.1 (2012). DOI: 10.1103/PhysRevD.85.013002. arXiv: 1109.5304.

[206] K. J. Bae, M. Endo, K. Hamaguchi, and T. Moroi. "Diphoton Excess and Running Couplings". In: *Physics Letters B* 757 (2016), pp. 493–500. DOI: 10.1016/j.physletb.2016.04.031. arXiv: 1602.03653.

[207] G. Arcadi, P. Ghosh, Y. Mambrini, and M. Pierre. "Scrutinizing a di-photon resonance at the LHC through Moscow zero". In: *Journal of Cosmology and Astroparticle Physics* 2016.11 (2016), pp. 054–054. DOI: 10.1088/1475-7516/2016/11/054. arXiv: 1608.04755.

[208] P. Anastasopoulos, M. Bianchi, E. Dudas, and E. Kiritsis. "Anomalies, anomalous U(1)'s and generalized Chern-Simons terms". In: *J. High Energy Phys.* 2006.11 (2006), p. 057. DOI: 10.1088/1126-6708/2006/11/057. arXiv: hep-th/0605225.

[209] B. de Wit, P. G. Lauwers, and A. Van Proeyen. "Lagrangians of $N = 2$ Supergravity - Matter Systems". In: *Nucl.Phys.* B255 (1985), pp. 569–608. DOI: 10.1016/0550-3213(85)90154-3.

[210] I. Antoniadis, E. Kiritsis, and T. Tomaras. "A D-brane alternative to unification". In: *Physics Letters B* 486.1 (2000), pp. 186–193. DOI: 10.1016/S0370-2693(00)00733-4. arXiv: hep-ph/0004214.

[211] E. Dudas, A. Falkowski, and S. Pokorski. "Deconstructed U(1) and Supersymmetry Breaking". In: *Physics Letters B* 568.3 (2003), pp. 281–290. DOI: 10.1016/j.physletb.2003.06.038. arXiv: hep-th/0303155.

[212] Y. Farzan and A. R. Akbarieh. "Decaying vector dark matter as an explanation for the 3.5 keV line from galaxy clusters". In: *J. Cosmol. Astropart. Phys.* 2014.11 (2014), p. 015. DOI: 10.1088/1475-7516/2014/11/015.

[213] A. Ismail, A. Katz, and D. Racco. "On dark matter interactions with the Standard Model through an anomalous Z". In: *J. High Energ. Phys.* 2017.10 (2017), p. 165. DOI: 10.1007/JHEP10(2017)165.

[214] G. Arcadi, P. Ghosh, Y. Mambrini, M. Pierre, and F. S. Queiroz. "Z' portal to Chern-Simons Dark Matter". In: *J. Cosmol. Astropart. Phys.* 2017.11 (2017), p. 020. DOI: 10.1088/1475-7516/2017/11/020. arXiv: 1706.04198.

[215] S.-M. Choi, Y. Hochberg, E. Kuflik, H. M. Lee, Y. Mambrini, H. Murayama, and M. Pierre. "Vector SIMP dark matter". In: *J. High Energ. Phys.* 2017.10 (2017), p. 162. DOI: 10.1007/JHEP10(2017)162.

[216] E. Dudas, L. Heurtier, Y. Mambrini, and B. Zaldivar. "Extra U(1), effective operators, anomalies and dark matter". In: *J. High Energ. Phys.* 2013.11 (2013), p. 83. DOI: 10.1007/JHEP11(2013)083.

[217] L. D. Landau. "On the angular momentum of a system of two photons". In: (). DOI: 10.1016/B978-0-08-010586-4.50070-5.

[218] C. N. Yang. "Selection Rules for the Dematerialization of a Particle into Two Photons". In: *Phys. Rev.* 77.2 (1950), pp. 242–245. DOI: 10.1103/PhysRev.77.242.

[219] V. Pleitez. "Angular momentum and parity of a two gluon system". In: (2018). arXiv: 1801.09294.

[220] W. Beenakker, R. Kleiss, and G. Lustermans. "No Landau-Yang in QCD". In: *arXiv:1508.07115 [hep-ph]* (2015). arXiv: 1508.07115.

[221] V. Pleitez. "The angular momentum of two massless fields revisited". In: (2015). arXiv: 1508.01394.

[222] M. Cacciari, L. Del Debbio, J. R. Espinosa, A. D. Polosa, and M. Testa. "A note on the fate of the Landau-Yang theorem in non-Abelian gauge theories". In: *Physics Letters B* 753 (2016), pp. 476–481. DOI: 10.1016/j.physletb.2015.12.053. arXiv: 1509.07853.

[223] H. Ruegg and M. Ruiz-Altaba. "The Stueckelberg Field". In: *International Journal of Modern Physics A* 19.20 (2004), pp. 3265–3347. DOI: 10.1142/S0217751X04019755. arXiv: hep-th/0304245.

[224] G. Salesi and L. Deleidi. "Helicity-0 spinning particles". In: (2015). arXiv: 1506.04471.

[225] Fayyazuddin and Riazuddin. *Modern Introduction to Particle Physics*. Singapore: World Scientific Pub Co Inc, 1992. 676 pp.

[226] Jupyter Development Team. "Jupyter Notebooks – a publishing format for reproducible computational workflows". In: *Stand Alone* (2016). DOI: 10.3233/978-1-61499-649-1-87.

[227] M. B. Green and J. H. Schwarz. "Anomaly Cancellation in Supersymmetric $D = 10$ Gauge Theory and Superstring Theory". In: *Phys.Lett.* 149B (1984), pp. 117–122. DOI: 10.1016/0370-2693(84)91565-X.

[228] H. Sahlmann. "Loop quantum gravity - a short review". In: (2010).

[229] N. Huggett and T. Vistarini. "Deriving General Relativity From String Theory". In: 2014.

[230] C. C. Speake and C. M. Will. "Tests of the weak equivalence principle". In: *Class. Quantum Grav.* 29.18 (2012), p. 180301. DOI: 10.1088/0264-9381/29/18/180301.

[231] P. Touboul et al. "MICROSCOPE Mission: First Results of a Space Test of the Equivalence Principle". In: *Phys. Rev. Lett.* 119.23 (2017), p. 231101. DOI: 10.1103/PhysRevLett.119.231101.

[232] C. Bonvin and P. Fleury. "Testing the equivalence principle on cosmological scales". In: *Journal of Cosmology and Astroparticle Physics* 2018.5 (2018), pp. 061–061. DOI: 10.1088/1475-7516/2018/05/061. arXiv: 1803.02771.

[233] C. M. Will. "The confrontation between general relativity and experiment: An update". In: *Physics Reports* 113.6 (1984), pp. 345–422. DOI: 10.1016/0370-1573(84)90119-4.

[234] T. Damour and A. M. Polyakov. "The String Dilaton and a Least Coupling Principle". In: *Nuclear Physics B* 423.2 (1994), pp. 532–558. DOI: 10.1016/0550-3213(94)90143-0. arXiv: hep-th/9401069.

[235] T. Damour. "Theoretical aspects of the equivalence principle". In: *Class. Quantum Grav.* 29.18 (2012), p. 184001. DOI: 10.1088/0264-9381/29/18/184001.

[236] P. J. Orlando, R. B. Mann, K. Modi, and F. A. Pollock. "A Simple Test of the Equivalence Principle(s) for Quantum Superpositions". In: *Classical and Quantum Gravity* 33.19 (2016), 19LT01. DOI: 10.1088/0264-9381/33/19/19LT01. arXiv: 1511.02943.

[237] G. Rosi, G. D'Amico, L. Cacciapuoti, F. Sorrentino, M. Prevedelli, M. Zych, C. Brukner, and G. M. Tino. "Quantum test of the equivalence principle for atoms in superpositions of internal energy eigenstates". In: *Nature Communications* 8 (2017), p. 15529. DOI: 10.1038/ncomms15529. arXiv: 1704.02296.

[238] The LIGO Scientific Collaboration and the Virgo Collaboration. "GW170104: Observation of a 50-Solar-Mass Binary Black Hole Coalescence at Redshift 0.2". In: *Physical Review Letters* 118.22 (2017). DOI: 10.1103/PhysRevLett.118.221101. arXiv: 1706.01812.

[239] F. Dyson. "Is a graviton detectable?" In: *Int. J. Mod. Phys. A* 28.25 (2013), p. 1330041. DOI: 10.1142/S0217751X1330041X.

[240] C.-Q. Geng, D. Huang, Y. Tang, and Y.-L. Wu. "Note on 125 GeV spin-2 particle". In: *Physics Letters B* 719.1 (2013), pp. 164–169. DOI: 10.1016/j.physletb.2013.01.016.

[241] M. Fierz and W. Pauli. "On Relativistic Wave Equations for Particles of Arbitrary Spin in an Electromagnetic Field". In: *Proceedings of the Royal Society of London. Series A, Mathematical and Physical Sciences* 173.953 (1939), pp. 211–232.

[242] D. G. Boulware and S. Deser. "Can Gravitation Have a Finite Range?" In: *Phys. Rev. D* 6.12 (1972), pp. 3368–3382. DOI: 10.1103/PhysRevD.6.3368.

[243] N. Boulanger, T. Damour, L. Gualtieri, and M. Henneaux. "Inconsistency of interacting, multi-graviton theories". In: *Nuclear Physics B* 597.1 (2001), pp. 127–171. DOI: 10.1016/S0550-3213(00)00718-5. arXiv: hep-th/0007220.

[244] T. Gregoire, M. D. Schwartz, and Y. Shadmi. "Massive Supergravity and Deconstruction". In: *Journal of High Energy Physics* 2004.7 (2004), pp. 029–029. DOI: 10.1088/1126-6708/2004/07/029. arXiv: hep-th/0403224.

[245] S. G. Nibbelink and M. Peloso. "Chiral gravity as a covariant formulation of massive gravity". In: *Class. Quantum Grav.* 22.7 (2005), p. 1313. DOI: 10.1088/0264-9381/22/7/008.

[246] S. Groot Nibbelink, M. Peloso, and M. Sexton. "Nonlinear properties of vielbein massive gravity". In: *Eur. Phys. J. C* 51.3 (2007), p. 741. DOI: 10.1140/epjc/s10052-007-0311-x.

[247] C. de Rham, G. Gabadadze, and A. J. Tolley. "Resummation of Massive Gravity". In: *Phys. Rev. Lett.* 106.23 (2011), p. 231101. DOI: 10.1103/PhysRevLett.106.231101.

[248] S. F. Hassan and R. A. Rosen. "Bimetric Gravity from Ghost-free Massive Gravity". In: (2011). DOI: 10.1007/JHEP02(2012)126.

[249] S. F. Hassan and R. A. Rosen. "Resolving the Ghost Problem in Nonlinear Massive Gravity". In: *Phys. Rev. Lett.* 108.4 (2012), p. 041101. DOI: 10.1103/PhysRevLett.108.041101.

[250] S. F. Hassan, A. Schmidt-May, and M. von Strauss. "On Consistent Theories of Massive Spin-2 Fields Coupled to Gravity". In: *Journal of High Energy Physics* 2013.5 (2013). DOI: 10.1007/JHEP05(2013)086. arXiv: 1208.1515.

[251] A. Schmidt-May. "Nonlinear interactions for massive spin-2 fields". In: *arXiv:1602.07520 [astro-ph, physics:gr-qc, physics:hep-th]* (2016). arXiv: 1602.07520.

[252] H. M. Lee, M. Park, and V. Sanz. "Gravity-mediated (or composite) dark matter". In: *Eur. Phys. J. C* 74.2 (2014), p. 2715. DOI: 10.1140/epjc/s10052-014-2715-8.

[253] S. Kraml, U. Laa, K. Mawatari, and K. Yamashita. "Simplified dark matter models with a spin-2 mediator at the LHC". In: *The European Physical Journal C* 77.5 (2017). DOI: 10.1140/epjc/s10052-017-4871-0. arXiv: 1701.07008.

[254] A. Carrillo-Monteverde, Y.-J. Kang, H. M. Lee, M. Park, and V. Sanz. "Dark matter direct detection from new interactions in models with spin-two mediators". In: *J. High Energ. Phys.* 2018.6 (2018), p. 37. DOI: 10.1007/JHEP06(2018)037.

[255] H. M. Lee, M. Park, and V. Sanz. "Gravity-mediated (or Composite) Dark Matter Confronts Astrophysical Data". In: *Journal of High Energy Physics* 2014.5 (2014). DOI: 10.1007/JHEP05(2014)063. arXiv: 1401.5301.

[256] A. Schmidt-May and M. von Strauss. "Recent developments in bimetric theory". In: *Journal of Physics A: Mathematical and Theoretical* 49.18 (2016), p. 183001. DOI: 10.1088/1751-8113/49/18/183001. arXiv: 1512.00021.

[257] E. Babichev, L. Marzola, M. Raidal, A. Schmidt-May, F. Urban, H. Veermäe, and M. von Strauss. "Gravitational Origin of Dark Matter". In: *Physical Review D* 94.8 (2016). DOI: 10.1103/PhysRevD.94.084055. arXiv: 1604.08564.

[258] K. Aoki and S. Mukohyama. "Massive gravitons as dark matter and gravitational waves". In: *Physical Review D* 94.2 (2016). DOI: 10.1103/PhysRevD.94.024001. arXiv: 1604.06704.

[259] X. Chu and C. Garcia-Cely. "Self-interacting Spin-2 Dark Matter". In: *Physical Review D* 96.10 (2017). DOI: 10.1103/PhysRevD.96.103519. arXiv: 1708.06764.

[260] Y. Tang and Y.-L. Wu. "On thermal gravitational contribution to particle production and dark matter". In: *Physics Letters B* 774 (2017), pp. 676–681. DOI: 10.1016/j.physletb.2017.10.034.

[261] S. Deser. "Self-Interaction and Gauge Invariance". In: *General Relativity and Gravitation* 1.1 (1970), pp. 9–18. DOI: 10.1007/BF00759198. arXiv: gr-qc/0411023.

[262] G. F. Giudice, R. Rattazzi, and J. D. Wells. "Quantum gravity and extra dimensions at high-energy colliders". In: *Nuclear Physics B* 544.1 (1999), pp. 3–38. DOI: 10.1016/S0550-3213(99)00044-9.

[263] T. R. Taylor and G. Veneziano. "Dilaton couplings at large distances". In: *Physics Letters B* 213.4 (1988), pp. 450–454. DOI: 10.1016/0370-2693(88)91290-7.

[264] P. Binétruy and E. Dudas. "Nambu mass hierarchies in low energy string models". In: *Physics Letters B* 338.1 (1994), pp. 23–30. DOI: 10.1016/0370-2693(94)91338-2.

[265] P. Binetruy and E. Dudas. "Fermion mass hierarchies in low energy supergravity and superstring models". In: *Nuclear Physics B* 442.1 (1995), pp. 21–46. DOI: 10.1016/S0550-3213(95)00069-0. arXiv: hep-ph/9411413.

[266] P. Binetruy and E. Dudas. "Dynamical mass matrices from effective superstring theories". In: *Nuclear Physics B* 451.1 (1995), pp. 31–52. DOI: 10.1016/0550-3213(95)00345-S. arXiv: hep-ph/9505295.

[267] C. Kounnas, I. Pavel, and F. Zwirner. "Towards a dynamical determination of parameters in the Minimal Supersymmetric Standard Model". In: *Physics Letters B* 335.3 (1994), pp. 403–415. DOI: 10.1016/0370-2693(94)90371-9. arXiv: hep-ph/9406256.

[268] S. Dimopoulos and G. F. Giudice. "Macroscopic Forces from Supersymmetry". In: *Physics Letters B* 379.1 (1996), pp. 105–114. DOI: 10.1016/0370-2693(96)00390-5. arXiv: hep-ph/9602350.

[269] I. Antoniadis, S. Dimopoulos, and G. Dvali. "Millimetre-Range Forces in Superstring Theories with Weak-Scale Compactification". In: (1997). DOI: 10.1016/S0550-3213(97)00808-0.

[270] F. Feruglio. "Are neutrino masses modular forms?" In: (2017).

[271] J. C. Criado and F. Feruglio. "Modular Invariance Faces Precision Neutrino Data". In: *SciPost Physics* 5.5 (2018). DOI: 10.21468/SciPostPhys.5.5.042. arXiv: 1807.01125.

[272] G. D. Coughlan, W. Fischler, E. W. Kolb, S. Raby, and G. G. Ross. "Cosmological problems for the polonyi potential". In: *Physics Letters B* 131.1 (1983), pp. 59–64. DOI: 10.1016/0370-2693(83)91091-2.

[273] T. Banks, D. B. Kaplan, and A. E. Nelson. "Cosmological implications of dynamical supersymmetry breaking". In: *Phys. Rev. D* 49.2 (1994), pp. 779–787. DOI: 10.1103/PhysRevD.49.779.

[274] B. de Carlos, J. A. Casas, F. Quevedo, and E. Roulet. "Model Independent Properties and Cosmological Implications of the Dilaton and Moduli Sectors of 4-d Strings". In: *Physics Letters B* 318.3 (1993), pp. 447–456. DOI: 10.1016/0370-2693(93)91538-X. arXiv: hep-ph/9308325.

[275] A. Kusenko, M. Loewenstein, and T. T. Yanagida. "Moduli dark matter and the search for its decay line using Suzaku X-ray telescope". In: *Physical Review D* 87.4 (2013). DOI: 10.1103/PhysRevD.87.043508. arXiv: 1209.6403.

[276] T. Moroi and L. Randall. "Wino Cold Dark Matter from Anomaly-Mediated SUSY Breaking". In: *Nuclear Physics B* 570.1 (2000), pp. 455–472. DOI: 10.1016/S0550-3213(99)00748-8. arXiv: hep-ph/9906527.

[277] B. S. Acharya, P. Kumar, K. Bobkov, G. Kane, J. Shao, and S. Watson. "Non-thermal Dark Matter and the Moduli Problem in String Frameworks". In: *Journal*

of High Energy Physics 2008.6 (2008), pp. 064–064. DOI: 10.1088/1126-6708/2008/06/064. arXiv: 0804.0863.

[278] B. S. Acharya, P. Kumar, G. Kane, and S. Watson. "A Non-thermal WIMP Miracle". In: *Physical Review D* 80.8 (2009). DOI: 10.1103/PhysRevD.80.083529. arXiv: 0908.2430.

[279] S. Watson. "Reevaluating the Cosmological Origin of Dark Matter". In: 21 (2010), pp. 305–324. DOI: 10.1142/9789814307505_0007. arXiv: 0912.3003.

[280] R. Allahverdi, B. Dutta, R. N. Mohapatra, and K. Sinha. "A Supersymmetric Model for Dark Matter and Baryogenesis Motivated by the Recent CDMS Result". In: *Physical Review Letters* 111.5 (2013). DOI: 10.1103/PhysRevLett.111.051302. arXiv: 1305.0287.

Résumé en Français

Dans cette thèse, nous considérons des modèles de physique des particules qui pourraient expliquer la nature de la matière noire. Au Chap. 1, nous avons discuté des principales indications selon lesquelles environ 27% du contenu énergétique de l'univers aujourd'hui est composé d'un type de matière qui n'émet ni n'absorbe de lumière de manière détectable, la matière noire (DM) *, mais dont l'influence gravitationnelle sur la matière ordinaire est cruciale pour comprendre les observations astrophysiques et cosmologiques. Au Chap. 2, nous fournissons des détails techniques concernant le point de départ de toute analyse présente dans les travaux considérés: les équations des fluides et leurs termes de collision. Nous discutons également de l'évolution cosmologique d'espèces de particules en tenant compte de la possibilité de production d'entropie ("reheating") due à la désintégration des champs lourds, ce qui est important pour décrire l'évolution de la DM dans l'univers. Au Chap. 3, nous avons examiné les mécanismes permettant d'établir l'abondance des reliques de la DM. Aux Chaps. 4, 5 et 6, nous présentons les résultats originaux de notre recherche. Nos conclusions et perspectives ont été présentées au Chap. 7. Nous tenterons ici d'exposer brièvement la discussion de cette thèse aux lecteurs francophones.

Remarques introductives

Le comportement des étoiles dans les galaxies est mieux compris si nous supposons la présence de halos de matière gravitante qui ne contribuent pas à la luminosité mesurée. Les courbes de rotation des galaxies (Fig. 1.1), ainsi que des études permettant de déduire les masses des amas de galaxies, peuvent être expliquées avec l'inclusion de la DM [14] ou de modifications de la gravitation newtonienne (MOND) [11]. L'analyse des amas de galaxies semble toutefois favoriser l'interprétation des particules de la DM par rapport aux modèles MOND (Figs. 1.2 et 1.3). D'autre part, nous avons besoin d'un contenu énergétique présent il y a longtemps qui n'était pas affecté par la lumière et qui catalysait l'agglutination gravitationnelle de la matière baryonique pour donner naissance aux structures à grande échelle que nous voyons aujourd'hui. La cartographie de ces structures met en évidence l'existence de la DM et établit des liens sérieux dans les modèles MOND (Fig. 1.4).

Les connaissances actuelles sur le processus de formation des structures, les observations des spectres du fond diffus cosmologique (CMB) et les prédictions confirmées de la nucléosynthèse primordiale (BBN) montrent que la plus grande partie du contenu en DM a été établie sous forme de relique cosmique avant découplage des photons du CMB. Ils indiquent également que la contribution de la DM à la densité énergétique de l'univers

*Dans ce résumé, nous conserverons tous les acronymes en anglais.

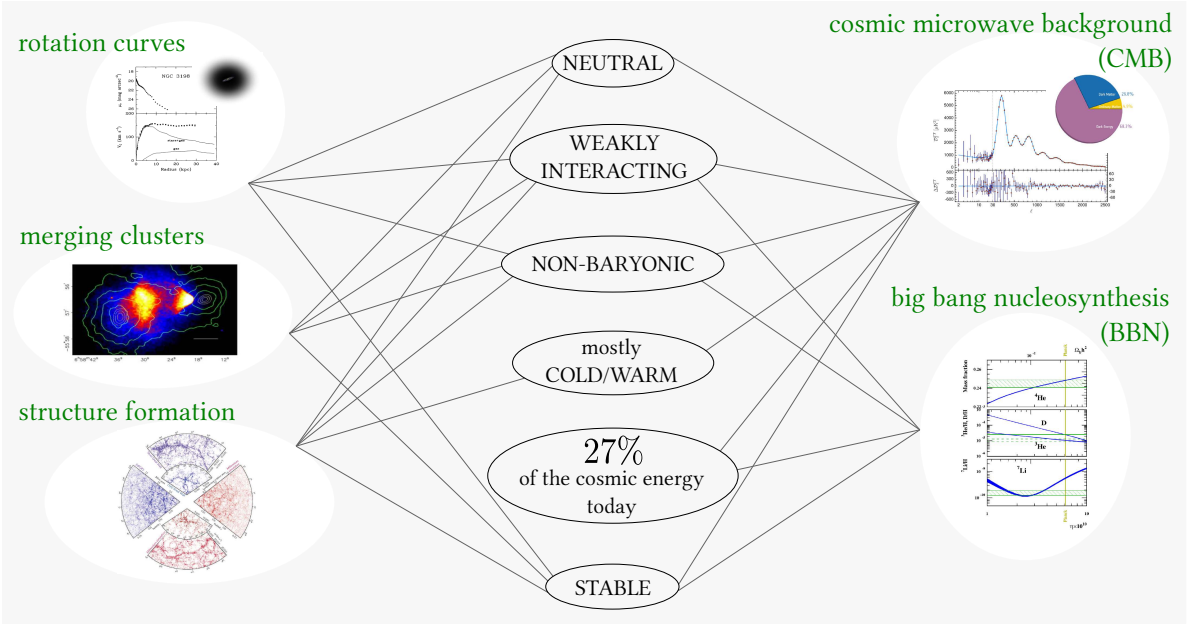

FIGURE 1 – *Puzzle de la matière noire.*

aujourd'hui est d'environ 27%, ce qui est déduit principalement des résultats du télescope Planck [155]. Si ces deux composants de la matière non-baryonique (qui sont et étaient présents dans l'univers) sont constitués du même type de particules, ils devraient être stables, électromagnétiquement neutres (sombres), et s'ils interagissaient de manière non gravitationnelle avec la matière visible, de telles interactions doivent être très faibles puisqu'elles n'ont pas encore été détectées. De telles propriétés doivent donc être garanties dans tout modèle qui entend expliquer la DM du point de vue de la physique des particules. Dans la figure 1, nous avons schématisé la relation entre les preuves de l'existence de particules de matière noire et les propriétés qu'elles devraient avoir.

Le vingtième siècle a été témoin de la consolidation des descriptions quantitatives de phénomènes aux échelles subatomique et cosmologique. D'une part, nous avons la naissance de la mécanique quantique et de la relativité restreinte qui ont conduit à la théorie quantique des champs. Ce formalisme nous a permis de décrire les interactions fondamentales – électromagnétique, faible et forte. D'autre part, nous observons l'émergence de la théorie gravitationnelle d'Einstein, qui considère l'interaction gravitationnelle comme un effet du contenu énergétique (matière et lumière) incurvant l'espace-temps, la relativité générale (GR).

Le modèle standard de la physique des particules (SM), construit sur la base de la théorie des champs quantiques et du principe d'invariance de jauge, en plus d'être cohérent mathématiquement, possède toutes ses prédictions confirmées expérimentalement avec une grande précision au cours des dernières décennies. Malgré tout, il existe des raisons à la fois expérimentales et théoriques d'élargir le modèle standard: masse des neutrinos, asymétrie matière/antimatière, problème de hiérarchie, etc.

Le modèle cosmologique standard (ΛCDM), construit sur la base de la GR, a pour piliers observationnels l'expansion cosmique, le CMB, la BBN, la matière noire froide (CDM) et l'énergie noir (éventuellement une constante cosmologique, Λ). Cela englobe également la tentative de comprendre l'origine des perturbations gravitationnelles en générant les

structures que nous observons aujourd'hui (modèles inflationaires). Nous avons également ici des raisons d'élargir ce modèle, telles que le problème de la constante cosmologique et les problèmes à petite échelle de la CDM.

La matière noire est un problème macroscopique mais, comme nous l'avons vu, il s'agit probablement de particules. Cela signifie que de telles particules doivent être intégrées dans une certaine extension de SM, qui ne possède pas de candidats à DM. Dans le même temps, nous devons également nous assurer qu'ils sont conformes à ce que ΛCDM explique déjà, en faisant partie ou en une extension viable. Le 21ème siècle, si notre espèce survit, sera certainement témoin de progrès significatifs dans cette interface entre la physique des particules et la cosmologie, avec d'innombrables expériences cherchant à détecter de nouvelles particules, l'avancement de l'astronomie par ondes gravitationnelles, des études encore plus précises de CMB, etc. Notamment, la compréhension des premiers instants de l'univers dépend en grande partie du comportement des particules aux hautes énergies - les transitions de phase pour lesquelles l'univers est certainement passé, par exemple, peuvent être dues à des ruptures de symétrie de jauge. En fait, la découverte du boson de Higgs nous a permis d'étudier le processus avant lequel les interactions faibles et électromagnétiques étaient unifiées. Cela motive également la recherche de l'unification des interactions électrofaibles et fortes, les théories de la grande unification (GUT), qui se produiraient normalement à des échelles supérieures à 10^{16}GeV, éventuellement par brisure de symétrie à des échelles intermédiaires, $10^{10} - 10^{16}$ GeV.

Des modèles BSM bien motivés peuvent prendre en charge des candidats à DM qui ont des couplages avec des particules de SM suffisamment fortes pour être détectées par les expériences actuelles. La classe principale de ces candidats est celle des WIMPs, particules massives d'interaction faible. L'abondance reliques de WIMP avec des masses à l'échelle électrofaible ($10-1000$ GeV) est produite thermiquement et s'adapte facilement à la plage observée – le "miracle WIMP".

Cependant, le fait que les expériences ne les ont pas détectées motive toujours la prise en compte des particules massives d'interaction très faibles (FIMPs), dont la production a lieu de manière non thermique. Une difficulté théorique dans ce cas consiste à adapter de manière satisfaisante les couplages très faibles. Dans ce contexte, lier la production de la DM à des échelles intermédiaires est une option intéressante, car dans de nombreux cas, les candidats à DM sont inévitablement des FIMPs. En outre, l'échelle de reheating (production de particules de SM après la période inflationaire, avec production d'entropie) se situant dans de nombreux scénarios dans l'interval $10^7 - 10^{10}$ GeV, l'abondance des FIMPs a probablement été établie au cours de reheating. Des champs lourds sont en effet nécessaires dans des scénarios théoriquement bien motivés tels que le GUT, le see-saw (génération de masse de neutrinos), la baryogenèse (génération d'asymétrie matière-antimatière) et l'inflation. Contrairement au "miracle WIMP", nous prenons la liberté - comme nous nous en excusons - d'appeler une telle connexion la "merveille FIMP". Cela n'est pas une connexion miraculeux, mais cela implique une appréciation de ce que nous ne pouvons toujours pas toucher directement. Évidemment, dans le but d'aller au-delà de l'émerveillement vers le développement de la phénoménologie des FIMPs.

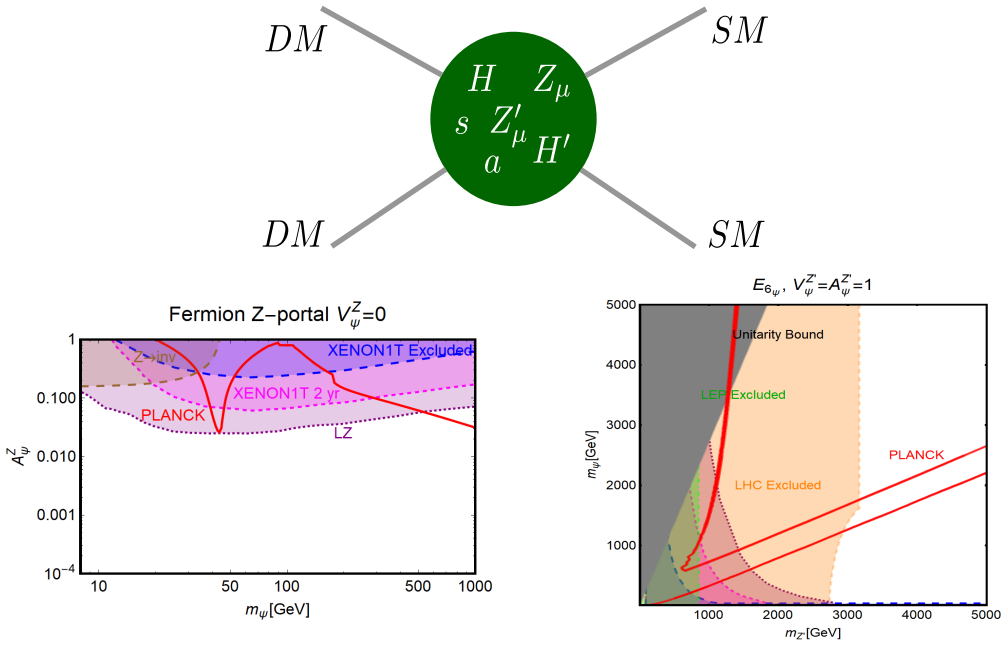

FIGURE 2 – *Panneau supérieur: représentation schématique des processus considérés en Réf. [1]. Résultats représentatifs des liens sur les scénarios simplifiés avec des WIMP fermioniques: portail Z (à gauche) et portail Z' dans un modèle inspiré par le GUT E_{6_ψ} (à droite).*

du “miracle WIMP"...

Dans notre premier travail [1], nous avons examiné une grande variété de modèles simplifiés de WIMP et de médiateurs (portails) entre les secteurs visible et sombre avec des masses comprises entre 10 et 1000 GeV. Ces modèles étaient fortement liés par des expériences de détection directe (LUX, XENON1T et future LZ, XENON1T2y), et de manière complémentaire par colliseurs (LHC, LEP) et par des expériences de détection indirectes (FERMI). Nous concluons que la plupart des scénarios considérés sont déjà exclu. Les portails spin-0 BSM (scalaire et pseudo-scalaire) et spin-1 (SM et BSM) dont les WIMP sont des fermion de Majorana sont toujours viables. Dans la figure 2, nous illustrons les liens expérimentaux forts (régions ombrées en couleur) sur les régions de l'espace des paramètres qui fournissent l'abondance correcte de la DM (rouge) dans les cas où la DM est un fermion de Majorana dans le modèle de portail Z (à gauche) et un fermion de Dirac dans le portail Z' (à droite).

Nous avons exploré le régime de masse faible (échelle MeV) des DM et de photon sombre comme médiateur dans un modèle très prédictif, une extension de jauge du SM [2]. Les mesures précises des spectres du CMB, complété par des expériences à la recherche de photon sombre et de matière noir, laissent une petite fenêtre pour la production thermique de la DM. Cependant, ce scénario serait partiellement en accord avec les limites expérimentales si un champ lourd s'était décomposé après le découplage de la DM, et la densité relique serait diluée par les facteurs Δ comme ceux observés sur la figure 3 (à gauche). Un tel phénomène serait même inévitable s'il existait une physique BSM à l'échelle d'énergie entre 1 GeV et 10^{19} GeV dans l'univers. Nous avons également étudié le même candidat à DM comme une FIMP, pour un mélange cinétique assez infime entre

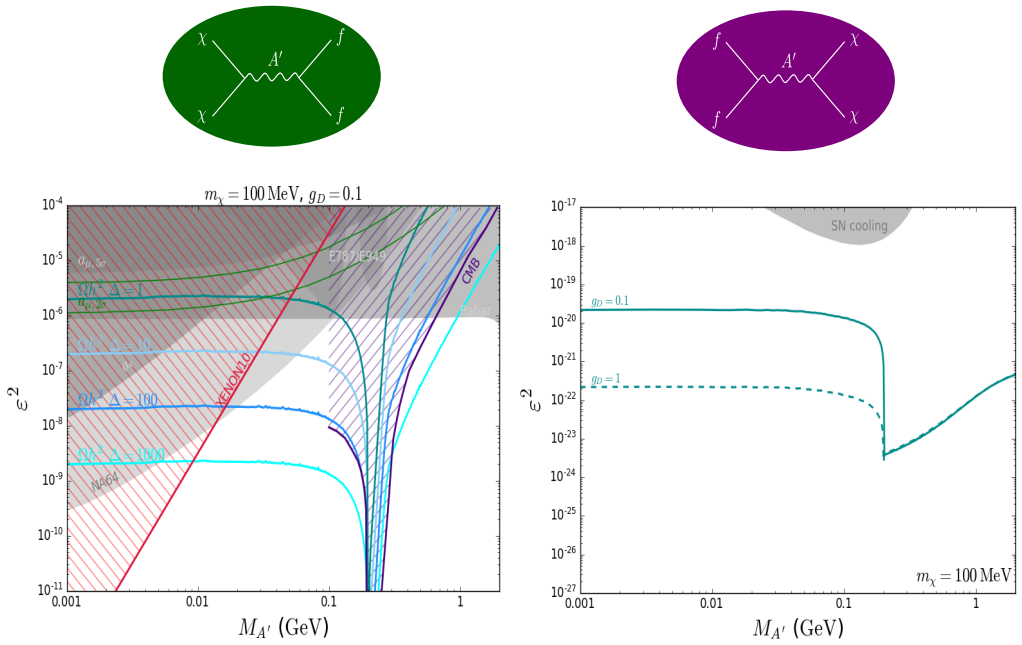

FIGURE 3 – *Résultats pour un WIMP à l'échelle MeV (à gauche) et FIMP (à droite) dans le modèle de portail de photons sombres à l'échelle MeV [2].*

les photons ordinaires et les photons sombres (panneau à droite de la figure 3). La production non-thermique de la DM est capable de fournir la densité relique correcte tout en évitant les contraintes d'observation, en particulier celles liées au refroidissement de Supernova. Ce travail a été considéré comme une motivation de physique fondamentale pour la mission proposée e-ASTROGAM (Enhanced ASTROGAM) [3], destinée à sonder les phénomènes astrophysiques dans la gamme des énergies des photons de 0.3 MeV à 3 GeV.

... à une "merveille FIMP"

Les fermions lourds non standard sont présents dans de nombreux scénarios BSM, par exemple pour la génération des masses minuscules des neutrinos, et nous avons étudié des portails BSM spin-0 et spin-1 qui sont affaiblis par de tels fermions lourds. Dans le premier cas, encore en développement [7], la matière noire est la composante pseudoscalaire d'un champ complexe présentant une symétrie $U(1)$ globale dont la rupture génère la masse des fermions lourds BSM. Nous étudions actuellement les contraintes possibles sur de tels scénarios, notamment sur la matière noire tiède. Le second scénario suppose une symétrie locale $U(1)$ sous laquelle les fermions BSM et les candidats de matière noire sont chargé [5]. Dans ce cas, les fermions lourds sont déjà nécessaires pour que la théorie soit cohérente, une fois que l'annulation des anomalies de jauge résultant de cette extension génère les couplages généralisés de Chern-Simons que nous utilisons pour produire de la matière noire. Dans les deux cas, donc, en supposant que les fermions BSM lourds sont chargés sur des groupes standard, nous pouvons générer une connexion effective *très faible* entre les secteurs sombre et visible.

Nous avons systématiquement constaté que, pour une Z' à l'échelle intermédiaire, avec une masse dans la gamme $10^{10} - 10^{14}$ GeV, l'espace des paramètres fournissant la quantité

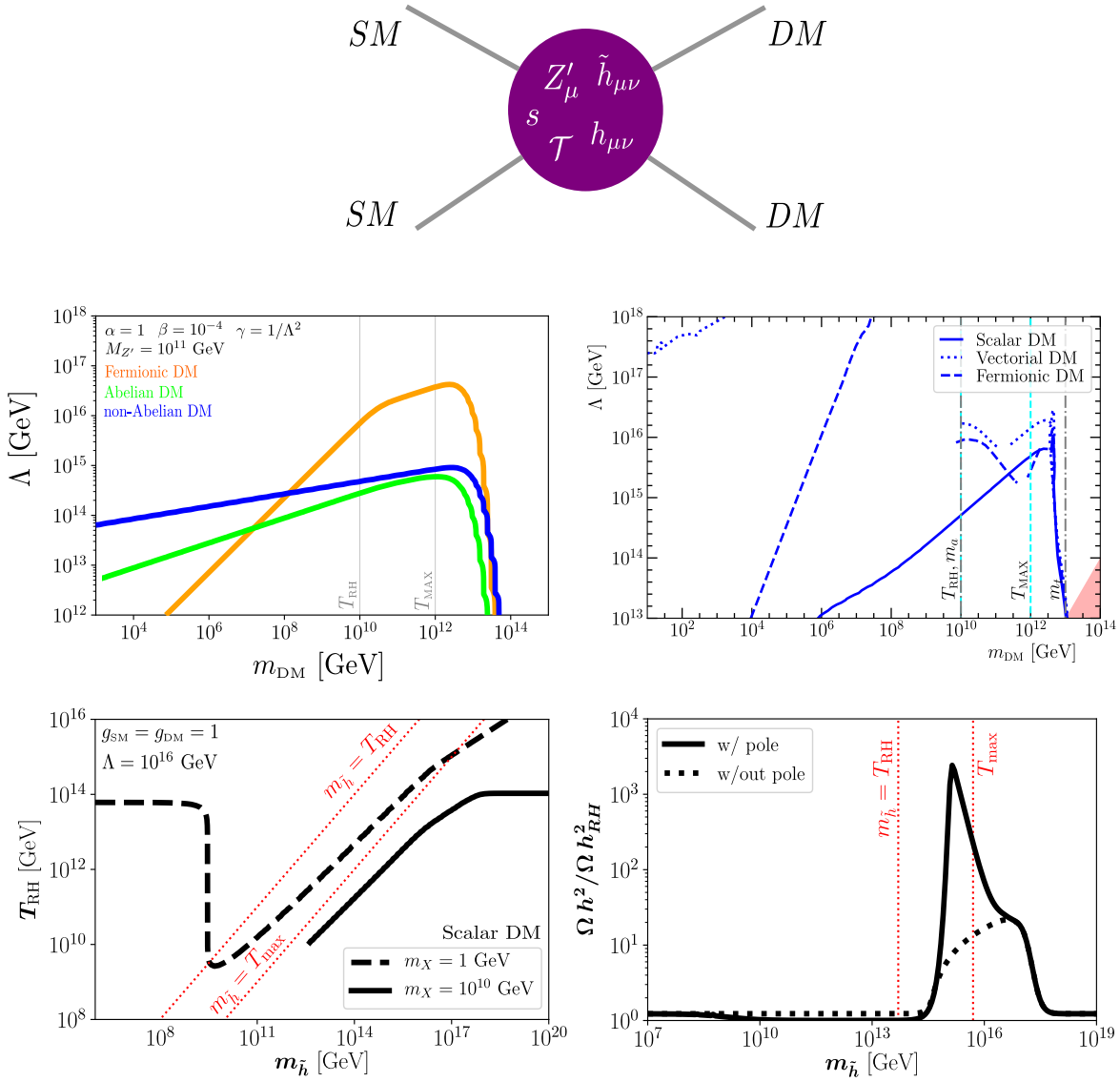

FIGURE 4 – *Panneau supérieur: représentation schématique des processus considérés en [4–7]. Panneau central: L'espace des paramètres du portail Z' (à gauche) et du portail moduli (à droite). Panneau inférieur: L'espace des paramètres du portail spin-2 (à gauche) et, dans ce contexte, l'effet de pôle lors du reheating (à droite).*

correcte de matière noire dans l'univers est telle que la nouvelle échelle de physique de la théorie (Λ), et donc les fermions sur lequel nous intégrons, se situe au moins au-dessus de l'échelle intermédiaire. La masse de matière noire, cependant, peut facilement varier de l'échelle TeV (s'il s'agit d'un fermion) ou même de l'échelle keV (s'il s'agit d'un vecteur) à un ordre de grandeur supérieur à la température maximale atteinte par le réservoir thermique. Ceci peut être vu dans le panneau central à gauche de la Fig. 4.

Des problèmes ouverts du modèle standard de la physique des particules peuvent être résolus par des extensions structurelles non minimales telles que la supersymétrie et la théorie des cordes. Dans de telles extensions, la gravité peut être systématiquement incorporée dans une description de la nature unifiée avec les autres interactions fondamentales, dont la relativité générale et le modèle standard en tant que théories efficaces avec des particules lourdes non standard dans le spectre. Dans ce contexte, des *interactions très faibles* entre les champs du modèle standard et ce secteur non standard, composé par exemple de champs spin-2 et de moduli, serait plutôt obligatoire pour que la description effective soit cohérente. En conséquence, ce type de cadre permet naturellement l'immersion de la matière noire produit de façon non thermique.

Nous avons étudié la production non thermique des candidats de matière noire scalaire, fermionique et vectoriel à partir de tous les champs de modèle standard via l'échange de spin-2 sans masse et massif [4] et de moduli [6], dont les espaces de paramètres sont exposé respectivement dans les panneaux inférieur gauche et central droit de la Fig. 4.

Si les masses des médiateurs sont proches de l'échelle de reheating, leur production résonante pendant le période de reheating peut être énorme, abaissant considérablement les valeurs de température de réchauffage (panneaux inférieur gauche dans Fig. 4) et augmentant les valeurs de la nouvelle échelle de physique (panneaux central droit dans Fig. 4) dans les contours fournissant la densité relique correcte de la matière noire. Nous avons montré que le "facteur d'amplification" de l'importance de la production pendant le reheating ne dépend généralement que de la quantité $T_{\rm MAX}/T_{\rm RH}$, qui est complètement défini par la théorie inflationaire. Cependant, lorsque le taux de production ne peut être approché par une loi de puissance, le facteur d'amplification devient fortement dépendant de la physique du secteur produisant la matière noire, comme on peut le voir dans le panneau inférieur droit dans Fig. 4.

Au-delà de l'émerveillement

Le puzzle de la matière noire souffre de nombreuses incertitudes théoriques et astrophysiques. Dans cette optique, les prochaines étapes de cette ligne de recherche pourraient être guidées par:

- déployer des efforts de calcul pour tester la validité des approximations usuelles et mieux explorer numériquement l'espace des paramètres des modèles;
- établir un lien entre la théorie de la matière noire et les problèmes ouverts de la physique des particules et de la cosmologie, principalement la génération des masses des neutrinos et de l'asymétrie baryonic;
- en essayant de comprendre comment les environnements astrophysiques affectent la matière noire d'un point de vue indépendant du modèle.

Pour relier la physique de la matière noire aux premiers stades de l'univers, il est nécessaire de travailler plus soigneusement à la compréhension des processus de thermalisation entre la matière noire, l'inflaton et les autres particules susceptibles de participer à sa production. Le formalisme de l'équation du fluide utilisé dans cette thèse ne serait pas approprié et n'est qu'une première approche de ce problème.

Les effets provenant de corrections de température finies et de facteurs d'amplification de Bose de la statistique quantique pourraient être importants dans les environnements à haute énergie et à forte densité, respectivement. Leurs effets possibles sur l'évolution de la matière noire dans l'univers primordial et éventuellement sur les environnements astrophysiques méritent d'être explorés.

Les analyses des spectres CMB étant de plus en plus précises, et donc la possibilité de contraindre des modèles inflationaires spécifiques motive l'étude de la production de matière noire avec une influence directe des candidats à l'inflaton.

À une époque où nous commençons à être en mesure de détecter les ondes gravitationnelles et éventuellement la lumière des premières étoiles, il convient d'étudier les signatures astrophysiques et les conséquences cosmologiques de la matière noire de manière aussi générique et complémentaire que possible.